



Hyperuniform states of matter

Salvatore Torquato

Department of Chemistry, Department of Physics, Princeton Institute for the Science and Technology of Materials, and Program in Applied and Computational Mathematics, Princeton University, Princeton, NJ 08544, USA



ARTICLE INFO

Article history:

Accepted 2 March 2018
Available online 31 March 2018
Editor: Mark Bowick

ABSTRACT

Hyperuniform states of matter are correlated systems that are characterized by an anomalous suppression of long-wavelength (i.e., large-length-scale) density fluctuations compared to those found in garden-variety disordered systems, such as ordinary fluids and amorphous solids. All perfect crystals, perfect quasicrystals and special disordered systems are hyperuniform. Thus, the hyperuniformity concept enables a unified framework to classify and structurally characterize crystals, quasicrystals and the exotic disordered varieties. While disordered hyperuniform systems were largely unknown in the scientific community over a decade ago, now there is a realization that such systems arise in a host of contexts across the physical, materials, chemical, mathematical, engineering, and biological sciences, including disordered ground states, glass formation, jamming, Coulomb systems, spin systems, photonic and electronic band structure, localization of waves and excitations, self-organization, fluid dynamics, number theory, stochastic point processes, integral and stochastic geometry, the immune system, and photoreceptor cells. Such unusual amorphous states can be obtained via equilibrium or nonequilibrium routes, and come in both quantum-mechanical and classical varieties. The connections of hyperuniform states of matter to many different areas of fundamental science appear to be profound and yet our theoretical understanding of these unusual systems is only in its infancy. The purpose of this review article is to introduce the reader to the theoretical foundations of hyperuniform ordered and disordered systems. Special focus will be placed on fundamental and practical aspects of the disordered kinds, including our current state of knowledge of these exotic amorphous systems as well as their formation and novel physical properties.

© 2018 Elsevier B.V. All rights reserved.

Contents

1. Introduction	3
1.1. Disordered hyperuniform systems are distinguishable states of matter	5
1.2. Hyperuniformity of heterogeneous materials	6
1.3. Further generalizations of the hyperuniformity concept	6
1.4. Overview	7
2. Basic definitions and preliminaries	7
2.1. Point processes	7
2.2. Lattices and periodic point configurations	9
2.3. Two-phase heterogeneous media	12
3. Local number fluctuations	13
3.1. Ensemble-average formulation of the number variance	13
3.1.1. Hyperspherical windows	15
3.2. Number variance for a single point configuration	16

E-mail address: torquato@princeton.edu.

3.3. Number variance for a single periodic point configurations.....	17
4. Local volume-fraction fluctuations in two-phase media	18
5. Mathematical foundations of hyperuniformity: Point configurations.....	19
5.1. Vanishing of normalized infinite-wavelength number fluctuations	19
5.2. Distinctions between equilibrium and nonequilibrium infinite-wavelength density fluctuations	20
5.3. Asymptotics via ensemble-average formulation and three hyperuniformity classes.....	20
5.3.1. Asymptotics of the number variance	21
5.3.2. Asymptotics from power-law structure factors	23
5.4. Asymptotics for a single point configuration	24
5.5. Asymptotics for periodic point configurations	24
5.6. Hyperuniform order metrics	26
5.7. Nonspherical windows	28
6. Mathematical foundations of hyperuniformity: Two-phase media.....	30
6.1. Vanishing of infinite-wavelength volume-fraction fluctuations	30
6.1.1. Asymptotic behavior of the volume-fraction variance for two-phase systems	31
6.1.2. Three classes of hyperuniform two-phase systems	31
6.2. Asymptotics from power-law spectral densities	32
6.3. Design of hyperuniform two-phase materials with prescribed spectral densities	32
6.4. Interrelations between number and volume-fraction variances	32
6.5. Spectral densities for packings	33
6.6. Nonspherical windows	34
7. Hyperuniformity as a critical-point phenomenon and scaling laws	35
7.1. Direct correlation function for hyperuniform systems and new critical exponents	35
7.2. Critical behavior of g_2 -invariant hyperuniform point configurations	37
7.2.1. Step-function g_2	37
7.2.2. Step+Delta function g_2	40
8. Hyperuniform disordered classical ground states	41
8.1. Stealthy configurations via collective-coordinate optimizations	41
8.2. Can disordered stealthy particle configurations tolerate arbitrarily large holes?	44
8.3. Configurations with designed hyperuniform structure factors via collective coordinates.....	44
8.3.1. Underconstrained systems.....	45
8.3.2. Perfect-glass paradigm	45
8.4. Ensemble theory for stealthy hyperuniform disordered ground states	46
8.4.1. General results	46
8.4.2. Pseudo hard spheres in Fourier space and pair statistics	47
8.4.3. Number variance and translational order metric τ	48
8.4.4. Entropically favored (most probable) states and ground-state manifold	49
8.4.5. Comparison of stealthy configurations to some common states of matter	50
8.4.6. Excited (vibrational) states	51
9. 1D hyperuniform patterns derived from random matrices, zeta function and prime numbers.....	52
9.1. Random matrices and the Riemann zeta function	52
9.2. Prime numbers	56
10. Hyperuniform determinantal point processes.....	56
10.1. General considerations	57
10.2. Fermi-sphere point processes	57
10.3. Two-dimensional Ginibre ensemble: one-component plasma	59
10.4. Weyl-Heisenberg ensemble	61
10.5. Multicomponent hard-sphere plasmas	61
11. Classical nonequilibrium systems	61
11.1. Ordered and disordered jammed particle packings	62
11.1.1. Jamming categories	62
11.1.2. Geometric-structure approach and order maps	63
11.1.3. Jamming-hyperuniformity conjecture	64
11.1.4. Numerical simulations of MRJ-like states and effective hyperuniformity	64
11.1.5. Critical slowing down as a disordered jammed state is approached	66
11.1.6. "Effective" hyperuniformity criterion	66
11.1.7. Toward the ideal MRJ state	66
11.1.8. Is hyperuniformity also a signature of MRJ packings of aspherical particles?	67
11.2. Driven nonequilibrium systems and critical absorbing states	67
11.2.1. Hyperuniformity in absorbing-state models	68
11.2.2. Interpretation of the ideal MRJ sphere packing as a critical-absorbing state	70
12. Natural disordered hyperuniform systems	70
12.1. Avian photoreceptor cells	70
12.2. Receptor organization in the immune system	72
13. Generalizations of the hyperuniformity concept	72
13.1. Fluctuations in the interfacial area	73

13.2. Random scalar fields	74
13.3. Random vector fields	75
13.4. Statistical anisotropic structures.....	77
13.5. Spin systems	79
14. Novel bulk physical properties of disordered hyperuniform materials.....	79
14.1. Thermodynamic properties	80
14.2. Wave characteristics	80
14.3. Transport properties	81
14.4. Mechanical properties	81
14.5. Structurally anisotropic materials.....	82
15. Effect of imperfections on hyperuniform states	82
16. Nearly hyperuniform systems.....	83
16.1. Growing length scale on approach to a hyperuniform state.....	84
16.2. Amorphous silicon and electronic band gaps.....	84
16.3. Polymeric materials: liquid state and glass formation	84
16.3.1. Equilibrium liquids	84
16.3.2. Glassy systems	85
17. Discussion and outlook.....	86
Acknowledgments	87
Appendix. Gauss circle problem and its generalizations	87
References	88

1. Introduction

The quantitative characterization of density fluctuations in many-particle systems is a fundamental and practical problem of great interest in the physical, materials, mathematical and biological sciences. It is well known that density fluctuations contain crucial thermodynamic and structural information about many-particle system both away from [1–6] and near critical points [7–12]. The one-dimensional point patterns associated with the eigenvalues of random matrices and energy levels of integrable quantum systems have been characterized by their density fluctuations [13–15]. The quantification of density fluctuations has been used to reveal the fractal nature of structures within living cells [16]. The measurement of galaxy density fluctuations is a powerful way to quantify and study the large-scale structure of the Universe [17,18]. Structural fluctuations play a critical role in charge transfer in DNA [19], thermodynamics of polyelectrolytes [20,21], and dynamics in glass formation [22]. Depletion phenomena that occur in various molecular systems near interfaces are due to density fluctuations [23,24]. Knowledge of density fluctuations in vibrated granular media has been used to probe the structure and collective motions of the grains [25]. Local density fluctuations have been recently used to distinguish the spatial distribution of cancer cells from that of normal, healthy cells [26].

The unusually large suppression of density fluctuations at long wavelengths (large length scales) is central to the hyperuniformity concept, whose broad importance for condensed matter physics and materials science was brought to the fore only about a decade ago in a study that focused on fundamental theoretical aspects, including how it provides a unified means to classify and structurally characterize crystals, quasicrystals and special disordered point configurations [27]. Hyperuniform systems are poised at an exotic critical point in which the direct correlation function, defined via the Ornstein-Zernike relation [6], is long-ranged [27], in diametric contrast to standard thermal critical points in which the total correlation function is long-ranged and the corresponding structure factor $S(\mathbf{k})$ diverges to infinity as the wavenumber $|\mathbf{k}|$ goes to zero [7–12]. A hyperuniform (or superhomogeneous [28]) many-particle system in d -dimensional Euclidean space \mathbb{R}^d is one in which (normalized) density fluctuations are completely suppressed at very large length scales, implying that the structure factor $S(\mathbf{k})$ tends to zero in the limit $|\mathbf{k}| \rightarrow 0$. Equivalently, a hyperuniform system is one in which the number variance $\sigma_N^2(R) \equiv \langle N(R)^2 \rangle - \langle N(R) \rangle^2$ of particles within a spherical observation window of radius R grows more slowly than the window volume in the large- R limit, i.e., slower than R^d . Typical disordered systems, such as liquids and structural glasses, have the standard asymptotic volume scaling $\sigma_N^2(R) \sim R^d$ and hence are not hyperuniform (see the left panel of Fig. 1). Periodic point configurations (such as the one shown in the middle panel of Fig. 1) are an obvious class of hyperuniform systems, since the number fluctuations are concentrated near the window boundary and hence have the surface-area scaling $\sigma_N^2(R) \sim R^{d-1}$. Less trivially, many perfect quasicrystals [29–31] possess the same surface-area scaling as perfect crystals [32,33]. Surprisingly, there is a special class of disordered particle configurations that have the same asymptotic number-variance scaling behavior as crystals (see the right panel of Fig. 1), as well as those that have asymptotic scalings that lie between surface-area and volume growth rates (as discussed in Section 5.3).

Fig. 2 shows the number variance (scaled by R^3) as a function of R for four different point configurations in three dimensions at unit density: two disordered nonhyperuniform systems, the Poisson (uncorrelated) point process and a low-density equilibrium hard-sphere fluid, and two different hyperuniform systems, one ordered and the other disordered. For a three-dimensional Poisson point process at unit density, the scaled variance $\sigma_N^2(R)/R^3$ is the constant $4\pi/3$ for all R . The scaled variance for a hard-sphere fluid decreases as R increases but quickly plateaus to a constant asymptotically. By contrast, for a hyperuniform system, this scaled number variance tends to decrease as R increases, apart from small-scale variations,

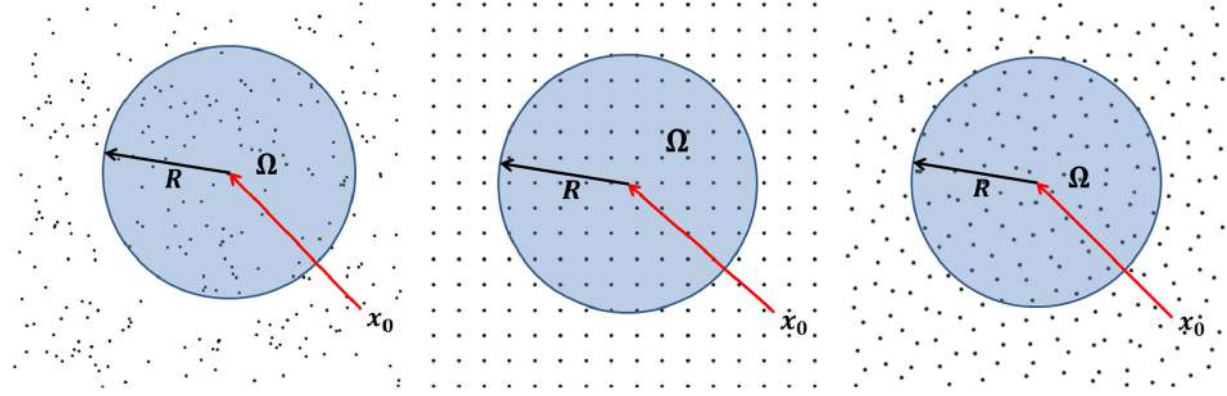


Fig. 1. Schematics indicating an observation window Ω , in this case a circular window in two dimensions, and its centroid x_0 for a disordered nonhyperuniform (left panel), periodic (middle panel), and disordered hyperuniform (right panel) point configurations. In each of these examples, the density of points within a window will fluctuate as the window position varies. Appendix briefly describes the related problem of determining how the number of points grows with window size when the window position is fixed and centered at one of the points of the point configuration.

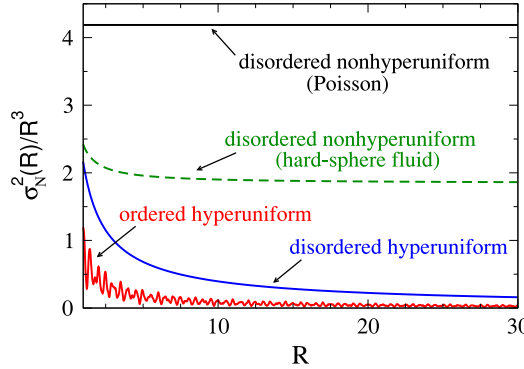


Fig. 2. Number variance $\sigma_N^2(R)$, scaled by R^3 , versus R for four different many-particle systems in three dimensions at unity density: disordered nonhyperuniform Poisson (uncorrelated), disordered nonhyperuniform (hard-sphere fluid), disordered hyperuniform (fermionic) [34], and ordered (simple cubic lattice) hyperuniform point configurations.

and completely vanishes in the large- R asymptotic limit. For a large class of nonspherical convex windows, hyperuniform point configurations are characterized by a number variance $\sigma_N^2(\mathbf{R})$ that when scaled by the window volume $v_1(\mathbf{R})$ tends to zero in the large-window limit, i.e.,

$$\lim_{v_1(\mathbf{R}) \rightarrow \infty} \frac{\sigma_N^2(\mathbf{R})}{v_1(\mathbf{R})} = 0, \quad (1)$$

where \mathbf{R} represents the geometrical parameters that define the window shape. In Section 5.7, we will discuss some anomalous situations in which the number variance for a hyperuniform system can grow even more slowly than the window surface area or as fast or faster than the window volume for some window shapes.

Disordered hyperuniform systems and their manifestations were largely unknown in the scientific community about a decade and a half ago; only a few examples were known then [27,28,35]. Now there is a realization that these systems play a vital role in a number of problems across the physical, materials, mathematical, and biological sciences. Specifically, we now know that these exotic states of matter can exist as both *equilibrium* and *nonequilibrium* phases, including classical disordered (noncrystalline) ground states [36–43], disordered hard-sphere plasmas [44,45], maximally random jammed (MRJ) hard-particle packings [46–54], jammed athermal soft-sphere models of granular media [55,56], jammed thermal colloidal packings [57,58], jammed bidisperse emulsions [59], dynamical processes in ultracold atoms [60], nonequilibrium phase transitions [61–69], avian photoreceptor patterns [70], receptor organization in the immune system [71], “perfect” glasses [72,73], certain quantum ground states (both fermionic and bosonic) [34,74], the distribution of the nontrivial zeros of the Riemann zeta function [34,75], and the eigenvalues of various random matrices [14,76].

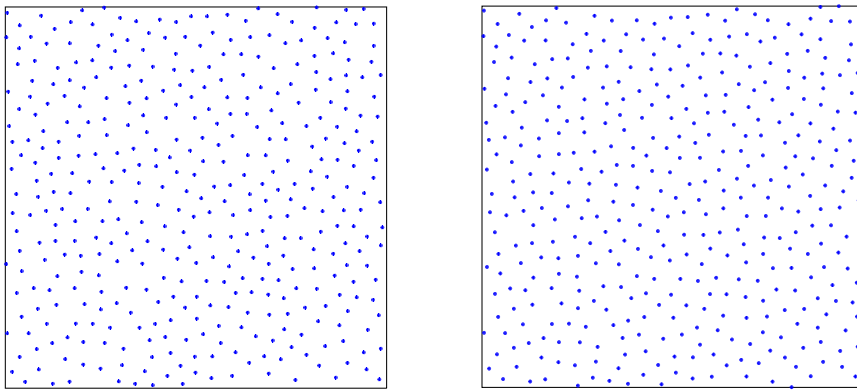


Fig. 3. A disordered *nonhyperuniform* many-particle configuration (left) that is derived from a dense packing of hard disks generated via the random sequential addition process at saturation with $S(0) \approx 0.059$ [77,78] and a disordered *hyperuniform* many-particle configuration (right) taken from Ref. [79]. The latter is obtained by very tiny collective displacements of the particles in the left panel using the collective-coordinate procedure reviewed in Section 8. Although the large-scale density fluctuations of these two systems are dramatically different, the distinctions are very difficult to detect by eye, since there is a tendency to focus on the structural similarities at short length scales. Thus, it can often be said that disordered hyperuniform point processes have a “hidden” order on large length scales.

1.1. Disordered hyperuniform systems are distinguishable states of matter

What qualifies as a distinguishable state of matter? Traditional criteria include, but are not limited to the following characteristics: (1) it is a homogeneous phase in thermodynamic equilibrium; (2) interacting entities are microscopic objects, e.g., atoms, molecules or spins; and (3) often, phases are distinguished by symmetry-breaking and/or some qualitative change in some bulk property. The liquid–gas phase transition is an example in which there is concomitant latent heat but no symmetry breaking. Modern developments demand broader criteria to identify a distinguishable state of matter, which inevitably involves some level of subjectivity. Additional criteria include the following attributes: (1) reproducible long-lived metastable or nonequilibrium phases (e.g., spin glasses and structural glasses); (2) interacting entities need not be microscopic, but can include building blocks that can interact across a wide range of length scales, e.g., colloids, polymers and DNA, to produce mesoscale materials; and (3) endowed with unique properties. New states of matter become more compelling if they give rise to or require new ideas and/or experimental/theoretical tools and are technologically important.

Isotropic disordered hyperuniform materials meet all of these criteria. They are exotic ideal states of matter that lie between a crystal and liquid: they are like perfect crystals in the way they suppress large-scale density fluctuations, a special type of long-range order and yet are like liquids or glasses in that they are statistically isotropic with no Bragg peaks and hence lack any *conventional* long-range order. These unusual attributes appear to endow such materials with novel physical properties, as described below. Importantly, disordered hyperuniform systems can be obtained via equilibrium or nonequilibrium routes, and come in both quantum-mechanical and classical varieties. Disordered hyperuniform systems can have a *hidden order not apparent on large length scales*; see Fig. 3 for a vivid example. Fig. 4 shows a typical scattering pattern for a crystal and another for a disordered isotropic hyperuniform system in which there is a circular region around the origin where there is no scattering, an extraordinary pattern for an amorphous material. Having become aware of what features to look for in scattering patterns, disordered hyperuniform systems are now being identified in various contexts across the fields of physics, materials science, chemistry, mathematics, engineering and biology [34,36–73,79–88].

The practical import of the hyperuniformity concept in the context of condensed matter physics started to become apparent soon after it was shown that two- and three-dimensional classical systems of particles interacting with certain soft long-ranged pair potentials could counterintuitively freeze into highly-degenerate disordered hyperuniform states at absolute zero temperature with “stealthy” scattering patterns, such as the one shown in the right panel of Fig. 4 [36,38]. These exotic situations run counter to the common expectation that liquids freeze into crystal structures with high symmetry (e.g., face-centered cubic and diamond crystals). In a subsequent computer simulation study [89], it was shown that cellular network solids derived from such stealthy hyperuniform configurations of particles possess large, *isotropic* photonic band gaps comparable in size to photonic crystals, which was previously thought to be impossible. This enabled investigators to design disordered hyperuniform cellular solids with unprecedented waveguide geometries unhindered by crystallinity and anisotropy, and robust to defects [90,91]. A variety of groups have recently fabricated various disordered hyperuniform materials at the micro- and nano-scales, including those for photonic applications [91–95], surface-enhanced Raman spectroscopy [96], the realization of a terahertz quantum cascade laser [97], self-assembly of diblock copolymers [98], periodically-driven emulsions [63], and self-assembled two-dimensional jammed packings of bidisperse droplets [59]. Recent computational investigations on stealthy hyperuniform systems have been directed toward optical [99], photonic [100–102], phononic [103], diffusion and conduction transport [87,104], and frequency-dependent

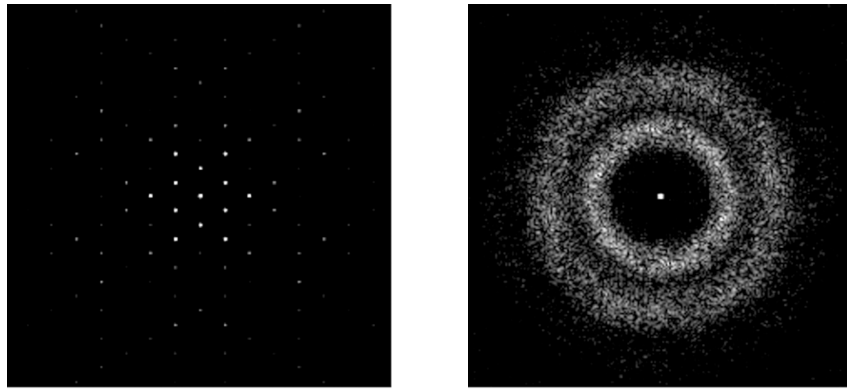


Fig. 4. Scattering patterns for two distinctly different hyperuniform point configurations: a six-fold symmetric crystal (left) and a disordered “stealthy” hyperuniform many-particle system (right) [36,38,40]. Observe that in the stealthy disordered case, apart from forward scattering, there is a circular region around the origin in which there is no scattering, a highly exotic situation for an amorphous state of matter.

dielectric constant behaviors [86–88] and applications. Moreover, another computational study revealed that the electronic bandgap of amorphous silicon widens as it tends toward a hyperuniform state [105]. Recent X-ray scattering measurements indicate that amorphous-silicon samples can be made to be nearly hyperuniform [106]. Thus, an ability to control and design disordered hyperuniform states of matter could lead to the discovery of novel materials.

The hyperuniformity concept has brought new attention to the importance of quantifying the large-scale structural correlations in amorphous systems, regardless of whether they are hyperuniform. This has been borne out in recent studies concerning molecular jamming processes that underlie glass-formation in polymeric materials [80,83], and quantifying the large-scale structure of amorphous ices and transitions between their different forms [84]. Understanding structural and physical properties of a system as it approaches a hyperuniform state or whether near hyperuniformity is signaling crucial large-scale structural changes in a system will be shown to be fundamentally important and is expected to lead to new insights about condensed phases of matter. Indeed, the hyperuniformity concept has suggested a “nonequilibrium index” for glasses [50] as well as new correlation functions from which one can extract relevant growing length scales as a function of temperature as a liquid is supercooled below its glass transition temperature [50,107], a problem of intense interest in the glass physics community [22,108–114].

1.2. Hyperuniformity of heterogeneous materials

The hyperuniformity concept was generalized to the case of heterogeneous materials [32], which are composed of domains of different materials (“phases”) [115,116]. Heterogeneous materials abound in Nature and synthetic situations. Examples include composite and porous media, metamaterials, biological media (e.g., plant and animal tissue), foams, polymer blends, suspensions, granular media, cellular solids, colloids [115]. In the case of two-phase media (defined in Section 2.3), one relevant fluctuating quantity is the local phase volume fraction within an observation window; see Fig. 5. The simplest characterization of such fluctuations is the local volume-fraction variance $\sigma_v^2(R)$ associated with a d -dimensional spherical window of radius R that uniformly samples the space [115,117–120], which is the counterpart to the number variance $\sigma_N^2(R)$ for point configurations. The hyperuniformity condition in the context of volume-fraction fluctuations in a two-phase heterogeneous system is one in which the variance $\sigma_v^2(R)$ for large R goes to zero more rapidly than the inverse of the window volume, i.e., R^{-d} [32]. This is equivalent to the condition that the relevant spectral function, called the spectral density $\tilde{\chi}_v(\mathbf{k})$ (defined in Section 2.3) tends to zero as the wavenumber $|\mathbf{k}|$ goes to zero. This generalization of the hyperuniformity concept has been fruitfully applied to characterize a variety of disordered two-phase systems [48,52,58,121–123] and to the rational design of digitized hyperuniform two-phase media (or, equivalently, two-state spin systems) with tunable disorder [87,124].

1.3. Further generalizations of the hyperuniformity concept

The hyperuniformity concept has very recently been broadened along four different directions. This includes generalizations to treat fluctuations in the interfacial area (one of the Minkowski functionals [125,126]) in heterogeneous media and surface-area driven evolving microstructures, random scalar fields (e.g., spinodal decomposition), random vector fields (e.g., velocity fields in turbulence and transport in random media), and statistically anisotropic many-particle systems (e.g., structures that respond to external fields) and two-phase media [81].

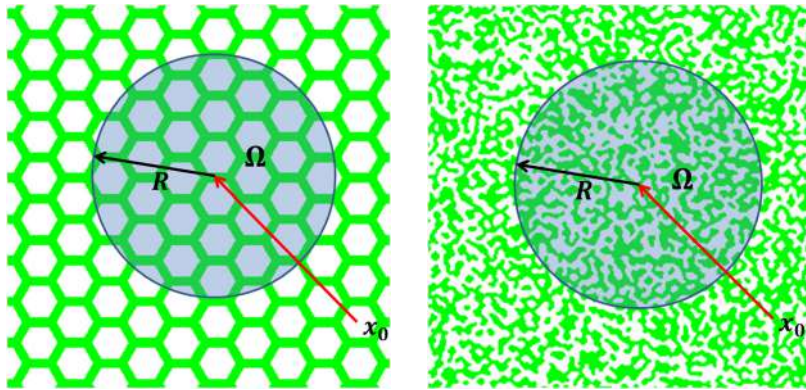


Fig. 5. Schematics indicating an observation window Ω , in this case a circular window in two dimensions, and its centroid \mathbf{x}_0 for a periodic heterogeneous medium (left) and a general disordered heterogeneous medium (right). In each of these examples, the phase volume fraction or interfacial area within a window will fluctuate as the window position varies.

1.4. Overview

The connections of hyperuniform states of matter to many different areas of fundamental science appear to be profound and yet our theoretical understanding of these unusual states of matter is still in its nascent stages of development. The purpose of this review article is directed toward introducing the reader to the theoretical foundations of hyperuniform ordered and disordered systems and their implications. Special focus will be placed on the disordered variety, describing our current state of knowledge of disordered hyperuniform systems and their formation, stressing both fundamental and practical aspects of such exotic states of amorphous matter.

This review article is organized as follows: in Section 2, we summarize basic definitions and concepts. Formulas for the local number variance of point configurations in different settings are derived and/or presented in Section 3. In Section 4, we derive formulas for the local volume-fraction variance of two-phase media. Sections 5 and 6 focus on the mathematical foundations of hyperuniformity for point configurations and two-phase media, respectively, including the three possible hyperuniformity classes. In Section 7, we demonstrate that hyperuniform point configurations are poised at exotic critical points and describe the critical behaviors of so-called g_2 -invariant hyperuniform point processes. A Fourier-based optimization procedure to generate a wide class of hyperuniform point configurations with targeted structure factors that are the classical ground states of certain soft long-ranged interactions is described in Section 8. In Section 9, we discuss the one-dimensional disordered hyperuniform point patterns derived from random matrices and the Riemann zeta function. Disordered hyperuniform determinantal point processes are described in Section 10. In Section 11, we report on a variety of disordered nonequilibrium systems that are putatively hyperuniform, including disordered jammed particle packings and absorbing-state models. A description of disordered hyperuniform patterns that arise in biological systems, including photoreceptor cells in avian retina and the immune system is presented in Section 12. The generalizations of the hyperuniformity concept to treat fluctuations in the interfacial area in heterogeneous media and surface-area driven evolving microstructures, random scalar fields, random vector fields, and statistically anisotropic many-particle systems and two-phase media is taken up in Section 13. In Section 14, we describe novel bulk physical properties of disordered hyperuniform materials that have recently come to light. We discuss how the degree of hyperuniformity of a perfect hyperuniform system is affected by the introduction of imperfections in Section 15. Section 16 addresses the importance of quantifying large-scale density fluctuations of many-particle systems, regardless of whether they are hyperuniform, and discusses nearly hyperuniform systems. Concluding remarks and an outlook for the field are given in Section 17. Appendix briefly discusses the Gauss circle problem and its generalizations, and links to integrable quantum systems.

2. Basic definitions and preliminaries

2.1. Point processes

A stochastic point process in d -dimensional Euclidean space \mathbb{R}^d is defined as a mapping from a probability space to configurations of points $\mathbf{x}_1, \mathbf{x}_2, \mathbf{x}_3, \dots$. The reader is referred to Refs. [125,127] for a more detailed mathematical description. It is noteworthy that this random setting is quite general. It incorporates cases in which the location of the points are deterministically known, such as a lattice or crystal. We will often call a particular realization of a point process a *point configuration*.

A point process is completely statistically characterized by specifying the countably infinite set of n -particle probability density functions $\rho_n(\mathbf{r}_1, \mathbf{r}_2, \dots, \mathbf{r}_n)$ ($n = 1, 2, 3, \dots$) [128]. The distribution-valued function $\rho_n(\mathbf{r}_1, \mathbf{r}_2, \dots, \mathbf{r}_n)$ has a probabilistic interpretation: apart from trivial constants, it is the probability density function associated with finding n different

points at positions $\mathbf{r}_1, \dots, \mathbf{r}_n$ and hence has the nonnegativity property

$$\rho_n(\mathbf{r}_1, \mathbf{r}_2, \dots, \mathbf{r}_n) \geq 0 \quad \forall \mathbf{r}_i \in \mathbb{R}^d \quad (i = 1, 2, \dots, n). \quad (2)$$

The point process is *statistically homogeneous* or *translationally invariant* if for every constant vector \mathbf{y} in \mathbb{R}^d , $\rho_n(\mathbf{r}_1, \mathbf{r}_2, \dots, \mathbf{r}_n) = \rho_n(\mathbf{r}_1 + \mathbf{y}, \mathbf{r}_2 + \mathbf{y}, \dots, \mathbf{r}_n + \mathbf{y})$, which implies that the point process occupies all of space and

$$\rho_n(\mathbf{r}_1, \mathbf{r}_2, \dots, \mathbf{r}_n) = \rho^n g_n(\mathbf{r}_{12}, \dots, \mathbf{r}_{1n}), \quad (3)$$

where ρ is the *number density* (number of points per unit volume in the infinite-volume limit) and $g_n(\mathbf{r}_{12}, \dots, \mathbf{r}_{1n})$ is the *n-particle correlation function*, which depends on the relative positions $\mathbf{r}_{12}, \mathbf{r}_{13}, \dots$, where $\mathbf{r}_{ij} \equiv \mathbf{r}_j - \mathbf{r}_i$. Unless otherwise stated, we will assume that statistically homogeneous point processes are also *ergodic*, i.e., any single realization of the ensemble is representative of the ensemble in the infinite-volume limit and hence a *volume average* in the infinite-volume limit is equal to the ensemble average [115].

For translationally invariant point processes without *long-range order*, $g_n(\mathbf{r}_{12}, \dots, \mathbf{r}_{1n}) \rightarrow 1$ when the points (or “particles”) are mutually far from one another, i.e., as $|\mathbf{r}_{ij}| \rightarrow \infty$ ($1 \leq i < j < n$), $\rho_n(\mathbf{r}_1, \mathbf{r}_2, \dots, \mathbf{r}_n) \rightarrow \rho^n$. Thus, the deviation of g_n from unity provides a measure of the degree of spatial correlations between the particles. Note that for a translationally invariant *Poisson* (spatially uncorrelated) point process, $g_n = 1$ is unity for all values of its argument.

We call $g_2(\mathbf{r}) = g_2(-\mathbf{r})$ the pair correlation function. It is useful to introduce the total correlation function $h(\mathbf{r})$ of a translationally invariant point process, which is related to the pair correlation function via

$$h(\mathbf{r}) \equiv g_2(\mathbf{r}) - 1 \quad (4)$$

and decays to zero for large $|\mathbf{r}|$ in the absence of long-range order. Note that $h(\mathbf{r}) = 0$ for all \mathbf{r} for a translationally invariant Poisson point process. If the point process is also statistically isotropic (rotational invariant), these pair statistics are functions only of the radial distance $r = |\mathbf{r}|$, i.e., $g_2(\mathbf{r}) = g_2(r)$ and $h(\mathbf{r}) = h(r)$. The *cumulative coordination number* $Z(r)$, defined to be the expected number of points found in a sphere of radius r centered at an arbitrary point of the point process, is a monotonically increasing function of r that is related to the radial pair correlation function as follows:

$$Z(r) = \rho s_1(1) \int_0^r x^{d-1} g_2(x) dx, \quad (5)$$

where

$$s_1(r) = \frac{2\pi^{d/2} r^{d-1}}{\Gamma(d/2)} \quad (6)$$

is the surface area of a d -dimensional sphere of radius r and $\Gamma(x)$ is the gamma function.

A collection of spheres in d -dimensional Euclidean space \mathbb{R}^d is called a *sphere packing* if no two spheres overlap. Clearly, the positions of the sphere centers of a packing constitute an infinite point configuration when the spheres uniformly occupy the space. An important characteristic of a packing is its packing fraction ϕ , which is the fraction of space \mathbb{R}^d covered by the spheres.

Before describing relevant spectral functions, it is useful to introduce the following definition of the Fourier transform of a function $f(\mathbf{r})$ that depends on the vector \mathbf{r} in d -dimensional Euclidean space \mathbb{R}^d :

$$\tilde{f}(\mathbf{k}) = \int_{\mathbb{R}^d} f(\mathbf{r}) \exp[-i(\mathbf{k} \cdot \mathbf{r})] d\mathbf{r}, \quad (7)$$

where \mathbf{k} is a wave vector and $(\mathbf{k} \cdot \mathbf{r}) = \sum_{i=1}^d k_i r_i$ is the conventional Euclidean inner product of two real-valued vectors. The function $f(\mathbf{r})$ can generally represent a tensor of arbitrary rank. When it is well-defined, the corresponding inverse Fourier transform is given by

$$f(\mathbf{r}) = \left(\frac{1}{2\pi}\right)^d \int_{\mathbb{R}^d} \tilde{f}(\mathbf{k}) \exp[i(\mathbf{k} \cdot \mathbf{r})] d\mathbf{k}. \quad (8)$$

If f is a radial function, i.e., f depends only on the modulus $r = |\mathbf{r}|$ of the vector \mathbf{r} , its Fourier transform is given by

$$\tilde{f}(k) = (2\pi)^{\frac{d}{2}} \int_0^\infty r^{d-1} f(r) \frac{J_{(d/2)-1}(kr)}{(kr)^{(d/2)-1}} dr, \quad (9)$$

where $k = |\mathbf{k}|$ is wavenumber or modulus of the wave vector \mathbf{k} and $J_v(x)$ is the Bessel function of the first kind of order v . The inverse transform of $\tilde{f}(k)$ is given by

$$f(r) = \frac{1}{(2\pi)^{\frac{d}{2}}} \int_0^\infty k^{d-1} \tilde{f}(k) \frac{J_{(d/2)-1}(kr)}{(kr)^{(d/2)-1}} dk. \quad (10)$$

An important nonnegative spectral function $S(\mathbf{k})$, called the *structure factor* (or power spectrum), is defined as follows:

$$S(\mathbf{k}) = 1 + \rho \tilde{h}(\mathbf{k}), \quad (11)$$

where $\tilde{h}(\mathbf{k})$ is the Fourier transform of $h(\mathbf{r})$. This quantity is directly related to the scattering-intensity function $S(\mathbf{k})$, defined in (24), when forward scattering is excluded. While $S(\mathbf{k})$ is a nontrivial function for spatially correlated point processes, it is trivially given by

$$S(\mathbf{k}) = 1 \quad \text{for all } \mathbf{k} \quad (12)$$

for a translationally invariant Poisson point process. Correlated disordered systems are characterized by structure factors that deviate from unity for some wave vectors; well-known examples include typical liquids [6] as well as disordered equilibrium [6,115] and nonequilibrium [78] sphere packings. However, the preponderance of such disordered systems are not hyperuniform.

We note that the value of the total correlation function at the origin, $h(\mathbf{r} = \mathbf{0})$, provides a simple sum rule on its Fourier transform or $S(\mathbf{k})$ must obey, namely, $\rho h(\mathbf{r} = \mathbf{0}) = (2\pi)^{-d} \int_{\mathbb{R}^d} [S(\mathbf{k}) - 1] d\mathbf{k}$. For any point configuration in which the minimal pair distance is some positive number, $g_2(\mathbf{r} = \mathbf{0}) = 0$ or $h(\mathbf{r} = \mathbf{0}) = -1$, and hence the sum rule becomes

$$\frac{1}{(2\pi)^d} \int_{\mathbb{R}^d} [S(\mathbf{k}) - 1] d\mathbf{k} = -\rho. \quad (13)$$

Examples of point configurations that satisfy (13) include the centers of spheres in a sphere packing or the vertices of polyhedral tiles of space.

A hyperuniform [27] or superhomogeneous [28] point configuration is one in which the structure factor $S(\mathbf{k})$ tends to zero as the wavenumber $k \equiv |\mathbf{k}|$ tends to zero, i.e.,

$$\lim_{|\mathbf{k}| \rightarrow 0} S(\mathbf{k}) = 0, \quad (14)$$

implying that single scattering of incident radiation at infinite wavelengths is completely suppressed. As we will see, this class of point configurations includes perfect crystals, a large class of perfect quasicrystals [32,33] and special disordered many-particle systems. Note that structure-factor definition (11) and the hyperuniformity requirement (14) dictate that the volume integral of $\rho h(\mathbf{r})$ over all space is exactly equal to -1 , i.e.,

$$\rho \int_{\mathbb{R}^d} h(\mathbf{r}) d\mathbf{r} = -1, \quad (15)$$

which is a direct-space *sum rule* that a hyperuniform point process must obey. This means that $h(\mathbf{r})$ must exhibit negative correlations, i.e., *anticorrelations*, for some values of \mathbf{r} .

Stealthy point processes are those in which the structure factor is exactly zero for a subset of wave vectors [36,38,40], meaning that they completely suppress single scattering for these wave vectors. *Stealthy hyperuniform* patterns are a subclass of hyperuniform systems in which $S(\mathbf{k})$ is zero for a range of wave vectors around the origin, i.e.,

$$S(\mathbf{k}) = 0 \quad \text{for } 0 \leq |\mathbf{k}| \leq K, \quad (16)$$

where K is some positive number. As we will see, perfect crystals are stealthy hyperuniform patterns. An example of a disordered stealthy and hyperuniform scattering pattern is shown in the right panel of Fig. 4.

It is instructive to compare pair statistics in direct and Fourier spaces to one another for several different two-dimensional point configurations. Figs. 6 and 7 show these pair statistics for the Poisson point process and an equilibrium hard-disk fluid, respectively, both of which are not hyperuniform. It is readily seen that both structure factors are positive at $k = 0$. Figs. 8 and 9 depict corresponding functions for two different disordered hyperuniform systems: a fermionic point process and a stealthy hyperuniform point configuration, respectively. These systems will be described more fully in Sections 8 and 10. It suffices to state here that whereas $S(\mathbf{k})$ goes to zero linearly in $k \equiv |\mathbf{k}|$ in the limit $k \rightarrow 0$ for the fermionic example, $S(\mathbf{k})$ is not only zero at the origin, but is “gapped”, i.e., it is zero for a contiguous range of wavenumbers around the origin, for the stealthy pattern. Finally, Fig. 10 shows the angular-averaged pair statistics for the triangular lattice. Like the disordered stealthy example, $S(\mathbf{k})$ is gapped for the lattice, but unlike the former, possesses long-range order as reflected by the presence of Bragg peaks out to infinity.

2.2. Lattices and periodic point configurations

A lattice Λ in \mathbb{R}^d is a subgroup consisting of integer linear combinations of vectors that constitute a basis for \mathbb{R}^d , and thus, it represents a special subset of point processes. Here, the space can be geometrically divided into identical regions F called fundamental cells, each of which contains just one point specified by the lattice vector

$$\mathbf{p} = n_1 \mathbf{a}_1 + n_2 \mathbf{a}_2 + \cdots + n_{d-1} \mathbf{a}_{d-1} + n_d \mathbf{a}_d, \quad (17)$$

where \mathbf{a}_i are the basis vectors for a fundamental cell and n_i spans all the integers for $i = 1, 2, \dots, d$. We denote by v_F the volume of F . A lattice is called a *Bravais* lattice in the physical sciences. Every lattice has a dual (or reciprocal) lattice Λ^* in which the lattice sites are specified by the dual (reciprocal) lattice vector $\mathbf{q} \cdot \mathbf{p} = 2\pi m$ for all \mathbf{p} , where $m = 0, \pm 1, \pm 2, \pm 3, \dots$

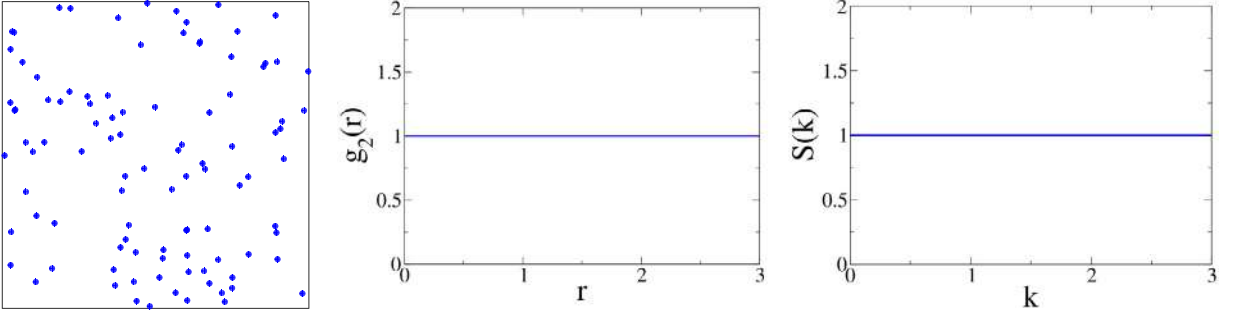


Fig. 6. (Left) Portion of a Poisson point configuration. (Middle) Corresponding ensemble-averaged pair correlation function $g_2(r)$ versus pair distance r in the infinite-volume limit. (Right) Corresponding ensemble-averaged structure factor $S(k)$ versus wavenumber k in the infinite-volume limit.

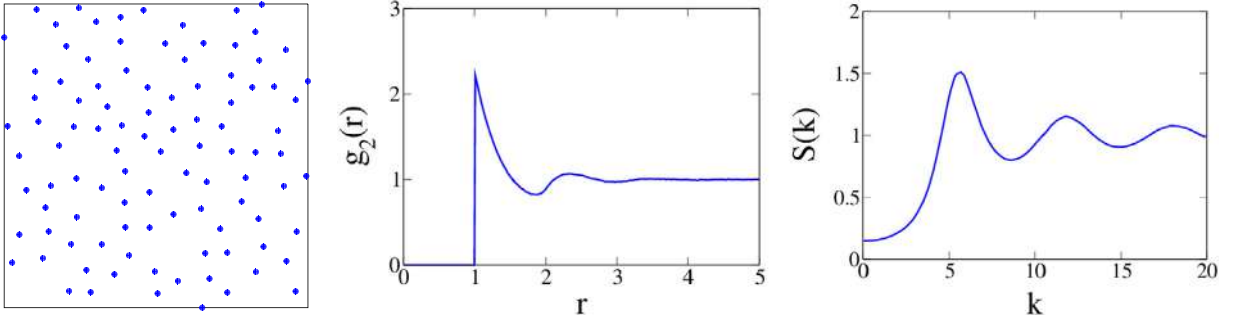


Fig. 7. (Left) Portion of a configuration of an equilibrium distribution of hard circular disks with packing fraction $\phi = 0.4$. Only the centers of the disks are shown. (Middle) Corresponding ensemble-averaged pair correlation function $g_2(r)$ versus pair distance r in the infinite-volume limit in units of the disk diameter. (Right) Corresponding ensemble-averaged structure factor $S(k)$ versus wavenumber k in the infinite-volume limit.

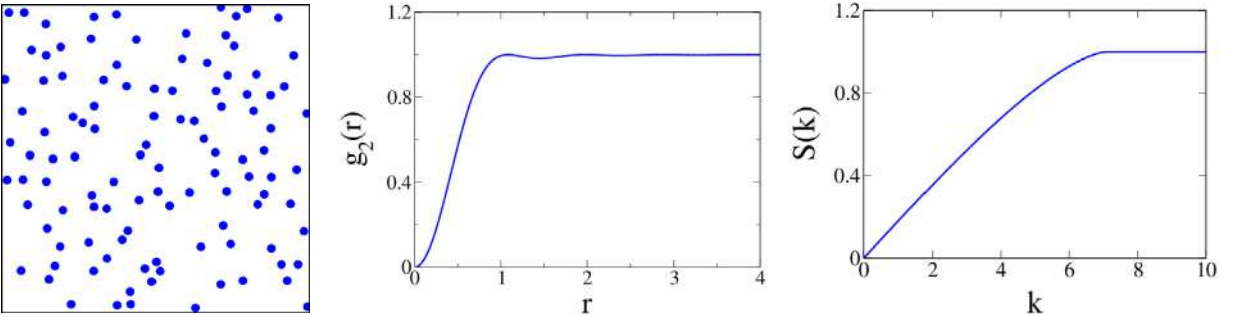


Fig. 8. (Left) Portion of a configuration of a fermionic (determinantal) point process at unit density [34]. (Middle) Corresponding ensemble-averaged pair correlation function $g_2(r)$ versus pair distance r in the infinite-volume limit. (Right) Corresponding ensemble-averaged structure factor $S(k)$ versus wavenumber k in the infinite-volume limit.

The dual fundamental cell F^* has volume $v_{F^*} = (2\pi)^d/v_F$. This implies that the number density ρ_Λ of Λ is related to the number density ρ_{Λ^*} of the dual lattice Λ^* via the expression

$$\rho_\Lambda \rho_{\Lambda^*} = 1/(2\pi)^d. \quad (18)$$

Common d -dimensional lattices include the *hypercubic* \mathbb{Z}^d , *checkerboard* D_d , and root A_d lattices, defined, respectively, by

$$\mathbb{Z}^d = \{(x_1, \dots, x_d) : x_i \in \mathbb{Z}\} \quad \text{for } d \geq 1 \quad (19)$$

$$D_d = \{(x_1, \dots, x_d) \in \mathbb{Z}^d : x_1 + \dots + x_d \text{ even}\} \quad \text{for } d \geq 3 \quad (20)$$

$$A_d = \{(x_0, x_1, \dots, x_d) \in \mathbb{Z}^{d+1} : x_0 + x_1 + \dots + x_d = 0\} \quad \text{for } d \geq 1, \quad (21)$$

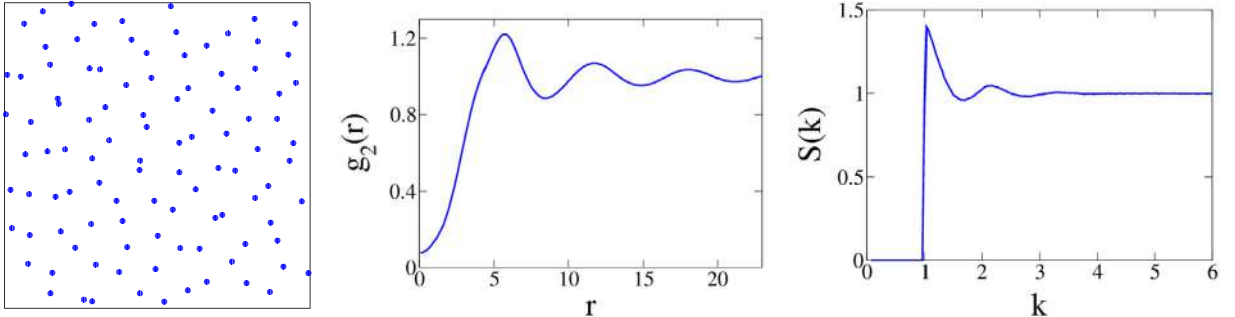


Fig. 9. (Left) Portion of a configuration of a disordered stealthy hyperuniform ground state at unit density [40]. (Middle) Corresponding ensemble-averaged pair correlation function $g_2(r)$ versus pair distance r in the infinite-volume limit. (Right) Corresponding ensemble-averaged structure factor $S(k)$ versus wavenumber k in the infinite-volume limit.

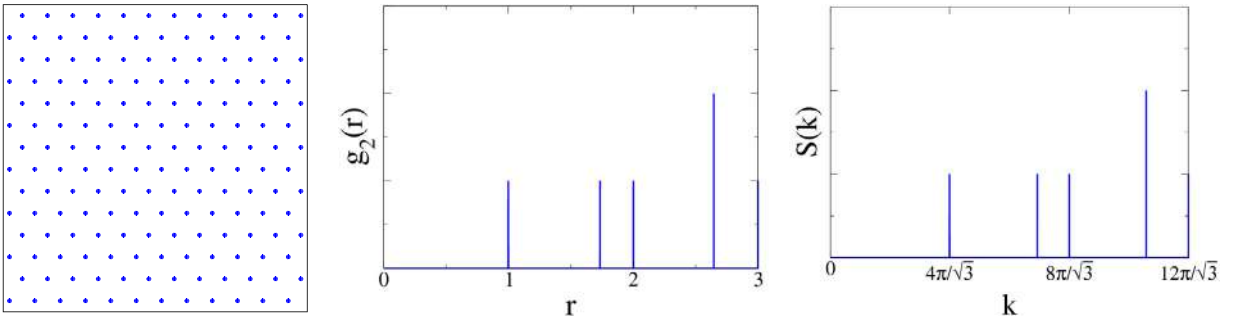


Fig. 10. (Left) Portion of an infinite triangular lattice. (Middle) Corresponding angular-averaged pair correlation function $g_2(r)$ versus pair distance r in units of the nearest-neighbor distance. (Right) Corresponding angular-averaged structure factor $S(k)$ versus wavenumber k .

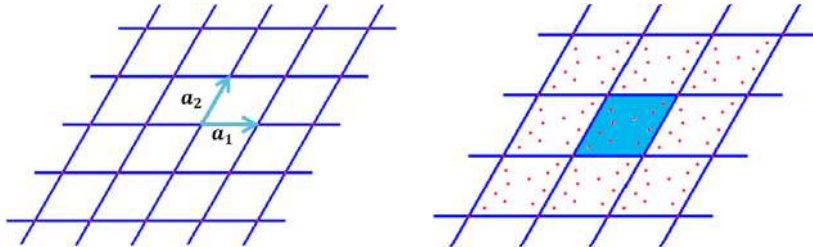


Fig. 11. (Bravais) lattice with one particle per fundamental cell (left panel) and a periodic crystal with multiple particles per fundamental cell (right panel).

where \mathbb{Z} is the set of integers; x_1, \dots, x_d denote the components of a lattice vector of either \mathbb{Z}^d or D_d ; and x_0, x_1, \dots, x_d denote the components of a lattice vector of A_d . The d -dimensional lattices \mathbb{Z}_*^d , D_d^* and A_d^* are the corresponding dual lattices. Following Conway and Sloane [129], we say that two lattices are *equivalent* or *similar* if one becomes identical to the other possibly by a rotation, reflection, and change of scale, for which we use the symbol \equiv . The A_d and D_d lattices are d -dimensional generalizations of the face-centered-cubic (FCC) lattice defined by $A_3 \equiv D_3$; however, for $d \geq 4$, they are no longer equivalent. In two dimensions, $A_2 \equiv A_2^*$ defines the triangular lattice. In three dimensions, $A_3^* \equiv D_3^*$ defines the body-centered-cubic (BCC) lattice. In four dimensions, the checkerboard lattice and its dual are equivalent, i.e., $D_4 \equiv D_4^*$. The hypercubic lattice $\mathbb{Z}^d \equiv \mathbb{Z}_*^d$ and its dual lattice are equivalent for all d .

A periodic point configuration (crystal) is a more general notion than a lattice, since it is obtained by placing a fixed configuration of N points (where $N \geq 1$) within a fundamental cell F of a lattice Λ , which is then periodically replicated. Thus, the point configuration is still periodic under translations by Λ , but the N points can occur anywhere in F ; see Fig. 11. Crystals are characterized by long-range translational and orientational order with crystallographic symmetries.

A quasicrystal lacks translational periodicity but possesses long-range orientational order with prohibited crystallographic symmetries, including five-fold symmetry and three-dimensional icosahedral symmetry [29–31]. Levine and Steinhardt correctly predicted that the diffraction pattern of a quasicrystal would show a dense set of Bragg peaks with such prohibited crystallographic symmetries [30,31].

An arbitrary single periodic point configuration of N points within F of a lattice Λ is specified by its *microscopic density* $n(\mathbf{r})$ at position \mathbf{r} , which is defined by

$$n(\mathbf{r}) = \sum_{j=1}^N \delta(\mathbf{r} - \mathbf{r}_j), \quad (22)$$

where $\delta(\mathbf{r})$ is a d -dimensional Dirac delta function. It is useful for both theoretical and practical reasons to introduce the *complex collective density variable* $\tilde{n}(\mathbf{k})$, which is simply the Fourier transform of the microscopic density (22):

$$\tilde{n}(\mathbf{k}) = \sum_{j=1}^N \exp(-i\mathbf{k} \cdot \mathbf{r}_j), \quad (23)$$

where \mathbf{k} is a wave vector in Λ^* . This quantity enables one to determine the *scattering-intensity* function $S(\mathbf{k})$, which is proportional to the total intensity measured in elastic scattering radiation experiments [4,6]. Specifically, the scattering-intensity function is mathematically defined as

$$S(\mathbf{k}) = \frac{|\tilde{n}(\mathbf{k})|^2}{N}, \quad (24)$$

which is a nonnegative real function with inversion-symmetry, i.e.,

$$S(\mathbf{k}) = S(-\mathbf{k}) \quad (25)$$

that obeys the bounds

$$0 \leq S(\mathbf{k}) \leq N \quad (\mathbf{k} \neq \mathbf{0}) \quad (26)$$

with $S(\mathbf{0}) = N$.

For a single periodic configuration with a finite number of N points within a fundamental cell, the scattering intensity $S(\mathbf{k})$ is identical to the structure factor $S(\mathbf{k})$ [cf. (11)], excluding its value at $\mathbf{k} = \mathbf{0}$ (forward scattering). Any such configuration contains a spherical region around the origin $\mathbf{k} = \mathbf{0}$ in whose interior there is no scattering for $|\mathbf{k}| < |\mathbf{k}_{\text{Bragg}}|$, where $\mathbf{k}_{\text{Bragg}}$ is the minimal positive wave vector, and hence is stealthy, as defined by the structure factor condition (16).

For an ensemble of periodic point configurations generated from a point process within F , the ensemble average of $S(\mathbf{k})$ in a certain infinite-size limit is directly related to the structure factor $S(\mathbf{k})$ defined in Eq. (11) via

$$\lim_{N, v_F \rightarrow \infty} \langle S(\mathbf{k}) \rangle = (2\pi)^d \rho \delta(\mathbf{k}) + S(\mathbf{k}), \quad (27)$$

where

$$\rho \equiv \lim_{N \rightarrow \infty, v_F \rightarrow \infty} \frac{N}{v_F} \quad (28)$$

is the constant *number density*. This is the so-called *thermodynamic limit*, where it is assumed (unless otherwise stated) that the limiting point process is ergodic.

Note that for a single periodic point configuration at number density ρ , the radial (angular-averaged) pair correlation function can be written as

$$g_2(r) = \sum_{i=1}^{\infty} \frac{Z_i}{\rho s_1(r_i)} \delta(r - r_i), \quad (29)$$

where Z_i is the expected coordination number at radial distance r_i (number of points that are exactly at a distance $r = r_i$ from a point of the point process) such that $r_{i+1} > r_i$ and $\delta(r)$ is a radial Dirac delta function.

2.3. Two-phase heterogeneous media

A random heterogeneous medium is a partition of d -dimensional Euclidean space \mathbb{R}^d into disjoint regions (phases) with interfaces that are known only probabilistically [115]. Such media are ubiquitous in nature and synthetic situations; examples include composites, sandstones, granular media, polymer blends, colloids, animal and plant tissue, gels, foams, and concrete. Throughout this article, we will consider *two-phase* heterogeneous media for simplicity. Since one can always construct a heterogeneous medium by “decorating” a point process with possibly overlapping closed sets (e.g., spheres and polyhedra) or by some other mapping derived from a point process, characterizing the statistical properties of a heterogeneous medium represents a more general problem than the study of point configurations; namely, the latter systems are recovered as a special limit of the former.

Consider a two-phase random heterogeneous medium, which is a domain of space $\mathcal{V} \subseteq \mathbb{R}^d$ of volume V that is partitioned into two disjoint regions: a phase 1 region $\mathcal{V}_1(\omega)$ of volume fraction ϕ_1 and a phase 2 region $\mathcal{V}_2(\omega)$ of volume fraction ϕ_2 such

that $\mathcal{V} = \mathcal{V}_1 \cup \mathcal{V}_2$ for some realization ω of an underlying probability space [115]. The statistical properties of each phase of the system are specified by the countably infinite set of n -point probability functions $S_n^{(i)}$, which are defined by [115,125,130,131]:

$$S_n^{(i)}(\mathbf{x}_1, \dots, \mathbf{x}_n) = \left\langle \prod_{i=1}^n \mathcal{I}^{(i)}(\mathbf{x}_i; \omega) \right\rangle, \quad (30)$$

where angular brackets denote an ensemble average and $\mathcal{I}^{(i)}(\mathbf{x}; \omega)$ is the indicator function for phase i defined by

$$\mathcal{I}^{(i)}(\mathbf{x}; \omega) = \begin{cases} 1, & \mathbf{x} \in \text{phase } i \\ 0, & \text{otherwise.} \end{cases} \quad (31)$$

The n -point probability function $S_n^{(i)}(\mathbf{x}_1, \dots, \mathbf{x}_n)$ gives the probability of finding the vectors $\mathbf{x}_1, \dots, \mathbf{x}_n$ all in phase i . If the medium is statistically homogeneous, $S_n^{(i)}(\mathbf{x}_1, \dots, \mathbf{x}_n)$ is translationally invariant and, in particular, the one-point probability function is independent of position and equal to the volume fraction of phase i :

$$S_1^{(i)}(\mathbf{x}) = \phi_i, \quad (32)$$

while the two-point probability function $S_2^{(i)}(\mathbf{r})$ depends on the displacement vector $\mathbf{r} \equiv \mathbf{x}_2 - \mathbf{x}_1$. If the medium is also statistically isotropic, then $S_2^{(i)}(\mathbf{r})$ is a radial function (where $r = |\mathbf{r}|$), which gives the probability of finding the end points of a line segment of length r in phase i .

For statistically homogeneous media, the two-point correlation function for phase 2 is simply related to that for phase 1 via the expression $S_2^{(2)}(\mathbf{r}) = S_2^{(1)}(\mathbf{r}) - 2\phi_1 + 1$, and hence the *autocovariance* function is given by

$$\chi_V(\mathbf{r}) \equiv S_2^{(1)}(\mathbf{r}) - \phi_1^2 = S_2^{(2)}(\mathbf{r}) - \phi_2^2, \quad (33)$$

for phase 1 is equal to that for phase 2. Generally, for $\mathbf{r} = 0$,

$$S_2^{(i)}(\mathbf{0}) = \phi_i, \quad \chi_V(\mathbf{0}) = \phi_1\phi_2 \quad (34)$$

and in the absence of any *long-range* order,

$$\lim_{|\mathbf{r}| \rightarrow \infty} S_2^{(i)}(\mathbf{r}) \rightarrow \phi_i^2, \quad \lim_{|\mathbf{r}| \rightarrow \infty} \chi_V(\mathbf{r}) \rightarrow 0. \quad (35)$$

We call the Fourier transform of $\chi_V(\mathbf{r})$,

$$\tilde{\chi}_V(\mathbf{k}) = \int_{\mathbb{R}^d} \chi_V(\mathbf{r}) \exp[-i(\mathbf{k} \cdot \mathbf{r})] d\mathbf{r}, \quad (36)$$

the *spectral density*, which again can be measured in the laboratory from scattering experiments [132,133]. This quantity is the heterogeneous-medium analog of the structure factor $S(\mathbf{k})$ for point configurations [cf. (11)]. In light of the second equality in (34), it immediately follows that the spectral density generally obeys the following sum rule:

$$\frac{1}{(2\pi)^d \phi_1 \phi_2} \int_{\mathbb{R}^d} \tilde{\chi}_V(\mathbf{k}) d\mathbf{k} = 1. \quad (37)$$

A hyperuniform two-phase medium is one in which the spectral density $\tilde{\chi}_V(\mathbf{k})$ tends to zero as the wavenumber $k \equiv |\mathbf{k}|$ tends to zero [32], i.e.,

$$\lim_{|\mathbf{k}| \rightarrow 0} \tilde{\chi}_V(\mathbf{k}) = 0. \quad (38)$$

This hyperuniformity condition together with definition (36) imply that the volume integral of $\chi_V(\mathbf{r})$ over all space vanishes identically, i.e.,

$$\int_{\mathbb{R}^d} \chi_V(\mathbf{r}) d\mathbf{r} = 0, \quad (39)$$

which is a direct-space *sum rule* that a hyperuniform two-phase system must obey. This means that $\chi_V(\mathbf{r})$ cannot be strictly positive and hence must exhibit anticorrelations (i.e., negative correlations) for some values of \mathbf{r} .

3. Local number fluctuations

3.1. Ensemble-average formulation of the number variance

Consider general statistically homogeneous point processes in d -dimensional Euclidean space \mathbb{R}^d . Density fluctuations as measured by the number variance within a window of a given shape is entirely determined by pair statistics and a certain geometric property of the window. Here we provide a derivation of the local number variance formula in the ensemble

setting following Torquato and Stillinger [27]. Consider a d -dimensional observation window Ω of convex shape and let \mathbf{R} symbolize the parameters that characterize its geometry and its fixed orientation with respect to the point process. For example, in the case of a d -dimensional ellipsoidal (hyperellipsoid) or d -dimensional cubical (hypercubic) window, \mathbf{R} would represent the semi-axes of the ellipsoid or side length of the cube, respectively, as well as the window orientation. For statistical anisotropic point processes, it can be judicious to choose a nonspherical window to be consistent with symmetries of the underlying point processes (see Section 13.4) but, often, hyperspherical windows are convenient choices. Let us introduce the window indicator function

$$w(\mathbf{x} - \mathbf{x}_0; \mathbf{R}) = \begin{cases} 1, & \mathbf{x} - \mathbf{x}_0 \in \Omega, \\ 0, & \mathbf{x} - \mathbf{x}_0 \notin \Omega, \end{cases} \quad (40)$$

for a window occupying region $\Omega \subset \mathbb{R}^d$ with centroidal position \mathbf{x}_0 . Let $N(\mathbf{x}_0; \mathbf{R})$ denote the number of points within the window in a realization of the ensemble, which is given explicitly by

$$N(\mathbf{x}_0; \mathbf{R}) = \sum_{i=1}^N w(\mathbf{r}_i - \mathbf{x}_0; \mathbf{R}). \quad (41)$$

The ensemble-average number of points contained within the window in the thermodynamic (infinite-volume) limit is simply

$$\langle N(\mathbf{R}) \rangle = \rho v_1(\mathbf{R}), \quad (42)$$

where

$$v_1(\mathbf{R}) = \int_{\mathbb{R}^d} w(\mathbf{r}; \mathbf{R}) d\mathbf{r} \quad (43)$$

is the window volume. The translational invariance (statistical homogeneity) of the point configuration renders the ensemble average $\langle N(\mathbf{x}_0; \mathbf{R}) \rangle$ independent of the window coordinate \mathbf{x}_0 , and so we suppress it in (42).

Similarly, ensemble averaging the square of $N(\mathbf{x}_0; \mathbf{R})$ and using (42) gives the *local number variance* as

$$\begin{aligned} \sigma_N^2(\mathbf{R}) &\equiv \langle N^2(\mathbf{R}) \rangle - \langle N(\mathbf{R}) \rangle^2 \\ &= \int_{\mathbb{R}^d} \rho_1(\mathbf{r}_1) w(\mathbf{r}_1 - \mathbf{x}_0; \mathbf{R}) d\mathbf{r}_1 + \int_{\mathbb{R}^d} \int_{\mathbb{R}^d} [\rho_2(\mathbf{r}_1, \mathbf{r}_2) - \rho_1(\mathbf{r}_1)\rho_1(\mathbf{r}_2)] w(\mathbf{r}_1 - \mathbf{x}_0; \mathbf{R}) w(\mathbf{r}_2 - \mathbf{x}_0; \mathbf{R}) d\mathbf{r}_1 d\mathbf{r}_2 \end{aligned}$$

where $\rho_1(\mathbf{r})$ and $\rho_2(\mathbf{r}_1, \mathbf{r}_2)$ are the one- and two-particle probability density functions, respectively (see Section 2.1). Invoking statistical homogeneity, leads to the following simple expression for the number variance in terms of the total correlation function $h(\mathbf{r})$ [cf. (4)] that is independent of \mathbf{x}_0 :

$$\sigma_N^2(\mathbf{R}) = \langle N(\mathbf{R}) \rangle \left[1 + \rho \int_{\mathbb{R}^d} h(\mathbf{r}) \alpha_2(\mathbf{r}; \mathbf{R}) d\mathbf{r} \right], \quad (44)$$

where

$$\alpha_2(\mathbf{r}; \mathbf{R}) = \frac{v_2^{\text{int}}(\mathbf{r}; \mathbf{R})}{v_1(\mathbf{R})} \quad (45)$$

is called the *scaled intersection volume* function and

$$v_2^{\text{int}}(\mathbf{r}; \mathbf{R}) = \int_{\mathbb{R}^d} w(\mathbf{x}_0; \mathbf{R}) w(\mathbf{x}_0 + \mathbf{r}; \mathbf{R}) d\mathbf{x}_0 \quad (46)$$

is the intersection volume $v_2^{\text{int}}(\mathbf{r}; \mathbf{R})$ of two windows (with the same orientations) whose centroids are separated by the displacement vector \mathbf{r} . Note that $\alpha_2(\mathbf{r}; \mathbf{R})$ has compact support (non-zero only when two windows overlap) and, by definition, $\alpha_2(\mathbf{r} = \mathbf{0}; \mathbf{R}) = 1$. Formula (44) was also derived by Landau and Lifschitz [3], although they did not explicitly indicate the scaled intersection volume function $\alpha_2(\mathbf{r}; \mathbf{R})$. Martin and Yalcin [134] derived the corresponding formula for charge fluctuations in classical Coulombic systems.

For finite size windows, the integral in (44) will exist for bounded $h(\mathbf{r})$ because $\alpha_2(\mathbf{r}; \mathbf{R})$ has finite support. For infinitely large windows, $\alpha_2(\mathbf{r}; \mathbf{R}) = 1$, and integrability requires that $h(\mathbf{r})$ decays faster than $|\mathbf{r}|^{-d}$. For systems in thermal equilibrium, this will be the case for pure phases away from standard critical points, e.g., liquid–gas and magnetic varieties. The structure factor $S(\mathbf{k})$ [defined by (11)] at $\mathbf{k} = \mathbf{0}$ tends to $+\infty$ as a thermal critical point is approached, implying that $h(\mathbf{r})$ becomes long-ranged with a power-law tail that decays slower than $|\mathbf{r}|^{-d}$ [8–12], which is a manifestation of the underlying fractal structure [11,12]. Such fractal systems can be thought of as *anti-hyperuniform* with *hyperfluctuations*, since they are the antithesis of a hyperuniform system in which $\lim_{|\mathbf{k}| \rightarrow 0} S(\mathbf{k}) = 0$; see Section 5.1 for further discussion.

There is a dual Fourier representation of the local number variance formula [27]. Specifically, using Parseval's theorem for Fourier transforms, formula (44) for an arbitrarily shaped (regular) window can be expressed in terms of the structure

factor [defined by (11)] and the nonnegative function $\tilde{\alpha}_2(\mathbf{k}; \mathbf{R})$, the Fourier transform of $\alpha_2(\mathbf{r}; \mathbf{R})$ [27]:

$$\sigma_N^2(\mathbf{R}) = \langle N(\mathbf{R}) \rangle \left[\frac{1}{(2\pi)^d} \int_{\mathbb{R}^d} S(\mathbf{k}) \tilde{\alpha}_2(\mathbf{k}; \mathbf{R}) d\mathbf{k} \right]. \quad (47)$$

Note that

$$\tilde{\alpha}_2(\mathbf{k}; \mathbf{R}) = \frac{\tilde{w}^2(\mathbf{k}; \mathbf{R})}{v_1(\mathbf{R})} \geq 0, \quad (48)$$

where $\tilde{w}(\mathbf{k}; \mathbf{R})$ is the Fourier transform of the window indicator function (40), and

$$\frac{1}{(2\pi)^d} \int_{\mathbb{R}^d} \tilde{\alpha}_2(\mathbf{k}; \mathbf{R}) d\mathbf{k} = \alpha_2(\mathbf{r} = 0; \mathbf{R}) = 1. \quad (49)$$

It immediately follows from (47) that the number variance is strictly positive whenever $v_1(\mathbf{R}) > 0$ [27].

3.1.1. Hyperspherical windows

Many of the subsequent results will be given for the case of a d -dimensional spherical (hyperspherical) window of radius R centered at position \mathbf{x}_0 . The general window indicator function (40) becomes $w(\mathbf{x} - \mathbf{x}_0; R) = \Theta(R - |\mathbf{x} - \mathbf{x}_0|)$, where $\Theta(x)$ is the Heaviside step function

$$\Theta(x) = \begin{cases} 0, & x < 0, \\ 1, & x \geq 0. \end{cases} \quad (50)$$

Thus, the function $v_1(\mathbf{R})$, defined by (43), becomes the volume of a d -dimensional spherical window of radius R :

$$v_1(R) = \frac{\pi^{d/2}}{\Gamma(1 + d/2)} R^d. \quad (51)$$

The scaled intersection volume $\alpha_2(r; R)$, which has support in the interval $[0, 2R]$ in the range $[0, 1]$, has the following integral representation in any dimension:

$$\alpha_2(r; R) = c(d) \int_0^{\cos^{-1}[r/(2R)]} \sin^d(\theta) d\theta, \quad (52)$$

where $c(d)$ is the d -dimensional constant given by

$$c(d) = \frac{2\Gamma(1 + d/2)}{\pi^{1/2} \Gamma[(d + 1)/2]}. \quad (53)$$

Torquato and Stillinger [128] found the following series representation of $\alpha_2(r; R)$ for $r \leq 2R$ and for any d :

$$\alpha_2(r; R) = 1 - c(d)x + c(d) \sum_{n=2}^{\infty} (-1)^n \frac{(d-1)(d-3)\cdots(d-2n+3)}{(2n-1)[2 \cdot 4 \cdot 6 \cdots (2n-2)]} x^{2n-1}, \quad (54)$$

where $x = r/(2R)$. For even dimensions, relation (54) is an infinite series because it involves transcendental functions, but for odd dimensions, it truncates such that $\alpha_2(r; R)$ is a univariate polynomial of degree d . For example, for the first three dimensions, the scaled intersection volumes are respectively given by

$$\alpha_2(r; R) = \left[1 - \frac{r}{2R} \right] \Theta(2R - r) \quad (d = 1), \quad (55)$$

$$\alpha_2(r; R) = \frac{2}{\pi} \left[\cos^{-1} \left(\frac{r}{2R} \right) - \frac{r}{2R} \left(1 - \frac{r^2}{4R^2} \right)^{1/2} \right] \Theta(2R - r) \quad (d = 2), \quad (56)$$

$$\alpha_2(r; R) = \left[1 - \frac{3}{4} \frac{r}{R} + \frac{1}{16} \left(\frac{r}{R} \right)^3 \right] \Theta(2R - r) \quad (d = 3). \quad (57)$$

The Fourier transform of $\alpha_2(r; R)$ is given by

$$\tilde{\alpha}_2(k; R) = 2^d \pi^{d/2} \Gamma(1 + d/2) \frac{[J_{d/2}(kR)]^2}{k^d}. \quad (58)$$

The left panel of Fig. 12 shows plots of $\alpha_2(r; R)$ as a function of r for the first five space dimensions. For any space dimension, $\alpha_2(r; R)$ is a monotonically decreasing function of r . At a fixed value of r in the interval $(0, 2R)$, $\alpha_2(r; R)$ is a monotonically decreasing function of the dimension d . The right panel of Fig. 12 depicts corresponding plots of the normalized Fourier transform of the scaled intersection volume, $\tilde{\alpha}_2(k; R)/R^d$, as a function of the wavenumber. For any d , this is always a nonnegative decaying oscillating function of k .

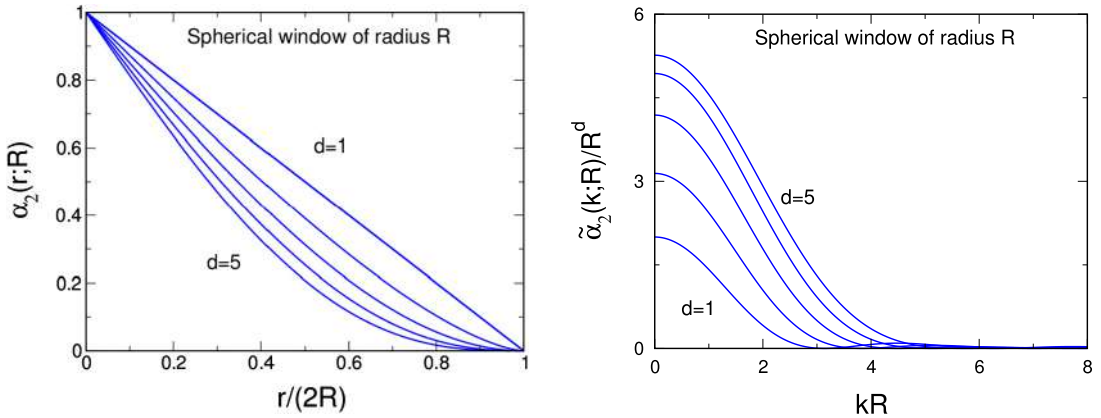


Fig. 12. Left panel: The scaled intersection volume $\alpha_2(r; R)$ for spherical windows of radius R as a function of r for the first five space dimensions, the uppermost curve corresponding to $d = 1$. Right panel: The corresponding Fourier transform normalized by R^d , $\tilde{\alpha}_2(k; R)/R^d$, as a function of k , the uppermost curve corresponding to $d = 5$.

For statistically homogeneous and isotropic point processes, the two-point statistical descriptors in both direct and Fourier spaces, $h(\mathbf{r})$ and $S(\mathbf{k})$, become radial functions, and hence for hyperspherical windows, the number-variance formulas (44) and (47) simplify as follows:

$$\sigma_N^2(R) = \rho v_1(R) \left[1 + \rho s_1(1) \int_0^\infty r^{d-1} h(r) \alpha_2(r; R) dr \right] \quad (59)$$

$$= \rho v_1(R) \left[\frac{s_1(1)}{(2\pi)^d} \int_0^\infty k^{d-1} S(k) \tilde{\alpha}_2(k; R) dk \right], \quad (60)$$

where $s_1(r)$ is the surface area of a d -dimensional sphere of radius r [cf. (6)], and $\alpha_2(r; R)$ and $\tilde{\alpha}_2(k; R)$ are given by (52) and (58), respectively. Importantly, these relations are also applicable for periodic or quasiperiodic structure when the pair statistics are appropriately averaged over angles. After integration by parts, relation (60) leads to an alternative representation of the number variance [33]:

$$\sigma_N^2(R) = -\frac{\rho v_1(R)}{(2\pi)^d} \int_0^\infty Z(k) \frac{\partial \tilde{\alpha}_2(k; R)}{\partial k} dk, \quad (61)$$

where

$$Z(k) = s_1(1) \int_0^k S(q) q^{d-1} dq \quad (62)$$

is the *integrated* or *cumulative* intensity function within a sphere of radius k of the origin in reciprocal space. The function $Z(k)$ has advantages over the structure factor $S(k)$ in the characterization of the hyperuniformity of quasicrystals and other point processes with dense Bragg peaks [33].

3.2. Number variance for a single point configuration

Following Torquato and Stillinger [27], here we consider the local number variance of a single point configuration consisting of a large number of points N in a large region of \mathbb{R}^d of volume V , which is necessarily a volume-average formulation. Fluctuations for a fixed window size arise because we let the window uniformly sample the space. Since one is always concerned with infinite-point configurations in \mathbb{R}^d , we ultimately take the thermodynamic limit. However, even in this limit, the volume-average formulation can lead to different results from those obtained in the ensemble-average formulation when the system is *non-ergodic*. Thus, strictly speaking, the corresponding variances should be notationally distinguished (e.g., Ref. [27] designates the volume-average variance as $\overline{N^2(R)} - \overline{N(R)}^2$). For simplicity, we will henceforth invoke ergodicity, enabling us to equate volume-averages with ensemble averages, and hence continue to designate $\sigma_N^2(R)$ to be the number variance. We consider a d -dimensional spherical window of radius R , keeping in mind that the results below apply as well (with obvious notational changes) to convex windows of arbitrary shape. Invoking ergodicity, the local number variance for a single infinite configuration is given by

$$\sigma_N^2(R) = \rho v_1(R) \left[1 - \rho v_1(R) + \frac{1}{N} \sum_{i \neq j} \alpha_2(r_{ij}; R) \right]. \quad (63)$$

Observe that the last term within the brackets is a pairwise sum, the summand of which is exactly zero for $r_{ij} > 2R$, even for infinitely large systems.

The scaled intersection volume $\alpha_2(r_{ij}; R)$ appearing in (63) is a nonnegative monotonically decreasing function of r_{ij} with compact support (see Fig. 12) and hence can be viewed as a *repulsive* pair potential between a point i and a point j . It is noteworthy that finding the global minimum of $\sigma_N^2(R)$ is equivalent to determining the ground state for the pair potential function $\alpha_2(r; R)$ [27]. More generally, one could devise an optimization scheme in which a *targeted* value of the variance (rather than an extremal value) is sought.

3.3. Number variance for a single periodic point configurations

For periodic point configurations, Fourier analysis leads to an alternative representation of the local number variance. We begin by sketching the derivation for the case of a (Bravais) lattice Λ in \mathbb{R}^d and consider a d -dimensional spherical window of radius R [27,135]. For this situation the number of points $N(\mathbf{x}_0; R)$ within a window centered at \mathbf{x}_0 [cf. (41)] within a fundamental cell F of volume v_F is clearly a periodic function of the window position \mathbf{x}_0 and thus it can be expanded in a Fourier series as

$$N(\mathbf{x}_0; R) = \rho v_1(R) + \sum_{\mathbf{q} \neq \mathbf{0}} a(\mathbf{q}) e^{i\mathbf{q} \cdot \mathbf{x}_0} \quad (64)$$

where \mathbf{q} represents the reciprocal lattice vectors that specifies the dual lattice Λ^* , defined in Section 2.2, and

$$a(\mathbf{q}) = \frac{1}{v_F} \left(\frac{2\pi}{|\mathbf{q}|R} \right)^{d/2} R^d J_{d/2}(|\mathbf{q}|R) \quad (65)$$

are the corresponding Fourier coefficients. The number variance $\sigma_N^2(R)$ is obtained by uniformly sampling the centroid of the window over the fundamental cell and hence is defined as follows:

$$\sigma_N^2(R) \equiv \frac{1}{v_F} \int_F [N(\mathbf{x}_0; R) - \rho v_1(R)]^2 d\mathbf{x}_0. \quad (66)$$

Application of Parseval's theorem for Fourier series to the right-hand side of this equation [27] yields

$$\sigma_N^2(R) = \sum_{\mathbf{q} \neq \mathbf{0}} a^2(\mathbf{q}) = \frac{R^d}{v_F^2} \sum_{\mathbf{q} \neq \mathbf{0}} \left(\frac{2\pi}{|\mathbf{q}|} \right)^d J_{d/2}^2(|\mathbf{q}|R). \quad (67)$$

Since the summand in the infinite sum (67) is nonnegative, any corresponding partial sum yields a lower bound on $\sigma_N^2(R)$. In one dimension, the integer lattice \mathbb{Z} is the unique lattice, and from (67) it follows that its number variance takes the simple form

$$\sigma_N^2(R) = \frac{2}{\pi^2} \sum_{m=1}^{\infty} \frac{\sin^2(2\pi mR/D)}{m^2}, \quad (68)$$

where $D = v_F$ is the lattice spacing. This integer-lattice variance is a bounded periodic function with period $D/2$ and is equal to the quadratic function $2x(1 - 2x)$ for $0 \leq x \leq 1/2$, where $x = R/D$ (see the left panel of Fig. 13).

The generalization of the variance formula (67) for a lattice to a periodic point configuration (crystal) in \mathbb{R}^d in which there are M points (where $M \geq 1$) at position vectors $\mathbf{r}_1, \mathbf{r}_2, \dots, \mathbf{r}_M$ within a fundamental cell F of a lattice Λ is straightforward [27]. We simply state this expression for such a d -dimensional crystal:

$$\sigma_N^2(R) = \frac{R^d}{v_F^2} \sum_{\mathbf{q} \neq \mathbf{0}} \left(\frac{2\pi}{|\mathbf{q}|} \right)^d J_{d/2}^2(|\mathbf{q}|R) \left[M + 2 \sum_{j < k}^M \cos[\mathbf{q} \cdot (\mathbf{r}_k - \mathbf{r}_j)] \right], \quad (69)$$

where again \mathbf{q} denotes the reciprocal lattice vectors of the dual lattice Λ^* . In the special case of one dimension with a fundamental cell of length D , this formula reduces to relation (87) of Torquato and Stillinger [27]:

$$\sigma_N^2(R) = \frac{2}{\pi^2} \sum_{m=1}^{\infty} \frac{\sin^2(2\pi mR/D)}{m^2} \left[M + 2 \sum_{j < k}^M \cos[2\pi m(r_k - r_j)/D] \right], \quad (70)$$

where, without loss of generality, the particle positions are ordered such that $r_j \leq r_{j+1}$ ($j = 1, 2, \dots, M - 1$). In the corresponding expression given in Ref. [27] [Eq. (85)], one of the points is chosen to be at the origin, resulting in two sums, both of which are missing a factor of 2. The right panel of Fig. 13 shows the number variance $\sigma_N^2(R)$ of a one-dimensional crystal with a two-particle basis in which $M = 2$ and $r_2 - r_1 = D/4$. Again, we see that the variance is a bounded function, as it must be for any one-dimensional periodic point pattern (crystal).

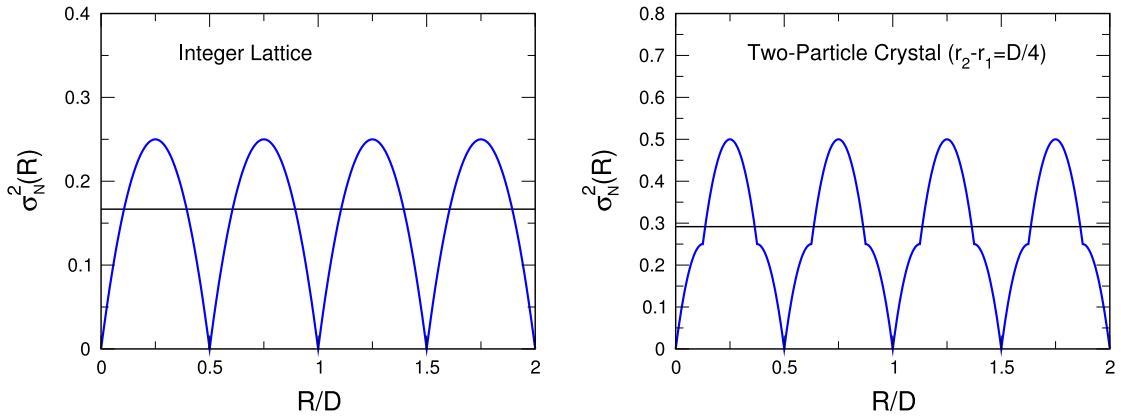


Fig. 13. Left panel: The quadratic periodic variance function $\sigma_n^2(R)$ for the one-dimensional integer lattice given by (68), where D is the length of the fundamental cell. The horizontal line is the average $\bar{\lambda} = 1/6$, as predicted by (115). Right panel: The piecewise-quadratic periodic variance function $\sigma_n^2(R)$ for the one-dimensional two-particle crystal for the case $r_2 - r_1 = D/4$, as predicted by (70). The horizontal line is the average $\bar{\lambda} = 7/24$, as predicted by (115).

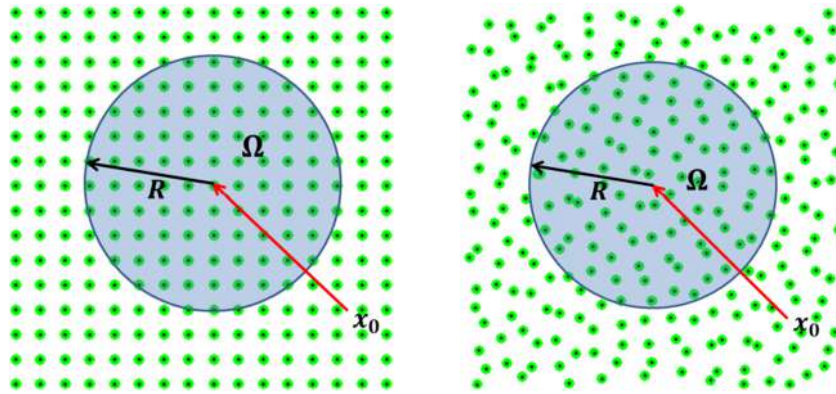


Fig. 14. Schematics indicating an observation window Ω for a periodic heterogeneous medium (left) and disordered hyperuniform heterogeneous medium (right) obtained by decorating the point patterns shown in the middle and right panels of Fig. 4, respectively, with nonoverlapping circular disks.

4. Local volume-fraction fluctuations in two-phase media

As noted earlier, a heterogeneous medium is a spatial set that can be regarded to be more general than a point configuration; see Section 2.3. Of particular interest to us is local volume-fraction fluctuations in two-phase heterogeneous media [117–120] and the generalization of hyperuniformity in this more general context [32]. An explicit formula for the former in terms of the relevant two-point descriptor was derived by Lu and Torquato [118]. Here we briefly review the derivation of this fluctuation formula.

While the global volume fraction, defined by (32), is a fixed constant for a homogeneous two-phase medium, the volume fraction within an observation window $\Omega \subset \mathcal{V}$ fluctuates as the window samples the space. For simplicity, we consider a d -dimensional spherical window of radius R in two-phase media; see Fig. 14. The associated *local volume fraction* $\tau_i(\mathbf{x}_0; R)$ of phase i within a window of radius R centered at position \mathbf{x}_0 is specified explicitly by

$$\tau_i(\mathbf{x}_0; R) = \frac{1}{v_1(R)} \int \mathcal{I}^{(i)}(\mathbf{x}) w(\mathbf{x} - \mathbf{x}_0; R) d\mathbf{x}, \quad (71)$$

where $v_1(R)$ is the window volume, $\mathcal{I}^{(i)}(\mathbf{x})$ is the phase indicator function defined by (45), and w is the corresponding window indicator function defined by (40). The variance $\sigma_v^2(R)$ in the local volume fraction is defined by

$$\sigma_v^2(R) \equiv \langle \tau_i^2(\mathbf{x}; R) \rangle - \phi_i^2, \quad (72)$$

which trivially related to the so-called *coarseness* [118].

Following Ref. [118], it is straightforward to show that the volume-fraction variance can be expressed in terms of the autocovariance function $\chi_v(\mathbf{r})$, defined by (33), as follows:

$$\sigma_v^2(R) = \frac{1}{v_1(R)} \int_{\mathbb{R}^d} \chi_v(\mathbf{r}) \alpha_2(r; R) d\mathbf{r}, \quad (73)$$

where $\alpha_2(r; R)$ is the scaled intersection volume defined by (52). The alternative Fourier representation that is dual to (73) is trivially obtained by applying Parseval's theorem to (73):

$$\sigma_v^2(R) = \frac{1}{v_1(R)(2\pi)^d} \int_{\mathbb{R}^d} \tilde{\chi}_v(\mathbf{k}) \tilde{\alpha}_2(k; R) d\mathbf{k}. \quad (74)$$

It should not go unnoticed that the local volume-fraction formulas (73) and (74) are functionally very similar to the number-variance formulas (44) and (47) for point configurations, respectively; the integrands involve the scaled intersection volume function α_2 multiplied by the relevant two-point statistical descriptors for each case.

5. Mathematical foundations of hyperuniformity: Point configurations

This section is concerned with the mathematical foundations of hyperuniformity for point configurations. We discuss hyperuniformity conditions for general point processes, asymptotic behaviors of the number variance and scaling behavior of pair statistics in both direct and Fourier spaces, the three possible hyperuniformity classes, hyperuniformity order metrics, and effect of window shape on the number variance.

5.1. Vanishing of normalized infinite-wavelength number fluctuations

Consider the Fourier-representation of the number variance (47) for a general point process in \mathbb{R}^d . Let the window grow infinitely large in a self-similar (i.e., shape- and orientation-preserving) fashion. In this limit, which we will denote simply by $v_1(\mathbf{R}) \rightarrow \infty$, the function $\tilde{\alpha}_2(\mathbf{k}; \mathbf{R})$ appearing in (47) tends to $(2\pi)^d \delta(\mathbf{k})$, where $\delta(\mathbf{k})$ is a d -dimensional Dirac delta function. For a large class of point configurations and window shapes (spherical and nonspherical), application of this limiting result and dividing the variance (47) by $\langle N(\mathbf{R}) \rangle = \rho v_1(\mathbf{R})$ yields

$$\lim_{v_1(\mathbf{R}) \rightarrow \infty} \frac{\sigma_N^2(\mathbf{R})}{\langle N(\mathbf{R}) \rangle} = \lim_{|\mathbf{k}| \rightarrow 0} S(\mathbf{k}) = 1 + \rho \int_{\mathbb{R}^d} h(\mathbf{r}) d\mathbf{r}. \quad (75)$$

Observe that the general variance formula (75) and the hyperuniformity requirement $\lim_{|\mathbf{k}| \rightarrow 0} S(\mathbf{k}) = 0$, defined by (14), then dictate that

$$\lim_{v_1(\mathbf{R}) \rightarrow \infty} \frac{\sigma_N^2(\mathbf{R})}{v_1(\mathbf{R})} = 0, \quad (76)$$

implying that the variance for a hyperuniform system grows more slowly than the window volume. This direct-space hyperuniformity condition provides the justification for the description of relation (1). In other words, formula (76) states that hyperuniform point processes have vanishing *normalized* density fluctuations at large length scales, where the normalization factor $v_1(\mathbf{R})$ is proportional to the asymptotic number variance of a typical disordered system (e.g., Poisson point process or standard liquid state). In the instance of spherical windows of radius R , condition (76) signifies that the number variance $\sigma_N^2(R)$ must grow slower than the window volume, i.e., R^d , for large R . In the case of lattices and special window shapes and orientations, the direct-space hyperuniformity condition (75) may not apply. Such subtle anomalous situations are described in Section 5.7.

In the case of hyperspherical windows of radius R , *nonhyperuniform* systems possess a normalized variance $\sigma_N^2(R)/v_1(R)$ that does not vanish in the limit $R \rightarrow \infty$ such that for large R

$$\frac{\sigma_N^2(R)}{v_1(R)} = f(R), \quad (77)$$

where $f(R)$ is some positive system-dependent function of R . For typical disordered nonhyperuniform systems (e.g., Poisson point processes, liquids and glasses), $f(R)$ tends to a system-dependent constant. However, for systems in which $S(\mathbf{k})$ becomes unbounded in the limit $|\mathbf{k}| \rightarrow 0$, $f(R)$ tends to an increasing function of R , and thus can be thought of as *anti-hyperuniform* with *hyperfluctuations*, since they are the antithesis of a hyperuniform system. Examples of such systems include those at thermal critical points [7–12], all of which have *fractal* structures. Point processes derived from certain Poisson hyperplane tessellations for $d \geq 2$ represent a class of hyperfluctuating systems in which it can be rigorously shown that the number variance grows like R^{2d-1} [136,137]; see also Ref. [138] for related heuristically derived hyperfluctuating scalings.

5.2. Distinctions between equilibrium and nonequilibrium infinite-wavelength density fluctuations

Let us now recall the well-known *fluctuation–compressibility theorem* that links the isothermal compressibility of equilibrium single-component many-particle ensembles at number density ρ and temperature T to infinite-wavelength density fluctuations [6]. In particular, for “open” systems in equilibrium, one has

$$\rho k_B T \kappa_T = \frac{\langle N^2 \rangle_* - \langle N \rangle_*^2}{\langle N \rangle_*} = S(\mathbf{k} = \mathbf{0}) = 1 + \rho \int_{\mathbb{R}^d} h(\mathbf{r}) d\mathbf{r}, \quad (78)$$

where k_B is Boltzmann’s constant, $\langle \rangle_*$ denotes an average in the grand canonical ensemble, and N is the fluctuating number of particles in the system due to equality of the chemical potential with a particle reservoir. Observe that the form of the scaled variance (75) in the infinite-wavelength limit is identical to that for equilibrium systems in the infinite-system limit, as given by relation (78). The important distinction is that result (75) is derived by considering fluctuations that arise from moving an asymptotically large window from point to point in infinite, “closed” generally *nonequilibrium* systems. Sampling density fluctuations associated with such asymptotically large windows can be viewed as ensembles of very large “open” systems. On the other hand, the “window” in the grand canonical ensemble is the infinite system itself and hence the density fluctuations described in (78) arise from density variations in the equilibrium ensemble members. We again stress that (75) is valid whether the system is in equilibrium or not. When the system is out of equilibrium, then of course, the global density fluctuations cannot be linked to the isothermal compressibility, as in the fluctuation–compressibility relation (78).

Importantly, conditions under which equilibrium systems are hyperuniform can be derived from this fluctuation–compressibility theorem (78). For example, any ground state ($T = 0$) in which the isothermal compressibility κ_T is bounded and positive must be hyperuniform because the structure factor $S(\mathbf{k} = \mathbf{0})$ must be zero according to relation (78). This includes crystal ground states as well as exotic disordered ground states, such as stealthy ones [36,38,40] discussed in Section 8. More generally, we infer from (78) that if the product $T \kappa_T$ tends to a nonnegative constant c in the limit $T \rightarrow 0$, then the ground-state of this system in this zero-temperature limit must be nonhyperuniform if $c > 0$ or hyperuniform if $c = 0$. By the same token, this means that increasing the temperature by an arbitrarily small positive amount when a system is initially at hyperuniform ground state will destroy perfect hyperuniformity, since $S(\mathbf{k} = \mathbf{0})$ must deviate from zero by some small amount determined by the temperature dependence of the product $\kappa_T T$ for small T . This indirectly implies that phonons or vibrational modes for sufficiently small T generally destroy the hyperuniformity of ground states [40], as detailed in Section 8.4.6. Moreover, in order to have a hyperuniform system that is in equilibrium at any positive T , the isothermal compressibility must be zero, i.e., the system must be thermodynamically incompressible [139]; see Refs. [27,34] and [72] as well as Sections 9 and 10.3 for some examples.

Since supercooled liquids and glasses are systems out of equilibrium, the fluctuation–compressibility relation (78) is generally not satisfied. This motivated Hopkins, Stillinger and Torquato [50] to introduce and apply the *nonequilibrium index* X defined to be

$$X \equiv \frac{S(\mathbf{k} = \mathbf{0})}{\rho k_B T \kappa_T} - 1. \quad (79)$$

Nonzero values of this index quantifies the degree to which a system under study deviates from thermal equilibrium ($X = 0$). This index has been applied to study nonequilibrium hard-sphere packings [50], well-known atomic models of glasses [107], and “perfect” glasses [72].

5.3. Asymptotics via ensemble-average formulation and three hyperuniformity classes

The local number variance $\sigma_N^2(R)$ is generally a function that can be decomposed into a global part that grows with the window radius R and a local part that oscillates on small length scale (e.g., mean nearest-neighbor distance) about the global contribution; see Fig. 2. Using the ensemble-average formulation, we will analyze the large- R asymptotic behavior of the variance $\sigma_N^2(R)$ for a d -dimensional spherical window of radius R associated with general hyperuniform systems, which includes perfect periodic, perfect quasiperiodic and special disordered point configurations. Nonspherical windows will be briefly considered in Section 5.7.

Using either of the ensemble-average representations (59) or (60) of $\sigma_N^2(R)$, it is straightforward to show that the global asymptotic growth rate is determined by the large-distance behavior of the total correlation function $h(\mathbf{r})$ [cf. (4)] or, equivalently, by the small-wavenumber behavior of the structure factor $S(\mathbf{k})$, respectively. We show that the asymptotic growth behaviors of $\sigma_N^2(R)$ fall into three distinct classes: class I in which the growth is proportional to the window surface area R^{d-1} , class II in which the growth is proportional to $\ln(R) R^{d-1}$, and class III in which the growth is proportional to $R^{d-\alpha}$, where $\alpha \in (0, 1)$ is an exponent. Since the variance cannot grow more slowly than R^{d-1} for a spherical window [140], class I embodies the *strongest* form of hyperuniformity. By contrast, systems that fall in class III in which α tends to zero represent the *weakest* form of hyperuniformity.

In what follows, we denote by D a characteristic “microscopic” length scale of the system. It is useful to introduce the dimensionless density ϕ defined by

$$\phi = \rho v_1(D/2) = \rho \frac{\pi^{d/2}}{2^d \Gamma(1 + d/2)} D^d. \quad (80)$$

In some cases, it is convenient to take D to be the mean nearest-neighbor distance between the points. If the point configuration is derived from a packing of identical nonoverlapping spheres of diameter D or if the minimum pair distance in a point process is D , ϕ is simply the fraction of space covered by nonoverlapping spheres of diameter D . In other instances, it may be useful to choose $D = \rho^{-1/d}$, which is equivalent to setting the number density to be unity (i.e., $\rho = 1$). This choice will be convenient when comparing the number variances for different systems.

5.3.1. Asymptotics of the number variance

Direct substitution of the expansion (54) of $\alpha_2(r; R)$ into the ensemble-average expression (59), and assuming that the resulting integrals separately converge, yields the following asymptotic formula for the variance:

$$\sigma_N^2(R) = 2^d \phi \left[A_N(R) \left(\frac{R}{D} \right)^d + B_N(R) \left(\frac{R}{D} \right)^{d-1} + o\left(\frac{R}{D}\right)^{d-1} \right] \quad (R \rightarrow \infty), \quad (81)$$

where $o(x)$ signifies all terms of order less than x , D is a characteristic microscopic length mentioned above, and $A_N(R)$ and $B_N(R)$ are, respectively, d -dependent asymptotic coefficients that multiply terms proportional to the window volume (R^d) and window surface area (R^{d-1}). The “volume” and “surface-area” coefficients are explicitly given by the following the volume integrals involving the total correlation function $h(\mathbf{r})$, respectively:

$$A_N(R) = 1 + \rho \int_{|\mathbf{r}| \leq 2R} h(\mathbf{r}) d\mathbf{r} = 1 + \frac{\phi}{v_1(D/2)} \int_{|\mathbf{r}| \leq 2R} h(\mathbf{r}) d\mathbf{r} \quad (82)$$

and

$$B_N(R) = -\frac{\phi c(d)}{2D v_1(D/2)} \int_{|\mathbf{r}| \leq 2R} h(\mathbf{r}) |\mathbf{r}| d\mathbf{r}, \quad (83)$$

where $c(d)$ is a d -dependent constant defined by (53). The restriction on the integration domains to be a spherical region of radius $2R$ is imposed by the finite support of the scaled intersection volume (52) and hence results in volume and surface-area coefficients that generally depend on R . The asymptotic formula (81) is more general than the one presented in Ref. [27] in that it allows for coefficients A_N and B_N that depend on R without any assumptions about their convergence properties.

Observe that the volume coefficient $A_N(R)$ in the limit $R \rightarrow \infty$ is equal to the nonnegative structure factor $S(\mathbf{k})$ [cf. (11)] in the zero-wavenumber limit i.e.,

$$\bar{A}_N \equiv \lim_{R \rightarrow \infty} A_N(R) = \lim_{|\mathbf{k}| \rightarrow 0} S(\mathbf{k}) \geq 0. \quad (84)$$

We call \bar{A}_N the *global* volume coefficient. It is well known that disordered point configurations associated with equilibrium molecular systems with a wide class of interaction potentials (e.g., hard-sphere, square-well, and Lennard-Jones interactions) yield positive values of the coefficient \bar{A}_N in gaseous, liquid, and many solid states. Indeed, \bar{A}_N will be positive for any equilibrium system possessing a positive compressibility at positive temperatures; see fluctuation–compressibility theorem (78). The coefficient \bar{A}_N is positive for a wide class of nonequilibrium disordered point configurations, including the random sequential addition (RSA) packing process [77,78]. Anti-hyperuniform systems (e.g., standard thermal critical-point states) are at the extreme end of nonhyperuniformity in which \bar{A}_N is infinitely large. To summarize, there is an enormous class of disordered point configurations in which \bar{A}_N is strictly positive and hence nonhyperuniform; indeed, this is typically true.

According to relations (14) and (15), a hyperuniform system is one in which the volume coefficient vanishes in the limit $R \rightarrow \infty$, i.e.,

$$\bar{A}_N = \lim_{|\mathbf{k}| \rightarrow 0} S(\mathbf{k}) = 0. \quad (85)$$

A *class I* hyperuniform system is one in which the surface-area coefficient $B_N(R)$ converges to a constant in the limit $R \rightarrow \infty$ and hence, according to relation (81), $\sigma_N^2(R)$ grows like the window surface area, as specified by

$$\sigma_N^2(R) \sim 2^d \phi \bar{B}_N \left(\frac{R}{D} \right)^{d-1} \quad (R \rightarrow \infty), \quad (86)$$

where

$$\bar{B}_N = \lim_{R \rightarrow \infty} B_N(R) = -\frac{\phi d \Gamma(d/2)}{2D v_1(D/2) \Gamma(\frac{d+1}{2}) \Gamma(\frac{1}{2})} \int_{\mathbb{R}^d} h(\mathbf{r}) |\mathbf{r}| d\mathbf{r} \quad (87)$$

is the *global* surface-area coefficient, which is positive for a hyperuniform system [27]. Class I systems include disordered point configurations in which $h(\mathbf{r})$ decays to zero sufficiently fast for large $|\mathbf{r}|$; for example, exponentially fast or faster (as in g_2 -invariant systems [27] discussed in Section 7.2, one-component plasmas described in Section 10.3 and Weyl–Heisenberg ensembles mentioned in Section 10.4 [141]) or faster than the power-law $1/|\mathbf{r}|^{d+1}$, as in some stealthy hyperuniform disordered systems [40] discussed in Section 8. Moreover, \bar{B}_N converges for statistically homogeneous point configurations that are derived from a perfect crystal (uniform translations of the entire crystal over the fundamental cell) and a large

class of perfect quasicrystals, all of which are characterized by Bragg peaks in reciprocal space, and hence belong to class I hyperuniform systems. In Section 15, we will see that a wide class of “randomly” perturbed crystal structures [138,142–144] also belong to class I. It is notable that the global surface-area coefficient \bar{B}_N provides a measure of the degree to which class I hyperuniform systems suppresses large-scale density fluctuations [27,32], as we detail further below.

For one-dimensional class I hyperuniform systems, the number variance is exactly (not asymptotically) given by

$$\sigma_N^2(R) = 2\phi B_N(R), \quad (88)$$

where $B_N(R)$ is given by (83) with $d = 1$ [27], implying that the fluctuations are bounded, i.e., do not grow with R . Aizenman, Goldstein and Lebowitz [145] proved general conditions under which a one-dimensional system possesses a bounded variance.

If the point process in \mathbb{R}^d (hyperuniform or not) can be characterized by radial total correlation function, i.e., $h(\mathbf{r}) = h(r)$, where $r \equiv |\mathbf{r}|$, the volume coefficient (82) and surface-area coefficient (83) are expressible in terms of certain moments of the radial total correlation function, namely,

$$\bar{A}_N = 1 + d2^d \phi \langle x^{d-1} \rangle, \quad (89)$$

$$\bar{B}_N = -\frac{d^2 2^{d-1} \Gamma(d/2)}{\Gamma(\frac{d+1}{2}) \Gamma(\frac{1}{2})} \phi \langle x^d \rangle, \quad (90)$$

where

$$\langle x^n \rangle = \int_0^\infty x^n h(Dx) dx \quad (91)$$

is the n th moment of $h(x)$ and $x = r/D$ is a dimensionless distance. Clearly, the total correlation function is a radial function for statistically homogeneous and isotropic point processes as well as for periodic point configurations in which one averages displacements between pairs of points over angles; see relation (29). According to the previous analysis, we see that if $\bar{A}_N = 0$, the condition for the variance to grow as the surface area implies that the d th moment of h must be strictly negative [27], i.e.,

$$\langle x^d \rangle < 0. \quad (92)$$

By contrast, point processes in which the global surface-area coefficient vanishes ($\bar{B}_N = 0$) is referred to as a *hyposurficial* system [27]. Thus, hyposurficial systems obey the following sum rule:

$$\int_0^\infty r^d h(r) dr = 0, \quad (93)$$

where $h(r)$ represents the radial total correlation function for a statistically homogeneous and isotropic point process or angular-averaged total correlation function in the case of a statistically anisotropic system. We see that for the integral (93) to converge, $h(r)$ must decay to zero faster than $1/r^{d+1}$ for large r in space dimension d . Since the variance is strictly positive [27] and cannot grow more slowly than the surface area of a spherical window [140], it follows that any such system cannot simultaneously be hyperuniform and hyposurficial, i.e., the volume coefficient \bar{A}_N [cf. (84)] and surface-area coefficient \bar{B}_N [cf. (87)] cannot both be zero. A homogeneous Poisson point configuration is a simple example of a hyposurficial system. A less trivial example of hyposurficial system is a certain hard-core point process in \mathbb{R}^d ; see Ref. [27] for details. It has recently come to light that hyposurficiality arises in non-equilibrium phase transitions involving amorphous ices [146].

Importantly, two other hyperuniform classes are possible if the coefficient $B_N(R)$ converges to a function of R (not a constant) in the limit $R \rightarrow \infty$. For example, if the total correlation function is controlled by the following radial power-law decay:

$$h(\mathbf{r}) \sim \frac{1}{|\mathbf{r}|^{d+1}} \quad (|\mathbf{r}| \rightarrow \infty), \quad (94)$$

a similar asymptotic analysis of (87) leads to a number variance that asymptotically grows like $\sigma_N^2(R) \sim R^{d-1} \ln(R)$, since $B_N(R) \sim \ln(R)$, which we refer to as class II hyperuniform systems. Examples include some quasicrystals [33], classical disordered ground states [37,72], zeros of the Riemann zeta function [34,75], eigenvalues of random matrices [14], fermionic point processes [34], superfluid helium [74,147], maximally random jammed packings [46–51,53,54,121,122], perturbed lattices [142], density fluctuations in early Universe [17,18,148], and perfect glasses [72]. On the other hand,

$$h(\mathbf{r}) \sim \frac{1}{|\mathbf{r}|^{d+\alpha}} \quad (|\mathbf{r}| \rightarrow \infty), \quad (95)$$

yields a number variance that scales like $R^{d-\alpha}$, where $0 < \alpha < 1$, since $B_N(R) \sim R^{1-\alpha}$. We refer to such hyperuniform systems as class III structures. Examples within this class include classical disordered ground states [139], random organization models [62,64], perfect glasses [72], and perturbed lattices [144].

Table 1

Hyperuniform point configurations can exist as both as equilibrium and nonequilibrium phases, and come in both quantum-mechanical and classical varieties. This table provides a summary of model systems that fall into the three hyperuniformity classes based on the use of d -dimensional spherical windows of radius R to sample for the number variance $\sigma_N^2(R)$. Class I embodies the strongest form of hyperuniformity and structures of class III in which α tends to zero represent the weakest form of hyperuniformity.

Class	Models
I: $\sigma_N^2(R) \sim R^{d-1}$	All crystals [27], many quasicrystals [32,33], stealthy and other hyperuniform disordered ground states [36–38,40,72], perturbed lattices [138,142–144,148], g_2 -invariant disordered point processes [27], one-component plasmas [35,149], hard-sphere plasmas [44,45], random organization models [66], perfect glasses [72], and Weyl–Heisenberg ensembles [141].
II: $\sigma_N^2(R) \sim R^{d-1} \ln(R)$	Some quasicrystals [33], classical disordered ground states [37,72], zeros of the Riemann zeta function [34,75], eigenvalues of random matrices [14], fermionic point processes [34], superfluid helium [74,147], maximally random jammed packings [46,48,49,51,53], perturbed lattices [142], Density fluctuations in early Universe [17,18,148], and perfect glasses [72].
III: $\sigma_N^2(R) \sim R^{d-\alpha}$ ($0 < \alpha < 1$)	Classical disordered ground states [139], random organization models [62,64], perfect glasses [72], and perturbed lattices [144].

5.3.2. Asymptotics from power-law structure factors

Let us consider hyperuniform systems that are characterized by a structure factor with a radial power-law form in the vicinity of the origin [27,32,46]:

$$S(\mathbf{k}) \sim |\mathbf{k}|^\alpha \quad (|\mathbf{k}| \rightarrow 0) \quad (96)$$

with scaling exponent $\alpha > 0$. (Note that it is not possible to construct a hyperuniform system for which $\alpha \leq 0$, since the number variance would then grow at least as fast as the volume of the observation window.) Analysis of the Fourier-representation of the number variance (47) reveals that large- R asymptotic behavior of $\sigma_N^2(R)$ is controlled by the power-law form (96), and depends on the value of the exponent α as follows:

$$\sigma_N^2(R) \sim \begin{cases} R^{d-1}, & \alpha > 1 \quad (\text{CLASS I}) \\ R^{d-1} \ln R, & \alpha = 1 \quad (\text{CLASS II}) \\ R^{d-\alpha}, & 0 < \alpha < 1 \quad (\text{CLASS III}) \end{cases} \quad (97)$$

We see that the scaling regimes in which $\alpha > 1$, $\alpha = 1$ and $0 < \alpha < 1$ correspond to class I, II and III hyperuniform systems, respectively. Table 1 provides a summary of model systems that fall into these three hyperuniformity classes. Almost all of these examples are expounded upon in Sections 7.2 and 8–11.

We stress that the hyperuniform power-law form (96) of the structure factor may or may not imply a power-law decay in the corresponding total correlation function $h(\mathbf{r})$ [cf. (4)] for large $|\mathbf{r}|$. The following are three possible outcomes when $\alpha > 0$:

A. Whenever $S(\mathbf{k})$ is analytic at the origin (i.e., admits a Taylor series and so only involves even integer powers of $|\mathbf{k}|$ through all orders), the exponent α in (96) must be a positive even integer and $h(\mathbf{r})$ must decay to zero exponentially fast (or faster) as $|\mathbf{r}| \rightarrow \infty$, prohibiting a power-law decay of $h(\mathbf{r})$. Such hyperuniform systems are of class I.

B. Whenever $S(\mathbf{k})$ is nonanalytic at the origin (including cases in which α is an odd integer) and sufficiently smooth away from the origin such that it is $\lfloor \alpha \rfloor + \lfloor d/2 \rfloor$ times differentiable, where $\lfloor x \rfloor$ is the floor function (largest integer less than or equal to x), the asymptotic behavior of the total correlation function is given by the following inverse power-law form:

$$\rho h(\mathbf{r}) \sim -\frac{C_1(\alpha, d)}{|\mathbf{r}|^{d+\alpha}} \quad (|\mathbf{r}| \rightarrow \infty), \quad (98)$$

which is sufficiently short-ranged such that its volume integral over all space exists. Here

$$C_1(\alpha, d) = \frac{2^\alpha \Gamma(1 + \alpha/2) \Gamma((d + \alpha)/2) \sin(\pi\alpha/2)}{\pi^{1+d/2}} \quad (99)$$

is a constant that depends on the exponent α and d , and it is assumed that the coefficient multiplying $|\mathbf{k}|^\alpha$ in (96) is unity. Note that the presence of the term $\sin(\pi\alpha/2)$ in (98) requires the exponent α to lie in one of the intervals $(0, 2)$, $(4, 6)$, $(8, 10)$, and so forth, in order for the total correlation function to have the asymptotic power-law form (98). Otherwise, $h(\mathbf{r})$ must decay to zero faster than a power law for sufficiently large $|\mathbf{r}|$. Therefore, positive even-integer values of α are types of “limiting values” that overcome the otherwise dominant $|\mathbf{r}|^{-(d+\alpha)}$ asymptotic scaling of $h(\mathbf{r})$.

This latter case leads to the following natural question: What is the corresponding form of the small-wavenumber structure factor when $h(\mathbf{r})$ is controlled by the power law

$$h(\mathbf{r}) \sim -\frac{1}{|\mathbf{r}|^{d+\alpha}} \quad (|\mathbf{r}| \rightarrow \infty), \quad (100)$$

where α is a positive even integer? In such situations, it is straightforward to show that the corresponding structure factor is no longer a pure power law but contains a multiplicative logarithmic factor, i.e.,

$$S(\mathbf{k}) \sim -|\mathbf{k}|^\alpha \ln(|\mathbf{k}|) \quad (|\mathbf{k}| \rightarrow 0). \quad (101)$$

Nonetheless, it is also easy to demonstrate that this still leads to a number variance that grows like the window surface area R^{d-1} and hence lies within class I hyperuniform systems.

C. Whenever $S(\mathbf{k})$ is nonanalytic at the origin such that it is less than $\lfloor \alpha \rfloor + \lfloor d/2 \rfloor$ times differentiable, the scaling form (96) corresponds to a total correlation function whose large- r behavior is still controlled by the inverse power-law form (98) but modulated by a sinusoidal function of the radial distance r , i.e.,

$$\rho h(\mathbf{r}) \sim -\frac{C_2(\alpha, d)s(r; d)}{|\mathbf{r}|^{d+\alpha}} \quad (|\mathbf{r}| \rightarrow \infty), \quad (102)$$

where $C_2(\alpha, d)$ and $s(r; d)$ are a positive constant and d -dependent sinusoidal function, respectively, whose specific forms depend on the differentiability of the structure factor.

In cases B and C such that α lies in the interval $(0, d)$, we will see in Section 7.1 that the direct correlation function $c(\mathbf{r})$, defined via the Ornstein–Zernike relation, becomes long-ranged in the sense that its volume integral is unbounded. Such behavior is in diametric contrast to standard thermal critical points in which $h(\mathbf{r})$ is long-ranged [7–12], and hence a system at a hyperuniform state has been called an “inverted” critical point [27].

For some infinite point configurations, e.g., lattices, the associated variance oscillates around some global average behavior [27] (see Fig. 2), which may make it difficult to determine smoothly its asymptotic behavior. In such cases, it is advantageous to use the *cumulative moving average* of the variance $\overline{\sigma_N^2}(R)$ [150], defined as

$$\overline{\sigma_N^2}(R) \equiv \frac{1}{R} \int_0^R \sigma_N^2(x) dx, \quad (103)$$

to ascertain the large- R asymptotic behavior of $\sigma_N^2(R)$.

5.4. Asymptotics for a single point configuration

Consider a single infinite hyperuniform point configuration. For large R , the large-scale variations in R will grow as R^{d-1} , and so we have from (63) that [27]

$$\sigma_N^2(R) = \Lambda(R) \left(\frac{R}{D} \right)^{d-1}, \quad (104)$$

where

$$\Lambda(R) = 2^d \phi \left(\frac{R}{D} \right) \left[1 - 2^d \phi \left(\frac{R}{D} \right)^d + \frac{1}{N} \sum_{i \neq j}^N \alpha_2(r_{ij}; R) \right] \quad (105)$$

is the asymptotic “surface-area” function that contains the small-scale variations in R . In the case of class I hyperuniform point configurations, it is useful to average the function $\Lambda(R)$ over R , yielding the constant

$$\overline{\Lambda} = \lim_{L \rightarrow \infty} \frac{1}{L} \int_0^L \Lambda(R) dR. \quad (106)$$

This constant is trivially related to the surface-area coefficient B_N , defined by (83), as follows:

$$\overline{\Lambda} = 2^d \phi B_N = \frac{-2^{d-1} \phi^2 d \Gamma(d/2)}{D v_1(D/2) \Gamma(\frac{d+1}{2}) \Gamma(\frac{1}{2})} \int_{\mathbb{R}^d} h(\mathbf{r}) r d\mathbf{r}. \quad (107)$$

Because the formula for the coefficient $\overline{\Lambda}$ is defined for a single realization, one can employ it to obtain a particular point configuration that minimizes it, i.e.,

$$\min_{\mathcal{C}} \overline{\Lambda}, \quad (108)$$

where \mathcal{C} denotes configuration space.

5.5. Asymptotics for periodic point configurations

All periodic point configurations that have a finite number of particles in the fundamental cell belong to class I hyperuniform systems, as we show below. For a lattice Λ , one easily obtains an asymptotic expression for the variance for large R by replacing the Bessel function in (67) by the dominant term of its asymptotic expansion [27], yielding

$$\sigma_N^2(R) = \Lambda(R) \left(\frac{R}{D} \right)^{d-1} + o \left(\frac{R}{D} \right)^{d-1}, \quad (109)$$

where D is a characteristic microscopic length scale, say a lattice spacing, and the function

$$\Lambda(R) = \frac{2^{d+1}\pi^{d-1}D^{2d}}{v_F^2} \sum_{\mathbf{q} \neq \mathbf{0}} \frac{\cos^2[|\mathbf{q}|R - (d+1)\pi/4]}{(|\mathbf{q}|D)^{d+1}}, \quad (110)$$

describes small-scale variations in R and \mathbf{q} is a reciprocal lattice vector of the dual lattice Λ^* . The function $\Lambda(R)$ is bounded and fluctuates around a constant (see Figs. 13 and 15), implying that lattices belong to class I hyperuniform systems. This constant is equal to the averaged surface-area coefficient $\bar{\Lambda}$ defined by (106) and hence is given by the following convergent sum:

$$\bar{\Lambda} = \frac{2^d\pi^{d-1}D^{2d}}{v_F^2} \sum_{\mathbf{q} \neq \mathbf{0}} \frac{1}{(|\mathbf{q}|D)^{d+1}}. \quad (111)$$

We see that finding the lattice in \mathbb{R}^d that minimizes the constant $\bar{\Lambda}$ is equivalent to finding the dual of the ground-state lattice associated with the inverse power-law pair potential $q^{-(d+1)}$ in reciprocal space in dimension d . Note that for the integer lattice \mathbb{Z} , the number variance $\sigma_N^2(R)$ is exactly equal to the function $\Lambda(R)$, i.e., there are no correction terms in formula (109) beyond the first term.

Remarkably, the averaged surface-area coefficient $\bar{\Lambda}$ is intimately connected to the Epstein zeta function $Z_\Lambda(s)$ of number theory [151]. For a lattice at unit density, this function is defined as follows [151]:

$$Z_\Lambda(s) = \sum_{\mathbf{p} \neq \mathbf{0}} \frac{1}{|\mathbf{p}|^{2s}} \quad (\text{Re}(s) > d/2), \quad (112)$$

where \mathbf{p} is a vector of the lattice Λ . It is clear from (111) that the dual of the lattice that minimizes the Epstein zeta function $Z_\Lambda(s = (d+1)/2)$ among all lattices will minimize the asymptotic coefficient for the number variance among lattices. It is known in two dimensions that the triangular lattice minimizes the Epstein zeta function [151–153] among all lattices, and in three dimensions, the FCC is at least a local minimum among lattices [151,153]. Sarnak and Strömbergsson [151] proved that for dimensions 4, 8, and 24, the densest known lattice packings (checkerboard lattice D_4 , E_8 root lattice and Leech lattice L_{24}) are at least local minima. (Note it was recently proved that the E_8 and L_{24} lattices are the densest packings among all possible packings in dimensions 8 [154] and 24 [155], respectively.) However, it is almost certainly not true in higher dimensions that the minimizers of the Epstein zeta function are lattice structures, since the densest packings are likely to be nonperiodic [128].

For a periodic point pattern in which the fundamental cell contains M points, the asymptotic formula (109) still applies, but where fluctuating surface-area coefficient $\Lambda(R)$ is given by

$$\Lambda(R) = \frac{2^{d+1}\pi^{d-1}D^{2d}}{v_F^2} \sum_{\mathbf{q} \neq \mathbf{0}} \frac{\cos^2[|\mathbf{q}|R - (d+1)\pi/4]}{(|\mathbf{q}|D)^{d+1}} \left[M + 2 \sum_{j < k}^M \cos[\mathbf{q} \cdot (\mathbf{r}_k - \mathbf{r}_j)] \right], \quad (113)$$

which immediately follows from relation (69). The fact that the function $\Lambda(R)$ function is bounded implies that periodic point configurations belong to class I hyperuniform systems. The corresponding global average is given by

$$\bar{\Lambda} = \frac{2^d\pi^{d-1}D^{2d}}{v_F^2} \sum_{\mathbf{q} \neq \mathbf{0}} \frac{1}{(|\mathbf{q}|D)^{d+1}} \left[M + 2 \sum_{j < k}^M \cos[\mathbf{q} \cdot (\mathbf{r}_k - \mathbf{r}_j)] \right]. \quad (114)$$

This expression simplifies considerably for $d = 1$ [27]:

$$\bar{\Lambda} = -\frac{M(M-3)}{12} + \sum_{j < k}^M f(r_k - r_j), \quad (115)$$

where $f(x)$ is the following convex quadratic nonnegative function for $0 \leq x \leq 1/2$:

$$f(x) = \frac{1}{\pi^2} \sum_{m=1}^{\infty} \frac{1 + 2 \cos(2\pi mx)}{m^2} = \frac{1}{2} - 2x(1-x). \quad (116)$$

From formula (115), it is straightforward to prove that the integer lattice \mathbb{Z} yields the global minimum of $\bar{\Lambda} = 1/6$ among all infinite point patterns [27].

One can also evaluate the asymptotic coefficient $\bar{\Lambda}$ for infinite periodic point configurations using the angular-averaged pair correlation function relation (29) and the ensemble-average formula (107), but this is a subtle calculation that must be carried out with care. The integrand can be appropriately modified so that a limiting convergent expression for the

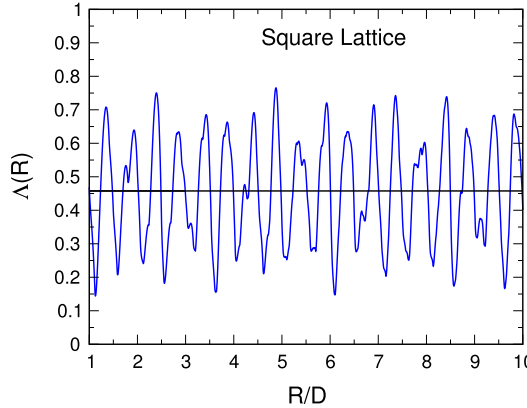


Fig. 15. The asymptotic surface-area function $\Lambda(R)$ for the square lattice for $1 \leq R \leq 10$, where D is the lattice spacing. The horizontal line is the asymptotic average value $\bar{\Lambda} = 0.457649$ [27].

surface-area coefficient emerges as follows [27]:

$$\bar{\Lambda} = \lim_{\gamma \rightarrow 0^+} \frac{2^{d-1} \phi d}{D \Gamma(\frac{1}{2})} \left[\frac{\phi \pi^{d/2}}{v_1(D/2) \gamma^{\frac{d+1}{2}}} - \frac{\Gamma(d/2)}{\Gamma(\frac{d+1}{2})} \sum_{i=1}^{\infty} Z_i r_i e^{-\gamma r_i^2} \right], \quad (117)$$

where Z_i is the *expected* coordination number at a radial distance r_i , as defined in Eq. (29).

5.6. Hyperuniform order metrics

The global surface-area coefficient $\bar{\Lambda}$, which is trivially related to \bar{B}_N , has been shown to provide a useful measure of the degree to which large-scale density fluctuations is suppressed in class I hyperuniform systems [27,32]. Thus, the magnitude of $\bar{\Lambda}$ provides a way to quantitatively distinguish structures among those that belong to the strongest form of hyperuniformity. In order to compare different hyperuniform systems to one another, one must choose a way to normalize $\bar{\Lambda}$ so that it is scale-independent. One choice used in Refs. [27] and [32] is $\bar{\Lambda}|_{D=1}/\phi^{(d-1)/d}$, where $\phi = \rho v_1(1/2)$ is the dimensionless density defined by (80). Another choice that we will employ here is the evaluation of the global surface-area coefficient at unit density, which we denote by $\bar{\Lambda}|_{\rho=1}$. In d -dimensions, the two normalized surface-area coefficients are related by

$$\bar{\Lambda}|_{\rho=1} = (v_1(1/2))^{(d-1)/d} \frac{\bar{\Lambda}|_{D=1}}{\phi^{(d-1)/d}}. \quad (118)$$

By normalizing the asymptotic coefficient $\bar{\Lambda}|_{\rho=1}$ by the corresponding result for the variance-minimizing structure, which we denote by $\bar{\Lambda}_{\min}|_{\rho=1}$, Zachary and Torquato [32] defined a scalar quantity

$$\psi_N = \frac{\bar{\Lambda}_{\min}|_{\rho=1}}{\bar{\Lambda}|_{\rho=1}} \quad (119)$$

that lies between 0 and 1.

Table 2 lists values of the scale-independent surface-area coefficients for various ordered and disordered point processes in one dimension, including point configurations derived from the quasiperiodic Fibonacci chain by taking the endpoints of each segment. It is seen that the integer lattice has the lowest hyperuniformity metric in the list. Indeed, it has been proved that the integer lattice globally minimizes $\bar{\Lambda}|_{\rho=1}$ among all point processes [27]. The step-function g_2 and step+delta-function g_2 are two disordered g_2 -invariant point processes described in Section 7.2. The two-particle crystals refer to periodic system with a 2-particle basis in which $r_2 - r_1 = 1/4$ (see Fig. 13) and $r_2 - r_1 = 2/5$. The “uncorrelated lattice gas” is constructed by tessellating the real line into regular intervals and then a single point is placed in each interval (independently of the others) according to a uniform random distribution, a type of “perturbed lattice” discussed in more detail in Section 15. Notice that the quasiperiodic Fibonacci chain (see Ref. [31] for a definition) has a hyperuniformity order metric that falls between the minimal value for the integer lattice and that of the uncorrelated lattice gas. Interestingly, it has recently been determined that there are some one-dimensional quasicrystals that belong to class II [33].

Table 3 lists values of the scale-independent surface-area coefficient for various ordered and disordered point processes in two dimensions. Rankin [152] proved that the triangular lattice has the smallest normalized surface-area coefficient for circular windows among all two-dimensional lattices, which is borne out in **Table 3**. However, there is no proof that the triangular lattice minimizes $\bar{\Lambda}|_{\rho=1}$ among all infinite two-dimensional hyperuniform point patterns for circular windows.

Table 2

Hyperuniformity order metrics $\overline{A}|_{\rho=1}$, $\overline{A}|_{D=1}$ and ψ_N for selected one-dimensional class I hyperuniform point patterns. Except for the Fibonacci-chain result [32], all of the results are taken from Ref. [27]. In the case of point patterns with a minimal pair separation of D , the dimensionless density represents ϕ the packing fraction.

Pattern	$\overline{A} _{\rho=1}$	$\overline{A} _{D=1}$	ψ_N
\mathbb{Z}	0.16667	0.16667	1.00000
two-particle crystal ($r_2 - r_1 = 2/5$)	0.18666	0.18666	0.89286
step+delta-function g_2	0.18750	0.18750	0.88889
Fibonacci chain	0.20110	0.20110	0.82878
step-function g_2	0.25	0.25	0.66667
two-particle crystal ($r_2 - r_1 = 1/4$)	0.29167	0.29167	0.57143
uncorrelated lattice gas	0.33333	0.33333	0.50000

Table 3

Hyperuniformity order metrics $\overline{A}|_{\rho=1}$, $\overline{A}|_{D=1}/\phi^{1/2}$ and ψ_N for selected two-dimensional class I hyperuniform point patterns [27,32]. In the case of point patterns with a minimal pair separation of D , the dimensionless density ϕ represents the packing fraction. The order metrics for the triangular, square, honeycomb, kagomé, step-function g_2 , step+delta-function g_2 , and one-component plasma structure were obtained Ref. [27], while those for the other structures were determined in Ref. [32].

Pattern	$\overline{A} _{\rho=1}$	$\overline{A} _{D=1}/\phi^{1/2}$	ψ_N
A_2 (triangular)	0.450511	0.50835	1.000000
\mathbb{Z}^2 (square)	0.457648	0.51640	0.98443
disordered stealthy; $\chi = 0.496$	0.46438	0.52400	0.97015
disordered stealthy; $\chi = 0.402$	0.47693	0.53816	0.94463
honeycomb	0.502513	0.56703	0.89652
kagomé	0.520206	0.58699	0.86603
octagonal quasicrystal	0.52790	0.59567	0.85340
step+delta-function g_2	0.531922	0.60021	0.846949
Penrose tiling	0.53220	0.60052	0.84651
Rectangular kagomé	0.54051	0.60990	0.83349
disordered stealthy; $\chi = 0.302$	0.54285	0.61254	0.82990
4.8.8 tessellation	0.620243	0.69987	0.72635
step-function g_2	0.752252	0.84883	0.598883
one-component plasma	1.000000	1.12838	0.45051

Nonetheless, it is expected that the triangular lattice is the global minimizer. Among the limited set of structures listed in this table, the one-component plasma has the largest order metric. The point configurations associated with the two quasicrystal structures, vertices of the Penrose and octagonal tilings, have order-metric values that lie closer to the minimal value than that for the one-component plasma. There are uncountably many distinct quasicrystals that have the same symmetry, same fundamental repeating units (e.g. tiles, clusters of atoms or molecules), and same support for their diffraction patterns, but which have different space-filling arrangements of the repeating units and different peak intensities for their diffraction patterns. These distinct quasicrystals are said to belong to different *local isomorphism* classes [30,31,156]. It has recently come to light that the degree of hyperuniformity in the case of quasicrystals depends on the local isomorphism class [157]. It was specifically shown that within the local isomorphism class the Penrose tiling, all of which belong to class I hyperuniform systems, the minimal order metric is achieved by the Penrose tiling (about 83% smaller than the maximal value in this set) [157].

Table 4 lists values of the scale-independent surface-area coefficients for various ordered and disordered point processes in three dimensions. The previous results for one- and two-dimensional hyperuniform systems might lead one to conjecture that the Bravais lattice associated with the densest packing of congruent spheres in any space dimension d provides the minimal value of $\overline{A}|_{\rho=1}$ for spherical windows. However, in three dimensions, this is definitely not true. The minimum value of $\overline{A}|_{\rho=1}$ in three dimensions appears to be achieved for the BCC lattice, which is the lattice dual to the FCC lattice, corresponding to the densest sphere packing [158]. We see that the global surface-area coefficient for the fcc lattice is very slightly larger than that of the BCC lattice. Based on our remarks earlier about the Epstein zeta function, one can only say that the BCC structure is a local minimum of $\overline{A}|_{\rho=1}$ among (Bravais) lattices. Note that the “tunneled” FCC and HCP crystal structures listed in the table are conjectured to have the lowest density among all strictly jammed packings of identical spheres [159]; see Section 11.1.2 for jamming definitions. However, while there is no proof that BCC is a global minimizer among all infinite three-dimensional hyperuniform point patterns of $\overline{A}|_{\rho=1}$, it is reasonable to conjecture that this is the case. Among the limited set of structures listed in this table, the one associated with the step-function g_2 (see Section 7.2) has the largest order metric.

Table 5 lists values of the scale-independent surface-area coefficient $\overline{A}|_{\rho=1}$ for selected lattices across dimensions up to $d = 8$ [32]. This includes the hypercubic \mathbb{Z}^d , checkerboard D_d , root A_d , E_6 and E_8 lattices as well as their corresponding reciprocal (dual) lattices [129]. Among the lattices described in Table 5, the smallest value of $\overline{A}|_{\rho=1}$ is given by D_d^* for $d = 4$ and $d = 5$, and by E_d^* for $d = 6, 7$ and 8 . For $d = 4$ and $d = 8$, the best known solutions for the sphere packing and number-variance problems are identical, namely, $D_4 \equiv D_4^*$ and $E_8 \equiv E_8^*$, respectively. These lattices are no longer optimal for dimensions in the range $5 \leq d \leq 7$ [160]. It is noteworthy that for the first three space dimensions, the best known

Table 4

Hyperuniformity order metrics $\overline{A}|_{\rho=1}$, $\overline{A}|_{D=1}/\phi^{2/3}$ and ψ_N for selected three-dimensional class I hyperuniform point patterns [27,32]. In the case of point patterns with a minimal pair separation of D , the dimensionless density ϕ represents the packing fraction. The order metrics for the BCC, FCC, HCP, SC, diamond, damped-oscillating g_2 , step-function g_2 and step+delta-function g_2 were obtained Ref. [27], while those for the other structures were determined in Ref. [32].

System	$\overline{A} _{\rho=1}$	$\overline{A} _{D=1}/\phi^{2/3}$	ψ_N
D_3^* (BCC)	0.808633	1.24476	1.00000
D_3 (FCC)	0.809127	1.24552	0.99939
HCP	0.809237	1.24569	0.99926
\mathbb{Z}^3 (SC)	0.837502	1.28920	0.96553
disordered stealthy; $\chi = 0.43$	0.842810	1.29737	0.95949
D_3^+ (diamond)	0.921772	1.41892	0.87726
tunneled FCC	0.922994	1.42080	0.87610
würzite	0.923669	1.42184	0.87546
tunneled HCP	0.927963	1.42845	0.87141
damped-oscillating g_2	0.940904	1.44837	0.85942
step+delta-function g_2	0.991893	1.52686	0.81524
step-function g_2	1.46166	2.25000	0.55323

Table 5

Hyperuniformity order metric $\overline{A}|_{\rho=1}$ for selected lattice families in the first eight space dimensions [32]. Also included are the maximal packing fractions ϕ of the lattices in each dimension. Note that the E_d and E_d^* lattice families are only uniquely defined for $d \geq 6$; a hyphen therefore indicates that information for these lattices is not available in lower dimensions.

d	$\mathbb{Z}^d(\phi)$	$A_d(\phi)$	$A_d^*(\phi)$
1	0.166667 (1)	0.166667 (1)	0.166667 (1)
2	0.457648 ($\pi/4$)	0.450511 ($\sqrt{3}\pi/6$)	0.450511 ($\sqrt{3}\pi/6$)
3	0.837502 ($\pi/6$)	0.809127 ($\sqrt{2}\pi/6$)	0.808633 ($\sqrt{3}\pi/8$)
4	1.24273 ($\pi^2/32$)	1.17426 ($\sqrt{5}\pi^2/40$)	1.17134 ($\sqrt{5}\pi^2/50$)
5	1.60656 ($\pi^2/60$)	1.478629 ($\sqrt{3}\pi^2/45$)	1.46911 ($5\sqrt{5}\pi^2/432$)
6	1.88060 ($\pi^3/384$)	1.67639 ($\sqrt{7}\pi^3/336$)	1.65351 ($9\sqrt{7}\pi^3/5488$)
7	2.04468 ($\pi^3/840$)	1.753865 ($\pi^3/210$)	1.708372 ($49\sqrt{7}\pi^3/61440$)
8	2.10564 ($\pi^4/6144$)	1.720951 ($\pi^4/1152$)	1.64504 ($2\pi^4/6561$)
d	$D_d(\phi)$	$D_d^*(\phi)$	$E_d(\phi)$
1	0.166667 (1)	0.166667 (1)	–
2	0.457648 ($\pi/4$)	0.457648 ($\pi/4$)	–
3	0.809127 ($\sqrt{2}\pi/6$)	0.808633 ($\sqrt{3}\pi/8$)	–
4	1.15803 ($\pi^2/16$)	1.15803 ($\pi^2/16$)	–
5	1.44268 ($\sqrt{2}\pi^2/30$)	1.44018 ($\pi^2/30$)	–
6	1.62341 ($\pi^3/96$)	1.61020 ($\pi^3/192$)	1.58945 ($\sqrt{3}\pi^3/144$)
7	1.69005 ($\sqrt{2}\pi^3/210$)	1.65356 ($\pi^3/420$)	1.60262 ($\pi^3/105$)
8	1.65765 ($\pi^4/768$)	1.58318 ($\pi^4/3072$)	1.48166 ($\pi^4/384$)
d	$E_d^*(\phi)$		
1	–		
2	–		
3	–		
4	–		
5	–		
6	1.587410 ($\sqrt{3}\pi^3/162$)		
7	1.59861 ($9\sqrt{3}\pi^3/2240$)		
8	1.48166 ($\pi^4/384$)		

solutions of the sphere-packing and number-variance problems (or their “dual” solutions) are directly related to those of two other well-known problems in discrete geometry: the *covering* and *quantizer* problems [129], but such relationships may or may not exist for $d > 4$, depending on the peculiarities of the dimensions involved [160].

5.7. Nonspherical windows

The preponderance of previous theoretical investigations concerning the local number variance of point processes have focused on the use of spherical windows. Spherical windows offer many advantages over nonspherical shapes. For example, the mathematical properties of the number variance are easier to derive when spherical windows are employed, regardless of the symmetries of the underlying point process. This may no longer be true when nonspherical windows are used

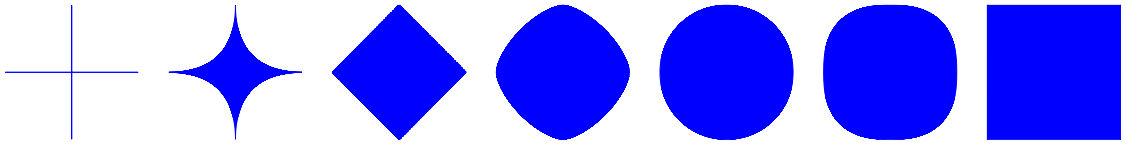


Fig. 16. Superdisk shapes for various values of the deformation parameter p , as adapted from Ref. [150]. Superdisks are defined by the equation $|x|^{2p} + |y|^{2p} = L^{2p}$, where L is a characteristic length and p is the deformation parameter. From the left to the right $p = 0, 0.25, 0.5, 0.75, 1, 1.25$, and ∞ .

and the point pattern is periodic. Moreover, spherical windows have been employed experimentally when direct-space configurational information is available via microscopy [58], for example.

Nonetheless, it is valuable to understand what is the effect of window shape on the number variance and the general conditions under which results for nonspherical windows are not qualitatively similar to those for spherical windows. Nonspherical windows may be good choices to employ to better reflect the symmetries of the underlying point process, e.g., sampling liquid crystals with oriented ellipsoidal windows. Square- and cubic-shaped windows in two and three dimensions, respectively, are convenient shapes to use when analyzing real material images, which are necessarily digitized into square pixels or cubic voxels, respectively.

It is well-known that the large-window asymptotic behavior of the variance $\sigma_N^2(\mathbf{R})$ for rectangular windows with certain orientations in the special case of the square lattice \mathbb{Z}^2 can be anomalously different from that of circular windows [161–163]. For example, for the square lattice and a rectangular window with a very irrational orientation with respect to the x -axis, the variance grows as $\ln R$ [162]. In these studies, however, the variance was used mainly as a mathematical tool to study properties of natural and irrational numbers, and hyperuniformity was not a consideration.

Kim and Torquato [150] have recently carried out a comprehensive study of the effect of window shape on the number variance from the perspective of hyperuniformity. Recall that in Section 5.1 it was noted that the direct-space hyperuniform condition (76) that the number variance grow asymptotically more slowly than the window volume in usual circumstances is equivalent to the Fourier-space hyperuniformity condition (14). However, for lattices and certain window shapes that share the symmetries of the lattices, the variance growth rate can depend on the shape as well as the orientation of the window, and in some cases, the growth rate can be faster than the window volume (see Ref. [150] and references therein), which may lead one to falsely conclude that accompanying hyperfluctuations is due to the system being nonhyperuniform. Kim and Torquato [150] showed that such anomalous behavior can be completely circumvented by sampling the nonspherical window uniformly over all window orientations. Specifically, the direct-space hyperuniformity requirement (76) generalizes in the following way:

$$\lim_{v_1(\mathbf{R}) \rightarrow \infty} \frac{\langle \sigma_N^2(\mathbf{R}) \rangle_0}{v_1(\mathbf{R})} = 0, \quad (120)$$

where $\langle \sigma_N^2(\mathbf{R}) \rangle_0$ is the orientationally-averaged number variance. It was also shown that for any hyperuniform point pattern in \mathbb{R}^d (ordered or not), the orientationally-averaged variance has the following common asymptotic behavior:

$$\frac{\langle \sigma_N^2(\mathbf{R}) \rangle_0}{s_1(\mathbf{R})} \approx -\rho^2 \kappa(d) \int_{|\mathbf{r}| \leq 2L_{\mathbf{R}}} h(\mathbf{r}) |\mathbf{r}| d\mathbf{r} \quad (v_1(\mathbf{R}) \rightarrow \infty), \quad (121)$$

for any convex window shape. Here, $L_{\mathbf{R}}$ is the largest distance from the centroid of the window to its surface, $s_1(\mathbf{R})$ is the surface area of the window, and $\kappa(d) = \Gamma(d/2)/(2\Gamma(1/2)\Gamma((1+d)/2))$. This formula generalizes previous results for the square and triangular lattices in two dimensions [161,164] and analogous results for charge fluctuations in two- and three-dimensional systems [134]. The asymptotic expression (121) also implies that if a point process is statistically isotropic, i.e., $h(\mathbf{r}) = h(|\mathbf{r}|)$, the general expression (44) for the number variance should exhibit the same asymptotic behavior up to a constant multiplicative factor, regardless of the window shape [150].

To illustrate the richness of the dependence of the window shape on the number variance, Kim and Torquato investigated the behavior of the number variance by sampling the square lattice using “superdisk” windows. A superdisk is the two-dimensional shape defined by $|x_1|^{2p} + |x_2|^{2p} = L^{2p}$ where p is the positive *deformation parameter* and L is a characteristic length scale. If the deformation parameter p is smaller than 0.5, a superdisk is concave, and it interpolates smoothly between a cross ($p = 0$) and a perfect square ($p = 0.5$). On the other hand, if $p \geq 0.5$, a superdisk is convex and continuously transforms from a square ($p = 0.5$) to the circle ($p = 1$) and then back to a square of side length $2L$ in the limit $p \rightarrow \infty$, as shown in Fig. 16. Superdisk windows with a fixed orientation with respect to the underlying square lattice were studied for cases in which $p \geq 1$. It was shown that the cumulative moving average of the number variance $\sigma_N^2(L)$ [defined by (103)] exhibits the power-law behavior $\overline{\sigma_N^2}(L) \sim L^\gamma$ for large L . The exponent γ takes on the expected value of unity at the circle point ($p = 1$) and increases continuously and monotonically from this value as the deformation parameter p increases until it achieves its maximum value of $\gamma = 2$ at the perfect square limit ($p \rightarrow \infty$); see Fig. 17. Thus, for square windows, the number variance grows like the window area (proportional to L^2) [150], which is inconsistent with the usual direct-space hyperuniformity condition (76). Referring to the middle panel in Fig. 17, we see that at rational angles (tangent of which belongs to the rational

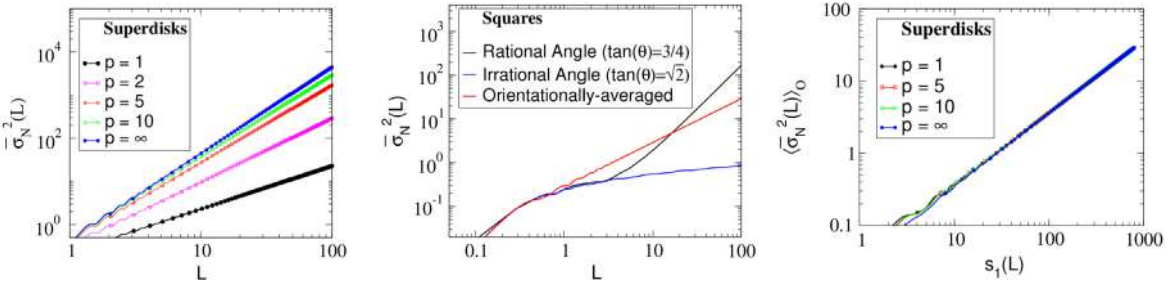


Fig. 17. Left panel: Log-log plot of the cumulative moving average of the number variance $\bar{\sigma}_N^2(L)$ of the square lattice as a function of the characteristic length scale L of superdisk windows for selected values of the deformation parameter p . The symmetry axes of superdisk window and the square lattice are coincident. The number variance exhibits power-law behavior, i.e., $\bar{\sigma}_N^2(L) \sim L^\gamma$ where $\gamma \in [1, 2]$. For circular windows ($p = 1$), the number variance grows like the window perimeter ($\gamma = 1$). However, as p increases from unity, the exponent γ increases continuously and monotonically from unity until it achieves its maximum value of $\gamma = 2$ at the square limit ($p \rightarrow \infty$). Middle panel: Log-log plot of the cumulative moving average of the number variance $\bar{\sigma}_N^2(L)$ versus the side length $2L$ in the case of a square window ($p \rightarrow \infty$) at a rational angle (showing growth rate proportional to the window area), an irrational angle (showing growth rate slower than the window perimeter) and the orientationally-averaged case (showing growth rate proportional to the window perimeter). Right panel: Log-log plot of cumulative moving average of the orientationally-averaged number variance $\langle \bar{\sigma}_N^2(L) \rangle_0$ as a function of the perimeter of superdisk window $s_1(L)$.

numbers), the number variance grows as fast as the window area (L^2), but at irrational angles, the variance grows slower than the window perimeter, e.g., $\ln(L)$ [150], which is not possible for a circular window [162]. Moreover, as shown in the right panel of Fig. 17, the orientationally-averaged number variance $\langle \bar{\sigma}_N^2(L) \rangle_0$ exhibit the same asymptotic behavior for any $p \geq 1$, i.e., $\langle \bar{\sigma}_N^2(L) \rangle_0 \propto s_1(L)$, as predicted by (121), where $s_1(L)$ is the perimeter of superdisk window.

It is instructive to understand more mathematically the anomalous variance growth rates. We indicated in Section 5.1 that for the preponderance of point processes and window shapes, the function $\tilde{\alpha}_2(\mathbf{k}; \mathbf{R})$ appearing in (47) tends to $(2\pi)^d \delta(\mathbf{k})$ when the windows grow infinitely large in a self-similar fashion. However, when the underlying point pattern is a lattice, this direct-space condition may no longer apply if $\tilde{\alpha}_2(\mathbf{k}; \mathbf{R})$ can be decomposed into a product of functions associated with its lower-dimensional forms [150]. For example, the function $\tilde{\alpha}_2(\mathbf{k}; \mathbf{R})$ for a d -dimensional hypercubic window of side length $2L$ can be expressed as

$$\tilde{\alpha}_2(\mathbf{k}; L) = \prod_{i=1}^d \left(\frac{2 \sin(k_i L)}{k_i L} \right)^2, \quad (122)$$

where the multiplicand in (122) is the Fourier transform of the scaled intersection volume of a one-dimensional interval of length $2L$, $\tilde{\alpha}_2(k; L)$. The function $\tilde{\alpha}_2(\mathbf{k}; L)$ decreases slowly in the direction of any axis of symmetry. Due to the interplay between the Bragg peaks of the structure factor $S(\mathbf{k})$ and the slowly decaying function $\tilde{\alpha}_2(\mathbf{k}; L)$ (see Fig. 8 in Ref. [150]), the variance scales like $L^{2(d-1)}$ when the windows are perfectly aligned with the lattice and hence grows faster than the window volume for $d \geq 3$. Of course, one should not conclude from this result that lattices are not hyperuniform. Indeed, in the preponderance of situations, the structure-factor hyperuniformity condition (14) implies the direct-space hyperuniformity condition (76).

6. Mathematical foundations of hyperuniformity: Two-phase media

This section is concerned with the mathematical foundations of hyperuniformity for two-phase media in \mathbb{R}^d . We discuss hyperuniformity conditions for general two-phase media, asymptotic behaviors of the volume-fraction variance and scaling behavior of two-point statistics in both direct and Fourier spaces, the three possible hyperuniformity classes, design of general hyperuniform two-phase media, and spectral densities of packings.

6.1. Vanishing of infinite-wavelength volume-fraction fluctuations

Consider uniformly sampling a two-phase medium with a d -dimensional spherical window of radius R . While the local number variance $\sigma_N^2(R)$ for a general many-particle system (hyperuniform or not) grows with increasing R , the local volume-fraction variance $\sigma_v^2(R)$ for a general two-phase medium decays as R increases [117–120], implying that it vanishes in the limit $R \rightarrow \infty$. For typical disordered two-phase media, $\sigma_v^2(R)$ decays to zero like the inverse of the window volume, i.e., R^{-d} [118]. It has been shown that for sufficiently large window sizes, the full distribution function of the local volume fraction can be reasonably approximated by the normal distribution [119].

To understand the behavior of the variance $\sigma_v^2(R)$ for a hyperuniform two-phase medium, consider its Fourier representation given by relation (74). In the limit that the spherical window grows infinitely large, the function $\tilde{\alpha}_2(k; R)$ appearing in

(74) tends to $(2\pi)^d \delta(\mathbf{k})$. Therefore, multiplying the variance (74) by $v_1(R)$ and taking this limit yields

$$\lim_{v_1(R) \rightarrow \infty} v_1(R) \sigma_v^2(R) = \lim_{|\mathbf{k}| \rightarrow 0} \tilde{\chi}_v(\mathbf{k}) = \int_{\mathbb{R}^d} \chi_v(\mathbf{r}) d\mathbf{r}, \quad (123)$$

where $\tilde{\chi}_v(\mathbf{k})$ is the spectral density defined by relation (36). Note that the hyperuniformity requirement (38) and relation (123) dictate that

$$\lim_{v_1(R) \rightarrow \infty} v_1(R) \sigma_v^2(R) = 0, \quad (124)$$

which signifies that the local volume-fraction variance $\sigma_v^2(R)$ must tend to zero for large R more rapidly than the inverse of the window volume, i.e., like R^{-d} .

Very recently, Chieco et al. [165] introduced a hyperuniformity disorder length parameter in pixelized systems that is linked to the volume-fraction variance. The continuum limit of point patterns, where pixel size vanishes, was also considered.

6.1.1. Asymptotic behavior of the volume-fraction variance for two-phase systems

For a homogeneous and isotropic two-phase medium and a spherical observation window of radius R , substitution of the expansion (54) for the scaled intersection volume $\alpha_2(r; R)$ into (73) implies the following large- R asymptotic expansion for the volume-fraction variance:

$$\sigma_v^2(R) = A_v(R) \left(\frac{D}{R} \right)^d + B_v(R) \left(\frac{D}{R} \right)^{d+1} + o \left(\frac{D}{R} \right)^{d+1}, \quad (125)$$

where

$$A_v(R) = \frac{1}{v_1(D)} \int_{|\mathbf{r}| \leq 2R} \chi_v(\mathbf{r}) d\mathbf{r}, \quad (126)$$

$$B_v(R) = -\frac{c(d)}{2 D v_1(D)} \int_{|\mathbf{r}| \leq 2R} \chi_v(\mathbf{r}) |\mathbf{r}| d\mathbf{r}, \quad (127)$$

where $A_v(R)$ and $B_v(R)$ are dimensionless asymptotic coefficients that multiply terms proportional to R^{-d} and $R^{-(d+1)}$, respectively, D represents a characteristic “microscopic” length scale, and $c(d)$ is a d -dependent constant defined by (53). Note that the coefficient $A_v(R)$ in the limit $R \rightarrow \infty$ is proportional to the nonnegative spectral density $\tilde{\chi}_v(\mathbf{k})$ [cf. (36)] in the limit that the wavenumber tends to zero, i.e.,

$$\bar{A}_v \equiv \lim_{R \rightarrow \infty} A_v(R) \propto \lim_{|\mathbf{k}| \rightarrow 0} \tilde{\chi}_v(\mathbf{k}). \quad (128)$$

6.1.2. Three classes of hyperuniform two-phase systems

Analogous to the classification of hyperuniform point configurations, the asymptotic decay behaviors of $\sigma_v^2(R)$ for hyperuniform two-phase media fall into three distinct classes: class I in which the decay is like $1/R^{d+1}$, class II in which the decay is like $\ln(R)/R^{d+1}$, and class III in which the decay is like $1/R^{d+\alpha}$, where α is an exponent that lies in the open interval $(0, 1)$. The particular class is determined by the large- $|\mathbf{r}|$ behavior of the autocovariance function $\chi_v(\mathbf{r})$ or, equivalently, the behavior of the spectral density $\tilde{\chi}_v(\mathbf{k})$ in the zero-wavenumber limit.

In the case of class I systems, the coefficient \bar{A}_v , defined in (128), is exactly zero and the coefficient $B_v(R)$ converges to a constant in the limit $R \rightarrow \infty$ and hence, according to relation (125), $\sigma_v^2(R)$ decays like $1/R^{d+1}$ [32], as specified by

$$\sigma_v^2(R) \sim \bar{B}_v \left(\frac{D}{R} \right)^{d+1} \quad (R \rightarrow \infty), \quad (129)$$

where

$$\bar{B}_v = \lim_{R \rightarrow \infty} B_v(R) = -\frac{c(d)}{2 D v_1(D)} \int_{\mathbb{R}^d} \chi_v(\mathbf{r}) |\mathbf{r}| d\mathbf{r}, \quad (130)$$

Class I hyperuniform two-phase systems include those in which $\chi_v(\mathbf{r})$ decays to zero sufficiently fast for large $|\mathbf{r}|$, including two-phase media that are certain decorations of perfect periodic and disordered hyperuniform point patterns [72,79] (such as the ones depicted in Fig. 14) and a large class of perfect quasicrystal point patterns.

Two other hyperuniform classes are possible if the coefficient $B_v(R)$ does not converge to a constant in the limit $R \rightarrow \infty$. For example, if the autocovariance function is controlled by the following radial power-law decay:

$$\chi_v(\mathbf{r}) \sim \frac{1}{|\mathbf{r}|^{d+1}} \quad (|\mathbf{r}| \rightarrow \infty), \quad (131)$$

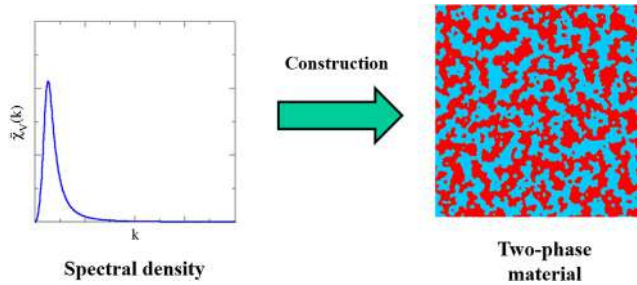


Fig. 18. A designed disordered hyperuniform spectral density with phase-inversion symmetry of class I and a corresponding constructed two-phase material in which $\phi_1 = \phi_2 = 1/2$.
Source: This figure is adapted from Ref. [87]

an asymptotic analysis of (127) leads to a volume-fraction variance that asymptotically decays like $\sigma_v^2(R) \sim R^{-(d+1)} \ln(R)$, since $B_v(R) \sim \ln(R)$, which we call class II hyperuniform two-phase systems. Examples include maximally random jammed packings of disks and spheres [48,52,53,121] and of nonspherical particles [121]. On the other hand, if

$$\chi_v(\mathbf{r}) \sim \frac{1}{|\mathbf{r}|^{d+\alpha}} \quad (|\mathbf{r}| \rightarrow \infty), \quad (132)$$

yields a volume-fraction variance that scales like $R^{-(d+\alpha)}$, where $0 < \alpha < 1$, since $B_v(R) \sim R^{1-\alpha}$. We refer to such hyperuniform two-phase systems as class III structures.

6.2. Asymptotics from power-law spectral densities

Let us consider the power-law behavior for spectral density in the vicinity of the origin

$$\tilde{\chi}_v(\mathbf{k}) \sim |\mathbf{k}|^\alpha \quad (|\mathbf{k}| \rightarrow 0) \quad (133)$$

for $\alpha > 0$. Associated with this scaling form are three different types of large- R scaling behaviors of the volume-fraction variance $\sigma_v^2(R)$ [32]:

$$\sigma_v^2(R) \sim \begin{cases} R^{-(d+1)}, & \alpha > 1 \quad (\text{CLASS I}) \\ R^{-(d+1)} \ln R, & \alpha = 1 \quad (\text{CLASS II}). \\ R^{-(d+\alpha)}, & 0 < \alpha < 1 \quad (\text{CLASS III}) \end{cases} \quad (134)$$

6.3. Design of hyperuniform two-phase materials with prescribed spectral densities

A Fourier-space based numerical construction procedure has recently been formulated to design a wide class of disordered hyperuniform two-phase materials with prescribed spectral densities, which enables one to tune the degree and length scales at which the anomalous suppression of volume-fraction fluctuations occur [87]. This is a generalization of the direct-space Yeong–Torquato construction procedure to generate two-phase media with prescribed autocovariance functions [115,166,167]. Clearly, the Fourier-space setting is the most natural one to employ for the purposes of constructing such disordered hyperuniform materials, since it enables one to very accurately control the behavior of the spectral density from very long to intermediate wavelengths. This technique was used to construct a family of phase-inversion-symmetric materials of class I with tunable topological connectedness properties (see Fig. 18) as well as disordered stealthy hyperuniform dispersions. As we see in Section 14, these two-phase materials have desirable effective physical properties.

6.4. Interrelations between number and volume-fraction variances

The asymptotic coefficients involved in volume-fraction fluctuations for class I two-phase systems have been related to those for number variance fluctuations for class I hyperuniform point processes in the case in which one of the phases consists of identical spherical inclusions of radius $a = D/2$ [32]. This was accomplished using the exact representation of two-point probability function S_2 for such systems in terms of the n -particle correlation functions g_n [115,130,131]. In particular, for a sphere packing at number density ρ , it was found that the coefficient \bar{A}_v , defined by (128), is exactly related to \bar{A}_N , defined by (82), according to

$$\bar{A}_v = \frac{\phi}{2^d} \bar{A}_N, \quad (135)$$

where

$$\phi = \rho v_1(a) \quad (136)$$

is the *packing fraction*, defined to be the fraction of space covered by the spheres. From relation (135), it immediately follows that a system of impenetrable spheres derived from a hyperuniform point configuration generates a hyperuniform heterogeneous medium with respect to fluctuations in the local volume fraction. This also follows directly via the spectral density, as will be described below.

A rigorous upper bound on \bar{B}_v in terms of \bar{B}_N , defined by (130) and (87), respectively, has been derived [32], namely,

$$\bar{B}_v \leq \frac{\phi}{2^d} \bar{B}_N. \quad (137)$$

This bound can be obtained from the more general inequality

$$\sigma_v^2(R) \leq \left(\frac{\phi}{\rho v_1(R)} \right)^2 \sigma_N^2(R) \quad (R \rightarrow \infty). \quad (138)$$

When the heterogeneous medium consists of identical *overlapping* spheres [115,168], the volume-fraction variance is generally greater than those for impenetrable inclusions at a fixed volume fraction ϕ [115,118,119]. This behavior arises since the exclusion-volume effects in the latter case induces a greater degree of uniformity in the underlying point process. However, at a *fixed reduced density* $\eta = \rho v_1(a)$, which is greater than the volume fraction of penetrable spheres, the general upper bound given in (137) with the replacement $\phi \rightarrow \eta$ will still hold.

6.5. Spectral densities for packings

For statistically homogeneous packings of congruent spheres of radius a in \mathbb{R}^d at number density ρ , the autocovariance function $\chi_v(r)$ of the particle (sphere) phase is known exactly in terms of the pair correlation function [115,169], yielding the autocovariance function as

$$\chi_v(\mathbf{r}) = \rho v_2^{int}(r; a) + \rho^2 v_2^{int}(r; a) \otimes h(\mathbf{r}), \quad (139)$$

where

$$m_v(r; a) = \Theta(a - r) = \begin{cases} 1, & r \leq a, \\ 0, & r > a, \end{cases} \quad (140)$$

is a spherical particle indicator function. Previously, this quantity has been designated as $m(r; a)$ [115,130]; we append the subscript v here in order to distinguish it from the interface indicator function of a sphere, denoted by $m_s(r; a)$, as detailed in Section 13.1. Moreover, $v_2^{int}(r; a) = v_1(a)\alpha_2(r; a)$ is the intersection volume of two spheres of radius a whose centers are separated by a distance r , where $v_1(a)$ and $\alpha_2(r; a)$ are defined as in (73), Fourier transformation of (139) gives the corresponding spectral density in terms of the structure factor [32,115,169]:

$$\tilde{\chi}_v(\mathbf{k}) = \phi \tilde{\alpha}_2(k; a) S(\mathbf{k}), \quad (141)$$

where $\tilde{\alpha}_2(k; a)$ is defined by (58).

It follows immediately from relation (141) that the hyperuniformity of a sphere packing in terms of volume-fraction fluctuations can only arise if the underlying point configuration (determined by the sphere centers) is itself hyperuniform, i.e., $\tilde{\chi}_v(\mathbf{k})$ inherits the hyperuniformity property (38) as well as its small-wavenumber behavior (i.e., its class) only through the structure factor, not $\tilde{\alpha}_2(k; a)$; see Ref. [79] for additional details. Accordingly, note that the spectral densities of maximally random jammed (MRJ) packings of identical spheres have been computed [52] and shown to be class II of hyperuniform two-phase systems, as expected due to the fact that the MRJ structure factor tends to zero linearly in $|\mathbf{k}|$ as $|\mathbf{k}| \rightarrow 0$ [46,50,53,54]. It is notable that relation (141) dictates that $\tilde{\chi}_v(\mathbf{k})$ is zero at those wave vectors where $S(\mathbf{k})$ is zero (i.e., where it is stealthy) as well as at the zeros of the function $\tilde{\alpha}_2(k; a)$, which is determined by the zeros of the Bessel function $J_{d/2}(ka)$. The function $\tilde{\chi}_v(\mathbf{k})$ will be zero at all of the zeros of $\tilde{\alpha}_2(k; a)$ for any disordered packing free of any Dirac delta functions (Bragg peaks), hyperuniform or not.

These results for the pair statistics in both direct and Fourier spaces have been generalized to the case of impenetrable spheres with a continuous or discrete size distribution at overall number density ρ [115,170]. In the case of a continuous distribution in radius \mathcal{R} characterized by a probability density function $f(\mathcal{R})$ that normalizes to unity,

$$\int_0^\infty f(\mathcal{R}) d\mathcal{R} = 1. \quad (142)$$

Let us denote the size average of a function $G(\mathcal{R})$ by

$$\langle G(\mathcal{R}) \rangle_{\mathcal{R}} \equiv \int_0^\infty f(\mathcal{R}) G(\mathcal{R}) d\mathcal{R}. \quad (143)$$

It is known that the packing fraction and the autocovariance function are given respectively by [115,170]

$$\phi = \rho \langle v_1(\mathcal{R}) \rangle_{\mathcal{R}} \quad (144)$$

and

$$\chi_v(\mathbf{r}) = \rho \langle v_2^{int}(r; \mathcal{R}) \rangle_{\mathcal{R}} + \rho^2 \left\langle \left\langle m_v(r; \mathcal{R}_1) \otimes m_v(r; \mathcal{R}_2) \otimes h(\mathbf{r}; \mathcal{R}_1, \mathcal{R}_2) \right\rangle_{\mathcal{R}_1} \right\rangle_{\mathcal{R}_2}, \quad (145)$$

where $h(\mathbf{r}; \mathcal{R}_1, \mathcal{R}_2)$ is the appropriate generalization of the total correlation function for the centers of two spheres of radii \mathcal{R}_1 and \mathcal{R}_2 separated by a distance r . Note that generally h is not symmetric with respect to interchange of the components, i.e., $h(\mathbf{r}; \mathcal{R}_1, \mathcal{R}_2) \neq h(\mathbf{r}; \mathcal{R}_2, \mathcal{R}_1)$. Fourier transformation of (145) gives the corresponding spectral density

$$\tilde{\chi}_v(\mathbf{k}) = \rho \langle \tilde{m}_v^2(k; \mathcal{R}) \rangle_{\mathcal{R}} + \rho^2 \left\langle \left\langle \tilde{m}_v(k; \mathcal{R}_1) \tilde{m}_v(k; \mathcal{R}_2) \tilde{h}(\mathbf{k}; \mathcal{R}_1, \mathcal{R}_2) \right\rangle_{\mathcal{R}_1} \right\rangle_{\mathcal{R}_2}. \quad (146)$$

The hyperuniformity condition for a polydisperse sphere packing is obtained by setting the right-hand side of (146) at $\mathbf{k} = \mathbf{0}$ equal to zero, implying that the second term involving $\tilde{h}(\mathbf{k}; \mathcal{R}_1, \mathcal{R}_2)$ must be equal to $-\rho \langle \tilde{m}_v^2(k = 0; \mathcal{R}) \rangle_{\mathcal{R}} = -\rho \langle v_1^2(\mathcal{R}) \rangle_{\mathcal{R}}$.

One can obtain corresponding results for spheres with M different radii a_1, a_2, \dots, a_M from the continuous case [115,171] by letting

$$f(R) = \sum_{i=1}^M \frac{\rho_i}{\rho} \delta(R - a_i), \quad (147)$$

where ρ_i is the number density of type- i particles, respectively, and ρ is the *total number density*. Substitution of (147) into (144), (145) and (146) yields the corresponding packing fraction, autocovariance function and spectral density, respectively, as

$$\phi = \sum_{i=1}^M \rho_i v_1(a_i), \quad (148)$$

$$\chi_v(\mathbf{r}) = \sum_{i=1}^M \rho_i v_2^{int}(r; a_i) + \sum_{i=1}^M \sum_{j=1}^M \rho_i \rho_j m_v(r; a_i) \otimes m_v(r; a_j) \otimes h(\mathbf{r}; a_i, a_j) \quad (149)$$

and

$$\tilde{\chi}_v(\mathbf{k}) = \rho \sum_{i=1}^M \tilde{m}_v^2(k; a_i) S(\mathbf{k}; a_i, a_i) + \rho \sum_{i \neq j}^M \tilde{m}_v(k; a_i) \tilde{m}_v(k; a_j) S(\mathbf{k}; a_i, a_j), \quad (150)$$

where

$$S(\mathbf{k}; a_i, a_j) = \frac{\rho_i}{\rho} \delta_{ij} + \frac{\rho_i \rho_j}{\rho} \tilde{h}(\mathbf{k}; a_i, a_j) \quad (151)$$

is the so-called *partial* structure factor associated with components i and j [6] and δ_{ij} is the Kronecker delta.

Remarks:

1. When each subpacking associated with each component is hyperuniform, i.e., $S(0; a_i, a_i) = 0$ for all i so that the first term on the right side of (150) is zero at $\mathbf{k} = \mathbf{0}$, the second term must also be identically zero at $\mathbf{k} = \mathbf{0}$ (sum of cross terms vanish), as shown elsewhere [79], leading to the hyperuniformity of the entire packing, i.e., $\tilde{\chi}_v(\mathbf{k} = \mathbf{0})$. Such a packing is called *multihyperuniform* [70]. Any decoration of a crystal in which each component is arranged in a periodic fashion is multihyperuniform. By contrast, constructing disordered multihyperuniform polydisperse packings is much more challenging. The photoreceptor mosaics in avian retina [70] and certain multicomponent hard-sphere plasmas [45] are such examples.

2. Generally speaking, examining the structure factor $S(\mathbf{k})$ of the point configurations derived from the centers of spheres in a polydisperse packing could lead one to incorrectly conclude that the packing is not hyperuniform. The proper way to ascertain hyperuniformity in this case is through a packing's spectral density $\tilde{\chi}_v(\mathbf{k})$ [48,52,121,122]. This approach has been profitably used to diagnose hyperuniformity in experimental studies of disordered jammed polydisperse packings of colloidal spheres and emulsions [58,59].

3. The discrete Fourier-space version of the spectral density (150) for a multicomponent hard-sphere packing in a fundamental cell under periodic boundary conditions was given in Ref. [121].

6.6. Nonspherical windows

It is noteworthy that there are anomalous circumstances in which the use of nonspherical observation windows yield a volume-fraction variance $\sigma_v^2(\mathbf{R})$ that do not decrease faster than the window volume, even though the two-phase system would be deemed to be hyperuniform according to the spectral condition (38). For example, using square windows with fixed

orientations, Zachary, Jiao and Torquato [122] studied the two-dimensional checkerboard model and square lattice decorated by identical squares, and showed that the corresponding volume-fraction variances decrease with increasing window size (while preserving the window shape) as slow as the inverse of the window volume, despite the fact that these systems are periodic and hence hyperuniform. Such anomalous fluctuations can arise for periodic two-phase media if nonspherical windows with fixed orientations share the symmetries of the periodic media. In the case of lattices, analogous anomalous fluctuations in the number of lattice points within certain shaped and oriented nonspherical windows can occur [150,162]; see Section 5.7.

7. Hyperuniformity as a critical-point phenomenon and scaling laws

In the ensuing discussion, we return to considering number fluctuations in point configurations. In their study of density fluctuations in fluid systems near the critical point, Ornstein and Zernike [172] defined the direct correlation function $c(\mathbf{r})$ via an integral equation that links it to the pair correlation function $g_2(\mathbf{r})$ or, equivalently, the total correlation function $h(\mathbf{r})$. Specifically, they proposed a decomposition of h into a “direct” part that involves only c and an “indirect” part that involves a convolution of c and h :

$$h(\mathbf{r}) = c(\mathbf{r}) + \rho c(\mathbf{r}) \otimes h(\mathbf{r}), \quad (152)$$

where \otimes denotes a convolution integral. This integral equation has primarily been used to study pair correlations of liquids in equilibrium [6], but it is perfectly well-suited to examine correlations in nonequilibrium systems, which are of general interest in the study of hyperuniform systems. Fourier transforming (152) and solving for $\tilde{h}(\mathbf{k})$ yields

$$\tilde{h}(\mathbf{k}) = \frac{\tilde{c}(\mathbf{k})}{1 - \rho \tilde{c}(\mathbf{k})}, \quad (153)$$

where $\tilde{c}(\mathbf{k})$ is the Fourier transform of $c(\mathbf{r})$.

A system at a thermal critical point, such as a liquid–vapor or magnetic critical point, has a fractal structure [11,12], which is characterized by hyperfluctuations, i.e., density fluctuations become unbounded, and in this sense is anti-hyperuniform. For general hyperfluctuating systems, we see from the fluctuation–compressibility theorem (78) that $\tilde{h}(\mathbf{k} = \mathbf{0})$ or, equivalently, the volume integral of $h(\mathbf{r})$ over all space is unbounded. Thus, $h(\mathbf{r})$ is a long-ranged function characterized by a power-law tail that decays to zero slower than $|\mathbf{r}|^{-d}$ [8,10–12,172]. On the other hand, relation (153) dictates that $\tilde{c}(\mathbf{k} = \mathbf{0})$ remains bounded at the critical point density defined by $\rho_c = \tilde{c}(\mathbf{k} = \mathbf{0})^{-1}$ and hence $c(\mathbf{r})$ is sufficiently short-ranged (roughly, the same range as an effective pair potential $v(\mathbf{r})$) in the sense that its volume integral over all space is bounded. Indeed, while there is no rigorous proof, there are strong theoretical arguments, using diagrammatic expansions, that show that the large-distance asymptotic behavior of the direct correlation of disordered phases is exactly proportional to the pair potential [173,174], i.e.,

$$c(\mathbf{r}) \sim -\beta v(\mathbf{r}) \quad (|\mathbf{r}| \rightarrow \infty), \quad (154)$$

where $\beta = (k_B T)^{-1}$ is an inverse temperature. In Fourier space, this is tantamount to

$$\tilde{c}(\mathbf{k}) \sim -\beta \tilde{v}(\mathbf{k}) \quad (|\mathbf{k}| \rightarrow 0), \quad (155)$$

where $\tilde{v}(\mathbf{k})$ is the Fourier transform of $v(\mathbf{r})$.

7.1. Direct correlation function for hyperuniform systems and new critical exponents

The direct correlation function $c(\mathbf{r})$ of a hyperuniform system behaves in an unconventional manner. We can express $\tilde{c}(\mathbf{k})$ in terms of $\tilde{h}(\mathbf{k})$ using relation (153):

$$\tilde{c}(\mathbf{k}) = \frac{\tilde{h}(\mathbf{k})}{S(\mathbf{k})} = \frac{\tilde{h}(\mathbf{k})}{1 + \rho \tilde{h}(\mathbf{k})}. \quad (156)$$

By definition, a hyperuniform system is one in which $\tilde{h}(\mathbf{k} = \mathbf{0}) = -1/\rho$, i.e., the volume integral of $h(\mathbf{r})$ exists, as, for example, in the case in which $h(\mathbf{r})$ is sufficiently short-ranged in the sense that it decays to zero faster than $|\mathbf{r}|^{-d}$. Interestingly, this means that the denominator on the right side of (156) vanishes at $\mathbf{k} = \mathbf{0}$ and therefore $\tilde{c}(\mathbf{k} = \mathbf{0})$ diverges to $-\infty$. This implies that the volume integral of $c(\mathbf{r})$ does not exist and hence the real-space direct correlation function $c(\mathbf{r})$ is long-ranged, i.e., decays slower than $|\mathbf{r}|^{-d}$. We see that this stands in diametric contrast to standard thermal critical points in which the total correlation function is long-ranged and the direct correlation function is sufficiently short-ranged such that its volume integral exists [7–9,11], as discussed immediately above. For this reason, it has been said that hyperuniform systems are at an “inverted” critical point [27].

Thus, in analogy with thermal critical points, one expects the direct correlation function for a hyperuniform state at critical reduced density ϕ_c to have the following power-law asymptotic decay for large $|\mathbf{r}|$ and sufficiently large d :

$$c(\mathbf{r}) \sim -\frac{1}{|\mathbf{r}|^{d-2+\eta}} \quad (|\mathbf{r}| \rightarrow \infty), \quad (157)$$

where $(2 - d) < \eta < 2$ is a new *critical* exponent associated with $c(\mathbf{r})$ for hyperuniform systems; the upper bound $\eta < 2$ ensures that $c(\mathbf{r})$ is a long-ranged function and the lower bound $\eta > 2 - d$ ensures that $c(\mathbf{r})$ decays at large distances. (The critical exponent η associated with $h(\mathbf{r})$ for thermal systems belonging to the standard Ising universality class is given exactly by 1/4 for $d = 2$ and approximately by 0.05 for $d = 3$; see Ref. [175].) This scaling form for $c(\mathbf{r})$ together with the Ornstein-Zernike relation (152) implies the following corresponding power-law form for the total correlation function at $\phi = \phi_c$:

$$h(\mathbf{r}) \sim -\frac{1}{|\mathbf{r}|^{d+2-\eta}} \quad (|\mathbf{r}| \rightarrow \infty), \quad (158)$$

which is always a sufficiently short-ranged function such that its volume integral over all space exists whenever $\eta < 2$. We say a system has *quasi-long-ranged* (QLR) correlations if $h(\mathbf{r})$ decays to zero like a power law $1/|\mathbf{r}|^a$ for large $|\mathbf{r}|$ with an exponent $a > d$ so that the volume integral of $h(\mathbf{r})$ exists.

It is notable that for any hyperuniform particle system derived from an equilibrium ensemble, we can associate an effective long-ranged interparticle pair potential $v(\mathbf{r})$ whose asymptotic form is given precisely by (157), i.e.,

$$\beta v(\mathbf{r}) \sim \frac{1}{|\mathbf{r}|^{d-2+\eta}} \quad (|\mathbf{r}| \rightarrow \infty), \quad (159)$$

where we have used relation (154). This effective repulsive potential can be regarded to be a *generalized* Coulombic interaction between “like-charged” particles. To maintain stability, the total potential energy must also include a “background” contribution of equal and opposite “charge”, i.e., the system must have *overall charge neutrality*. Notably, whenever $\eta = 0$ so that $S(\mathbf{k}) \sim |\mathbf{k}|^2$ as $|\mathbf{k}| \rightarrow 0$, the effective pair potential (159) reduces to the standard Coulombic interaction for $d \geq 3$ and hence the system belongs to class I; see Eq. (97). In summary, in order to drive an equilibrium many-particle system to a hyperuniform state, effective *long-ranged repulsive pair interactions* of the form (159) are required. On the other hand, long-ranged interactions are not necessary to achieve hyperuniformity if the system is out of equilibrium; prototypical nonequilibrium examples are MRJ particle packings that have pure short-ranged hard-particle interactions [46–49,51,53,54]. This and other nonequilibrium hyperuniform classes will be described in greater detail in Section 11.

Fourier transformation of the aforementioned large- $|\mathbf{r}|$ scaling laws for direct-space functions yield corresponding small- $|\mathbf{k}|$ scaling laws for hyperuniform systems. Specifically, the Fourier transform of the direct-correlation-function scaling (157) is given by

$$\tilde{c}(\mathbf{k}) \sim -\frac{1}{|\mathbf{k}|^\alpha} \quad (|\mathbf{k}| \rightarrow 0), \quad (160)$$

where α is the positive exponent introduced in (96), which determines the hyperuniformity class [cf. (97)] and is related to η via

$$\alpha = 2 - \eta. \quad (161)$$

Note that $\tilde{c}(\mathbf{k})$ contains a singularity at the origin, the order of which is determined by the exponent α . This implies that a length scale based on the volume integral $-\int_{\mathbb{R}^d} c(\mathbf{r}) d\mathbf{r}$ will grow as a hyperuniform state is approached, as specifically described in Section 16.1. The scaling law (160) combined with (156) yields the corresponding asymptotic form of the structure factor:

$$S(\mathbf{k}) \sim |\mathbf{k}|^\alpha \quad (|\mathbf{k}| \rightarrow 0). \quad (162)$$

Importantly, while the exponent α in the structure-factor scaling (162) can generally take on any real positive value up to infinity, it must obey the upper bound $\alpha < d$ in the scaling (160) in order for the direct correlation function $c(\mathbf{r})$ to decay at large distances. Note also that while the scaling (160) in the special case $\alpha = d$ is not integrable in Fourier space, one may sometimes be able to associate a long-range behavior of direct correlation function $c(\mathbf{r})$ that is not a power-law function; for example, a logarithmic law, i.e.,

$$c(\mathbf{r}) \sim -\beta v(\mathbf{r}) \sim \ln(|\mathbf{r}|) \quad (|\mathbf{r}| \rightarrow \infty), \quad (163)$$

which is recognized to be the two-dimensional Coulomb interaction. We will see in Sections 7.2, 9 and 10 that such effective “log-gas” interactions can arise in hyperuniform two-dimensional g_2 -invariant processes of class I, one-dimensional Coulombic systems of class II, and two-dimensional Coulombic systems of class I, respectively. Observe that when $\alpha = 1$ ($\eta = 1$), we conclude from (159) that the effective potential corresponds to a d -dimensional charged system but with Coulombic interactions in a higher $(d + 1)$ -dimensional space and hence is a hyperuniform system of class II, which is consistent with results reported in Ref. [176].

We can define critical exponents associated with the manner in which certain quantities diverge as the critical (hyperuniform) point is approached. Consider a point configuration with a reduced density ϕ that is nearly hyperuniform and which can be made hyperuniform by increasing and/or decreasing the density. We denote by ϕ_c the reduced density at the hyperuniform state. The reduced densities ϕ and ϕ_c play the same role as temperature T and critical temperature T_c , respectively, in the analogous thermal problem in the vicinity of a critical point. In some cases, the direct correlation

Table 6

Definitions of the critical exponents in the vicinity of or at a hyperuniform state. Here $S^{-1}(0)$ is the inverse of the structure factor at $\mathbf{k} = \mathbf{0}$, ξ is the correlation length, and $c(\mathbf{r})$ is the direct correlation function. The scaling laws for the latter apply for sufficiently large dimensions.

Exponent	Asymptotic behavior
γ	$S^{-1}(0) \sim (1 - \frac{\phi}{\phi_c})^{-\gamma} (\phi \rightarrow \phi_c^-)$
γ'	$S^{-1}(0) \sim (\frac{\phi}{\phi_c} - 1)^{-\gamma'} (\phi \rightarrow \phi_c^+)$
ν	$\xi \sim (1 - \frac{\phi}{\phi_c})^{-\nu} (\phi \rightarrow \phi_c^-)$
ν'	$\xi \sim (\frac{\phi}{\phi_c} - 1)^{-\nu'} (\phi \rightarrow \phi_c^+)$
η	$c(\mathbf{r}) \sim \mathbf{r} ^{2-d-\eta} (\phi = \phi_c)$
ξ	$c(\mathbf{r}) \sim \exp(- \mathbf{r} /\xi)/ \mathbf{r} ^{d-2+\eta} (\phi_c - \phi \ll 1)$

function of a many-particle system at a dimensionless density in the vicinity of a hyperuniform state, i.e., for $|\phi_c - \phi| \ll 1$, in sufficiently high dimensions has the following large- r asymptotic form:

$$c(\mathbf{r}) \sim \frac{\exp(-|\mathbf{r}|/\xi)}{|\mathbf{r}|^{d-2+\eta}}, \quad (164)$$

where ξ is the *correlation length*. If the system approaches a hyperuniform state from below the critical density ϕ_c , the correlation length and inverse of the structure factor at $k = 0$, $S^{-1}(0)$, which is proportional to $\tilde{c}(0)$, are described by the following scaling laws:

$$\xi \sim (1 - \frac{\phi}{\phi_c})^{-\nu} \quad (\phi \rightarrow \phi_c^-), \quad (165)$$

$$S^{-1}(0) \sim \left(1 - \frac{\phi}{\phi_c}\right)^{-\gamma}, \quad (\phi \rightarrow \phi_c^-), \quad (166)$$

where ν and γ are nonnegative critical exponents. Observe that $S^{-1}(0)$ is a measure of the degree of hyperuniformity of a system away from a critical point. Combination of three previous scaling laws leads to the following interrelation between the exponents:

$$\gamma = (2 - \eta)\nu. \quad (167)$$

Of course, the specific values of the critical exponents determine the “universality” class of the hyperuniform system. Analogous critical exponents can be defined for densities near but above ϕ_c . Table 6 provides a summary of the scaling laws and critical exponents.

In the following subsection, we describe so-called g_2 -invariant hyperuniform point configurations in which the critical behavior can be exactly determined in any dimension d .

7.2. Critical behavior of g_2 -invariant hyperuniform point configurations

A g_2 -invariant process is one in which a chosen nonnegative form for the pair correlation function g_2 remains invariant over a nonvanishing density range while keeping all other relevant macroscopic variables fixed [177]. The upper limiting “terminal” density is the point above which the nonnegativity condition on $S(\mathbf{k})$ [cf. (11)] would be violated. Thus, at the terminal or critical density, if $S(\mathbf{k} = \mathbf{0}) = 0$, the system is hyperuniform, if realizable. In Ref. [27], a variety of g_2 -invariant processes in \mathbb{R}^d in which the number variance scales like the window surface area (i.e., belong to class I) were exactly studied. Here we summarize some of those exact results by reporting the corresponding surface-area coefficients, structure factors, direct correlation functions, and associated critical exponents.

7.2.1. Step-function g_2

The simplest g_2 -invariant process that was considered by Torquato and Stillinger [27] is one in which a radial pair correlation function is defined by the unit step function, i.e.,

$$g_2(r) = \Theta(r - D) \quad (168)$$

or, equivalently, a total correlation function $h(r) = -\Theta(D - r)$. Any system with such pair correlations corresponds to a packing of identical spheres with hard-core diameter D . In the special case of identical hard spheres in equilibrium in the limit $\rho \rightarrow 0$, g_2 is exactly given by this step-function form as well as those with finite densities, as described below. Substitution of $h(r) = -\Theta(D - r)$ into (11) gives the structure factor for ϕ in the range $0 \leq \phi \leq \phi_c$ to be

$$S(k) = 1 - \Gamma(1 + d/2) \left(\frac{2}{kD} \right)^{d/2} \left(\frac{\phi}{\phi_c} \right) J_{d/2}(kD), \quad (169)$$

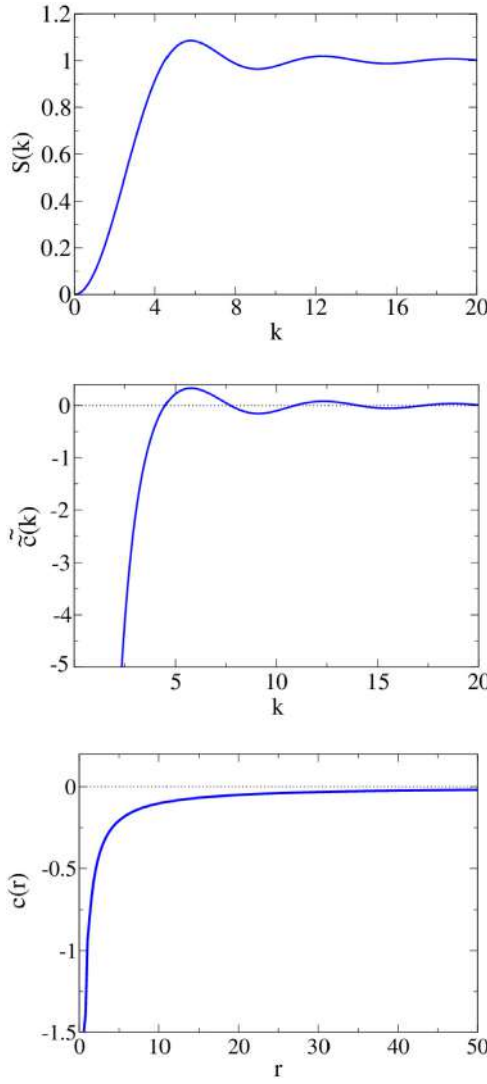


Fig. 19. Results for the sphere packing corresponding to the step-function g_2 -invariant process in three dimensions at the critical hyperuniform packing density $\phi_c = 1/8$, where the hard-core diameter D is taken to be unity. Top panel: Structure factor. Middle panel: Fourier transform of the direct correlation function. Bottom panel: Direct correlation function.

where

$$\phi_c = \frac{1}{2^d} \quad (170)$$

is the terminal or critical density, which is the density at which this system is hyperuniform. The fact that $h(r)$ is exactly zero for all $r > D$ results in a structure factor $S(k)$ that is analytic not only at the origin, but for all k . The Ornstein–Zernike relation (156) yields an exact expression for the Fourier transform of the direct correlation function:

$$\tilde{c}(k) = \frac{-\left(\frac{2\pi}{kD}\right)^{d/2} D^d J_{d/2}(kD)}{1 - \Gamma(1 + d/2) \left(\frac{2}{kD}\right)^{d/2} \left(\frac{\phi}{\phi_c}\right) J_{d/2}(kD)}. \quad (171)$$

Notably, Ref. [178] provides numerical evidence that the step-function g_2 is to a good approximation realizable by systems of impenetrable d -dimensional spheres (with $d = 1$ and $d = 2$) for densities up to the terminal density. Thus, satisfying the nonnegativity conditions on $g_2(r)$ and $S(k)$ in this instance is sufficient to ensure realizability of such a point process to within numerical accuracy. Fig. 19 shows results for the sphere packing corresponding to the step-function g_2 -invariant process in three dimensions at the critical hyperuniform packing density $\phi_c = 1/8$.

Combination of (168), (89) and (87) yields the volume and surface-area coefficients as

$$A_N = S(k=0) = 1 - 2^d \phi, \quad B_N = \frac{\bar{\Lambda}}{2^d \phi} = \frac{2^{d-2} d^2 \Gamma(d/2)}{\Gamma((d+3)/2) \Gamma(1/2)} \phi. \quad (172)$$

The reduced density ϕ defined by (80) (equivalent to the covering fraction of the hard cores of diameter D) lies in the range $0 \leq \phi \leq \phi_c$, where

$$\phi_c = \frac{1}{2^d} \quad (173)$$

is the terminal or critical density, i.e., the density at which the system is hyperuniform, where $A_N = 0$ and

$$B_N = \bar{\Lambda} = \frac{d^2 \Gamma(d/2)}{4 \Gamma((d+3)/2) \Gamma(1/2)}. \quad (174)$$

The values of the surface-area coefficient $\bar{\Lambda}$ for $d = 1, 2$ and 3 are given in Tables 2–4, respectively.

Thus, the small- k expansions of $S(k)$ and $\tilde{c}(k)$, which determine their behavior in the vicinity of the critical point, are respectively given by

$$S(k) = \left(1 - \frac{\phi}{\phi_c}\right) + \frac{1}{2(d+2)} \frac{\phi}{\phi_c} (kD)^2 + \mathcal{O}[(kD)^4] \quad (175)$$

and

$$\tilde{c}(k) = \frac{-v_1(D)}{\left(1 - \frac{\phi}{\phi_c}\right) + \frac{1}{2(d+2)} \frac{\phi}{\phi_c} (kD)^2 + \mathcal{O}[(kD)^4]}, \quad (176)$$

where $v_1(D)$ is the volume of a d -dimensional sphere of radius D [cf. (51)]. Comparison of Eqs. (175) and (176) to the scaling relations (162) and (166) yield the exponents $\eta = 0$ and $\gamma = 1$. At the critical point $\phi = \phi_c$, we see that

$$S(k) \sim k^2 \quad \text{and} \quad \tilde{c}(k) \sim -k^{-2} \quad (k \rightarrow 0). \quad (177)$$

The correlation length ξ can be extracted from relation (176), which can be rewritten as

$$k^2 \tilde{c}(k) + \xi^{-2} \tilde{c}(k) = -G, \quad kD \ll 1 \quad (178)$$

where

$$\xi = \frac{D}{[2(d+2)\phi_c]^{1/2}} \left(1 - \frac{\phi}{\phi_c}\right)^{-1/2}, \quad \phi \rightarrow \phi_c^-, \quad (179)$$

$$G = \frac{2(d+2)v_1(D)}{D^2} \frac{\phi_c}{\phi}, \quad (180)$$

Comparison of (179) to scaling relation (165) yields the exponent $\nu = 1/2$. The exponent values $\gamma = 1$, $\nu = 1/2$, and $\eta = 0$ are consistent with the interrelation (167). Inversion of (178) yields the partial differential equation

$$\nabla^2 c(r) - \xi^{-2} c(r) = G \delta(\mathbf{r}), \quad r \gg D, \quad (181)$$

where the spherically symmetric Laplacian operator ∇^2 in any dimension d is given by

$$\nabla^2 = \frac{1}{r^{d-1}} \frac{\partial}{\partial r} \left[r^{d-1} \frac{\partial}{\partial r} \right]. \quad (182)$$

We see that the direct correlation function in real space for large r is determined by the Green's function of the linearized Poisson–Boltzmann equation.

Let us first determine the solutions of (181) at the critical point $\phi = \phi_c$, where ξ diverges to infinity. Thus, the asymptotic behavior of $c(r)$ for $r \gg D$ is given by the infinite-space Green's function for the d -dimensional Laplace equation [115], and so we obtain

$$c(r) = \begin{cases} -6 \left(\frac{r}{D}\right), & d = 1, \\ 4 \ln \left(\frac{r}{D}\right), & d = 2, \\ -\frac{2(d+2)}{d(d-2)} \left(\frac{D}{r}\right)^{d-2}, & d \geq 3. \end{cases} \quad (183)$$

Observe that it is only for $d \geq 3$ that $c(r)$ follows the power-law form (160) with an exponent $\eta = 0$. The fact that η takes on an integer value is due to the fact that $\tilde{h}(k)$ is an analytic function. We will see in Section 10.3 that the real-space direct

correlation function of the one-component plasma [35,149,179–187] for $d \geq 2$ has precisely the same asymptotic form as the ones indicated in (183), albeit with different amplitudes (prefactors).

For fixed r and in the limit $\xi \rightarrow \infty$, the solutions of (181) are

$$c(r) = \begin{cases} -6 \frac{\phi_c}{\phi} \left(\frac{\xi}{D} \right) \exp(-r/\xi), & d = 1, \\ 4 \frac{\phi_c}{\phi} \ln \left(\frac{r}{D} \right) \exp(-r/\xi), & d = 2, \\ -\frac{2(d+2)\phi_c}{d(d-2)\phi} \left(\frac{D}{r} \right)^{d-2} \exp(-r/\xi), & d \geq 3. \end{cases} \quad (184)$$

On the other hand, observe that as $r \rightarrow \infty$ for fixed ξ , the asymptotic behavior changes according to the relation

$$c(r) = -\frac{(d+2)\sqrt{2\pi}\phi_c}{\Gamma(1+d/2)\phi} \left(\frac{D}{\xi} \right)^{(d-3)/2} \left(\frac{D}{r} \right)^{(d-1)/2} \exp(-r/\xi), \quad d \geq 1. \quad (185)$$

7.2.2. Step+Delta function g_2

Here we consider the g_2 -invariant process defined by a radial distribution function that consists of the aforementioned unit step function plus a delta function contribution that acts at $r = D$:

$$g_2(r) = \Theta(r - D) + \frac{Z}{\rho s_1(D)} \delta(r - D), \quad (186)$$

where Z is a nonnegative constant and $s_1(D)$ is the surface area of a sphere of radius D defined by (6). The function (186) was one of several examples studied by Torquato and Stillinger [177] to understand the relationship between short-range order and maximal density in sphere packings. In that investigation, Z was interpreted as the average contact coordination number. Here we consider their case IV in which the condition

$$Z = \frac{2^d d}{d+2} \phi \quad (187)$$

is obeyed in order to constrain the location of the minimum of $S(k)$ to be at $k = 0$, thus enforcing hyperuniformity. Here the reduced density ϕ lies in the range $0 \leq \phi \leq \phi_c$, and

$$\phi_c = \frac{d+2}{2^{d+1}} \quad (188)$$

is the critical density, which also results as a special limit of the pair correlation function corresponding to the dilute and narrow limit of the *square-well potential* studied by Sakai, Stillinger, and Torquato [188].

Substitution of (186) into (89) and (90) yields the volume and surface-area coefficients as

$$A_N = S(k=0) = 1 - \frac{2^{d+1}}{d+2} \phi, \quad B_N = \frac{\bar{\Lambda}}{2^d \phi} = \frac{2^{d-2} d^2 \Gamma(d/2)}{(d+2) \Gamma((d+3)/2) \Gamma(1/2)} \phi. \quad (189)$$

At the critical density, $A_N = 0$ and

$$\bar{\Lambda} = 2^d \phi_c B_N = \frac{d^2 (d+2) \Gamma(d/2)}{16 \Gamma((d+3)/2) \Gamma(1/2)}. \quad (190)$$

The values of the scale-independent surface-area coefficient $\bar{\Lambda}$ for $d = 1, 2$ and 3 are given in Tables 2–4, respectively.

The structure factor and Fourier transform of the direct correlation function can be exactly obtained for ϕ in the range $0 \leq \phi \leq \phi_c$ [27] and yields the following small- k behavior:

$$S(k) = \left(1 - \frac{\phi}{\phi_c} \right) + \frac{1}{8(d+2)(d+4)} \frac{\phi}{\phi_c} (kD)^4 + \mathcal{O}[(kD)^6] \quad (191)$$

and

$$\tilde{c}(k) = \frac{-2v_1(D)}{\left(1 - \frac{\phi}{\phi_c} \right) + \frac{1}{8(d+2)(d+4)} \frac{\phi}{\phi_c} (kD)^4 + \mathcal{O}[(kD)^6]}. \quad (192)$$

Comparison of expression (191) to the scaling relations (162) and (166) yield the exponents $\eta = -2$ and $\gamma = 1$. The correlation length ξ is defined via (192), which we rewrite as

$$k^4 \tilde{c}(k) + \xi^{-4} \tilde{c}(k) = -G, \quad kD \ll 1 \quad (193)$$

where

$$\xi = \frac{D}{[8(d+2)(d+4)\phi_c]^{1/4}} \left(1 - \frac{\phi}{\phi_c}\right)^{-1/4}, \quad \phi \rightarrow \phi_c^-, \quad (194)$$

$$G = \frac{16(d+2)(d+4)v_1(D)}{D^4} \frac{\phi_c}{\phi}. \quad (195)$$

Comparison of (194) to the power law (165) yields the exponent $\nu = 1/4$. The exponent values $\gamma = 1$, $\nu = 1/4$, and $\eta = -2$ are consistent with the interrelation (167). Inversion of (193) yields the partial differential equation

$$\nabla^4 c(r) + \xi^{-4} c(r) = -G\delta(\mathbf{r}), \quad r \gg D, \quad (196)$$

where $\nabla^4 \equiv \nabla^2 \nabla^2$ is the spherically symmetric *biharmonic operator*, and ∇^2 is given by (182).

The solutions of (196) at the critical point $\phi = \phi_c$ ($\xi \rightarrow \infty$) are given by the infinite-space Green's function for the d -dimensional biharmonic equation. It is only for $d \geq 5$ that the solutions admit a power law of the form (165) with an exponent $\eta = -2$, namely,

$$c(r) = -\frac{8(d+2)(d+4)}{d(d-2)(d-4)} \left(\frac{D}{r}\right)^{d-4}, \quad d \geq 5. \quad (197)$$

8. Hyperuniform disordered classical ground states

The “collective-coordinate” optimization procedure represents a powerful *reciprocal-space-based* approach to generate disordered hyperuniform classical many-particle systems in d -dimensional Euclidean space \mathbb{R}^d with prescribed (or targeted) structure factors. These particle configurations correspond to exotic disordered classical ground states of many particles interacting with certain bounded long-ranged interactions, including isotropic pair potentials [36–42, 139, 189, 190], anisotropic pair potentials [191], and two-, three- and four-body potential functions [37]. Not only are these ground states endowed with novel physical properties, such as photonic characteristics [89–94, 99, 101, 102], phononic band gaps [103], dielectric characteristics [86–88], and transport properties [87, 104] (see Section 14), but their corresponding excited (positive temperature) states are characterized by singular thermodynamic properties, as detailed in Section 8.4.6. In what follows, we first describe numerical procedures to generate a large class of tunable disordered hyperuniform ground-state configurations with high precision and then we discuss predictive ensemble theories for so-called “stealthy” ground states.

8.1. Stealthy configurations via collective-coordinate optimizations

The simplest setting involves the consideration of pairwise additive potentials $v(\mathbf{r})$ that are bounded and integrable such that their Fourier transforms $\tilde{v}(\mathbf{k})$ exist. If N identical point particles reside in a fundamental cell F of volume v_F in d -dimensional Euclidean space \mathbb{R}^d at positions $\mathbf{r}^N \equiv \mathbf{r}_1, \dots, \mathbf{r}_N$ under periodic boundary conditions, the total potential energy $\Phi_N(\mathbf{r}^N)$ [equal to the pairwise sum of the potential $v(\mathbf{r})$] also has the following Fourier representation:

$$\Phi_N(\mathbf{r}^N) = \frac{N}{2v_F} \left[\sum_{\mathbf{k}} \tilde{v}(\mathbf{k}) S(\mathbf{k}) - \sum_{\mathbf{k}} \tilde{v}(\mathbf{k}) \right], \quad (198)$$

where $S(\mathbf{k})$ is the single-configuration structure factor, as defined by (24). The key idea behind the collective-coordinate approach is to require that $\tilde{v}(\mathbf{k})$ be a bounded, positive function with support for wave vectors $\mathbf{k} \in \mathbf{Q}$, where \mathbf{Q} is a prescribed subregion of Fourier space, and if the particles are arranged so that $S(\mathbf{k})$ is driven to its minimum value of zero for all wave vectors where $\tilde{v}(\mathbf{k})$ has support (except $\mathbf{k} = \mathbf{0}$), then it is clear from relation (198) that the system must be at its ground state or global energy minimum. These ground-state configurations have been called “stealthy” [38] because the structure factor $S(\mathbf{k})$ is *constrained* to be zero for $\mathbf{k} \in \mathbf{Q}$ (except $\mathbf{k} = \mathbf{0}$), meaning that they completely suppress single scattering of incident radiation for these wave vectors.

For purposes of illustration, we will focus on the case in which \mathbf{Q} is taken to be a sphere of radius K centered at the origin, and hence by construction, such stealthy ground states are also hyperuniform, since the structure factor $S(\mathbf{k})$ is constrained to be zero within this “exclusion” sphere, implying no single scattering events from infinite wavelength down to a wavelength of the order of $2\pi/K$; see Fig. 4 for an example of such a scattering pattern. The corresponding class of stealthy radial potential functions $\tilde{v}(k)$ in \mathbb{R}^d have support within this sphere and the general functional form

$$\tilde{v}(\mathbf{k}) = V(k)\Theta(K - k), \quad (199)$$

where, for simplicity, $V(k)$ is infinitely differentiable in the open interval $(0, K)$ and $\Theta(x)$ is the Heaviside step function. The corresponding direct-space radial pair potential $v(r)$ is necessarily a delocalized, long-ranged function that is integrable in \mathbb{R}^d . Two specific families of potentials that fall within the class of stealthy interactions are the “power-law” and “overlap” potentials [40], examples of which are depicted in Figs. 20 and 21. While the form of the direct-space power-law potential is very similar to the weakly decaying Friedel oscillations of the electron density in a variety of systems, including molten

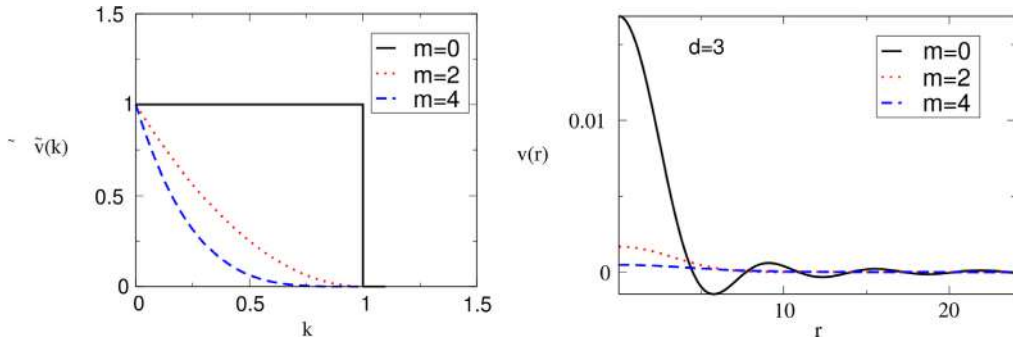


Fig. 20. Left panel: Fourier power-law potential $\tilde{v}(k)$ for the special cases $m = 0, 2$, and 4 that apply for any d with $V(0) = K = 1$. Right panel: Corresponding direct-space power-law potentials $v(r)$ in the instance $d = 3$.

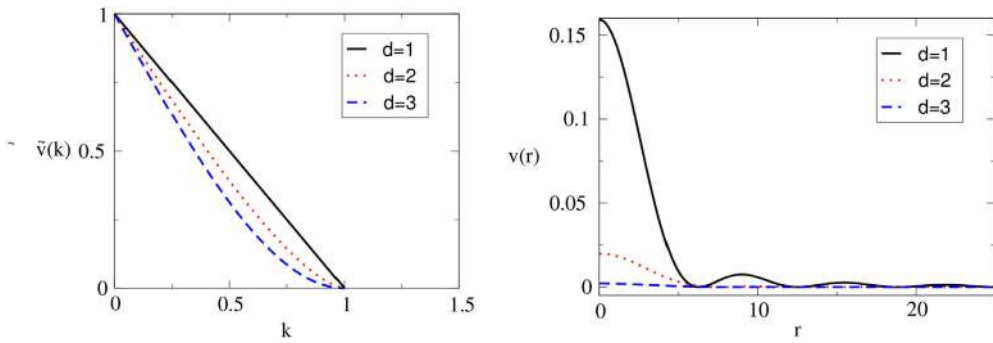


Fig. 21. Left panel: Fourier overlap potential $\tilde{v}(k)$ for the first three space dimensions with $V(0) = K = 1$. Right panel: Corresponding direct-space overlap potentials $v(r)$, which oscillate but are always non-negative.

metals as well as graphene [192,193], the overlap potential $v(r)$ mimics effective interactions that arise in certain polymer systems [194]. In either family of potentials, the direct-space potential $v(r)$ is controlled by an envelop that cannot decay slower than the inverse power law $1/r^{d+1}$; see Ref. [40] for additional details.

The nature of the ground-state configuration manifold (e.g., the degree of order) depends on the number of constrained wave vectors. As the number of \mathbf{k} vectors for which $S(\mathbf{k})$ is constrained to be zero increases, i.e., as K increases, the dimensionality of the ground-state configuration manifold per particle, d_c , decreases. Let $M(K)$ be the number of independently constrained wave vectors. The parameter $\chi = M(K)/[d(N - 1)]$, gives a measure of the relative fraction of constrained degrees of freedom compared to the total number of degrees of freedom $d(N - 1)$ (subtracting out the system translational degrees of freedom) [38], which, in the thermodynamic limit, is given by [40]

$$\rho \chi = \frac{v_1(K)}{2d(2\pi)^d}, \quad (200)$$

where $v_1(K)$ is the volume of a d -dimensional sphere (hypersphere) of radius K [cf. (51)]. We see that for fixed K and d , which sets the potential, the “tuning” parameter χ is inversely proportional to the number density ρ . The dimensionality of the configuration space per particle is given by $d_c = d(1 - 2\chi)$ for $0 \leq \chi \leq 1/2$ [40] and hence depends on χ or, equivalently, the density ρ . For sufficiently small χ , the ground states are highly degenerate and overwhelmingly disordered. Clearly, when the system is free of any constraints, i.e., if $\chi = 0$, it is structurally like a noninteracting classical ideal gas (even if it is not an ideal gas thermodynamically) [40]. This situation runs counter to traditional understanding that ideal-gas configurations correspond to the opposite zero-density limit of classical systems of particles. The reason for this inversion of limits is due to the fact that a compression of the system in direct space leads to a dilation of the lattice spacing in reciprocal space, thus expelling \mathbf{k} -vectors that can be constrained within the exclusion zone and thus increasing d_c . This compression process is schematically shown in Fig. 22 [40]. If χ is a positive but very small number, the ground states remain disordered and highly degenerate, even if d_c has now been suddenly reduced due to the imposed constrained degrees of freedom. While the ground-state manifold contains periodic configurations (e.g., Bravais lattices and lattices with a basis) in this “disordered” regime, these are sets of zero measure in the thermodynamic limit. When the configurational dimensionality collapses to zero in a low-density regime ($\chi = 1/2$), there can be concomitant phase transition to a crystal phase that depends on the space dimension and the ensemble under consideration [36,38,189,195].

Generally, a numerically obtained ground-state configuration depends on the number of particles N within the fundamental cell, initial particle configuration, shape of the fundamental cell, and particular optimization technique that is

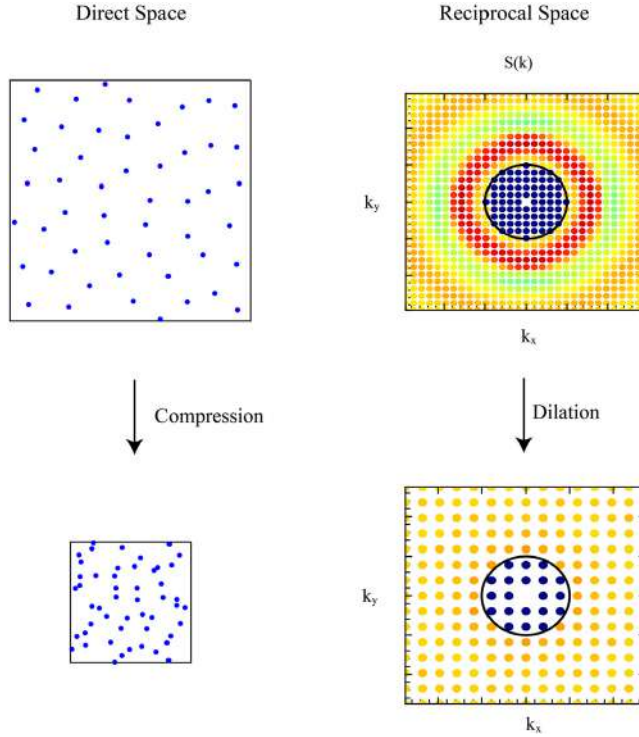


Fig. 22. Schematic taken from Ref. [40] that illustrates the inverse relationship between the number density ρ and relative fraction of constrained degrees of freedom χ for a fixed reciprocal-space exclusion-sphere of radius K (where dark blue \mathbf{k} points signify zero intensity with green, yellow, and red points indicating increasingly larger intensities) for a stealthy ground state. A compression of a disordered ground-state configuration with a fixed number of particles N in direct space leads to a dilation of the lattice spacing in reciprocal space, thus reducing the number of constrained wave vectors within the exclusion sphere and hence increasing the dimensionality of the ground-state manifold per particle d_c .

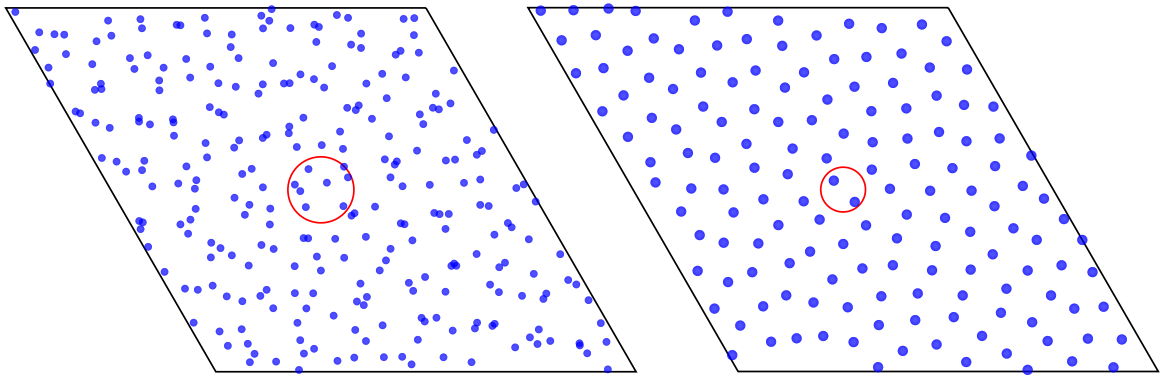


Fig. 23. Two stealthy two-dimensional configurations in a rhombical fundamental cell containing $N = 271$ particles with $\chi = 0.1$ (left panel) and $N = 151$ particles with $\chi = 0.4$ (right panel), as adapted from Ref. [41]. It is clear that the system with $\chi = 0.4$ has substantially more short-range order than the one with $\chi = 0.1$. The diameters of the circular windows shown in each figure represent the characteristic wavelength $2\pi/K$ above which single-scattering events are completely suppressed. In the case of $\chi = 0.4$, this means that no scattering occurs on length scales above that corresponding to approximately the mean-nearest-neighbor spacing.

used [40]. Various optimization techniques have been employed to find the globally energy-minimizing configurations for stealthy and other prescribed structure factors within an exceedingly small numerical tolerance [36–39,41,42,139, 189–191]. Figs. 23 and 24 show numerically obtained stealthy hyperuniform disordered configurations in both two and three dimensions at selective values of χ , as obtained from Ref. [41]. Regardless of the dimension, it is clear that the degree of short-range order (tendency for particles to repel one another) increases as χ increases [36,38,40,41].

The topography of the energy landscape in the disordered regime is sufficiently simple such that a variety of different optimization techniques yield the globally minimizing energy configurations with a 100% percent success rate from random

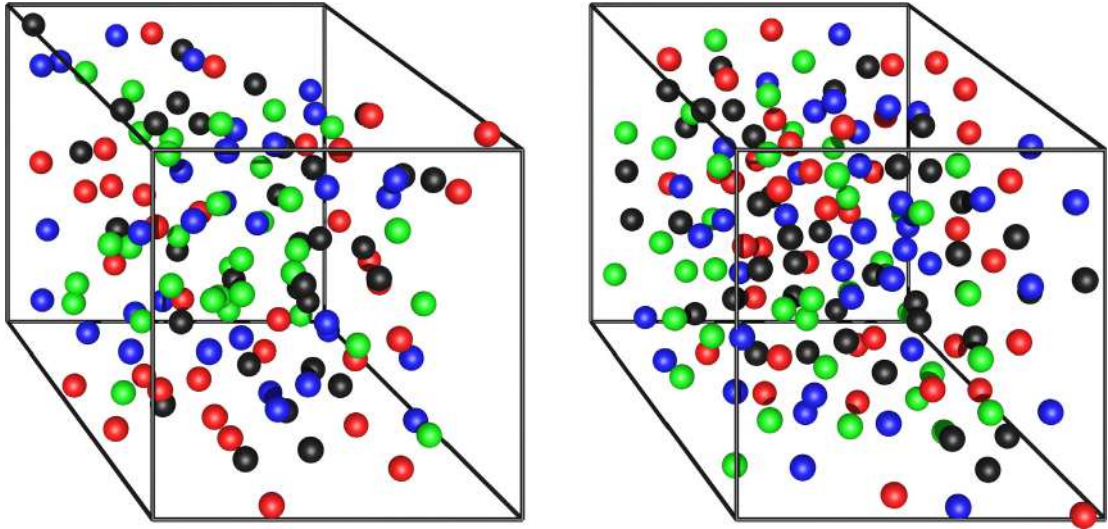


Fig. 24. Two stealthy three-dimensional configurations in a cubic fundamental cell containing $N = 131$ particles with $\chi = 0.1$ (left panel) and $N = 161$ particles with $\chi = 0.4$ (right panel), as adapted from Ref. [41]. As in the analogous two-dimensional cases exhibited in Fig. 23, the system with $\chi = 0.4$ has substantially more short-range order than the one with $\chi = 0.1$. The identical point particles are depicted as finite-sized spheres with different colors for visualization purposes.

or other initial conditions [41]. It turns out that disordered ground-state manifold has many directions in which the landscape is absolutely flat and fully connected [39,190]. Continuous perturbations from these states in configuration space can take the system from one ground state to another energetically degenerate ground state without any energy cost. Notably, while disordered stealthy hyperuniform ground states have positive bulk moduli [40], they cannot resist shear [39,190]. Thus, their Poisson ratios are equal to unity. Indeed, this is true for any $\chi < \chi_{\max}^*$, including those ground states in the ordered regime, except at the unique ground state associated with $\chi = \chi_{\max}^*$ [39,190]. Here χ_{\max}^* is the largest possible value of χ consistent with the stealthy constraint; see Section 8.4.1 for a more precise definition. The energy landscape becomes considerably more complex for $\chi > \chi_{\max}^*$, as discussed in Section 8.4.

More generally, stealthy configurations can be those ground states that correspond to minimizing $S(\mathbf{k})$ to be zero at other sets of wave vectors, not necessarily in a connected set around the origin; see Ref. [38] for specific examples. Of course, when $S(\mathbf{k})$ is not zero around the origin, the ground states are no longer hyperuniform.

8.2. Can disordered stealthy particle configurations tolerate arbitrarily large holes?

A “hole” in a many-particle system in d -dimensional Euclidean space \mathbb{R}^d is defined to be a spherical region of a certain radius that is empty of particle centers. The probability of finding a hole of arbitrarily large size in typical disordered many-particle systems in the infinite-system-size limit (e.g., equilibrium liquid states) is non-zero. Disordered hyperuniform systems could provide examples of disordered systems with bounded hole sizes because the formation of large holes might be inconsistent with hyperuniformity, which suppresses large-scale density fluctuations. However, we know that not all disordered hyperuniform systems prohibit arbitrarily large holes. For example, in a hyperuniform fermionic-point process in d spatial dimensions (see Section 10.2), the hole probability size scales as $\exp[-cr(d+1)]$ (where c is a constant) for large r and for the hyperuniform 2D one-component plasma (see Section 10.3) the hole probability scales as $\exp(-cr^4)$ for large r [196]. Hence, both of these systems allow arbitrarily large holes. Therefore, hyperuniformity alone is not a sufficient condition to guarantee boundedness of the hole size.

However, it is reasonable to conjecture that disordered stealthy systems have bounded hole sizes, since they strongly suppress density fluctuations for a finite range of wavelengths. A recent study presents strong evidence that disordered stealthy configurations across in any dimension cannot tolerate arbitrarily large holes in the infinite-system-size limit, i.e., the hole probability has compact support [43]. It was conjectured that maximum hole size depends inversely on K , and estimates of the corresponding dimension-dependent constant for $d = 1, 2$ and 3 were provided. Ghosh and Lebowitz have provided a rigorous proof of this hole conjecture [197]. This bounded-hole-size property of disordered stealthy systems apparently accounts for their novel thermodynamic and physical properties, including desirable band-gap, optical and transport characteristics [86,87,89,99,104]; see Section 14.

8.3. Configurations with designed hyperuniform structure factors via collective coordinates

The collective-coordinate technique has been applied to target even more general forms of the structure factor for a prescribed set of wave vectors such that the structure factor is not necessarily minimized to be zero in this set, e.g.,

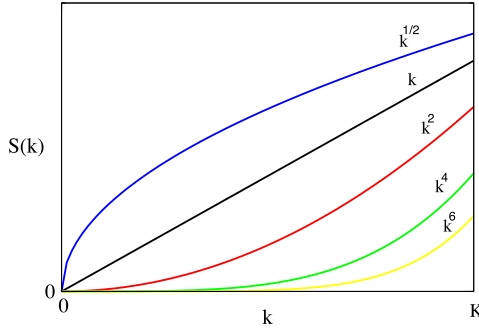


Fig. 25. Target power-law structure factor $S(\mathbf{k}) = |\mathbf{k}|^\alpha$ in the radial interval $0 \leq |\mathbf{k}| \leq K$ for selected values of the exponent α as carried out in Refs. [37] and [139]. The “stealthy” case corresponds to $\alpha \rightarrow \infty$ [36,38].

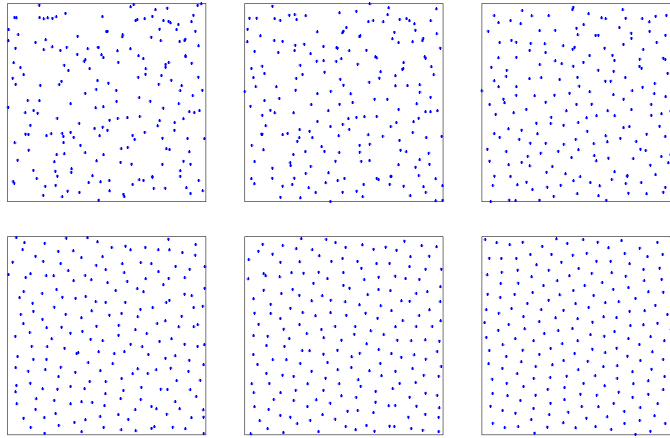


Fig. 26. Configurations of particles in two dimensions with prescribed power-law structure factors $S(\mathbf{k}) = |\mathbf{k}|^\alpha$ for $0 \leq |\mathbf{k}| \leq K$ corresponding to $\alpha = 1/2, 1, 2, 4, 6, \infty$ with $N = 200$ and $\chi = 0.47$. The class III case ($\alpha = 1/2$) is characterized by a large degree of particle clustering. Increasing the exponent α (left to right), increases the short-range order and decreases the tendency for particles to “cluster”. The limit $\alpha \rightarrow \infty$ corresponds to a stealthy hyperuniform disordered state (bottom right).

power-law forms and positive constants, called *equiluminous* systems [37,38,139]. In these more general situations, the resulting configurations are the ground states of interacting many-particle systems with 2-, 3- and 4-body interactions. Note that unlike stealthy ground states, $\chi = 1$ (not $\chi = 1/2$) is the critical value when one runs out of degrees of freedom that can be independently constrained in the large-system limit [40]. Here we briefly describe both underconstrained systems ($\chi < 1$) and so-called “perfect glasses”, which are overconstrained systems ($\chi > 1$).

8.3.1. Underconstrained systems

One can create disordered hyperuniform configurations that correspond to targeted structure factors with the power-law form $S(\mathbf{k}) = |\mathbf{k}|^\alpha$ in the radial interval $0 \leq |\mathbf{k}| \leq K$ for any positive value of the exponent α (see Fig. 25) thereby spanning the three hyperuniformity classes: I, II and III. Configurations corresponding to the targeted power-law structure factors depicted in Fig. 25 are illustrated in Fig. 26. We see that clustering of particles, characteristic of class III systems [37,139], is not inconsistent with hyperuniformity. This provides a vivid counterexample to the notion that the development of hyperuniformity goes hand in hand with the formation of short-range order and vice versa, as was suggested in Ref. [101]. It is seen that as the exponent α increases, short-range order increases and the tendency for particles to “cluster” decreases. All of the cases shown in Fig. 26 are underconstrained systems with $\chi = 0.471$, and hence cannot resist shear stresses [72].

8.3.2. Perfect-glass paradigm

It is well-known that rapid cooling of liquids below a certain temperature range can result in a transition to glassy states of matter that are structurally disordered with long-range order with the mechanical rigidity of a solid [4]. The traditional understanding of glasses includes their thermodynamic metastability with respect to crystals. A singular counterexample to this scenario is the *perfect glass* whereby interactions are designed to completely eliminate the possibilities of crystalline and quasicrystalline phases, while creating mechanically stable *hyperuniform* amorphous glasses down to absolute zero temperature [72]. Since the perfect-glass model completely banishes crystal and quasicrystal formation, it circumvents the

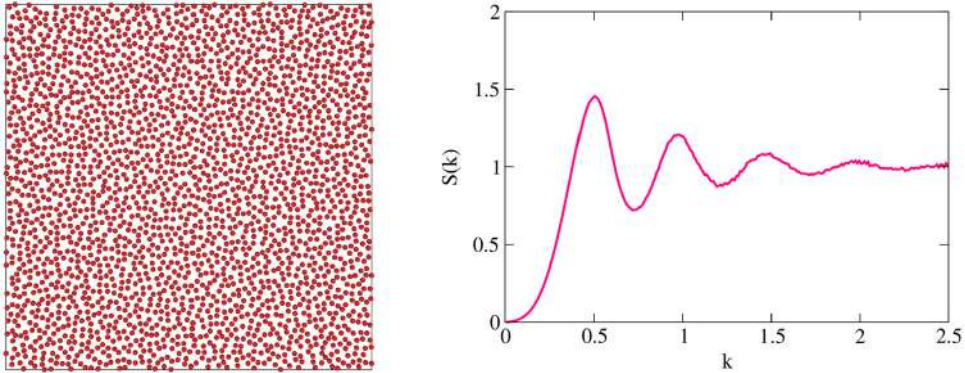


Fig. 27. Left panel: Snapshot of a 2D perfect-glass configuration of 2500 particles in which the structure factor is targeted to be the power-law form $S(\mathbf{k}) = |\mathbf{k}|^2$ with $\chi = 5.1$ and $K = 1$ [72]. Right panel: Resulting optimized structure factor.

Kauzmann paradox [198] in which the extrapolated entropy of a metastable supercooled liquid drops below that of the stable crystal and hence is distinguished from the associated *ideal glass*. Perfect-glass interactions are derived from the collective-coordinate optimization scheme by requiring the structure factor to have disordered hyperuniform power-law forms over a very wide range of wavenumbers around origin (indeed, overconstrained with $\chi > 1$), including values that automatically include all possible Bragg peaks. The resulting two-, three- and four-body interactions enable a perfect glass to resist both compressive and shear deformations. A perfect glass represents a soft-interaction analog of the maximally random jammed (MRJ) packings of hard particles [199,200]; see Section 11.1.2. These latter states can be regarded to be the epitome of a glass, since they are out of equilibrium, maximally disordered, hyperuniform, mechanically rigid with infinite bulk and shear moduli, and can never crystallize (infinitely “frustrated”) due to configuration-space trapping. A novel feature of equilibrium systems of identical particles interacting with a perfect-glass potential at positive temperature is that, due to their hyperuniformity, they have a non-relativistic speed of sound that is infinite.

It has recently been shown that the perfect-glass model possesses disordered classical ground states with an *enumeration entropy* $S_E = k_B \ln(\Omega_E)$ that is zero, where Ω_E is the number of *distinct* accessible structural patterns (aside from trivial symmetry operations) and k_B is the Boltzmann constant. This means that the disordered ground states of perfect glasses, an example of which is depicted in the left panel of Fig. 27, are configurationally unique such that they can always be superposed onto each other or their mirror image. Such “unique” disorder is a highly counterintuitive situation that heretofore had not been identified. Zero-enumeration entropy is normally associated with crystalline classical ground states, and the few previously known disordered classical ground states of many-particle systems are all highly degenerate states, including stealthy disordered ground states [40].

8.4. Ensemble theory for stealthy hyperuniform disordered ground states

The task of formulating an ensemble theory that yields analytical predictions for the structural characteristics and other properties of stealthy degenerate ground states in d -dimensional Euclidean space \mathbb{R}^d is highly nontrivial because the dimensionality of the configuration space depends on the number density ρ and there is a multitude of ways of sampling the ground-state manifold, each with its own probability measure for finding a particular ground-state configuration. Recently, some initial steps have been taken to develop an ensemble theory for stealthy ground states [40]. General exact relations for thermodynamic properties (energy, pressure, and isothermal compressibility) as well as exact conditions that both the ensemble-averaged pair correlation function $g_2(\mathbf{r})$ and ensemble-averaged structure factor $S(\mathbf{k})$ must obey for any d have been derived, which then can be applied to the ground-state of any well-defined stealthy ensemble as a function of ρ in any d .

8.4.1. General results

For a general stable radial pair potential function $v(\mathbf{r})$, it is well-known that the ensemble average of the energy (4) per particle u in the thermodynamic limit can be written in terms of the pair correlation function $g_2(\mathbf{r})$:

$$u \equiv \lim_{N \rightarrow \infty} \left\langle \frac{\Phi_N(\mathbf{r}^N)}{N} \right\rangle = \frac{\rho}{2} \int_{\mathbb{R}^d} v(\mathbf{r}) g_2(\mathbf{r}) d\mathbf{r} \quad (201)$$

where angular brackets denote an ensemble average and ρ is the number density in the thermodynamic limit. Let us now specialize to stealthy potential functions $\tilde{v}(\mathbf{k})$ with support in $0 \leq |\mathbf{k}| \leq K$ of the class specified by Eq. (199). It has been shown [40] that whenever particle configurations in \mathbb{R}^d exist such that $S(\mathbf{k})$ is constrained to achieve its minimum value of

zero for $0 \leq |\mathbf{k}| \leq K$, the system must be at its ground state or global energy minimum, and the average ground-state energy per particle u in any well-defined ensemble is given exactly by

$$u = v_0 \left[\frac{\rho}{2} - \gamma d \rho \chi \right], \quad (\rho_{\min}^* \leq \rho < \infty), \quad (202)$$

where $v_0 \equiv \tilde{v}(\mathbf{k} = \mathbf{0})$ denotes the Fourier-space potential at the origin and $\gamma = (2\pi)^d v(\mathbf{r} = \mathbf{0})/(v_0 v_1(K))$. The relation (202) follows from (201), energy duality relations [201,202], and the aforementioned stealthy conditions on $\tilde{v}(\mathbf{k})$ and $S(\mathbf{k})$. Importantly, the generally degenerate ground-state manifold is invariant to the specific choice of the stealthy function $\tilde{v}(k)$ at fixed ρ and d . Here ρ_{\min}^* is the minimal density associated with the dual of the densest Bravais lattice in direct space (as elaborated below), and $\gamma \in (0, 1]$ is a constant whose value depends on the specific form of the stealthy-potential class, but (as noted above) has no effect on the ground-state manifold. For stealthy potentials, the ground-state pressure p , as obtained from the average energy [$p = \rho^2 (\partial u / \partial \rho)_T$] for all possible values of ρ or χ , is given by the following simple expression:

$$p = \frac{\rho^2}{2} v_0, \quad (\rho_{\min}^* \leq \rho < \infty). \quad (203)$$

Hence, the isothermal compressibility $\kappa_T \equiv \rho^{-1} (\partial \rho / \partial p)_T$ of such a ground state is $\kappa_T = v_0 / \rho^2$. It is seen that as ρ tends to infinity, the compressibility tends to zero. Although the pressure obtained via the “virial relation” [6] is generally expected to be equivalent to that obtained from the energy route, for a certain class of stealthy potentials, the pressure obtained via the viral route may either be ill-defined or divergent [40]. This situation serves to illustrate the mathematical subtleties that can arise because of the long-ranged nature of stealthy potentials in direct space. These general exact relations can be profitably employed to test corresponding computer simulation results.

It is noteworthy that a particular periodic crystal with a finite basis is a stealthy hyperuniform ground state for all positive χ up to its corresponding maximum value χ_{\max} (or minimum value of the number density ρ_{\min}) determined by its first positive Bragg peak $\mathbf{k}_{\text{Bragg}}$ [minimal positive wave vector for which $S(\mathbf{k})$ is positive]. Reference [40] lists the pair χ_{\max} , ρ_{\min} for some common periodic patterns in one, two, three, and four dimensions, all of which are part of the ground-state manifold. At fixed d , we call ρ_{\min}^* the smallest possible value of ρ_{\min} , which corresponds to the density associated with the dual of the densest Bravais lattice in direct space, and represents the critical density value below which a stealthy ground state does not exist for all $k \leq |\mathbf{k}_{\text{Bragg}}^*|$. Correspondingly, χ_{\max}^* is the largest possible value of χ_{\max} . For $d = 1, 2, 3$ and 4, this critical minimal density occurs for the integer lattice ($\rho_{\min}^* = 1/(2\pi) = 0.15915\dots$) [189], triangular lattice ($\rho_{\min}^* = \sqrt{3}/(8\pi^2) = 0.06581\dots$) [36,195], body-centered cubic lattice ($\rho_{\min}^* = 1/(8\sqrt{2}\pi^3) = 0.00285\dots$) [38,195], and D_4 checkerboard lattice ($\rho_{\min}^* = 1/(32\pi^3) = 0.0003208\dots$) [40].

While the fact that periodic structures are part of the ground-state manifold does not provide any clues about their occurrence probability in some ensemble, one can show how their existence leads to disordered degenerate ground states arise as part of the ground-state manifold for sufficiently small χ , as we now briefly outline. It is notable that in the case $d = 1$, there is no non-Bravais lattice (periodic structure with a basis $n \geq 2$) for which χ_{\max} is greater than $1/2$, implying that the ground-state manifold is nondegenerate (uniquely the integer lattice) for $1/2 < \chi \leq 1$ [40]. This case is to be contrasted with the cases $d \geq 2$ where the ground-state manifold must be degenerate for $1/2 < \chi < \chi_{\max}^*$ and nondegenerate only at the point $\chi = \chi_{\max}^*$, as implied by the list of periodic structures summarized in Tables II–IV given in Ref. [40]. The following Lemma, together with the fact that any periodic crystal with a finite basis is a stealthy ground state can be used to demonstrate rigorously how complex aperiodic patterns can be ground states, entropically favored or not [40].

Lemma.—At fixed K , a configuration comprised of the union (superposition) of m different stealthy ground-state configurations in \mathbb{R}^d with $\chi_1, \chi_2, \dots, \chi_m$, respectively, is itself stealthy with a χ value given by

$$\chi = \left[\sum_{i=1} \chi_i^{-1} \right]^{-1}, \quad (204)$$

which is the harmonic mean of the χ_i divided by m .

8.4.2. Pseudo hard spheres in Fourier space and pair statistics

Unlike thermodynamic properties and certain general features of pair statistics, the specific functional forms of $g_2(\mathbf{r})$ and $S(\mathbf{k})$ and other structural functions depend on the stealthy ensemble under consideration [40]. Recently, a statistical-mechanical theory has been formulated in the canonical ensemble in the zero-temperature limit, i.e., the probability of observing a configuration is proportional to $\exp[-\Phi_N(\mathbf{r}^N)/(k_B T)]$ in the limit $T \rightarrow 0$. By exploiting an ansatz that the entropically favored (most probable) stealthy ground states in the canonical ensemble behave like “pseudo” equilibrium hard-sphere systems in Fourier space with an “effective packing fraction” that is proportional to χ , one can employ well-established integral-equation formulations for the pair statistics of hard spheres in direct space [6,115] to obtain accurate theoretical predictions for $g_2(\mathbf{r})$ and $S(\mathbf{k})$ for a moderate range of χ about $\chi = 0$ [40]. To get an idea of the large- r asymptotic behavior of the pair correlations, consider the total correlation function $h(r)$ in the limit $\chi \rightarrow 0$ for any d , which is exactly given by

$$\rho h(r) = - \left(\frac{K}{2\pi r} \right)^{d/2} J_{d/2}(Kr) \quad (\chi \rightarrow 0), \quad (205)$$

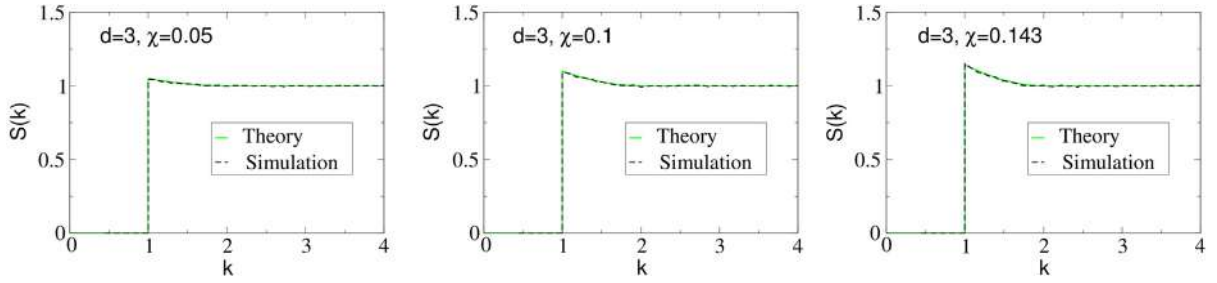


Fig. 28. Comparison of theoretical and simulation results for the radial structure factor $S(k)$ of three-dimensional stealthy systems for $\chi = 0.05, 0.1$, and 0.143 in the canonical ensemble, as taken from Ref. [40]. Here, $K = 1$.

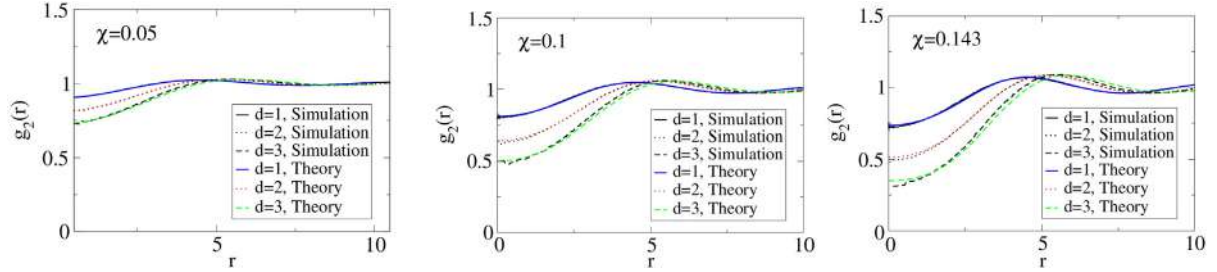


Fig. 29. Comparison of theoretical and simulation results for the radial pair correlation function $g_2(r)$ of stealthy systems for $\chi = 0.05, 0.1$, and 0.143 in the canonical ensemble across the first three space dimensions, as taken from Ref. [40]. Here, $K = 1$.

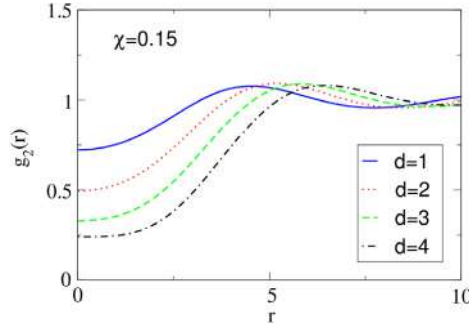


Fig. 30. Theoretical predictions for the radial pair correlation function $g_2(r)$ of stealthy systems for $\chi = 0.15$ in the canonical ensemble across the first four space dimensions, as taken from Ref. [40]. Here $K = 1$.

and for large r is given asymptotically by

$$\rho h(r) \sim -\frac{1}{r^{(d+1)/2}} \cos(r - (d+1)\pi/4) \quad (r \rightarrow +\infty). \quad (206)$$

Thus, the longed-ranged oscillations of $h(r)$ are controlled by the power law $-1/r^{(d+1)/2}$.

Fig. 28 shows that the structure factor $S(k)$ predicted by this pseudo-hard-sphere theory is in excellent agreement with the corresponding simulated quantities for $\chi = 0.05, 0.1$, and 0.143 for $d = 3$ in the case of radial stealthy potentials [40]. In Fig. 29, the theoretical results for the pair correlation function g_2 are compared to corresponding simulation results across the first three space dimensions. Again, we see excellent agreement between theory and simulations, which validates the pseudo-hard-sphere Fourier-space ansatz. Fig. 30 depicts the theoretical predictions for g_2 for $\chi = 0.15$ across the first four space dimensions. It is seen that increasing dimensionality increases short-range correlations.

8.4.3. Number variance and translational order metric τ

The aforementioned analytical results for $g_2(\mathbf{r})$ and $S(k)$ were employed to ascertain other structural characteristics of the entropically favored stealthy disordered ground states, including the local number variance, a new translational order metric τ , and nearest-neighbor functions across dimensions [40]. Fig. 31 compares the local number variance $\sigma^2(R)$ versus

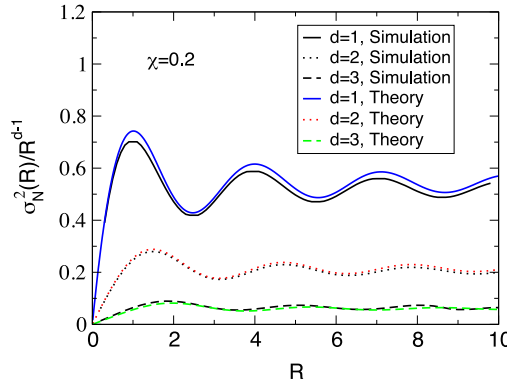


Fig. 31. Comparison of analytical and numerical results for the local number variance $\sigma_N^2(R)$ versus R of stealthy systems for $\chi = 0.2$ across the first three space dimensions, as obtained in Ref. [40]. Here, $K = 1$.

R for $\chi = 0.2$ across the first three space dimensions to corresponding simulation results. It is seen that the theoretical predictions are in good agreement with the simulations.

We have seen that both short- and long-scale correlations increase as χ increases. A useful scalar positive order metric τ that captures the degree to which translational order increases with χ across length scales was proposed in Ref. [40]:

$$\begin{aligned} \tau &\equiv \frac{1}{D^d} \int_{\mathbb{R}^d} h^2(\mathbf{r}) d\mathbf{r} \\ &= \frac{1}{(2\pi)^d D^d} \int_{\mathbb{R}^d} \tilde{h}^2(\mathbf{k}) d\mathbf{k}, \end{aligned} \quad (207)$$

where D denotes some characteristic length scale. Note that for an ideal gas (spatially uncorrelated Poisson point process), $\tau = 0$ because $h(r) = 0$ for all r . Thus, a deviation of τ from zero measures translational order with respect to the fully uncorrelated case. We see that both positive and negative correlations across length scales will make a positive contribution to τ , and hence is expected to be a sensitive detector of ordering in disordered systems. Because τ diverges for any *infinite* perfect crystal, it is a quantity that is better suited to distinguish the degree of pair correlations in amorphous systems. The metric τ has been profitably employed to characterize order in non-stealthy point and spin (or digitized) configurations, including equilibrium hard-disk and hard-sphere systems [104], amorphous ices [84] and binary digitized systems [124]. Note that for systems in the vicinity of liquid–gas and magnetic critical points, the order metric τ is infinitely large due to the fact that the structure factor diverges as $\mathbf{k} \rightarrow \mathbf{0}$ in the infinite-system-size limit. Thus, while caution should be exercised in interpreting τ as an order metric in the vicinity of a thermal critical point, it can be fruitfully employed to detect whether a disordered system is approaching a critical point.

Using the leading-order term in the χ -expansion for either $h(r)$ or $\tilde{h}(k)$ [cf. (205)] and relation (207) yields the following corresponding asymptotic expansion for τ for entropically-favored stealthy disordered ground states [40]:

$$\tau = \frac{4d^2(2\pi)^d}{v_1(1)} \chi^2 + \mathcal{O}(\chi^3), \quad (208)$$

where we have taken $D = K^{-1}$. Thus, for stealthy ground states in the canonical ensemble, the order metric τ grows quadratically with χ for small χ . Since the error is of order χ^3 , it was argued that the formula (208) will be a very good approximation of τ up to relatively large values of χ . Indeed, this is confirmed by simulations up to $\chi \approx 0.45$, as shown in Fig. 32. The dramatic rise of τ (by many orders of magnitude) as χ increases from small values to about $\chi = 0.45$ is a testament to its capacity to detect the increase of short-, intermediate and long-range order as χ increases.

8.4.4. Entropically favored (most probable) states and ground-state manifold

For χ between 0 and $1/2$, stealthy ground states are disordered and possess a configurational dimension per particle $d_C = d(1 - 2\chi)$. At $\chi = 1/2$, the configurational dimensionality per particle collapses to zero, and there is a concomitant phase transition to a stable crystal phase, the nature of which depends on the space dimension [40]. The entropically favored (most probable) ground-state phase diagram is schematically depicted in Fig. 33, which applies to the first four space dimensions in the canonical ensemble in the limit $T \rightarrow 0$. For $d = 1$, the only crystal phase allowed is the integer lattice, and hence there can be no phase coexistence. For $d = 2$, simulations [38,39,41,190] indicate that the stable crystal phase is the triangular lattice for $1/2 \leq \chi \leq \chi_{max}^*$. However, for $d = 3$, it is possible that there may be more than one crystal phase [41,42]. Since four dimensions is more similar to two dimensions in that the lattice corresponding to χ_{max}^* is equivalent to its dual, we would expect that the D_4 lattice is the stable crystal for $1/2 \leq \chi \leq \chi_{max}^*$, but this remains to be confirmed. While the configuration space is fully connected for sufficiently small χ , quantifying its topology as a function of

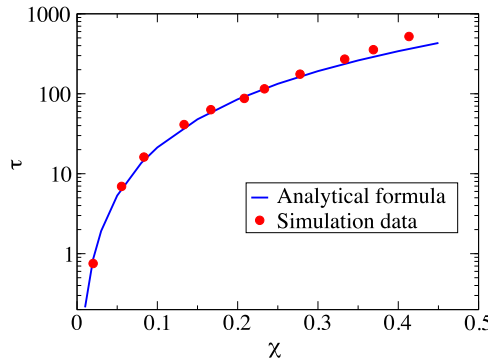


Fig. 32. Comparison of the analytical formula (208) for the τ order metric as a function of χ in three dimensions for entropically favored stealthy disordered ground states to corresponding simulation data obtained in Ref. [104].

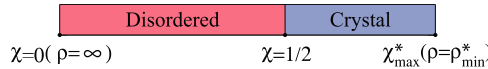


Fig. 33. Phase diagram for the entropically favored (most probable) stealthy ground states in the canonical ensemble as a function of χ , which applies to the first four space dimensions [40].

χ up to χ_{\max}^* is an outstanding open problem. At some intermediate range of χ , the topology of the ground-state manifold undergoes a sequence of one or more disconnection events, but this process is poorly understood and demands future study. In the limit $\chi \rightarrow \chi_{\max}^*$, the disconnection becomes complete at the unique crystal ground state.

The possible configurations that can arise as part of the ground-state manifold for $\chi > 1/2$, regardless of their probability of occurrence, not only include periodic crystals for $d \geq 2$, but also aperiodic structures, reflecting the complex nature of the energy landscape. For example, for some χ above 1/2, so-called “stacked-slider” phases are part of the stealthy ground-state manifold, even if they are not entropically favored. Stacked-slider phases were first discovered numerically from random (e.g., high-temperature) initial configurations in two dimensions in Ref. [36] and were originally called “wavy” crystals because they were observed to consist of particle columns that display a meandering displacement away from linearity. However, “stacked-slider phases” is a more suitable name for this phase for arbitrary space dimensions and this designation will be used henceforth. The authors of Ref. [36] easily distinguished stacked-slider phases from crystal phases by a lack of periodicity in direct space and a lack of Bragg peaks with crystallographic symmetry in its scattering pattern. On the other hand, stacked-slider phases were distinguished from disordered phases by the nature of their scattering patterns outside the exclusion region; specifically, while the structure factors of the former are positive for $|\mathbf{k}| > K$, those of the stacked-slider phases are induced to be zero at some \mathbf{k} ’s outside the exclusion sphere by virtue of the constraints imposed inside this region [36].

Guided by numerical results [36,42], it has recently been shown that stacked-slider phases can be constructed analytically by stacking lower-dimensional stealthy configurations in a higher-dimensional space such that different lower-dimensional “layers” (hyperplanes) can slide (translate) with respect to one another [42]; see two-dimensional examples shown in Fig. 34 and their corresponding scattering patterns in Fig. 35. The fact that the stacking directions are orthogonal to the sliding directions endow stacked-slider phases with unique orientational-order characteristics. More specifically, it was demonstrated that stacked-slider phases are generally nonperiodic, statistically anisotropic structures that possess long-range orientational order but have zero shear modulus [42]. Therefore, they are distinguishable states of matter distinct from stealthy disordered ground states without any Bragg peaks. Since stacked-slider phases are part of the ground-state manifold of stealthy potentials, they are also hyperuniform.

8.4.5. Comparison of stealthy configurations to some common states of matter

Stealthy disordered ground states as well as stealthy stacked-slider phases are distinguishable states of matter that are generally uniquely different from crystals, quasicrystals and some other common states of matter. Table 7 compares these states of matter. Unlike perfect crystals, perfect quasicrystals do not possess long-range translational order. Crystals, quasicrystals, and stacked-slider phases all have long-range orientational order, but with different symmetries. While crystals can only have two-fold, three-fold, four-fold, or six-fold rotational symmetries, quasicrystals have prohibited crystallographic rotational symmetries (e.g., five-fold symmetry in the plane or icosahedral symmetry in three dimensions [29–31]). Disordered stealthy ground states are isotropic and hyperuniform, cannot support shear stresses, and lack long-range translational and orientational order. Stacked-slider phases generally do not have any rotational symmetry, but the fact that their stacking directions are different from the sliding directions endows them with unique orientational order.

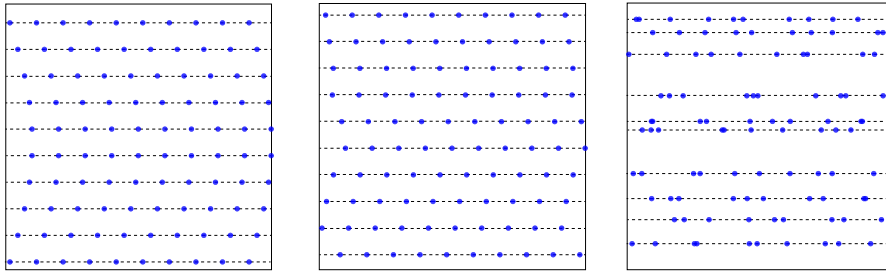


Fig. 34. Three examples of stealthy stacked-slider phases in \mathbb{R}^2 with $N = 100$ that are part of the ground-state manifold, even if not entropically favored. Left panel: Horizontal rows in the square lattice are coherently translated with respect to one another. Here $\chi = \pi/4$. Middle panel: Horizontal rows in the square lattice are randomly translated with respect to one another. Here $\chi = \pi/4$. Right panel: Horizontal stealthy disordered stackings of disordered stealthy 1D configurations. Here $\chi = \pi/18$ and each horizontal row has $\chi = 2/9$.

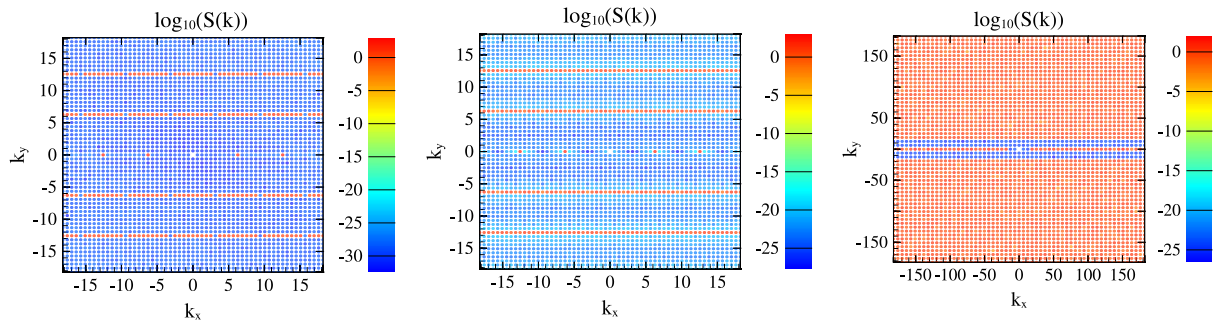


Fig. 35. The scattering patterns corresponding to the configurations to the left, middle and right panels, respectively, shown in Fig. 34. Note that in each example, there are wave vectors in which scattering is suppressed outside the circular exclusion region centered at the origin.

Table 7

Comparison of the properties of some common states of matter, as summarized in Ref. [41]. Here “crystals” and “quasicrystals” signify perfect crystals and perfect quasicrystals, respectively, without any defects (e.g., phonons and phasons). The checks and crosses indicate whether or not different phases have the attributes listed in the first column.

Source: This table is adapted from the one given in Ref. [42].

	Crystals [4,192]	Quasicrystals [29–31]	Stacked-slider phases [36,42]	Disordered stealthy ground states [36–38,40,41]	Typical liquid crystals [203]	Typical liquids [6]
Translational order	✓	✗	✗	✗	✗	✗
Orientational order	✓	✓	✓	✗	✓	✗
Hyperuniformity	✓	✓	✓	✓	✗	✗
Anisotropy	✓	✓	✓	✗	✓	✗
Positive shear modulus	✓	✓	✗	✗	✗	✗

8.4.6. Excited (vibrational) states

One can also derive accurate analytical formulas for the structure factor at the origin $S(\mathbf{k} = 0)$, and thermal expansion coefficient for the excited (vibrational) states associated with stealthy ground states at sufficiently small temperatures. Specifically, for small χ (large ρ) and small T , it has been shown that $S(0)$ varies linearly with T and proportional to χ [40]:

$$S(0) \sim C(d) \chi T, \quad (209)$$

in units $k_B = v_0 = K = 1$, where $C(d) = 2d(2\pi)^d/v_1(1)$ is a d -dependent constant. Fig. 36 shows that the prediction of relation (209) is in excellent agreement with MD simulation results in the case $d = 2$. An interesting conclusion to be drawn from this analysis is that $S(0)$ can be arbitrarily close to zero at positive temperatures when T is arbitrarily small. This means that, for all practical purposes, such systems at positive T are effectively hyperuniform. We remind the reader that perfect hyperuniformity is not necessarily required in order to achieve novel physical properties in technological applications.

Interestingly, at positive temperatures within the harmonic regime, particle systems interacting with isotropic stealthy pair potentials exhibit negative thermal expansion [39,190], which is an unusual behavior for single-component systems with isotropic interactions. When heated at constant pressure, the system attains a density maximum [39,190].

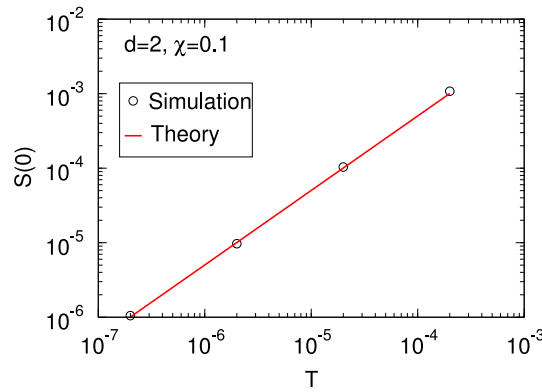


Fig. 36. Comparison of the theoretically predicted structure factor at the origin $S(0)$ versus absolute temperature T , as obtained from Eq. (209), to our corresponding simulation results for a two-dimensional stealthy system at $\chi = 0.1$. Here we take $k_B = v_0 = K = 1$.
Source: This figure is taken from Ref. [40].

9. 1D hyperuniform patterns derived from random matrices, zeta function and prime numbers

It is well known that there are remarkable connections between the statistical properties of certain random matrices, the zeros of the Riemann zeta function, classical Coulomb gases, and fermionic ground states [14,34,76,204–218], all of which can be regarded to be one-dimensional point configurations. These correspondences came to light through a chance meeting between Freeman Dyson and Robert Montgomery during tea time at the Institute for Advanced Study in Princeton, New Jersey in 1972. Underlying each of the aforementioned four seemingly disparate systems are certain one-dimensional disordered point processes whose statistical properties (under certain limits) are believed to be identical. Here we will re-examine these results through the “hyperuniformity lens”, including two other random matrices that are hyperuniform but are not connected to the Riemann zeta function. We conclude this section with some remarks about the unanticipated multiscale hyperuniform order in the prime numbers reported in very recent papers.

9.1. Random matrices and the Riemann zeta function

Random-matrix theory was pioneered by Wigner [204,205] in the 1950’s to model the statistics of the eigenvalues and eigenfunctions of complex many-body quantum systems by studying the spectrum of certain large random matrices. It was more fully developed by Dyson and Mehta in the 1960’s [206,208–211]. Wigner’s original study was concerned with neutron excitation spectra of heavy nuclei. Since this seminal work, random matrices have found applications in a host of fields including quantum chaos [13,219], nuclear physics [220], black holes [221,222], quantitative finance [223,224], complex energy landscapes [225] and number theory [212,216]. There are three prominent theories of random Hermitian matrices that model the Hamiltonians of a wide class of random dynamical systems; see the excellent book by Mehta [14]. If the Hamiltonian is symmetric under time reversal, the relevant theory is that of the Gaussian orthogonal ensemble (GOE), which consists of the sets of all $N \times N$ real symmetric matrices with the unique probability measure that is invariant under orthogonal transformations such that the individual matrix entries are independent random variables. The Gaussian symplectic ensemble (GSE) models Hamiltonians that are symmetric under time reversal but possess no rotational symmetry. The GSE consists of the sets of all $N \times N$ Hermitian quaternionic matrices with the unique probability measure that is invariant under symplectic transformations such that the individual matrix entries are independent random variables. On the other hand, the Gaussian unitary ensemble (GUE), which models random Hamiltonians without time reversal symmetry, is directly relevant to certain properties of the Riemann zeta function as described below. The GUE consists of the set of all $N \times N$ Hermitian matrices together with a Haar measure. This is the unique probability measure on the set of $N \times N$ Hermitian matrices that is invariant under conjugation by unitary matrices such that the individual matrix entries are independent random variables. The *universality conjecture* asserts that the n -particle correlations functions of a large class of random matrices exhibit a bulk universal behavior in the large N -limit depending only on the symmetry class of the matrix ensemble [14,216–218].

Dyson [14,208] showed that the eigenvalue distributions of the GOE, GUE and GSE are given by the Gibbs canonical distribution function $P_N(\mathbf{r}^N)$ that correspond to one-dimensional systems of certain charged point particles at unit number density with positions \mathbf{r}^N contained within an interval of length $L \subset \mathbb{R}$ at certain temperatures, i.e.,

$$P_N(\mathbf{r}^N) = \frac{1}{Z(N, L, T)} \exp[-\beta \Phi_N(\mathbf{r}^N)], \quad (210)$$

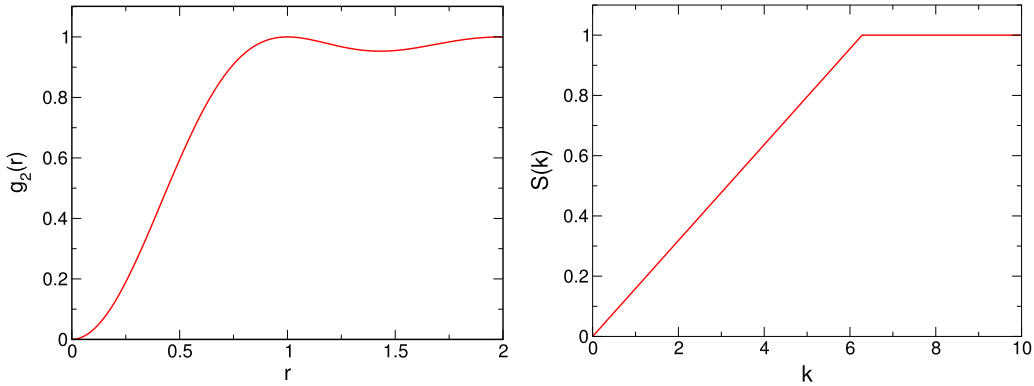


Fig. 37. Left panel: The pair correlation function $g_2(r)$ versus distance r for the eigenvalues of the GUE in the large- N limit, as given by (212), which is conjectured to be the same as the one characterizing the nontrivial zeros of the Riemann zeta function. Noninteracting spin-polarized fermions in their ground state in \mathbb{R} have the same pair correlation function, as will be discussed in Section 10. Right panel: The corresponding structure factor $S(k)$ [cf. (214)], as a function of wavenumber k .

where

$$\Phi_N(\mathbf{r}^N) = \frac{N}{2} \sum_{i=1}^N |\mathbf{r}_i|^2 - \sum_{i < j}^N \ln(|\mathbf{r}_i - \mathbf{r}_j|) \quad (211)$$

is total potential energy of the system, $Z(N, L, T)$ is the canonical partition function, and $\beta = (k_B T)^{-1}$ is a reciprocal temperature. The second term in (211) corresponds to point particles interacting via the two-dimensional repulsive logarithmic Coulomb potential, $v(r) = -\ln(r)$, whereas the first term in (211) is a harmonic potential that confines the charged particles by attracting them towards the origin. In the thermodynamic limit, the eigenvalue distributions of the GOE, GUE and GSE correspond configurationally to these Coulomb gases at reciprocal temperatures $\beta = 1, 2, 4$, respectively [14]. The confinement of the gas by a harmonic potential is absent in the closely related *circular ensembles* originally considered by Dyson.

In the particular case of the GUE in the limit $N \rightarrow \infty$ such that the mean gap distance between eigenvalues in the vicinity of the origin is suitably normalized, the pair correlation function at number density $\rho = 1$ is known exactly:

$$g_2(r) = 1 - \frac{\sin^2(\pi r)}{(\pi r)^2}. \quad (212)$$

The aforementioned normalization has the effect of magnifying the bulk of the eigenvalue density on \mathbb{R} such that (212) is well-defined. We see that this point process is always *negatively correlated*, i.e., $g_2(r)$ never exceeds unity (see Fig. 37) and is “repulsive” in the sense that $g_2(r) \rightarrow 0$ as r tends to zero. In fact, the pair correlation function tends to zero quadratically in r in this asymptotic limit; specifically,

$$g_2(r) = \frac{\pi^2}{3} r^2 - \frac{2\pi^4}{45} r^4 + \mathcal{O}(r^6) \quad (r \rightarrow 0). \quad (213)$$

The corresponding structure factor $S(k)$ for the GUE at unit number density is given by

$$S(k) = \begin{cases} \frac{k}{2\pi}, & 0 \leq k \leq 2\pi \\ 1, & k > 2\pi. \end{cases} \quad (214)$$

We see that structure factor goes to zero linearly in k as wavenumber goes to zero and is equal to unity for $k > 2\pi$. Hence, this one-dimensional point process is perfectly hyperuniform and disordered. This small- k behavior of the structure factor is reflected in a pair correlation whose decay envelope for large r is controlled by the inverse power law $1/r^2$; see the general relations (96) and (97). Clearly, the physical origin of the hyperuniformity of this point process is the long-range Coulombic interactions between the point particles.

It is noteworthy that Dyson [76] proved that the n -particle correlation function for the GUE in the thermodynamic limit is exactly given by the following determinant:

$$g_n(r_{12}, r_{13}, \dots, r_{1n}) = \det \left(\frac{\sin(\pi r_{ij})}{\pi r_{ij}} \right)_{i,j=1,\dots,n}. \quad (215)$$

Thus, the g_n for $n \geq 3$ are entirely determined by the pair correlation function g_2 .

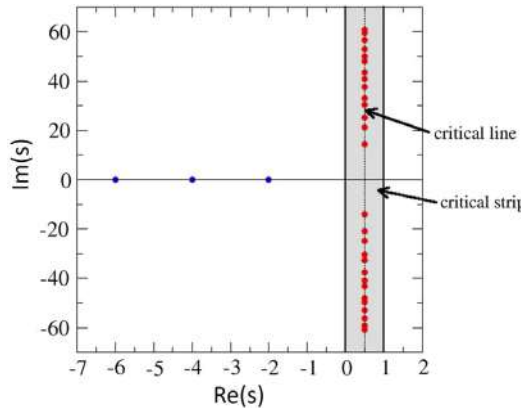


Fig. 38. A schematic of a few of the trivial zeros (blue circles) and nontrivial zeros (red circles) of the Riemann zeta function in the complex plane. It is known that all of the nontrivial zeros must lie in the “critical strip” defined by the open strip” $\{\zeta \in \mathbb{C} : 0 < \operatorname{Re}(\zeta) < 1\}$. Riemann conjectured that all of the nontrivial zeros of the zeta function lie along the critical line $1/2 + it$ with $t \in \mathbb{R}$.

There is a remarkable correspondence between the statistical properties of the eigenvalues of the GUE and those of the nontrivial zeros of the Riemann zeta function $\zeta(s)$. The latter is a function of a complex variable s and can be written as the following infinite series:

$$\zeta(s) = \sum_{n=1}^{\infty} \frac{1}{n^s}, \quad (216)$$

which converges for $\operatorname{Re}(s) > 1$. However, $\zeta(s)$ has a unique analytic continuation to the entire complex plane, excluding the simple pole at $s = 1$. According to the Riemann hypothesis, the nontrivial zeros of the zeta function lie along the critical line $s = 1/2 + it$ with $t \in \mathbb{R}$ in the complex plane; see Fig. 38. Montgomery [212] conjectured that the pair correlation function associated with the nontrivial zeros in the asymptotic limit (high on the critical line), when appropriately normalized, is given exactly by (212), which he did not realize until his chance meeting with Dyson, was identical to the GUE pair correlation. This correspondence was further established by Odlyzko [213], who numerically verified the Riemann hypothesis for the first 10^{13} nontrivial zeros of the zeta function and at much larger heights, and confirmed that its $g_2(r)$ agrees with (212). Rudnick and Sarnak [226] proved that, under the Riemann hypothesis, the nontrivial zeros have n -particle densities for any n given by (215). The reader is referred to the excellent review article by Katz and Sarnak [216], which discusses the connection between the zeros of zeta functions and classical symmetric groups, of which the three canonical random-matrix ensembles are but special cases.

For spin-polarized free fermions in \mathbb{R} (fermion gas) at number density $\rho = 1$, it is known that the pair correlation function in the *ground state* (i.e., completely filling the Fermi “sphere”) is given by

$$g_2(r) = 1 - \frac{\sin^2(k_F r)}{(k_F r)^2}, \quad (217)$$

where k_F is the Fermi radius, which is the one-dimensional analog of the well-known three-dimensional result [215]. Therefore, we see that when $k_F = \pi$, we obtain the GUE pair correlation function (212). The repulsive nature of the point process in this context arises physically from the Pauli exclusion principle. Exact generalizations of these one-dimensional point processes in d -dimensional Euclidean space \mathbb{R}^d for any d are discussed in Section 10.

The suitably normalized pair correlation functions for the GOE and GSE are known analytically [14] and given respectively by

$$g_2(r) = 1 - \frac{\sin^2(\pi r)}{(\pi r)^2} + \frac{1}{2(\pi r)^2} \left(\pi r \cos(\pi r) - \sin(\pi r) \right) \left(2 \operatorname{Si}(\pi r) - \pi \right) \quad (218)$$

and

$$g_2(r) = 1 - \frac{\sin^2(2\pi r)}{(2\pi r)^2} + \frac{1}{4(\pi r)^2} \left(2\pi r \cos(2\pi r) - \sin(2\pi r) \right) \operatorname{Si}(2\pi r), \quad (219)$$

where $\operatorname{Si}(x) \equiv \int_0^x (\sin(t)/t) dt$ is the sine integral. The left panel of Fig. 39 shows that the pair correlation functions for the GOE and GSE exhibit oscillations that are substantially suppressed and amplified, respectively, compared to that of the GUE (see Fig. 37). The small- r and large- r asymptotic behaviors of these pair correlation functions are different from one another and the GUE asymptotic behaviors. While the point particles associated with the GOE and GSE tend to repel one another for

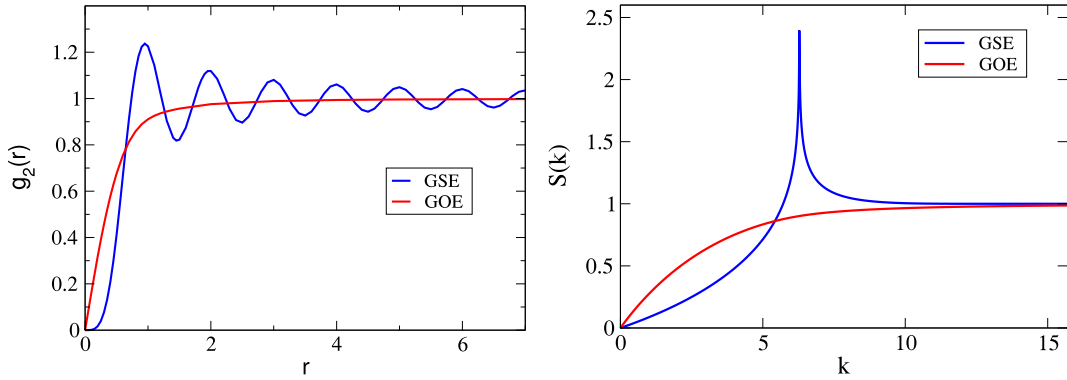


Fig. 39. Left panel: The pair correlation functions for the eigenvalues of the GOE and GSE in the large- N limit, as given by (218) and (219), respectively. Right panel: The corresponding structure factors, as given by (224) and (225).

small r (as they do in the GUE), $g_2(r)$ tends to zero as $r \rightarrow 0$ linearly in r in the former and quartically in r in the latter; more precisely,

$$g_2(r) = \frac{\pi^2}{6}r - \frac{\pi^4}{60}r^3 + \mathcal{O}(r^5) \quad (r \rightarrow 0) \quad (220)$$

and

$$g_2(r) = \frac{16\pi^4}{135}r^4 - \frac{128\pi^6}{4725}r^6 + \mathcal{O}(r^8) \quad (r \rightarrow 0). \quad (221)$$

By contrast, the GUE $g_2(r)$ in the small- r limit tends to zero quadratically, as seen in Eq. (213). Moreover, the large- r asymptotic behaviors for the GOE and GSE are given respectively by

$$g_2(r) = 1 - \frac{1}{(\pi r)^2} + \frac{1 + \cos^2(\pi r)}{(\pi r)^4} - \mathcal{O}\left(\frac{1}{r^6}\right) \quad (r \rightarrow \infty) \quad (222)$$

and

$$g_2(r) = 1 + \frac{\cos(2\pi r)}{4r} - \frac{2 + \pi \sin(\pi r)}{4(\pi r)^2} + \mathcal{O}\left(\frac{1}{r^4}\right) \quad (r \rightarrow \infty). \quad (223)$$

The closed-form exact expressions for the structure factors for the GOE and GSE corresponding to (218) and (219) are respectively given by [14]

$$S(k) = \begin{cases} \frac{k}{\pi} - \frac{k}{2\pi} \ln(k/\pi + 1), & 0 \leq k \leq 2\pi \\ 2 - \frac{k}{2\pi} \ln\left(\frac{k/\pi + 1}{k/\pi - 1}\right), & k > 2\pi. \end{cases} \quad (224)$$

and

$$S(k) = \begin{cases} \frac{k}{4\pi} - \frac{k}{8\pi} \ln(|1 - k/(2\pi)|), & 0 \leq k \leq 4\pi \\ 1, & k > 4\pi. \end{cases} \quad (225)$$

Observe that the GSE structure factor possesses a cusp at $k = 2\pi$, which is to be contrasted with the smooth GOE structure factor; see the right panel of Fig. 39. Moreover, like the GUE structure factor (214), we see that the structure factors of both the GOE and GSE tend to zero linearly in k in the limit $k \rightarrow 0$; specifically

$$S(k) = \frac{1}{\pi}k - \frac{1}{2\pi^2}k^2 + \mathcal{O}(k^3) \quad (k \rightarrow 0) \quad (226)$$

and

$$S(k) = \frac{1}{4\pi}k + \frac{1}{8\pi^2}k^2 + \mathcal{O}(k^3) \quad (k \rightarrow 0). \quad (227)$$

In the opposite large- k asymptotic limit, the GOE structure factor decays to unity like $1/k^2$, i.e.,

$$S(k) = 1 - \frac{\pi^2}{3k^2} + \frac{\pi^4}{5k^4} + \mathcal{O}\left(\frac{1}{k^6}\right) \quad (k \rightarrow \infty) \quad (228)$$

whereas $S(k) = 1$ for any $k > 4\pi$ in the case of the GSE.

The number variance in the large- R limit for any of the three random Hermitian matrices is given by

$$\sigma_N^2(R) = a_\beta \ln(R) + \mathcal{O}(1) \quad (R \rightarrow \infty), \quad (229)$$

where $a_\beta = 2/(\beta\pi^2)$, and $\beta = 1, 2, 4$ for GOE, GUE, and GSE, respectively, and thus they all belong to class II hyperuniform systems such that GSE suppresses density fluctuations to the greatest degree at large R . This logarithmic growth with R is consistent with a structure factor $S(k)$ that tends to zero linearly in k in the small-wavenumber limit; see the general relations (96) and (97).

9.2. Prime numbers

Patterns in the prime numbers have been a source of fascination for millenia. Although the prime numbers are deterministic, they traditionally have been viewed, by a variety of measures, as pseudo-random numbers. For example, in short intervals, say from a large number X to $X + \ln(X)$, Gallagher [227] proved that the spatial distribution of gaps in the primes following a Poisson distribution and hence can be treated as spatially uncorrelated.

On the other hand, it is well known that the prime numbers are directly linked to the zeros of the Riemann zeta function via *explicit* formulas [228]. Thus, one can in principle deduce information about the primes from information about the zeros of the zeta function. Accordingly, one might expect the primes to encode long-range hyperuniform correlations seen in the nontrivial Riemann zeros; see Fig. 37. On the surface, this expectation might seem to contradict Gallagher's results.

This conundrum motivated a very recent study by Zhang, Martelli and Torquato [229] in which the structure factor $S(k)$ for the primes was numerically computed in larger intervals than the ones considered by Gallagher, namely, an interval $[M, M + L]$ with M large (say, 10^{10}) and L/M a small positive number. These simulations strongly suggested that the structure factor in such intervals exhibits many well-defined Bragg-like peaks dramatically overwhelming a small “diffuse” contribution, indicating that the primes are more ordered than previously known. Motivated by this numerical study, recent theoretical studies were undertaken by Torquato, Zhang and de Courcy-Ireland [230,231] to understand the nature of the primes as a point process by quantifying the structure factor, pair correlation function, local number variance, and the τ order metric [cf. Eq. (207)] in various intervals. They considered the primes to be a special ‘lattice-gas’ model: the primes and odd composite integers are “occupied” and “unoccupied” sites, respectively, on an integer lattice of spacing 2 that contains all of the positive odd integers. Their main results were obtained for primes in the interval $[M, M + L]$ with M very large and the ratio L/M held constant, which enables one to treat them as a homogeneous point pattern. In Ref. [231], these authors used the Hardy–Littlewood circle method [232] to prove that the primes numbers in this regime are hyperuniform with unanticipated order on multiple length scales with pure point diffraction. Remarkably, the limiting form of the structure factor for the primes is characterized by dense Bragg peaks, like a quasicrystal, but positioned at certain rational wavenumbers, like a limit-periodic point pattern [233]. However, the primes show an erratic pattern of occupied and unoccupied sites, very different from the predictable and orderly patterns of standard limit-periodic systems. Therefore, the primes are the first example of a point pattern that is *effectively* limit-periodic. The discovery of this hidden multiscale order in the primes is in contradistinction to their traditional treatment as pseudo-random numbers. Effective limit-periodic systems represent a new class of many-particle systems with pure point diffraction patterns that deserve future investigation in physics, apart from their connection to the primes.

Torquato, Zhang and de Courcy-Ireland [230,231] also considered appreciably larger and smaller intervals for purposes of comparison. Using the τ order metric, they identified a transition between the order exhibited when L is comparable to M and the uncorrelated behavior when L is only logarithmic in M .

10. Hyperuniform determinantal point processes

One class of disordered point processes that exhibits exact hyperuniformity is *determinantal point processes*, which are characterized by a joint probability distribution given by the determinant of a finite-rank, positive, bounded, and self-adjoint operator. Determinantal point processes were introduced by Macchi [234], who originally called them fermion point processes because they are rooted in quantum fermionic statistics. Soshnikov [235] presented a review of this subject and discussed applications to random matrix theory, statistical mechanics, quantum mechanics, and representation theory. Examples of determinantal point processes arise in uniform spanning trees [236], self-avoiding random walks [237] and random polynomials [238], and have been reported both on the real line [34,239–241] and in higher Euclidean space dimensions [34,141,241].

10.1. General considerations

In what follows, we briefly review the mathematics of determinantal point processes. Without loss of generality, the number density is set to unity ($\rho = 1$) in the ensuing discussion. Let $H(\mathbf{r}) = H(-\mathbf{r})$ be a translationally invariant Hermitian-symmetric kernel of an integral operator \mathcal{H} . A translationally invariant *determinantal point process* in \mathbb{R}^d exists if the n -particle density functions for $n \geq 1$ are given by the following determinants:

$$\rho_n(\mathbf{r}_{12}, \mathbf{r}_{13}, \dots, \mathbf{r}_{1n}) = \det[H(\mathbf{r}_{ij})]_{i,j=1,\dots,n}. \quad (230)$$

By virtue of the nonnegativity of the ρ_n in the pointwise sense [cf. (2) and (230)], it follows that \mathcal{H} must have nonnegative minors and \mathcal{H} must be a nonnegative operator, which implies that $H(\mathbf{r})$ is positive semidefinite. The latter implies that the Fourier transform $\tilde{H}(\mathbf{k})$ of the kernel $H(\mathbf{r})$ is nonnegative. In particular, let

$$0 \leq \tilde{H}(\mathbf{k}) \leq 1 \quad \text{for all } \mathbf{k}, \quad (231)$$

and $H(\mathbf{0}) = 1$, implying the sum rule

$$\frac{1}{(2\pi)^d} \int_{\mathbb{R}^d} \tilde{H}(\mathbf{k}) d\mathbf{k} = 1. \quad (232)$$

It follows that a Fourier transform $\tilde{H}(\mathbf{k})$ that satisfies the inequalities (231) and sum rule (232) describes a determinantal point process with a pair correlation function $g_2(\mathbf{r})$ given by

$$g_2(\mathbf{r}) = 1 - |H(\mathbf{r})|^2, \quad (233)$$

such that

$$0 \leq g_2(\mathbf{r}) \leq 1 \quad \text{and} \quad g_2(\mathbf{0}) = 0, \quad (234)$$

and a n -particle density function given by (230). We see that the total correlation function is given by $h(\mathbf{r}) = -|H(\mathbf{r})|^2$ and therefore the corresponding structure factor is given by

$$S(\mathbf{k}) = 1 - \mathcal{F}[|H|^2](k), \quad (235)$$

where \mathcal{F} denotes the Fourier transform. To obtain a hyperuniform determinantal point process specified by some $H(\mathbf{r})$ that satisfies the aforementioned conditions, it is necessary and sufficient that $\tilde{H}(\mathbf{k})$ be an indicator function of a set ω in \mathbf{k} -space, i.e., $\tilde{H}(\mathbf{k}) = 1$ for $\mathbf{k} \in \omega$ and $\tilde{H}(\mathbf{k}) = 0$ otherwise [239].

10.2. Fermi-sphere point processes

The so-called Fermi-sphere point process [34] provides a d -dimensional generalization of the one-dimensional point processes corresponding to the eigenvalues of the GUE, the zeros of the Riemann zeta function or the fermionic gas, all of which were described in Section 9. This disordered hyperuniform point process belongs to class II and corresponds exactly to the one associated with the ground state of a noninteracting spin-polarized fermions in which the Fermi sphere is completely filled. The d -dimensional Fermi-sphere point process is a special determinantal point process obtained by taking $\tilde{H}(\mathbf{k})$ to be the indicator function of a (Fermi) sphere of radius $K = 2\sqrt{\pi} [\Gamma(1 + d/2)]^{1/d}$ [34]. This means that the n -particle densities given by (230) have a squared kernel $|H(\mathbf{r})|^2 = \tilde{\alpha}_2(r; K)/(2\pi)^d$ and hence, using (233), the pair correlation function of such a point process at unit density is given by

$$g_2(\mathbf{r}) = 1 - 2^d \Gamma(1 + d/2)^2 \frac{J_{d/2}^2(Kr)}{(Kr)^d}. \quad (236)$$

Moreover, the corresponding structure factor takes the form

$$S(\mathbf{k}) = 1 - \alpha_2(k; K), \quad (237)$$

where $\alpha_2(k; K)$ is the scaled intersection volume of two d -dimensional spheres of radius K separated by a distance k , i.e., the function $\alpha_2(r; R)$, specified by (52), with the replacements $r \rightarrow k$ and $R \rightarrow K$. It follows from the properties of $\alpha_2(k; K)$ in (237) that the structure factor $S(\mathbf{k})$ obeys the bounds $0 \leq S(\mathbf{k}) \leq 1$ for all \mathbf{k} , and achieves its maximum value of unity for $|\mathbf{k}| \geq 2K$.

Fig. 40 shows the pair statistics in both real and Fourier space for $d = 1$ and $d = 3$ at unit density. Perfect hyperuniformity is manifest in the small-wavenumber behavior of the structure factors. In both one and three dimensions, the point particles tend to repel one another, as reflected by the fact that $g_2(r) \rightarrow 0$ as r tends to zero. We also see that the amplitudes of the oscillations in $g_2(r)$ that are apparent for $d = 1$ are significantly reduced in the corresponding three-dimensional pair

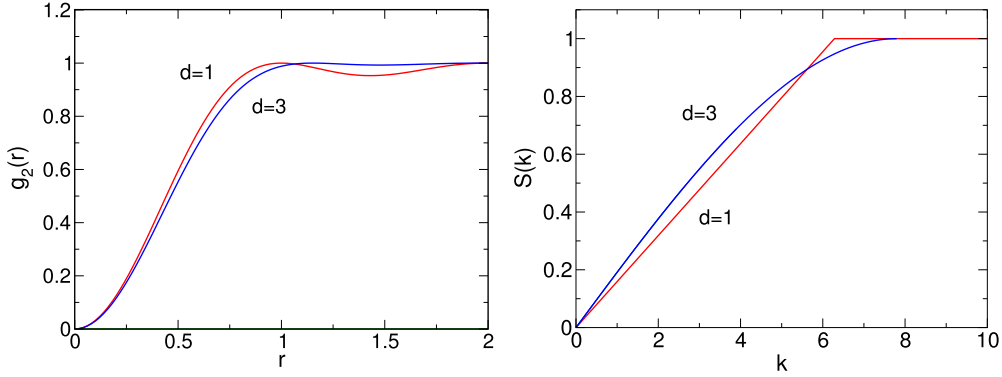


Fig. 40. Results for fermionic-sphere point processes. Left panel: Comparison of the pair correlation functions for $d = 1$ and $d = 3$, as obtained from (236). Right panel: The corresponding structure factors, as obtained from (237), tend to zero as $k \rightarrow 0$ linearly in k , and hence exhibit exact hyperuniformity within class II.

Source: These figures are adapted from those given in Ref. [34].

correlation function. By virtue of the asymptotic properties of the Bessel function of arbitrary order, the small- r and large- r forms of the pair correlation function (236) are respectively given by

$$g_2(r) = \frac{K^2}{d+2} r^2 - \frac{(d+3)K^4}{2(d+2)^2(d+4)} r^4 + \mathcal{O}(r^6) \quad (r \rightarrow 0) \quad (238)$$

and

$$g_2(r) = 1 - \frac{2\Gamma(1+d/2)\cos^2(rK - \pi(d+1)/4)}{K \pi^{d/2+1} r^{d+1}} \quad (r \rightarrow \infty). \quad (239)$$

We see that $g_2(r)$ tends to zero quadratically in r in the limit $r \rightarrow 0$, independent of the dimension. Moreover, $g_2(r)$ tends to unity for large pair distances with a decay rate that is controlled by the power law $-1/r^{d+1}$ for any $d \geq 1$, and hence the corresponding structure factor $S(k)$ at $\rho = 1$ tends to zero linearly in k in the limit $k \rightarrow 0$ such that

$$S(k) = \frac{c(d)}{2K} k + \mathcal{O}(k^3) \quad (k \rightarrow 0), \quad (240)$$

where $c(d)$ is a d -dependent positive constant given by (53). Hence, Fermi-sphere point processes belongs to class II hyperuniform systems (see Section 5.3). Generalizations of this determinantal process, called *Fermi-shells* point processes, also belong to class II [34].

It is notable that Fermi-sphere point processes in the high- d asymptotic limit can be characterized by an effective “hard-core” diameter that grows like the square root of d [34]. Moreover, in the high- d limit, the point process behaves effectively like a sphere packing with a coverage fraction of space that is no denser than $1/2^d$. This coverage fraction has a special significance in the study of sphere packings in high-dimensional Euclidean spaces, including Minkowski’s lower bound on the density of the densest lattice sphere packings [242] as well as exactly solvable disordered sphere-packing models [128,243].

Using (236) into (44), it has been shown [34] that the number variance $\sigma_N^2(R)$ for a spherical window of radius R of Fermi-sphere point processes in any dimension d for large R grows like

$$\sigma_N^2(R) = \frac{d\pi^{(d-4)/2}}{2\Gamma[(d+1)/2]\Gamma(1+d/2)^{1/d}} \ln(R)R^{d-1} + \mathcal{O}(R^{d-1}) \quad (R \rightarrow \infty). \quad (241)$$

This class-II hyperuniform growth law in three dimensions also arises in maximally random jammed sphere packings [46], which can be viewed as prototypical glasses because they are simultaneously perfectly mechanically rigid, maximally disordered and perfectly nonergodic. Since the coefficient multiplying $\ln(R)$ in (241) decays to zero exponentially fast as $d \rightarrow \infty$, the surface-area term R^{d-1} increasingly becomes the dominant one in the large- d limit.

Fig. 41 depicts realizations of the Fermi-sphere point processes in one and two dimensions, which were generated using an algorithm devised by Scardicchio, Zachary and Torquato [126] that was based on a formal description given by Hough et al. [244]. The reader is referred to Ref. [126] for details and applications of this algorithm.

It is noteworthy that the nearest-neighbor distribution functions for Fermi-sphere point processes were also evaluated and rigorously bounded [34]. Nearest-neighbor probability density functions give the probability of finding a nearest-neighbor point within some differential annulus a radial distance r around some reference position. The associated complementary cumulative functions give the probability of finding spheres of radius r centered at some reference position empty of any points, which are sometimes referred to as “hole” probabilities. Among other results, it was shown that the probability of finding a large spherical cavity of radius r in a d -dimensional Fermi-sphere point process behaves like a Poisson

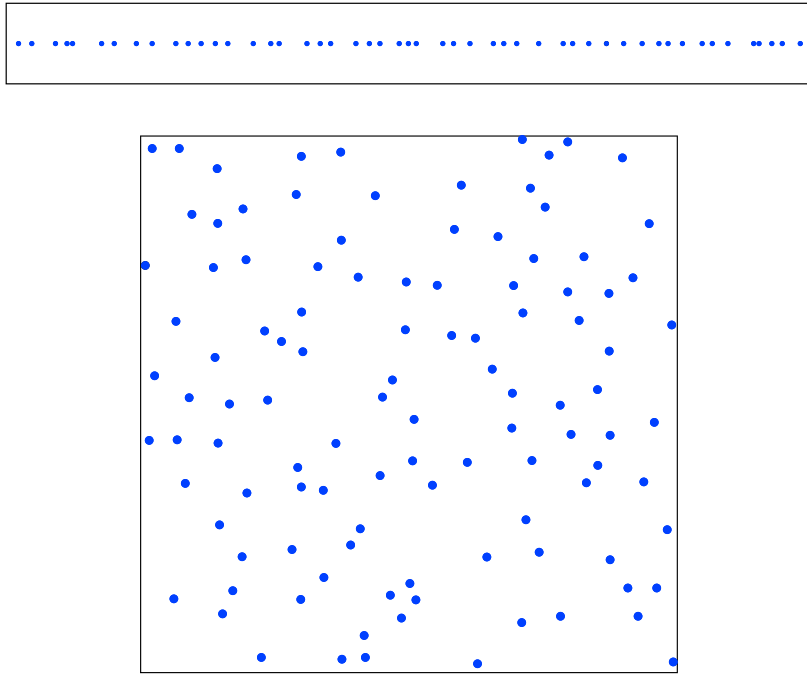


Fig. 41. Top panel: A realization of 50 points of a Fermi-sphere point process in a linear “box” subject to periodic boundary conditions generated from the algorithm described in Ref. [126]. Bottom panel: A realization of 100 points of a Fermi-sphere point process in a square box subject to periodic boundary conditions generated from the algorithm described in Ref. [126].

point process but in dimension $d + 1$, i.e., this probability is given by $\exp[-\kappa(d)r^{d+1}]$ for large r and finite d , where $\kappa(d)$ is a positive d -dependent constant.

Finally, we note that superfluid helium at zero temperature possesses a structure factor $S(\mathbf{k})$ equal to $\hbar |\mathbf{k}|/(mc)$ in the zero-wavenumber limit [74,147], where m is the mass of a helium molecule and c the speed of propagation of the phonons. Hence, this strongly interacting system of bosons in its ground state is hyperuniform of class II, as are spin-polarized free fermions as well as maximally random jammed packings of disks and spheres [46,48,52,53,121] and of nonspherical particles [49,51,121] via either $S(\mathbf{k})$ or the spectral density $\tilde{\chi}_V(\mathbf{k})$.

10.3. Two-dimensional Ginibre ensemble: one-component plasma

An example of a two-dimensional determinantal point process that exhibits hyperuniform behavior is generated by the Ginibre ensemble (corresponding to the complex eigenvalues of random complex matrices with independent Gaussian entries) [245], which is a special case of the so-called two-dimensional one-component plasma [35,149,179–187]. A one-component plasma (OCP) is an equilibrium system of identical point particles of charge e interacting via the log Coulomb potential and immersed in a rigid, uniform background of opposite charge to ensure overall charge neutrality, i.e., the total system potential energy is given by

$$\Phi_N(\mathbf{r}^N) = N \sum_{i=1}^N V(\mathbf{r}_i) - \sum_{i < j}^N \ln(|\mathbf{r}_i - \mathbf{r}_j|), \quad (242)$$

where $V(\mathbf{r})$ is the background potential and we set $e = 1$. For $\beta = 2$, the total correlation function for the OCP (Ginibre ensemble) in the thermodynamic limit has been ascertained exactly by Jancovici [149]:

$$h(r) = -\exp(-\rho\pi r^2). \quad (243)$$

This faster-than-exponential decay of $h(r)$ demonstrates that *quasi-long-ranged correlations* (power-law decays faster than $1/r^d$) are not required for a disordered system to be hyperuniform. Fig. 42 shows a finite configuration (under periodic boundary) for this case generated in Ref. [32] using the algorithm presented in Ref. [244] and elaborated in Ref. [241]. The corresponding structure factor is given by

$$S(k) = 1 - \exp\left(-\frac{k^2}{4\pi\rho}\right) \quad (244)$$

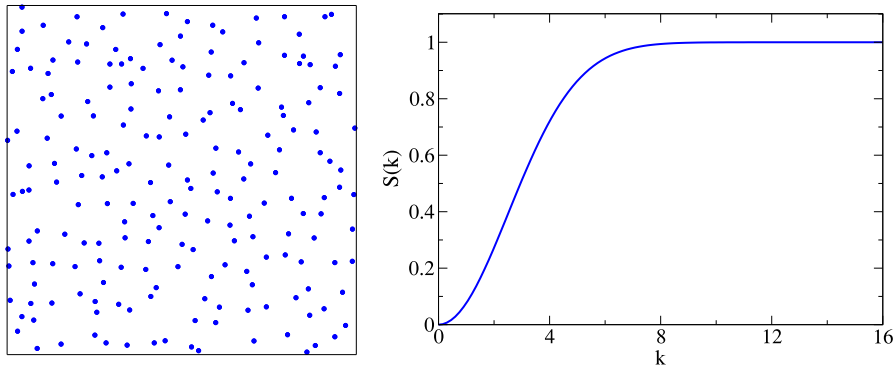


Fig. 42. Left panel: A realization of a point process generated from the Ginibre ensemble [245], which corresponds to the two-dimensional one-component plasma with $\beta = 2$ [32]. Right panel: The corresponding structure factor in the infinite-size limit at unit number density. Notice that, unlike the fermionic-sphere point processes (see Fig. 40), the structure factor is analytic everywhere and, in particular, goes to zero quadratically in k as $k \rightarrow 0$.

(see Fig. 42) and hence is analytic everywhere, in contrast to the fermionic-sphere structure factor, which is nonanalytic at $k = 0$ and $k = K$ in any d (see Section 10.2). Therefore, this system is hyperuniform with the following smooth small- k behavior:

$$S(k) \sim k^2 \quad (k \rightarrow 0). \quad (245)$$

According to Section 7.1, relation (245) implies that the Fourier transform of the direct correlation function is singular at the origin such that

$$\tilde{c}(k) \sim -\frac{1}{k^2} \quad (k \rightarrow 0), \quad (246)$$

the nonintegrability of which is a reflection of the long-ranged nature of the Coulomb interaction in (242), which is consistent with asymptotic logarithmic large-distance behavior of the direct correlation function $c(r)$ indicated in relation (163), i.e.,

$$c(r) = -\beta v(r) \sim \ln(r) \quad (r \rightarrow \infty). \quad (247)$$

The scaling laws (245) and (246) apply as well to the OCP in three and higher dimensions, and thus lead to the expected large- r Coulombic scaling laws for the direct correlation function and effective pair interactions for $d \geq 3$:

$$c(r) = -\beta v(r) \sim -\frac{1}{r^{d-2}} \quad (r \rightarrow \infty), \quad (248)$$

Thus, according to Section 5.3, OCP systems for $d \geq 2$, fall in class I hyperuniform systems. Notice that since the step-function g_2 -invariant processes are characterized by the same scaling laws for $S(k)$ and $\tilde{c}(k)$, the corresponding asymptotic scaling for the direct correlation function $c(r)$ is also purely Coulombic, as indicated in relation (183).

It bears re-emphasizing that the OCP provides a critical lesson, namely, point patterns do not need to possess quasi-long-ranged pair correlations in order to be hyperuniform, as evidenced by the Gaussian form of the total correlation function (243). Note that OCP fluid phases at other temperatures must always be hyperuniform because, due to overall charge neutrality with a rigid background, the reduced charge fluctuations are in correspondence with number fluctuations, both of which grow like the window surface area. Interestingly, the probability of finding a large spherical cavity of radius r in the 2D OCP behaves like a Poisson point process but in dimension four, i.e., this “hole” probability is given by $\exp(-cr^4)$ for large r [196].

Combination of either (59) and (243) or (60) and (244) exactly yields the local number variance for the 2D OCP with $\beta = 2$ to be

$$\sigma_N^2(R) = \pi R^2 \exp(-2\pi R^2) [I_0(2\pi R^2) + I_1(2\pi R^2)], \quad (249)$$

where $I_\nu(x)$ is a modified Bessel function of order ν . The corresponding large- R asymptotic behavior of the number variance is given by

$$\sigma_N^2(R) = R - \frac{1}{16\pi R} + \mathcal{O}\left(\frac{1}{R^3}\right) \quad (R \rightarrow \infty). \quad (250)$$

The local number variance rapidly saturates to its asymptotic value, as shown in Fig. 43.

We remark that Laughlin’s celebrated ansatz for the ground state wave function associated with the fractional quantum Hall effect is tantamount to a mapping to a classical 2D OCP in which the charges depend on the filling fraction [246]. Notably, Sandier and Serfaty [184] have rigorously established a link between the Ginzburg–Landau model for vortices in

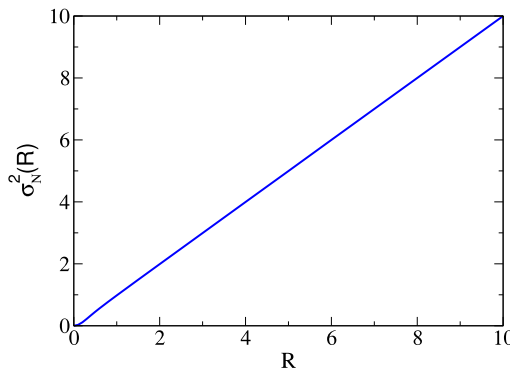


Fig. 43. The local number variance $\sigma^2(R)$ versus R for the 2D OCP, as given by (249). It is noteworthy that the large- R asymptotic limit of R [see relation (250)] is achieved at very small values of R (say $R > 1$).

superconductors in the critical regime and the 2D OCP. Here the interaction between the vortices is well-described by a 2D OCP in which the background potential $V(\mathbf{r}) = |\mathbf{r}|^2$.

Finally, we comment on superionic phases, including superionic ice [247], which is a special group of ice phases at high temperatures and pressures that may exist in ice-rich planets and exoplanets. In superionic ice, “liquid” hydrogen ions can coexist with a relatively rigid crystalline oxygen sublattice of opposite charge. Thus, it is expected that OCPs can be well-approximated by superionic ice under appropriate conditions. Recent evidence has emerged that this is indeed the case by virtue of the fact that the liquid hydrogen phase is nearly hyperuniform as measured by the structure factor [248]. Other solid-state superionic conductors at ambient temperatures and pressure, such as silver iodide (AgI) [249,250] used in batteries and sensors, should exhibit near hyperuniformity for the same reasons.

10.4. Weyl–Heisenberg ensemble

The infinite Weyl–Heisenberg ensemble is a class of determinantal point processes associated with the Schrödinger representation of the Heisenberg group. It has recently been proved that such determinantal point processes are perfectly hyperuniform [141]. This provides another class of examples of d-dimensional determinantal point processes that are hyperuniform beyond the aforementioned Fermi-type varieties [34,241]. It was also proved there that the number variance $\sigma_N^2(R)$ associated with a spherical observation window of radius R grows like the surface area of the window, i.e., as R^{d-1} , and hence are hyperuniform of class I. Explicit formulas for the corresponding total correlation functions $h(\mathbf{r})$ were obtained; they exhibit a large- $|\mathbf{r}|$ decay that is faster than exponential; specifically, like a Gaussian [141]. In the radial case, the structure factor $S(\mathbf{k})$ near the origin tends to zero quadratically in $|\mathbf{k}|$ in all space dimensions, and thus exhibits the same behavior as the Ginibre ensemble in two dimensions. We note that the Weyl–Heisenberg ensemble includes as a special case a multi-layer extension of the Ginibre ensemble modeling the distribution of electrons in higher Landau levels, which has recently been the object of study in the realm of the Ginibre-type ensembles associated with polyanalytic functions [251]. Moreover, this family of Weyl–Heisenberg ensembles includes new structurally anisotropic processes, and thus provides a rigorous means to explore “directional” hyperuniformity, which is a recent generalization of the hyperuniformity concept that is reviewed in Section 13.4.

10.5. Multicomponent hard-sphere plasmas

It has recently been recognized that multicomponent equilibrium plasmas made of *nonadditive* hard spheres with Coulombic interactions enable one to generate a very wide class of disordered hyperuniform as well as multihyperuniform systems at positive temperatures [44,45]. It is the infinite parameter space (particle size distribution, composition and non-additivity parameter) and long-ranged interactions afforded by them that provides greater tunability to achieve hyperuniform states. Specific theoretical and computational results have been obtained for two-component non-additive hard-disk plasmas in two dimensions [44,45]. In the case of multihyperuniform two-component hard-disk plasmas, it was shown that multihyperuniformity competes with phase separation and stabilizes a clustered phase [45].

11. Classical nonequilibrium systems

In this section, we report on a variety of disordered nonequilibrium systems that are putatively hyperuniform according to numerical/experimental protocols and analyses. Specifically, we describe the hyperuniformity characteristics of ordered and disordered jammed particle systems [27,48,50,52–54,56–59,121,252] and absorbing-state models [62–69].

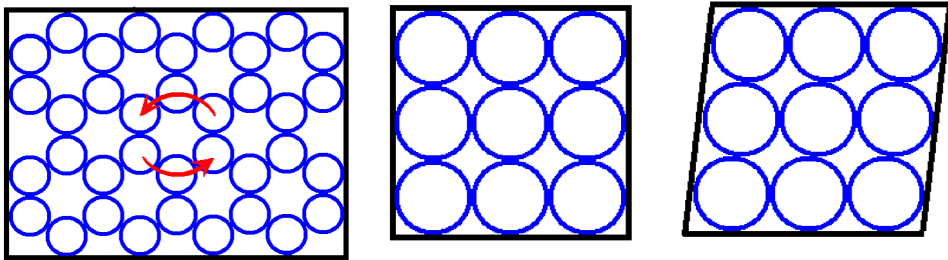


Fig. 44. Illustrations of jamming categories taken from Ref. [200]. Leftmost panel: The honeycomb-crystal packing within a rectangular hard-wall container is locally jammed, but is not collectively jammed (e.g., a collective rotation of a hexagonal particle cluster, as shown, will unjam the packing). Middle panel: Square-lattice packing within a square hard-wall container is collectively jammed. Rightmost panel: The square-lattice packing shown in the middle panel can be sheared and hence is not strictly jammed. Thus, we see that the square-lattice packing with square hard-wall boundary conditions can only be collectively jammed even in the infinite-volume limit.

11.1. Ordered and disordered jammed particle packings

Understanding the characteristics of jammed particle packings provides basic insights into the structure and bulk properties of crystals, glasses, and granular media and selected aspects of biological systems [200,253]. A *packing* is a large collection of hard (nonoverlapping) particles in either a finite-sized container or in d -dimensional Euclidean space \mathbb{R}^d [200,254]. Recall that the packing fraction ϕ is the fraction of space covered by the hard particles. “Jammed” packings are those particle configurations such that each particle is in contact with its nearest neighbors so that mechanical stability of a specific type is conferred to the packing, as defined more precisely below. Jammed packings have received considerable attention in the theoretical and experimental literature [48,55–58,200,253,255–265].

Preliminary results in 2003 indicated that disordered jammed packings of spheres exhibited hyperuniform behavior [27], which at that time was regarded to be a highly exotic large-scale property of a hard-sphere system. This result suggested a link between a certain class of jammed states and hyperuniformity. The most natural theoretical framework to understand this connection is the “geometric-structure” approach, which emphasizes the quantitative characterization of single-packing configurations without regard to their occurrence frequency in the algorithmic method used to produce them; see Ref. [200] and references therein. While a comprehensive review of this literature is beyond the scope of the present article, we briefly review those aspects of the geometric-structure approach that will aid in understanding the conditions under which jamming and hyperuniformity may or may not be linked.

11.1.1. Jamming categories

Much of the ensuing discussion focuses on packings of frictionless identical hard spheres in the absence of gravity. Three broad and mathematically precise hierarchical “jamming” categories of sphere packings can be distinguished depending on the nature of their mechanical stability [256,266]. In order of increasing stringency (stability), for a finite sphere packing, these are the following:

1. *Local jamming*: Each particle in the packing is locally trapped by its neighbors (at least $d + 1$ contacting particles, not all in the same hemisphere), i.e., it cannot be translated while fixing the positions of all other particles;
2. *Collective jamming*: Any locally jammed configuration in which no subset of particles can simultaneously be displaced so that its members move out of contact with one another and with the remainder set fixed; and
3. *Strict jamming*: Any collectively jammed configuration that disallows all uniform volume-decreasing strains of the system boundary is strictly jammed, implying that their bulk and shear moduli are infinitely large [266].

Importantly, the jamming category of a given sphere packing depends on the boundary conditions employed [123,256,266,267]. For example, hard-wall boundary conditions [256] generally yield different jamming classifications from periodic boundary conditions [267]. These jamming categories, which are closely related to the concepts of “rigid” and “stable” packings found in the mathematics literature [254], requires that the packing possesses no “rattlers”, which are particles that are free to move about their respective confining cages [200,268].

Fig. 44 shows examples of ordered locally and collectively jammed packings of circular hard disks in two dimensions within hard-wall containers. The honeycomb-crystal packing ($\phi = \pi/3^{3/2} = 0.605 \dots$ in the infinite-size limit) is only locally jammed because there are collective particle motions that will lead to its collapse, suggesting that there exist particle rearrangements and motions of the container boundary that can lead to collectively or strictly packings with a higher density. Such a densification process starting with the original *unsaturated* honeycomb packing could be accomplished, for example, using an “adaptive-shrinking-cell” optimization scheme [269,270]. A *saturated* packing of hard spheres is one in which there is no space available to add another sphere. Fig. 44 also shows that while the square-lattice packing within a hard-wall container ($\phi = \pi/4 = 0.785 \dots$ in the infinite-size limit) is collectively jammed, implying that it can be sheared to yield a denser packing that is strictly jammed, e.g., the triangular lattice packing (with $\phi = \pi/\sqrt{12} = 0.907 \dots$ in the infinite-size

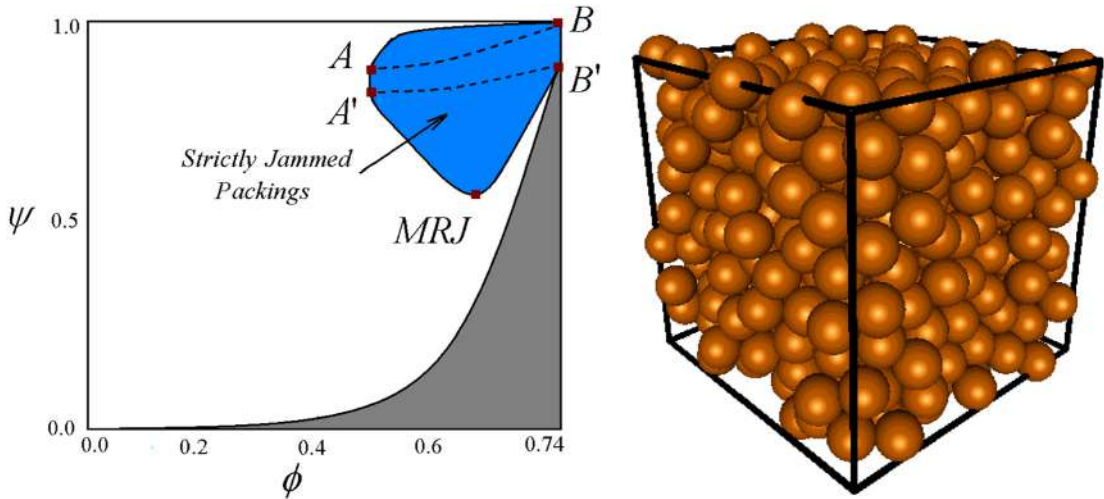


Fig. 45. Left panel: Schematic order map in the density-order (ϕ - ψ) plane for identical hard spheres, including strictly jamming states in \mathbb{R}^3 under periodic boundary conditions. White and blue regions contain the attainable packings, blue regions represent the jammed subspaces, and dark shaded regions contain no packings, as taken from Ref. [200]. The locus of points along the boundary of the jammed set are optimal points [159]. The locus of points A - A' correspond to the lowest-density jammed packings [159]. The locus of points B - B' correspond to the densest jammed packings (face-centered-cubic packing and its stacking variants). The point MRJ represents the maximally random jammed states, i.e., the most disordered states subject to the jamming constraint. The represented packings are not subject to rattler exclusion. Right panel: A three-dimensional MRJ -like configuration of 500 spheres with $\phi \approx 0.64$ produced using the Lubachevsky–Stillinger (LS) packing algorithm [277] with a fast expansion rate [255].

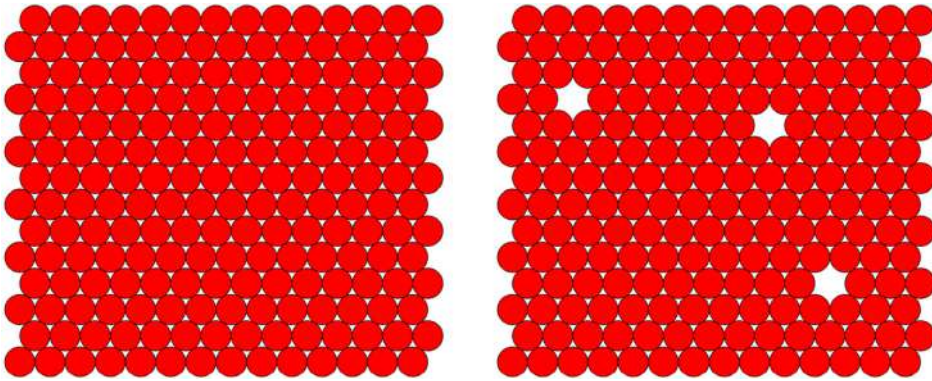


Fig. 46. Left panel: A portion of the infinite triangular-lattice circle packing, which is both strictly jammed and hyperuniform. Right panel: A portion of an infinite triangular-lattice circle packing in which a small fraction of particles are randomly removed such that there are no di-vacancies. This defective triangular-lattice packing is strictly jammed [278] but not hyperuniform.

limit). A portion of this infinite strictly jammed packing is shown in Fig. 46, which is not only hyperuniform but stealthy for the reasons noted in Section 8.4.

11.1.2. Geometric-structure approach and order maps

It is also valuable to quantify the degree of ordering in a packing, especially any that is jammed. To this end, a variety of scalar order metrics ψ have been employed and applied that depend on the configurational coordinates of a packing [200,255] with the normalization $0 \leq \psi \leq 1$, where $\psi = 0$ corresponds to the most disordered state (i.e., Poisson point process) and $\psi = 1$ is the most ordered state (e.g., fcc packing). Using the geometric-structure approach, one can construct an “order map” in the ϕ - ψ plane [200], where jammed packings form a subset in this map. The boundaries of the jammed region delineate extremal structures, including, for example, the maximally dense packings (the face-centered-cubic packing and its stacking variants with $\phi_{\max} = \pi/\sqrt{18} \approx 0.74$ [158]) and the least dense strictly jammed packings (conjectured to be the ‘tunneled crystals’ with $\phi_{\min} = 2\phi_{\max}/3 \approx 0.49$ [159]).

Among all strictly jammed sphere packings in \mathbb{R}^d , the one that exhibits maximal disorder (minimizes some given order metric ψ) is of special interest. This ideal state is called the maximally random jammed (MRJ) state [255]; see Fig. 45. The MRJ concept is geometric-structure based, since it refers to a single packing that is maximally disordered subject to the strict jamming constraint, regardless of its probability of occurrence in some packing protocol. Thus, the MRJ state is conceptually

and quantitatively different from random close packed (RCP) packings [271,272], which have recently been suggested to be the most probable jammed configurations within an ensemble [258]. The differences between these states are even starker in two dimensions, e.g., MRJ packings of identical circular disks in \mathbb{R}^2 have been shown to be dramatically different from their RCP counterparts, including their respective densities, average contact numbers, and degree of order [273]. The MRJ state under the strict-jamming constraint is a prototypical glass [159] in that it is maximally disordered (according to a variety of order metrics) without any long-range order (Bragg peaks) and perfectly rigid (i.e., the elastic moduli are indeed unbounded [200,266]). The jammed backbone of the MRJ state is *isostatic*, i.e., the number of exact contacts in the jamming limit is exactly equal to the number of degrees of freedom, once rattlers are removed; in the infinite-size limit, this implies that the average number of contacts per sphere is $2d$ in d dimensions [268,274,275]. Moreover, MRJ packings in \mathbb{R}^d are characterized by negative “quasi-long-range” (QLR) pair correlations in which the total correlation function $h(\mathbf{r})$ decay to zero asymptotically like $-1/|\mathbf{r}|^{d+1}$ [46,47,50,53,54]. Equivalently, this means that the structure factor $S(\mathbf{k})$ tends to zero linearly in $|\mathbf{k}|$ in the limit $|\mathbf{k}| \rightarrow 0$, and hence place putative MRJ sphere packings in the same hyperuniformity class as Fermi-sphere point processes (see Section 10.2) and superfluid helium in its ground state [74,147], i.e., they all belong to class II.

It is noteworthy that Minkowski correlation functions associated with the Voronoi cells of MRJ packings exhibit even stronger anti-correlations than those shown in the standard pair-correlation function [276].

11.1.3. Jamming-hyperuniformity conjecture

It is instructive now to state a conjecture due to Torquato and Stillinger concerning the conditions under which a certain class of infinite strictly jammed packings are *perfectly* hyperuniform.

Conjecture. *Any strictly jammed saturated infinite packing of identical spheres in \mathbb{R}^d is hyperuniform [27].*

To date, there is no rigorously known counterexample to this conjecture. What is the rationale behind the conjecture? First, the saturation condition is a necessary one because perfect hyperuniformity can be destroyed by “imperfections”. For example, the random removal of a finite fraction of circular disks from the perfect strictly jammed triangular-lattice packing such that there are no di-vacancies (absence of nearest-neighbor particles), as shown in Fig. 46, will result in a packing that is still strictly jammed [278] but will no longer be hyperuniform – the random defects induce diffuse scattering that has a nonzero intensity in the zero-wavenumber limit and hence $S(0) \neq 0$. Similarly, it is known that randomly removing a finite fraction of particles from the perfect strictly jammed fcc-lattice sphere packing such that there are no “tri-vacancies” to maintain strict jamming results in nonhyperuniform packings [278]. Moreover, it is known that collisions in equilibrium hard-sphere configurations along the stable “crystal” branch (see Fig. 47) and on approach to jammed ordered states (such as the triangular lattice and fcc lattice in two and three dimensions, respectively) are not hyperuniform due to large-scale collective vibrational motions and only become exactly hyperuniform when the ideal jammed state without any imperfections or defects is attained [54]. One expects to achieve exact hyperuniformity on the approach to disordered jammed states in the infinite-volume limit that are defect-free, including the complete absence of rattlers [53], as elaborated below. Thus, based on these considerations, it seems reasonable to conjecture that infinite strictly jammed saturated packings of identical spheres are perfectly hyperuniform.

We emphasize that the conjecture eliminates saturated packings that may have a rigid backbone but possess “rattlers” for two reasons: first, the whole (saturated) packing cannot be deemed to be “jammed” due to the presence of these movable particles [200,268] and second, they can be viewed as defects [53] that will prevent perfect hyperuniformity from being achieved. Current numerical packing protocols that have been used to generate putatively jammed disordered packings tend to contain a small concentration of rattlers [46,258,275,279,280], and hence such simulations cannot test this conjecture – notwithstanding recent numerical studies of necessarily finite disordered packings that call into question the link between jamming and perfect hyperuniformity [281–283]. While numerical simulations of MRJ-like states have these limitations as well as others (described immediately below), one can infer near or effective hyperuniformity, as we now detail.

11.1.4. Numerical simulations of MRJ-like states and effective hyperuniformity

Donev, Stillinger and Torquato [46] were the first to determine the extent to which large MRJ-like sphere packings in \mathbb{R}^3 were hyperuniform using a modified Lubachevsky–Stillinger molecular-dynamics packing protocol [284,285]. Under such an event-driven molecular dynamics, particles in a periodic simulation box (that is allowed to perform volume-preserving deformations) undergo thermal motion but also (quickly) grow in size at a certain expansion rate starting from a Poisson distribution of points until it ideally produces a jammed state with a diverging collision rate. Even though the packings contained a significant rattler fraction (about 2.5%), precluding their applicability to the aforementioned conjecture, Donev et al. [46] nonetheless found that a packing of 10^6 particles was to an excellent approximation hyperuniform with a structure factor that exhibits an unusual nonanalytic linear dependence near the origin, i.e., $S(\mathbf{k}) \sim |\mathbf{k}|$ as $|\mathbf{k}| \rightarrow 0$; see Fig. 48. This implies that QLR pair correlations in which $h(r)$ decays to zero with the power-law scaling $-1/r^4$ in accordance with the asymptotic analysis presented in Section 5.3. When the rattlers were removed from the packing, the structure factor at the origin had a substantially larger value, showing that the backbone alone is far from hyperuniform. This numerical finding supporting the link between “effective” hyperuniformity of a disordered packing and mechanical rigidity spurred a number of subsequent numerical and experimental investigations that reached similar conclusions either via $S(k)$ or the spectral density $\tilde{\chi}_v(k)$ [48,50,52,53,56–58,121]. In all cases, effective or near hyperuniformity is conferred because the majority of

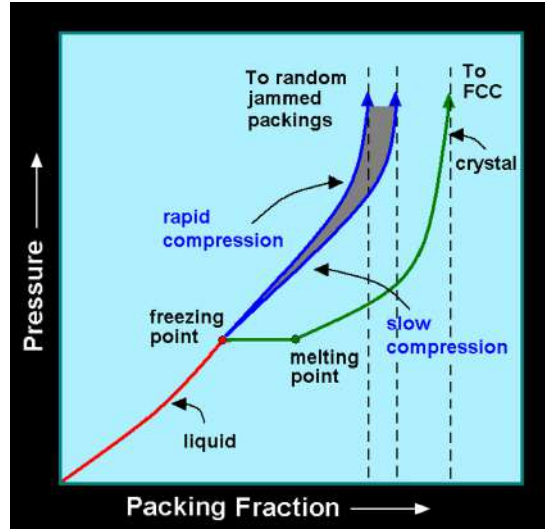


Fig. 47. The isothermal phase behavior of three-dimensional hard-sphere model in the pressure-packing fraction plane, as taken from Ref. [200]. An infinitesimal compression rate of the disordered liquid traces out the thermodynamic equilibrium path, shown in green, including a first-order freezing transition to a crystal branch that ends at the maximally dense fcc state ($\phi = \pi/\sqrt{18} = 0.740\dots$), which is strictly jammed and hyperuniform. Importantly, hard-sphere collisions along the stable crystal branch induce large-scale density fluctuations that destroy hyperuniformity unless the system is exactly at the close-packed fcc jamming point [54]. Rapid compressions of the liquid produce a range of amorphous metastable extensions of the liquid branch that jam only at their respective terminal densities. Ideally, the MRJ state could be regarded to be the end point of a metastable branch with the fastest compression rate consistent with jamming.

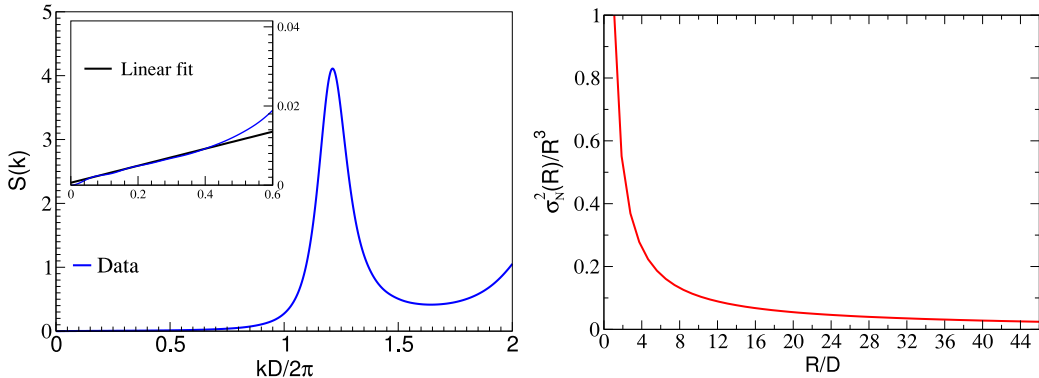


Fig. 48. Left panel: The structure factor $S(k)$ as a function of the dimensionless wavenumber $kD/(2\pi)$ for a million-particle packing of identical three-dimensional spheres at a putative MRJ state, where D is the hard-sphere diameter [46]. The inset shows the linear in $|\mathbf{k}|$ nonanalytic behavior at $\mathbf{k} = \mathbf{0}$ with $S(0) = 6 \times 10^{-4}$. Right panel: The corresponding scaled number variance $\sigma_N^2(R)/R^3$ versus R . The fact that $S(k)$ goes to zero linearly in $|\mathbf{k}|$ implies that $\sigma_N^2(R)$ grows like $R^2 \ln(R)$ for large R and hence $\sigma_N^2(R)/R^3$ is a decaying function of R , as it should be for a hyperuniform system.

the particles are contained in the strictly-jammed backbone. Indeed, it has been systematically shown that as a hard-sphere system, substantially away from a jammed state, is driven toward strict jamming through densification, $S(0)$ monotonically decreases until effective hyperuniformity is achieved at the putative MRJ state. Specifically, $S(0)$ was found to approach zero approximately linearly as a function of density from 93% to 99% of the jamming density, where extrapolating the linear trend in $S(0)$ to jamming density yielded $S(0) = -1 \times 10^{-4}$ [50]. This study clearly established a correlation between distance to jamming and hyperuniformity, and additionally introduced a “nonequilibrium index” X , defined by relation (79), describing the interplay between hyperuniformity and a dynamic measure of distance to jamming.

It is instructive to contrast the effective hyperuniform behavior of these nonequilibrium packings to that of nonhyperuniform identical hard spheres in equilibrium along the stable disordered (fluid) branch for packing fractions in the range $0 \leq \phi \leq \phi_F$, where the freezing point is $\phi_F \approx 0.494$ in three dimensions; see Fig. 47. At these packing-fraction extremes, $S(0) = 1$ and $S(0) = 0.02$ [6,268], respectively. The latter minimal value is still about two orders of magnitude larger than $S(0)$ reported for MRJ packings [50,268]. Moreover, the QLR behavior of $g_2(r)$ of MRJ states distinguishes it from that of the equilibrium hard-sphere fluid [6], which possesses a structure factor that is analytic at $\mathbf{k} = \mathbf{0}$ and thus has a pair-correlation function that decays exponentially fast to unity for large r .

Even though polydisperse packings are not part of the original Torquato–Stillinger conjecture [27], effective hyperuniformity can be observed in such packings [48,56–58,121] provided that the size distribution is suitably constrained and the rattler concentration is sufficiently small. It is even possible that the conjecture can be extended to strictly jammed saturated packings of polydisperse spheres; however, the determination of the additional conditions for such an extension is highly nontrivial. Nonetheless, jamming is again a crucial necessary property to attain near-hyperuniformity in two and three dimensions. Note that for packings of spheres with a size distribution and of nonspherical particles, it is the spectral density $\tilde{\chi}_v(\mathbf{k})$ (not the structure factor $S(\mathbf{k})$ associated with the points that define the particles centroidal positions) that must be computed [48]. Of course, the hyperuniformity condition is that $\tilde{\chi}_v(\mathbf{k})$ must vanish in the small-wavenumber limit, as specified by (38); see also Section 6.4.

As a practical matter, is important to note that ascertaining the hyperuniformity of limited samples sizes often encountered in simulations and laboratory experiments can often be done more accurately in direct space via the local variance than in reciprocal space via the appropriate spectral function [58].

11.1.5. Critical slowing down as a disordered jammed state is approached

A fascinating open question remains as to whether putative MRJ packings can be made to be even more hyperuniform than established to date or exactly hyperuniform with improved numerical protocols as the system size is made large enough. This is an extremely delicate question to answer because one must be able to ensure that true jamming is achieved to within a controlled tolerance as the system size increases without bound. However, any packing algorithm necessarily must treat a finite system and hence the smallest accessible positive wavenumber at which $S(k)$ or $\tilde{\chi}(k)$ can be measured is of the order of $2\pi/N^{1/d}$, where N is the number of particles. The situation is further complicated by noise at the smallest wavenumbers, numerical and protocol-dependent errors, and the reliance on extrapolations of such uncertain data to the zero-wavenumber limit.

It has been recently shown that various standard packing protocols struggle to reliably create packings that are jammed for even modest system sizes of $N \approx 10^3$ bidisperse disks in two dimensions [53]. Importantly, while these packings appear to be jammed by conventional tests, rigorous linear-programming jamming tests [267,286] reveal that they are not. Evidence suggests that deviations from hyperuniformity in putative MRJ packings can in part be explained by a shortcoming of the numerical protocols to generate exactly-jammed configurations as a result of a type of “critical slowing down” [53] as the packing’s collective rearrangements in configuration space become locally confined by high-dimensional “bottlenecks” through which escape is a rare event. Thus, a critical slowing down implies that it becomes increasingly difficult numerically to drive the value of $S(0)$ exactly down to its minimum value of zero if a true jammed critical state could be attained. Moreover, the inevitable presence of even a small fraction of rattlers generated by current packing algorithms destroys perfect hyperuniformity. In this regard, one should note that nearly hyperuniform point configurations can be made to be exactly hyperuniform by very tiny collective displacements via the collective-coordinate approach [37], which by construction enables the structure factor to be constrained to take exact targeted values at a range of wave vectors, as shown recently in Refs. [79] (see also Fig. 3) and [53].

In summary, the difficulty of ensuring jamming as N becomes sufficiently large to access the small-wavenumber regime in the structure factor as well as the presence of rattlers that degrade hyperuniformity makes it virtually impossible to test the Torquato–Stillinger jamming-hyperuniformity conjecture on disordered jammed packings via current numerical protocols.

11.1.6. “Effective” hyperuniformity criterion

Since hyperuniformity is an infinite-wavelength property of a point configuration in \mathbb{R}^d and numerical simulations as well as lab experiments are limited by system size and subject to error/noise, it is desirable from a practical viewpoint to devise a rough criterion for what one considers to be “effective” or “near” hyperuniformity. While this is ultimately subjective, an empirical operational definition that has been proposed [53] for such behavior is that the first dominant peak value of the structure factor relative to its estimated value at the origin is roughly of the order of 10^4 or larger; equivalently, the ratio

$$H \equiv \frac{S(\mathbf{k} = \mathbf{0})}{S(\mathbf{k}_{\text{peak}})} \quad (251)$$

is of the order of 10^{-4} or smaller, where \mathbf{k}_{peak} is the location of the first dominant peak of the structure factor. In the case of heterogeneous media, a similar “hyperuniformity metric” applies, except where $S(\mathbf{k})$ is replaced with the spectral density $\tilde{\chi}_v(\mathbf{k})$, as defined in Section 2.3.

11.1.7. Toward the ideal MRJ state

While one should not generally expect exact hyperuniformity for disordered packings with rattlers, it has been demonstrated that when jamming is ensured, disordered packings with a small fraction of rattlers can be very nearly hyperuniform, and deviations from hyperuniformity correlate with an inability to ensure jamming, suggesting that strict jamming and hyperuniformity are indeed linked [53]. This raises the possibility that the ideal MRJ packing possesses no rattlers such that the jammed backbone contains every sphere in the packing. This would imply that disordered isostatic sphere packings with rattlers possess a higher degree of order (than ideal MRJ packings without rattlers), even when the rattlers are included, because rattler cages require the caged particles and their neighbors be more correlated in order to house the rattlers. This possibility provides the impetus for the development of packing algorithms that produce large disordered strictly jammed

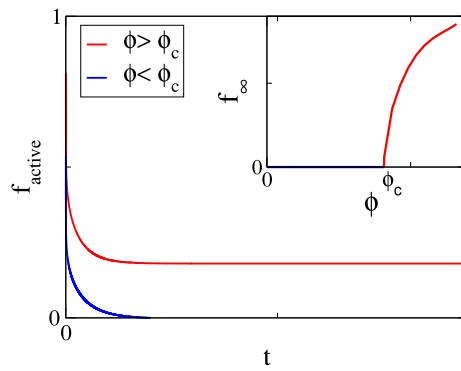


Fig. 49. Schematic illustrating the time (t) evolution of the fraction of active particles $f_{\text{active}}(t)$ below the critical packing fraction ϕ_c (blue curve) and above ϕ_c (red curve). The inset shows the behavior of the active fraction at infinite time f_{∞} as a function of the packing fraction ϕ . A second-order phase transition occurs at $\phi = \phi_c$, where the system is hyperuniform.

packings that are rattler free. Typical packing algorithms, to a good approximation, will produce disordered isostatic sphere packings with approximately 3% rattlers [200,268,277,287]. The Torquato–Jiao (TJ) sphere packing algorithm [280], which employs linear-programming techniques that become exact as jamming is approached, efficiently produces disordered, isostatic strictly jammed packings with unsurpassed numerical fidelity with a substantially lower rattler fraction of 1.5% when the number of spheres N is sufficiently small [275]. Thus, an outstanding, challenging task is the formulation of numerical packing protocols that generate not only rattler-free disordered isostatic packings but ones in which N is large enough to access very small wavenumbers in the structure factor to ascertain the degree of hyperuniformity as accurately as possible.

In the subsequent subsection on absorbing-state models, the ideal MRJ state will be interpreted as the end point of a nonequilibrium dynamical process of a many-particle system in which jamming is tantamount to being at a critical-absorbing state.

11.1.8. Is hyperuniformity also a signature of MRJ packings of aspherical particles?

Over the past decade there has been increasing interest in the effects of particle shapes on the characteristics of disordered jammed packings, since deviations from sphericity introduce rotational degrees of freedom. This implies that a nonspherical particle requires more contacts to stabilize mechanically than a sphere [259,284,285] and hence packings of the former are generally denser than sphere packings. Packings of aspherical particles are useful models of heterogeneous materials, granular media and structural glasses [115,259]. Nonspherical particles that have been studied include ellipsoids [48,259,260,263], “superballs” [48,288,289], “superellipsoids” [290], and polyhedra [270,291–295]. Numerical simulations have been performed that to a very good approximation produce MRJ-like isostatic packings of identical nonspherical particles in two and three dimensions, including ellipsoids and superballs [48,121,122] as well as polyhedra, such as the Platonic solids [49] and truncated tetrahedra [51]. In all of these cases, the spectral function (either the structure factor or spectral density) appears to go zero linearly in the wavenumber with a slope that depends on the particle shape [48,121,122]. Hence, these jammed disordered packings possess QLR pair correlations in which $h(r)$ or $\chi_V(r)$ decays asymptotically to zero with the scaling $-1/r^{d+1}$, showing that they belong to the same universality class as MRJ sphere packings. Thus, at least for this limited class of aspherical shapes, hyperuniformity (to a good approximation) appears to be a signature of the MRJ state.

11.2. Driven nonequilibrium systems and critical absorbing states

It is well-established that many-particle systems far from equilibrium typically possess long-range correlations; see, for example, [296–300]. Absorbing-state models are far-from-equilibrium many-body systems that provide excellent examples of nonequilibrium phase transitions between two distinct phases – an active phase, which is a steady state with never-ending dynamics, and an absorbing state where the dynamics cease – with a well-defined critical point [301]. Following an initial transient, any system below its critical state ultimately evolves to an absorbing state, in which each of the particles satisfies some local criterion for the cessation of its evolution under the dynamics. The details of what is this criterion and the nature of the dynamics defines the specific absorbing-state model. Whether the system is in the active or the absorbing phase is determined by the value of the control parameter (e.g., fraction of space covered by the particles), as will be detailed below.

At a given instant of time t , a system has fraction of active particles $f_{\text{active}}(t)$, and the active fraction decreases up to a steady-state value $f_{\infty} \equiv \lim_{t \rightarrow \infty} f_{\text{active}}(t)$ over time; see Fig. 49. If a control parameter, such as the packing fraction ϕ , is smaller than a critical value ϕ_c , the steady-state fraction f_{∞} becomes identically zero. As ϕ approaches the critical point ϕ_c from below, both the lifetime of the transient and appropriately defined correlation length diverge. When the parameter ϕ is larger than the critical point ϕ_c , the steady-state fraction f_{∞} is positive, and the system lies in the active phase. The

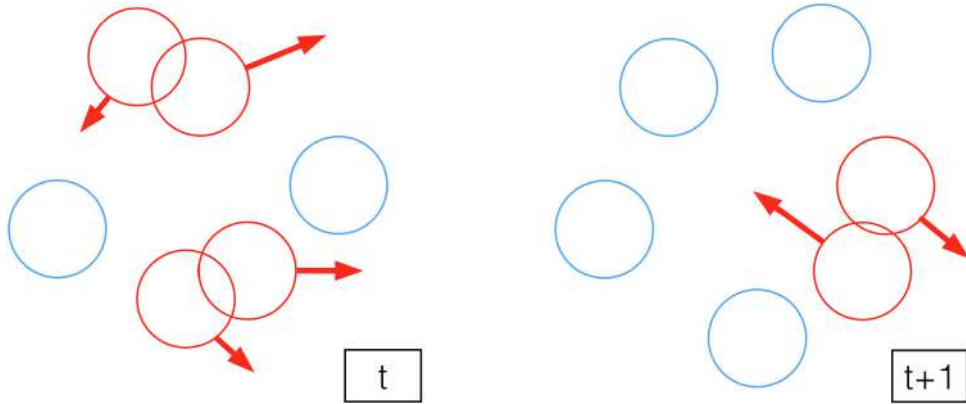


Fig. 50. Schematic indicating overlapping active particles (red) and nonoverlapping inactive particles (blue) at times t (left panel) and $t + 1$ (right panel). At time t , the maximum possible displacement vectors of active particles are indicated with arrows (whose directions and lengths are chosen according to some stochastic rule) and determine which of the particles are active or inactive at the next time step, i.e., at time $t + 1$.

transition bears a great resemblance to a second-order equilibrium phase transition [301–303]; see the inset of Fig. 49. It is natural to ask about the nature of the critical absorbing states, which is obtained by studying the absorbing phase as the control parameter approaches its critical value, ϕ_c . The recent numerical observations that several absorbing state models at criticality are effectively hyperuniform long-range pair correlations [62] together with the fact that such disordered systems may be realized experimentally [304,305] are significant developments.

11.2.1. Hyperuniformity in absorbing-state models

The properties of several absorbing-state models belonging to the conserved directed percolation universality class were numerically studied by Hexner and Levine [62]. The models examined include the conserved lattice gas in two and three dimensions [306], the Manna model in one dimension [301,307] and random organization models in one and two dimensions [305]. They found that at the critical point the absorbing states are effectively hyperuniform. The various models differ in the criteria that define which of the particles are active and the particle displacement rules. Regardless of their details, they found that the nonequilibrium phase transitions are characterized by a set of universal critical exponents that depend only on the dimensionality. Specifically, they found that the structure-factor exponent α defined in Eq. (96) is given by $\alpha \approx 0.425$, $\alpha \approx 0.45$ and $\alpha \approx 0.24$ in one, two and three dimensions, respectively. Therefore, according to the asymptotic number-variance scaling relation (97), these hyperuniform systems belong to class III; specifically, $\sigma_N^2(R) \sim R^{0.575}$ for $d = 1$, $\sigma_N^2(R) \sim R^{1.55}$ for $d = 2$, and $\sigma_N^2(R) \sim R^{2.76}$ for $d = 3$.

It is instructive to review briefly aspects of the random organization model that was put forward by Corté et al. [305] to understand how the irreversible collisions that generally produce diffusive chaotic dynamics in periodically sheared suspensions at low Reynolds number can also cause systems to self-organize to avoid future collisions. Such dynamics can lead to a non-fluctuating quiescent state with a dynamical phase transition separating it from fluctuating diffusive states. The model begins from an initial distribution of points (e.g., Poisson point process) in some region of d -dimensional Euclidean space \mathbb{R}^d , often taken to be a fundamental cell under periodic boundary conditions. Next, each point is surrounded by an “influence region” of some well-defined shape and size. Particles whose influence regions overlap with those of other particles are deemed active, and at the next time step, all active particles are translated by some distance (“kick”) in random directions; see Fig. 50. The kick sizes may be drawn randomly from a given distribution, which is taken to be short-ranged. This process is iterated until the system achieves a steady state (active phase) or the dynamics ends (absorbing phase). An anisotropically-shaped influence region is an appropriate choice for sheared systems, which was the original motivation for the model [304,305].

A particularly simple version of this model takes the influence region to be a d -dimensional sphere [64]. Because of the isotropy of this shape, the system evolves to a statistically isotropic distribution of particles. We have generated realizations of 100,000 particles in two dimensions that start from relative dense but *unsaturated* nonoverlapping random-sequential-addition of circular disks of diameter a [78,308,309] but with an influence circle of radius $D > a$ to allow particle overlaps (active particles). For a given value of D , the amplitude of a kick given to an active particle is randomly and uniformly chosen between 0 and $D/4$, and the system dynamics are followed until the steady-state conditions are established. The diameter is allowed to systematically increase in order to identify the critical packing fraction ϕ_c , at which point the system is a packing, i.e., identical hard circular disks of diameter D . A portion of a system at a critical absorbing state with $\phi_c = 0.407$ is shown in Fig. 51. (This value of the critical packing fraction is consistent with the one reported in Ref. [64] with this maximum displacement size.) The corresponding structure factor and number variance are also depicted in Fig. 51. Both quantities reveal that the critical state is effectively hyperuniform and belongs to class III [cf. Eq. (97)], since $\sigma_N^2(R) \sim R^{1.55}$. This is consistent with the results reported in Ref. [62]. Note that, as in the case of the generation of MRJ particle packings

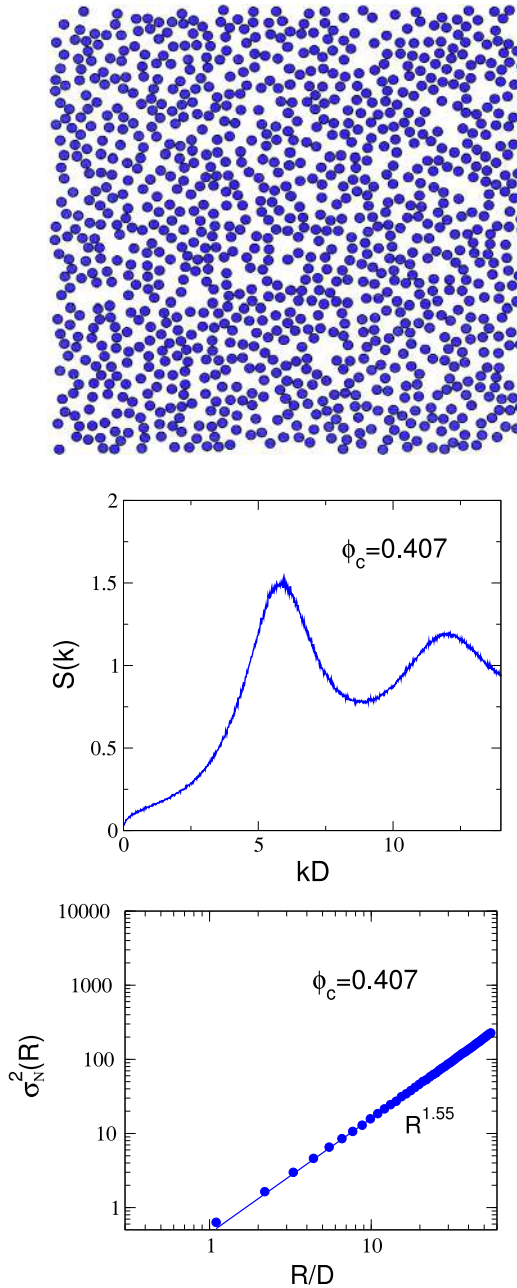


Fig. 51. Top panel: A portion of a system of 100,000 circular disks of diameter D at the critical state with packing fraction $\phi_c = 0.407$ as generated from the random organization model [305]. Middle panel: Corresponding structure factor $S(k)$ versus dimensionless wavenumber kD . Bottom panel: Corresponding logarithm of the number variance $\sigma_N^2(R)$ versus the logarithm of the window radius R , which shows a hyperuniform scaling of $R^{1.55}$, and hence belongs in class III; see Eq. (97).

(Section 11.1.5), a precise numerical determination of the critical point of absorbing-state models is nontrivial due to a critical slowing down of the system.

The discovery that periodically sheared low-Reynolds number non-Brownian systems can self-organize into a correlated absorbing state [305] has led to a flurry of activity on periodically-driven systems. Superconducting vortices in an oscillating magnetic field [310], driven glassy systems [311], compressed/expanded foams, emulsions in oscillating flow [63] have all been shown to have absorbing states. It has recently been found that periodically sheared frictional granular systems have an absorbing-state transition as well [312]. Moreover, at criticality, these absorbing-state systems are hyperuniform. Remarkably, it has been discovered that off criticality, “kicking” or reactivating these systems makes them more hyperuniform

with exponents that are comparable to those found for MRJ packings, i.e., the structure factor tends to $S(k) \sim k$ in the small wavenumber limit [66], and hence they belong to class II hyperuniform systems. Interestingly, a recent numerical study has shown how to design time-dependent suspension flows that judiciously combine the speed of chaotic advection to achieve hyperuniform states [67].

These models have been extended by introducing an additional symmetry beyond particle conservation, namely, when two particles interact, stochastic kicks are given that conserve their center of mass [66]. It was found that the active states are hyperuniform with a greater suppression of large-scale density fluctuations than those in previous random organization models; in fact, they belong to class I, as defined by (97). Large-scale fluctuations are determined by a competition between a noise term that generates fluctuations, and a deterministic term that reduces them.

11.2.2. Interpretation of the ideal MRJ sphere packing as a critical-absorbing state

Interestingly, an ideal MRJ sphere packing can be interpreted as a critical-absorbing state associated with a nonequilibrium absorbing phase transition. As usual, one must define the active and inactive particles as well as the dynamics. We propose the following absorbing-state models for disordered strictly jammed sphere packings. To begin, imagine an initial random configuration of a dilute concentration of N identical hard spheres that will undergo interparticle collisions via molecular dynamics within a fundamental simulation cell that is allowed to deform and shrink (on average) as a function of time in the spirit of an adaptive-shrinking cell scheme [269,270]. (Note that conceptually this is opposite to the modified event-driven molecular dynamics in which the particles are allowed to grow in a deforming volume-preserving simulation box that is not allowed to shrink in volume [284,285].) Active particles are those that can undergo collisions with themselves (or the container boundary in the case of a hard-wall container) and inactive particles are those that are frozen or at least locally jammed at any particular instant of time. The dynamics cease when the system reaches an absorbing state in which all of the particles are inactive, i.e., when the entire packing is strictly jammed, and hence achieves a critical absorbing state, but only from below. Notably, this implies that such critical absorbing states cannot possess rattlers because rattlers are active due to collisions with the rattlers cages. A rattler-free critical strictly-jammed absorbing state that is maximally random harkens back to the ideal MRJ state alluded to in Section 11.1.7, which would be hyperuniform according to the hyperuniformity-jamming conjecture (see Section 11.1.3). Depending on the initial conditions (spatial configuration and density) and simulation box deformations, the final (jammed) critical absorbing states can have a spectrum of degrees of ordering, including, for example, the maximally dense fcc lattice sphere packing.

12. Natural disordered hyperuniform systems

It has recently been discovered that disordered hyperuniformity can confer to biological systems optimal or nearly optimal functionality, including the avian retina [70] and the immune system [71], which are briefly reviewed here. It is likely that there are many other natural disordered hyperuniform materials or systems that have yet to be found.

12.1. Avian photoreceptor cells

Biology has recently taught us that disordered hyperuniform point patterns offer desirable color-sensing characteristics [70]. The purpose of a visual system is to sample light in such a way as to provide an animal with actionable knowledge of its surroundings that will permit it to survive and reproduce [313]. Often, this goal is achieved most effectively by a highly regular two-dimensional array of cone cells that evenly sample incoming light to produce an accurate representation of the visual scene. Cone cells are one of three types of photoreceptor cells in the retina of vertebrates that are responsible for color vision and function best in relatively bright light, as opposed to rod cells that are better able to detect dim light. According to classical sampling theory [314,315], the optimal arrangement of a two-dimensional array of light detectors is the triangular lattice. Indeed, studies suggest that any deviation from perfectly regularity will cause deterioration in the quality of the image produced by a retina [316]. Accordingly, many species have evolved an optimal or nearly optimal sampling arrangement of their photoreceptors, including the insect compound eye [317,318], many teleost fish [319–321] and some reptiles [322].

Diurnal birds have one of the most sophisticated cone visual systems of any vertebrate, consisting of five cone types: four single cones (violet, blue, green and red) that mediate color vision and double cones involved in luminance detection [323]; see Fig. 52. Despite the presence of numerous evolutionary specializations in the avian eye, the overall arrangement of bird cone photoreceptors is not ordered but rather is irregular [324,325]. The five avian cone types exist as five independent, spatial patterns, all embedded within a single monolayered epithelium. Each cell type of this *multicomponent* system is maximally sensitive to visible light in a limited but different range of wavelengths. Given the acute vision of birds and the utility of the perfect triangular-lattice arrangement of photoreceptors for color sensing [316], the presence of disorder in the spatial arrangement of avian cone patterns had been puzzling.

Recently, images of large two-dimensional arrays of chicken cone photoreceptors (~ 5000 cells per data set) were spatially analyzed and characterized using a host of sensitive statistical correlation functions and other microstructural descriptors [70]; see the left panel of Fig. 53. Among other quantities, the local number variances and the structure factors were ascertained. It was found that the disordered photoreceptor patterns are hyperuniform, a property that had previously not been identified in any living organism [70]. Remarkably, in a departure from any known physical system, the patterns of both the total population and the individual cell types are simultaneously hyperuniform, as shown by the corresponding

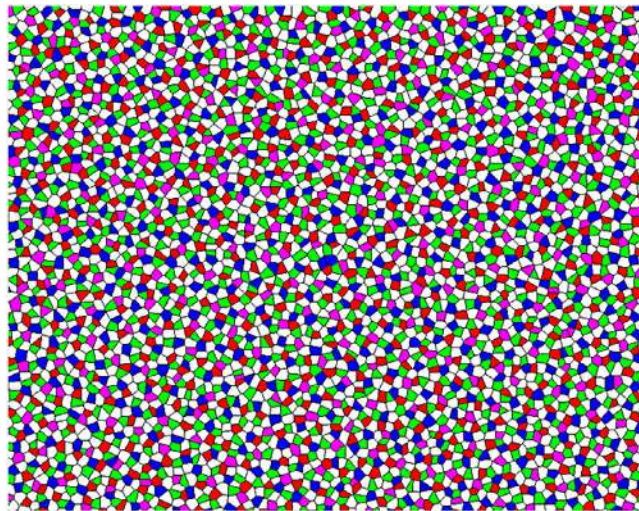


Fig. 52. Voronoi tessellation representation of the spatial distribution of the five types of light-sensitive cones in the chicken retina: violet, blue, green, red and white (representing double cones).

Source: Courtesy of Joseph Corbo and Timothy Lau, Washington University in St. Louis.

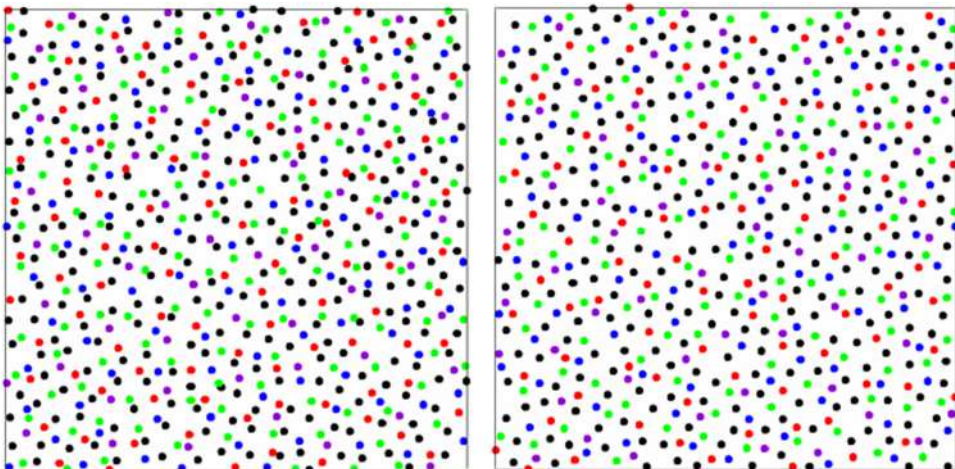


Fig. 53. Left panel: Experimentally obtained configurations representing the spatial arrangements of the five chicken cone photoreceptors. The colored dots (enlarged for visualization purposes) represent the centers of the cells. Here black dots represent the double cones. Right panel: Simulated point configurations representing the spatial arrangements of chicken cone photoreceptors.

Source: These figures are taken from Ref. [70].

structure factors depicted in Fig. 54. Such patterns are called “multihyperuniform” because multiple distinct subsets of the overall point pattern are themselves hyperuniform [70]. This singular property implies that if any such distinct subset is removed from the overall population, the remaining pattern is still hyperuniform. Multihyperuniform disordered structures could have implications for the design of materials with novel physical properties and therefore may represent a fruitful area for future research.

To model the avian photoreceptor patterns, Jiao et al. [70] considered a statistical-mechanical cell model with two types of effective cell-cell interactions: isotropic short-range hard-core repulsions between any pair of cells and isotropic longer-ranged soft-core repulsions between pairs of like-cells. The local-energy minimizing configurations of such a many-particle interacting system were simulated and shown to quantitatively capture, with high accuracy, the unique spatial characteristics of avian photoreceptor patterns, including multihyperuniformity [70]. Fig. 54 shows that there is excellent agreement between the structure factors obtained from the aforementioned statistical-mechanical cell model and their experimental counterparts for the total population and the individual cell types. This epithelium system stands in contrast to epithelia in mammalian skin, which has been shown not to be hyperuniform [326], since the latter, unlike the former, must be very pliable to deformations.

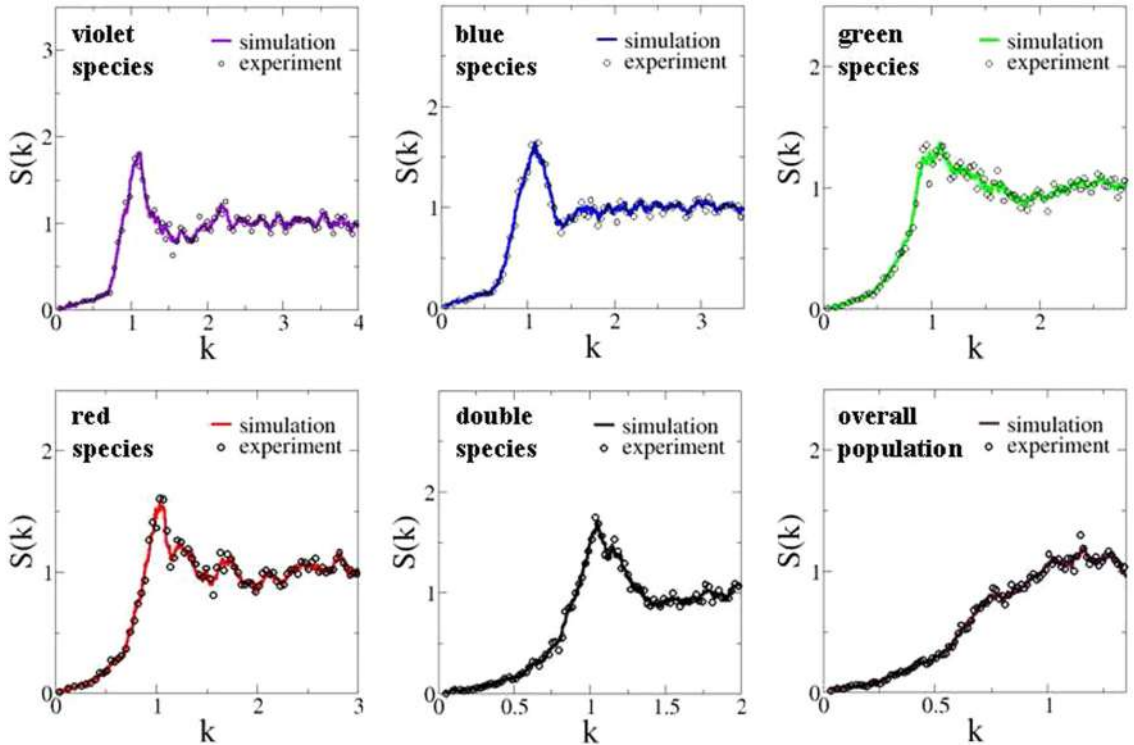


Fig. 54. Comparison of the structure factors $S(k)$ of the experimentally obtained and simulated point configurations representing the spatial arrangements of the individual cell types and total population, as presented in Ref. [70]. Multihyperuniformity is manifested in the fact that the individual cone types and the total population are hyperuniform.

12.2. Receptor organization in the immune system

A well-adapted immune system should be tuned to the pathogenic environment to reduce the cost of infections to the organism. Mayer et al. [71] devised a general theoretical framework to predict the optimal repertoire of lymphocyte receptors that minimizes the cost of infections contracted from a given distribution of pathogens. The model assumes that receptor repertoire is bounded in size and that receptors are “cross-reactive” (each antigen binds many receptors; each receptor binds many antigens) and the cost of an infection increases with time. An important question that they investigated is whether the cross-reactivity generically drives the optimal receptor distribution to cluster into peaks. They found that the optimal repertoire is strongly peaked on a discrete forest of receptors and showed that the width of these peaks decreases as numerical precision is increased, suggesting that in a continuous limit the optimum consists of a weighted sum of Dirac delta functions, i.e., distinct, discretely spaced receptors in different amounts in the shape space of the antigens. The peaks tended to repel each other and to organize into local tiling patterns. Remarkably, the optimal distribution of the peaks in shape space of the antigens were demonstrated to be disordered and hyperuniform, as determined by the structure factor at small wavenumbers. In biological terms, hyperuniformity means that the distribution of receptor peaks provides a much more uniform coverage of the antigen space than if the peaks were positioned randomly according to a Poisson distribution. As methods are developed to better characterize pathogenic landscapes and receptor cross-reactivity, the predictions for the composition of optimal repertoires derived from this theoretical framework may be directly compared with experiments.

13. Generalizations of the hyperuniformity concept

Given the fundamental as well as practical importance of disordered hyperuniform systems elucidated thus far, it is natural to explore generalizations of the hyperuniformity notion and its consequences. Recently, the hyperuniformity concept has been generalized to treat fluctuations in the interfacial area in multiphase heterogeneous media and surface-area driven evolving microstructures, random scalar fields, random vector fields, and statistically anisotropic many-particle systems and two-phase media [81]. The relevant mathematical underpinnings are briefly reviewed and illustrative examples are provided. In the instances of random vector fields and statistically anisotropic structures, it is crucial to note that the standard definition of hyperuniformity must be generalized so that it accounts for the dependence of the relevant spectral functions on the direction in which the origin in Fourier space is approached. These recent generalizations of hyperuniformity

are expected to provide scientists new avenues to understand a very broad range of phenomena across a variety of fields through the hyperuniformity “lens”.

13.1. Fluctuations in the interfacial area

Interfacial-area fluctuations are of importance whenever interfaces determine the underlying physical phenomena. This includes flow in porous media [115,116], diffusion and reaction in porous media (including nuclear magnetic resonance (NMR) relaxation processes) [115,327–329], and surface-energy driven coarsening phenomena, such as those that occur in spinodal decomposition and morphogenesis [330,331].

The global specific surface s (interface area per unit volume) is a one-point correlation function that is independent of position for a statistically homogeneous two-phase system in \mathbb{R}^d [115]. On the other hand, the specific surface fluctuates at a local level. It is straightforward to show that the local specific-surface variance associated with a d -dimensional spherical window of radius R is given by [81]

$$\sigma_s^2(R) = \frac{1}{s^2 v_1(R)} \int_{\mathbb{R}^d} \chi_s(\mathbf{r}) \alpha_2(r; R) d\mathbf{r}, \quad (252)$$

where $\chi_s(\mathbf{r})$ is the autocovariance function associated with the interface indicator function, $r = |\mathbf{r}|$, $\alpha_2(r; R)$ is the scaled intersection volume, defined by (52) and we have invoked statistical homogeneity. Again, application of Parseval's theorem to (252) yields the alternative Fourier representation of $\sigma_s^2(R)$ in terms of the spectral density $\tilde{\chi}_s(\mathbf{k})$:

$$\sigma_s^2(R) = \frac{1}{s^2 v_1(R)(2\pi)^d} \int_{\mathbb{R}^d} \tilde{\chi}_s(\mathbf{k}) \tilde{\alpha}_2(k; R) d\mathbf{k}. \quad (253)$$

A two-phase system is hyperuniform with respect to surface-area fluctuations if the spectral density $\tilde{\chi}_s(\mathbf{k})$ obeys the condition

$$\lim_{|\mathbf{k}| \rightarrow 0} \tilde{\chi}_s(\mathbf{k}) = 0, \quad (254)$$

which implies the sum rule

$$\int_{\mathbb{R}^d} \chi_s(\mathbf{r}) d\mathbf{r} = 0. \quad (255)$$

This hyperuniformity property is equivalent to requiring that the surface-area variance $\sigma_s^2(R)$ for large R goes to zero more rapidly than R^{-d} , which is the same condition as that for the volume-fraction variance discussed in the Introduction. Using precisely the same analysis as for point configurations [27,32,139], it is simple to show that three different hyperuniform scaling regimes arise from (253) when the surface-area spectral density goes to zero with the power-law form $\tilde{\chi}_s(\mathbf{k}) \sim |\mathbf{k}|^\alpha$:

$$\sigma_s^2(R) \sim \begin{cases} R^{-(d+1)}, & \alpha > 1 \\ R^{-(d+1)} \ln R, & \alpha = 1 \\ R^{-(d+\alpha)}, & 0 < \alpha < 1 \end{cases} \quad (R \rightarrow \infty). \quad (256)$$

Note that these scaling forms are exactly the same as those for volume-fraction fluctuations [cf. (134)].

For a packing of identical d -dimensional spheres in \mathbb{R}^d , the spectral density $\tilde{\chi}_s(\mathbf{k})$ is related to the structure factor $S(\mathbf{k})$ associated with the sphere centers as follows [81]:

$$\tilde{\chi}_s(\mathbf{k}) = \rho \tilde{m}_s^2(k; a) S(\mathbf{k}), \quad (257)$$

where

$$\tilde{m}_s(k; a) = \left(\frac{2\pi a}{k} \right)^{d/2} k J_{d/2-1}(ka) \quad (258)$$

is the Fourier transform of the interface indicator function $m_s(r; a)$ for a sphere of radius a [81]. From formula (257), it immediately follows that if the underlying point process is hyperuniform and/or stealthy, then the spectral density $\tilde{\chi}_s(\mathbf{k})$ inherits the same hyperuniformity property (254) [81]. Corresponding formulas for the autocovariance function and the associated spectral density for packings of hard spheres with a continuous or discrete size distribution were previously obtained [115,170] and collected in a more recent article [81] to analyze their hyperuniformity properties.

It is of interest to compare volume-fraction and surface-area fluctuations for the same two-phase system. The left panel of Fig. 55 shows the two spectral functions, $\tilde{\chi}_v(\mathbf{k})$ and $\tilde{\chi}_s(\mathbf{k})$, for the step-function g_2 -invariant packing process in three dimensions at the terminal density $\rho_c = 3/(4\pi)$ [27]; see also Section 7.2. The right panel of Fig. 55 depicts the corresponding local variances for the same system, as obtained from these spectral functions, and relations (74) and (253). Notice that the surface-area spectral function exhibits stronger and longer-ranged behavior compared to the volume-fraction spectral function, indicating that the former is a more sensitive microstructural descriptor. While both local variances decay like R^{-4} for large R , the surface-area variance is larger than its volume-fraction counterpart at a fixed value of R .

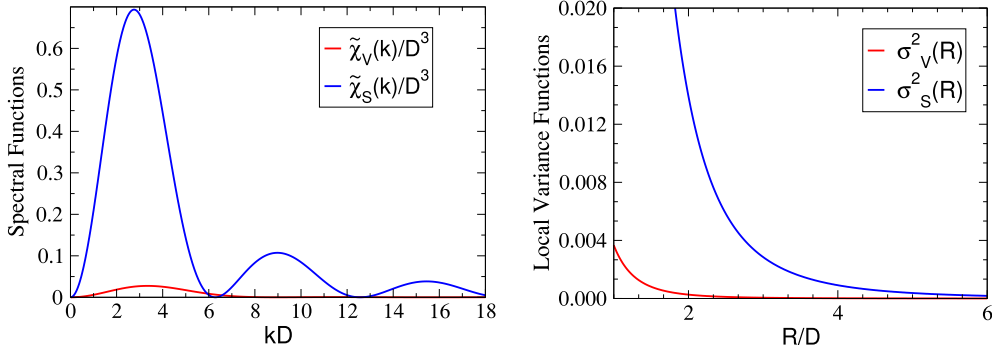


Fig. 55. Left panel: Comparison of the two hyperuniform spectral functions $\tilde{\chi}_V(k)$ (lower curve) and $\tilde{\chi}_S(k)$ versus wavenumber k for a packing of identical spheres corresponding to the step-function g_2 -invariant process in three dimensions at the hyperuniform terminal density $\rho_c = 3/(4\pi)$, as obtained in Ref. [27]. Here D is the diameter of a hard sphere. Right panel: Corresponding volume-fraction variance $\sigma_V^2(R)$ (lower curve) and surface-area variance $\sigma_S^2(R)$ versus window sphere radius R .

13.2. Random scalar fields

The hyperuniformity concept has been recently generalized to characterize fluctuations associated with random scalar fields in \mathbb{R}^d . Such fields can arise in a variety of physical contexts, including concentration and temperature fields in heterogeneous and porous media [115,116] as well as in turbulent flows [332,333], laser speckle patterns [334–337], and temperature fluctuations associated with the cosmic microwave background [17,338]. Other examples include spatial patterns that arise in biological and chemical systems that have been theoretically described by, for example, Cahn–Hilliard [330] and Swift–Hohenberg equations [331].

Consider a statistically homogeneous random scalar field $F(\mathbf{x})$ in \mathbb{R}^d that is real-valued with an autocovariance function

$$\psi(\mathbf{r}) = \left\langle (F(\mathbf{x}_1) - \langle F(\mathbf{x}_1) \rangle) (F(\mathbf{x}_2) - \langle F(\mathbf{x}_2) \rangle) \right\rangle, \quad (259)$$

where we have invoked the statistical homogeneity of the field, since $\mathbf{r} = \mathbf{x}_2 - \mathbf{x}_1$, which is a d -dimensional vector. We assume that the associated spectral density $\tilde{\psi}(\mathbf{k})$ (Fourier transform of the autocovariance) exists. The hyperuniformity condition is simply that the nonnegative spectral density obeys the small-wavenumber condition:

$$\lim_{|\mathbf{k}| \rightarrow 0} \tilde{\psi}(\mathbf{k}) = 0, \quad (260)$$

which implies the sum rule

$$\int_{\mathbb{R}^d} \psi(\mathbf{r}) d\mathbf{r} = 0. \quad (261)$$

The local variance associated with fluctuations in the field within a spherical window of radius R , denoted by $\sigma_F^2(R)$, is related to the autocovariance function or spectral function in the usual way:

$$\begin{aligned} \sigma_F^2(R) &= \frac{1}{v_1(R)} \int_{\mathbb{R}^d} \psi(\mathbf{r}) \alpha_2(r; R) d\mathbf{r}, \\ &= \frac{1}{v_1(R)(2\pi)^d} \int_{\mathbb{R}^d} \tilde{\psi}(\mathbf{k}) \tilde{\alpha}_2(k; R) d\mathbf{k}. \end{aligned} \quad (262)$$

It is interesting to note that one can construct models of two-phase or multiphase heterogeneous systems via level cuts of random scalar fields by choosing appropriate threshold levels to define the phases [339–344]. This approach is particularly useful in modeling *bicontinuous* media (two-phase media in which each phase percolates), such as microemulsions [339], carbonate rocks [342], Vycor glass [342], amorphous alloys, [344] and aerogels [345]. To derive a hyperuniform two-phase medium from a thresholded random field $F(\mathbf{r})$, the field must possess the special correlations required to yield an autocovariance function $\chi_V(\mathbf{r})$ that satisfies the rule (39) [81].

The study of hyperuniformity in random scalar fields is in its very early stages. Some recent results are worth noting. For example, it was proved that a class of random scalar fields derived from underlying hyperuniform point configurations are themselves hyperuniform [81]. Ma and Torquato [146] formulated methods to explicitly construct hyperuniform scalar fields and, by thresholding them, to ascertain whether the resulting two-phase random media were hyperuniform [146]. They specifically considered spatial patterns generated from Gaussian random fields, the Cahn–Hilliard equation for spinodal decomposition, and the Swift–Hohenberg equation for pattern formation. Gaussian random fields that have been used to

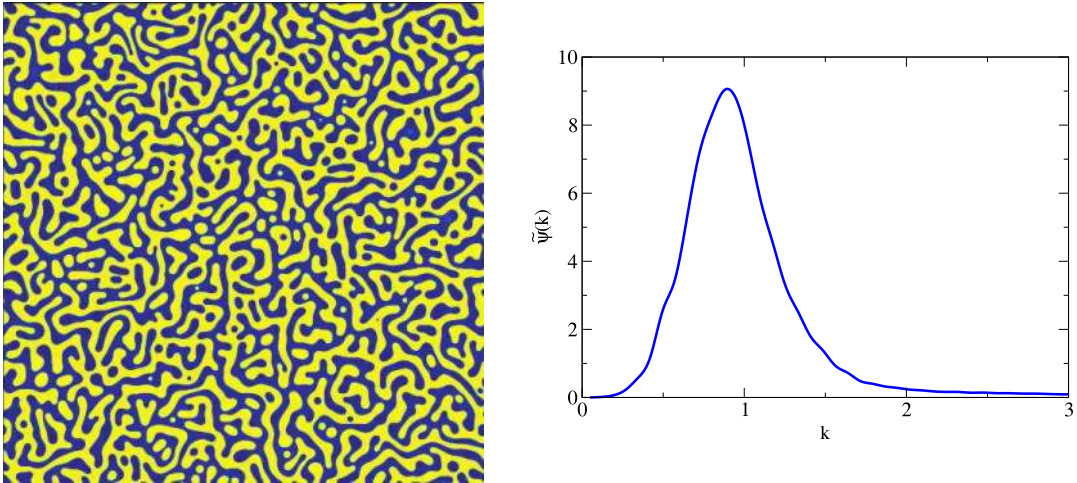


Fig. 56. Snapshot of a two-dimensional system undergoing a coarsening spinodal-decomposition process (left panel) as obtained from a numerical simulation of the Cahn–Hilliard equation reported in Ref. [146]. At this instant of time in the scaling regime, the system is hyperuniform, as evidenced by a scaled spectral density function $\tilde{\psi}(k)$, which is seen to vanish as the dimensionless wavenumber tends to zero (right panel). The reader is referred to Ref. [146] for the manner in which $\tilde{\psi}(k)$ and k are scaled.

model a variety of systems, including the microwave background radiation [17,338], heterogeneous materials [115] and laser speckle fields [334–337]. The time-evolving patterns that arise from spinodal decomposition via the Cahn–Hilliard description [330], which are ubiquitous in chemistry and biological systems. The Swift–Hohenberg equations that describe thermal convection in hydrodynamics [331] as well as a general model of emergent pattern formation [346].

Ma and Torquato demonstrated that it is straightforward to construct Gaussian random scalar fields that are hyperuniform. They also numerically studied the time evolution of spinodal decomposition patterns modeled by the Cahn–Hilliard equation and showed that these patterns are hyperuniform in the scaling regime. Fig. 56 shows a snapshot of such a hyperuniform two-dimensional realization as well as the corresponding spectral density $\tilde{\psi}(k)$. Consistent with hyperuniform behavior, the corresponding local variance $\sigma_f^2(a)$ was shown to decay like $1/a^3$ for large a , where a is the side length of a square window. Moreover, they also characterized labyrinth-like patterns generated by the Swift–Hohenberg equation, and found they are effectively hyperuniform. A toy “polycrystal” model was introduced to explain the features of the local field fluctuations and spectral densities of these labyrinth-like patterns. Finally, they showed that thresholding (level-cutting) a hyperuniform scalar field to produce a two-phase random medium can easily destroy the hyperuniformity of the progenitor scalar field. In particular, a thresholded disordered Gaussian random field is generally not hyperuniform. Several guidelines were provided to achieve effectively hyperuniform two-phase media obtained from thresholded scalar fields.

In summary, hyperuniformity can emerge in scalar fields, and the quantification of long-wavelength scalar field fluctuations provide useful ways to characterize the degree of global order of scalar fields and hence enables the classification of wide class of spatial patterns. These theoretical results are expected to guide experimentalists to synthesize new classes of hyperuniform materials with novel physical properties via coarsening processes and using state-of-the-art techniques, such as stereolithography and 3D printing.

It should be noted that when simulating random fields on the computer or when extracting them from experimentally obtained images, one must inevitably treat discrete or digitized renditions of the fields. The “pixels” or “voxels” (smallest components of the digitized systems in two and three dimensions, respectively) take on gray-scale intensities that span the intensity range associated with the continuous field. Thus, the discrete versions of relations (259) and (262) are to be applied in such instances; see, for example, Ref. [343].

13.3. Random vector fields

The hyperuniformity concept has been recently generalized to characterize fluctuations associated with random vector fields [81]. This was done in the context of divergence-free random vector fields for simplicity, but the basic ideas apply to more general vector fields. Excellent physical examples within this class of vectors fields occur in heterogeneous media, including divergence-free heat, current or mass flux fields, divergence-free electric displacement fields associated with dielectrics, divergence-free magnetic induction fields, and divergence-free low-Reynolds-number velocity fields [115,116]. Incompressible turbulent flow fields provide yet other very well-known set of examples [332,333].

Consider a statistically homogeneous divergence-free (solenoidal) random vector field $\mathbf{u}(\mathbf{x})$ in \mathbb{R}^d that is real-valued with zero mean. A key quantity is the autocovariance function $\Psi_{ij}(\mathbf{r})$ ($i, j = 1, 2, \dots, d$) associated with the vector field $\mathbf{u}(\mathbf{x})$, which

is a second-rank tensor field defined by

$$\Psi_{ij}(\mathbf{r}) = \langle u_i(\mathbf{x}) u_j(\mathbf{x} + \mathbf{r}) \rangle, \quad (263)$$

where we have invoked the statistical homogeneity of the field. Let $\tilde{\Psi}_{ij}(\mathbf{k})$ denote the spectral density tensor, i.e., the Fourier transform of the autocovariance tensor (263). The real-valued spectral density tensor is positive semi-definite, i.e., for an arbitrary real vector \mathbf{a} ,

$$a_i \tilde{\Psi}_{ij}(\mathbf{k}) a_j \geq 0, \quad \text{for all } \mathbf{k}, \quad (264)$$

where Einstein indicial summation notation is implied.

From the theory of turbulence of an incompressible fluid [332,333], it is well known that if an arbitrary divergence-free vector field $\mathbf{u}(\mathbf{x})$ is also isotropic, then the spectral density tensor must take the following general form:

$$\tilde{\Psi}_{ij}(\mathbf{k}) = \left(\delta_{ij} - \frac{k_i k_j}{k^2} \right) \tilde{\psi}(k), \quad (265)$$

where δ_{ij} is the Kronecker delta or identity tensor, and $\tilde{\psi}(k)$ is a nonnegative scalar radial function of the wavenumber $k = |\mathbf{k}|$. A random vector field is isotropic if all of its associated n -point correlation functions are independent of translations, rotations and reflections of the coordinates. Note that the trace of $\tilde{\Psi}_{ij}(\mathbf{k})$ is trivially related to $\tilde{\psi}(k)$, i.e.,

$$\tilde{\Psi}_{ii}(\mathbf{k}) = (d - 1)\tilde{\psi}(k), \quad (266)$$

and so we see that

$$\tilde{\Psi}_{ii}(\mathbf{k} = \mathbf{0}) = (d - 1)\tilde{\psi}(k = 0) = \int_{\mathbb{R}^d} \Psi_{ii}(\mathbf{r}) d\mathbf{r} \quad (267)$$

and

$$\Psi_{ii}(\mathbf{r} = \mathbf{0}) = \frac{(d - 1)}{(2\pi)^d} \int_{\mathbb{R}^d} \tilde{\psi}(k) d\mathbf{k}. \quad (268)$$

Now if the radial function $\tilde{\psi}(k)$ is continuous but positive at $k = 0$ (not hyperuniform), it immediately follows from the form (265) that the spectral tensor can only vanish (i.e., be hyperuniform) in *certain directions*. For example, the component $\tilde{\Psi}_{11}(\mathbf{k})$ is zero for $k = k_1$ (all wave vectors along the k_1 -axis) and the component $\tilde{\Psi}_{12}(\mathbf{k})$ is zero whenever $k_1 = 0$ or $k_2 = 0$. The fact that the value of $\tilde{\Psi}_{11}(\mathbf{k})$ depends on the direction in which the origin is approached means that it is nonanalytic at $\mathbf{k} = \mathbf{0}$. On the other hand, if $\tilde{\psi}(k)$ is hyperuniform and continuous at $k = 0$, then each component of $\tilde{\Psi}_{ij}(\mathbf{k})$ will inherit the radial hyperuniformity of $\tilde{\psi}(k)$, and hence is independent of the direction in which the origin is approached. For example, consider the situation in which $\tilde{\psi}(k)$ admits the following small-wavenumber expansion

$$\tilde{\psi}(k) = a_1 |\mathbf{k}|^\alpha + o(|\mathbf{k}|^\alpha), \quad (269)$$

where a_1 and α are positive constants and o signifies higher order terms. Note that whenever α is a noninteger or odd integer, $\tilde{\psi}(k)$ is a nonanalytic function at the origin due to a derivative discontinuity. (An analytic radial function would admit an expansion in even powers of the wavenumber only.) For any $\alpha > 0$, substitution of (269) in (265) reveals that the spectral tensor is radially hyperuniform near $\mathbf{k} = \mathbf{0}$ such that it vanishes as $|\mathbf{k}|^\alpha$.

Thus we see that one needs an even more general hyperuniformity concept in the case of a spectral tensor, namely, one in which hyperuniformity depends on the direction in which the origin is approached in Fourier space. Let \mathbf{k}_Q represent a d -dimensional unit vector emanating from the origin $\mathbf{k} = \mathbf{0}$. The field is said to be hyperuniform for a particular component $i = I$ and $j = J$ of the spectral tensor of a vector field (isotropic or not) in the direction \mathbf{k}_Q if

$$\lim_{t \rightarrow 0} \tilde{\Psi}_{ij}(t\mathbf{k}_Q) = 0, \quad (270)$$

where t is a scalar parameter. Note that there are many different unit vectors (directions) for a particular spectral tensor that can satisfy this condition, whether this set is countable, or it is uncountable because these unit vectors can occur in a continuous range of directions. Moreover, if the condition (270) applies independent of the direction of the unit vector, then it reduces to the standard spectral definition of hyperuniformity.

To illustrate the hyperuniformity concept in the context of a divergence-free isotropic vector field, consider the following hyperuniform radial function:

$$\tilde{\psi}(k) = c(d)(ka) \exp(-(ka)^2), \quad (271)$$

where

$$c(d) = \frac{\Gamma(d/2) a^d}{2^d \pi^{d/2} \Gamma((d + 1)/2)}, \quad (272)$$

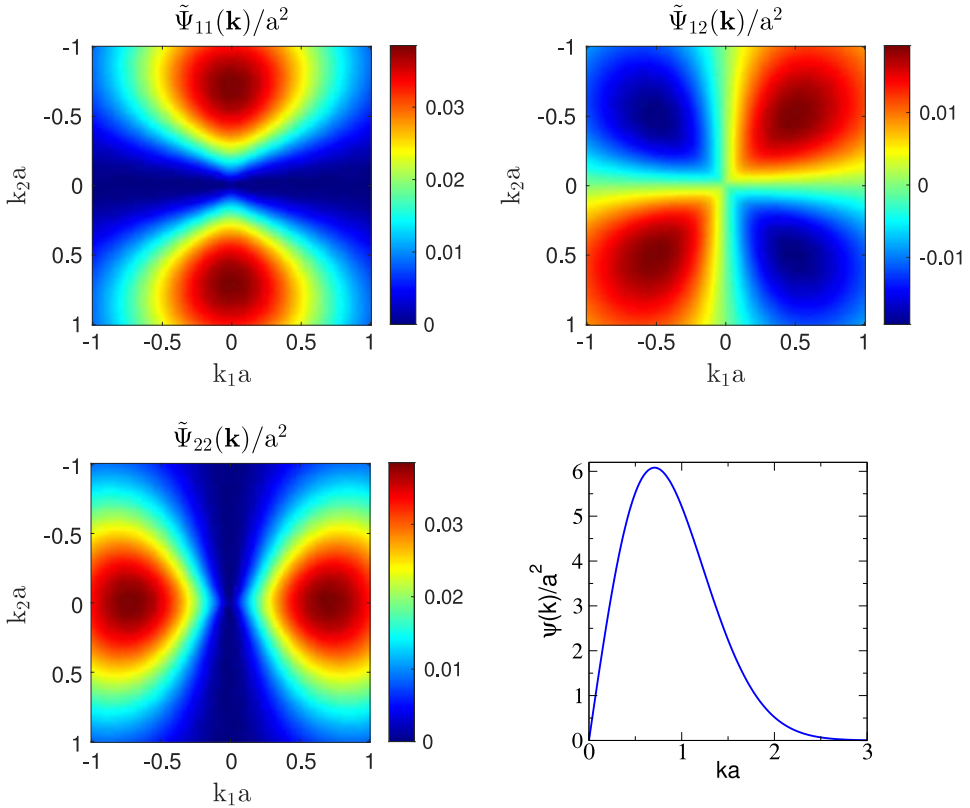


Fig. 57. Spectral patterns for the tensor components of a divergence-free isotropic vector field in \mathbb{R}^2 generated from the radial function $\psi(k)$, defined by (271) with $d = 2$, which is depicted on the right side of the bottom panel. Unlike the nonnegative 11- and 22-components, the 12-component can be both positive and negative, and so its color map indicating zero intensity (darkest shade) is different from those for the diagonal components.

Source: These figures are taken from Ref. [81].

where a is a characteristic length scale. In any dimension, this nonnegative spectral function corresponds to a realizable scalar field associated with an autocovariance function such that $\psi(r = 0) = 1$. For visual purposes, we examine the two-dimensional outcome when (271) is substituted into the spectral tensor (265). Fig. 57 shows three components of this symmetric tensor and the radial function $\tilde{\psi}(k)$. The hyperuniformity property in a compact region around the origin for all components is readily visible.

13.4. Statistical anisotropic structures

Other classes of disordered systems in which “directional” hyperuniformity is relevant include many-particle and heterogeneous systems that are statistically anisotropic, but statistically homogeneous. In such instances, the spectral function conditions (14), (38) and (254) should be replaced with the following ones, respectively:

$$\lim_{t \rightarrow 0} S(t\mathbf{k}_Q) = 0, \quad (273)$$

$$\lim_{t \rightarrow 0} \tilde{\chi}_V(t\mathbf{k}_Q) = 0, \quad (274)$$

$$\lim_{t \rightarrow 0} \tilde{\chi}_S(t\mathbf{k}_Q) = 0, \quad (275)$$

where the unit vector \mathbf{k}_Q is defined immediately above relation (270).

To illustrate the implications of such generalizations, the collective-coordinate optimization technique outlined in Section 8 was employed to create a many-particle system that is hyperuniform in only certain directions in Fourier space [81]. Specifically, the structure factor was constrained to be exactly zero within a lemniscate region around the origin $\mathbf{k} = \mathbf{0}$, implying that this entire region is stealthy (scattering is completely suppressed) but is hyperuniform in only certain directions; see the top panel of Fig. 58. Indeed, this anisotropic structure factor is attainable by like-linear “filamentary” chains of particles that run more or less horizontally (bottom panel of Fig. 58), which corresponds to the ground state of the

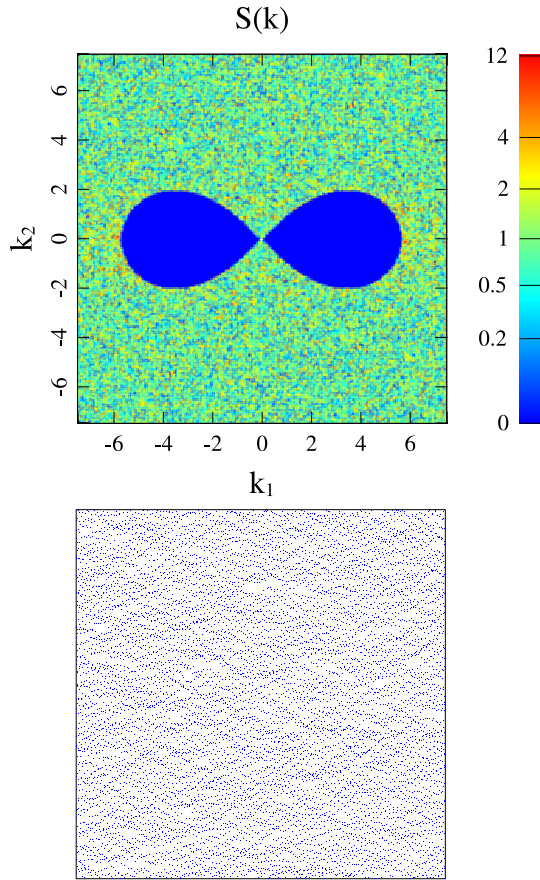


Fig. 58. Top panel: A targeted scattering pattern showing a lemniscate region around the origin in which the scattering intensity is exactly zero (darkest shade). This “stealthy” pattern clearly shows that hyperuniformity depends on the direction in which the origin $\mathbf{k} = \mathbf{0}$ is approached. Bottom panel: A statistically anisotropic ground-state configuration of 10,000 particles that corresponds to the unusual scattering pattern shown in the top panel, which is generated using the collective-coordinate optimization procedure [36,41,42] in a square simulation box under periodic boundary conditions.

Source: These figures are taken from Ref. [81].

associated bounded long-ranged anisotropic (directional) pair potential. These ground states will possess exotic physical properties, as described in Section 14.

For structurally anisotropic systems, one can choose an appropriately shaped nonspherical window occupying region Ω with fixed orientation that maximizes sensitivity of fluctuations in certain directions [81]. Fig. 59 schematically depicts a statistically homogeneous, anisotropic nematic liquid crystal configuration of particles and an appropriate window shape and orientational distribution to distinguish “directional” fluctuations associated with either the centroidal positions of the particles, volume fraction, or interfacial area of the particles. It is clear that window sampling in the direction indicated in Fig. 59 will produce fluctuations that are different from those obtained by sampling in the orthogonal direction.

Many-particle systems that respond to external fields are frequently described by anisotropic structure factors and thus represent a class of systems where directional hyperuniformity can potentially arise. Huang, Wang and Holm [347] have carried out molecular dynamics simulations of colloidal ferrofluids subjected to external fields that capture the salient structural features observed in corresponding experimental systems as measured by the structure factor. In these systems, structural anisotropy arises due to the formation of particle chains that tend to align in the direction of the applied magnetic field; see Fig. 60 taken from Ref. [347]. It is apparent that the system is effectively hyperuniform in the vertical direction.

Long-range hydrodynamic correlations among settling particles in a viscous liquid lead to complex many-body dynamics, exhibiting very large density fluctuations and large-scale dynamic structures when the particles are spheres or other centrally symmetric objects [348–351]. Goldfriend, Diamant and Witten studied [352] the over damped sedimentation of non-Brownian objects of irregular shape using fluctuating hydrodynamics. They showed that the anisotropic response of the objects to flow, caused by their tendency to align with gravity, directly suppresses density and velocity fluctuations in certain directions with varying intensities. This allows the suspension to avoid the anomalous fluctuations predicted for suspensions of spheres and other centrally symmetric particles. The suppression of density fluctuations in suspensions with irregularly-shaped particles leads to structures characterized by directional hyperuniformity.

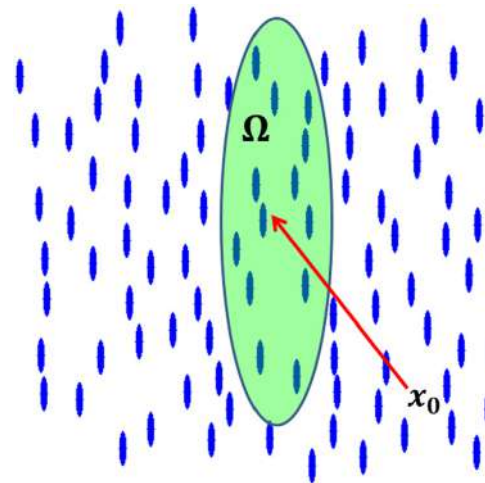


Fig. 59. Schematic illustration of a statistically homogeneous and anisotropic nematic liquid crystal configuration taken from Ref. [81]. An appropriately shaped window that occupies region Ω is also shown. Here x_0 denotes both the centroidal position and orientation of the window, the latter of which is chosen generally from a prescribed probability distribution that depends on the specific structure of interest.

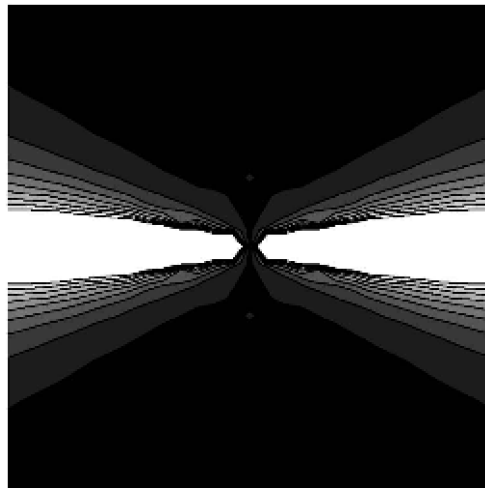


Fig. 60. Anisotropic structure factor of a colloidal ferrofluid in the plane in which the particle chains align, as obtained from Fig. 6 of Ref. [347]. Dark and light regions indicate low and high intensities, respectively. Observe that depending on the direction in which the origin is approached, the structure factor can exhibit effective hyperuniformity.

13.5. Spin systems

We note in passing that the hyperuniformity concept has recently been generalized to spin systems, including a capability to construct disordered stealthy hyperuniform spin configurations as classical ground states [82]. The discovered exotic disordered spin ground states, which are distinctly different from spin glasses [353], are the spin analogs of disordered stealthy hyperuniform many-particle ground states [36,38,40] that have been shown to be endowed with novel bandgap and wave characteristics [86–89,91,97,99–101,103]. The implications and significance of the existence of such disordered spin ground states warrant further study, including whether their bulk physical properties and excited states, like their many-particle system counterparts, are singularly remarkable, and can be experimentally realized.

14. Novel bulk physical properties of disordered hyperuniform materials

We noted in the Introduction that disordered hyperuniform states of matter lie between a crystal and liquid in that they are like perfect crystals in the way they suppress large-scale density fluctuations and yet are like liquids or glasses in that they are statistically isotropic with no Bragg peaks. These unusual attributes can endow such materials with novel equilibrium and

nonequilibrium bulk physical properties. Isotropic disordered hyperuniform materials may offer advantages over periodic materials with high crystallographic symmetries when the latter possess bulk physical properties that have undesirable directional dependence.

While our understanding of the bulk properties of disordered hyperuniform materials is nascent and thus represents a fertile area for future research, evidence is beginning to emerge that such materials have important practical and technological implications. Here we briefly review some of these developments.

14.1. Thermodynamic properties

Interparticle interactions in many-particle hyperuniform systems in thermal equilibrium must necessarily be long-ranged in order to achieve the requisite strong suppression of density fluctuations at large length scales. The anomalous thermodynamic properties of classical one-component plasmas, which must be hyperuniform at all temperatures due to overall charge neutrality with a rigid background of opposite charge, are well-documented [6,149,179,180,182] and hence will not be reviewed here. We saw in Section 8 that the ground states of isotropic stealthy pair potentials with a structure factor $S(\mathbf{k})$ that is constrained to be zero in a spherical region around the origin in reciprocal space (see Fig. 1) are remarkably disordered and highly degenerate provided that $\chi < 1/2$ [38,40]. Such pair interactions are bounded, oscillating, long-ranged functions and the resulting energy landscape is such that the disordered ground states cannot resist shear deformations. This feature distinguishes them from crystalline ground states associated with steep repulsive interactions (e.g., Lennard-Jones and hard-sphere potentials) whose shear moduli are positive. It has been shown that stealthy systems at low positive temperatures possess anomalous equilibrium properties, which again is attributed to the topography of the underlying energy landscape [39,190].

14.2. Wave characteristics

By mapping relatively large 2D disordered stealthy hyperuniform particle configurations, obtained via the collective-coordinate optimization procedure [36,38], to certain 2D trivalent dielectric networks via a Delaunay centroidal tessellation [89] (see left panel of Fig. 61) what was thought to be impossible at the time became possible, namely, the first disordered solids to have large *complete* (both polarizations and all directions) photonic band gaps comparable in size to those in photonic crystals, but with the additional advantage of perfect isotropy [89]. Under the constraint of statistical isotropy, it is the largest degree of stealthiness (χ nearly equal to 0.5) with an accompanying substantial degree of short-range order that is responsible for what appears to be the maximal complete band-gap size in disordered hyperuniform dielectric networks. (We have seen in Section 8 that short-range order increases with increasing χ in the disordered regime $0 \leq \chi \leq 1/2$ [36,38,41].) This computational study enabled the design and fabrication of disordered cellular solids with unprecedented waveguide geometries unhindered by crystallinity and anisotropy, and robust to defects [90,91]; see Fig. 61. Such materials are thus suitable for various applications, including lasers, sensors, and optical microcircuits [91]. Florescu, Steinhardt and Torquato [89] suggested that disordered hyperuniform solid networks had ramifications for electronic and phononic band gaps in disordered materials, which indeed has been borne out [103,105,106]; see also Section 16.2. A recent 2D numerical study by Froufe-Pérez et al. [101] of disordered photonic solids suggested that short-range order and hyperuniformity were more important than stealthiness in determining band gap formation, but the systems examined were relatively small and its not clear that the same conclusions would be drawn for larger systems, as explained immediately below.

A critical theoretical question is whether a complete isotropic photonic band gap persists in a disordered solid network in the infinite-system-size (thermodynamic) limit. Since most disordered systems, including many hyperuniform varieties, contain arbitrarily large “holes” (see Section 8.2), such inhomogeneities would seem to preclude them from possessing complete photonic band gaps in the thermodynamic limit. On the other hand, disordered stealthy hyperuniform systems cannot tolerate arbitrarily large holes [43], which we conjecture here to be a necessary condition to have a complete photonic band gap in the thermodynamic limit. This is precisely why one must be very careful in drawing conclusions about band gap size from numerical simulations because hole formation is an extremely rare event that is virtually impossible to see in the very limited simulation box sizes and number of configurations, especially those that make it is computationally feasible to solve Maxwell's electromagnetic equations.

The propagation of electromagnetic waves in hyperuniform two-phase dielectric media are predicted to be lossless in the long-wavelength limit. This prediction is derived from the corresponding “strong-contrast” expansions for the frequency-dependent effective dielectric constant ε_e [354]. Through lowest-order in the perturbation expansion as well as an accurate approximations for ε_e based on a resummation of the series the imaginary part of the effective dielectric constant depends on the volume integral over the autocovariance function $\chi_v(\mathbf{r})$, defined by (33). This means that the imaginary part, which accounts for attenuation (losses) due to incoherent multiple scattering in a typical disordered two-phase system, is identically zero for any hyperuniform material (to an excellent approximation) due to the sum rule (39) and hence waves can propagate without any dissipation. This suggests that “stealthy” disordered hyperuniform two-phase dielectric materials (to an excellent approximation) must be dissipativeless for a wider range of wavelengths [87]. Recent calculations of the frequency-dependent effective dielectric constant have been carried out for designed phase-inversion-symmetric disordered hyperuniform composites and disordered stealthy dispersions in two dimensions [87] as well as dispersions of MRJ spheres

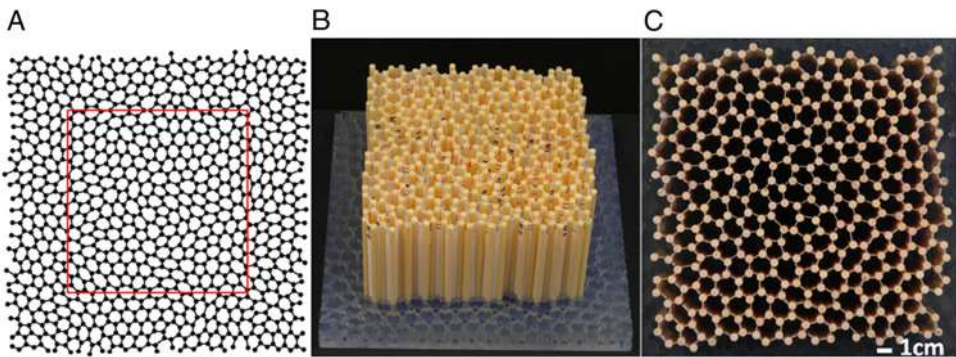


Fig. 61. Computational design of a 2D stealthy hyperuniform disordered network solid (cross-section) and corresponding fabricated three-dimensional structure built of “cylinders” and “walls”. (A) Delaunay centroidal tessellation of a stealthy hyperuniform point configurations decorated with cylinders and walls [89]. The area enclosed in the red box is the structure used in the experimental study. Side view (B) and top view (C) of the stealthy hyperuniform disordered structure used in the experiment, assembled with Al_2O_3 cylinders and walls [91].

Source: This figure is taken from Ref. [91].

in three dimensions [88]. It is notable that another recent study [86] has demonstrated that a Lunesburg lens (which focuses a plane wave or transforms a circular wave from a point source to a plane wave) based on a disordered hyperuniform design has superior radiation properties compared to those of previously reported metamaterial designs.

It is noteworthy that a recent computational study by Leseur, Pierrat and Carminati [99] has demonstrated that high-density materials made of non-absorbing subwavelength stealthy hyperuniform scatterers can be made transparent. More precisely, under very general conditions, such materials can be transparent for a range of wavelengths at densities for which an uncorrelated disordered material would be opaque due to multiple scattering.

As discussed in Section 12.1, Nature has shown us a disordered *multihyperuniform* design in the avian retina for acute color sensing [70]. This strongly suggests that the performance of color displays and sensors could be improved by the use of multihyperuniform color patterns, and hence represents a potentially technologically important area for future development.

14.3. Transport properties

Recently, stealthy disordered hyperuniform point configurations have been mapped to two-phase media by circumscribing each point with a possibly overlapping sphere of a common radius a : the “particle” and “void” phases are taken to be the space interior and exterior to the spheres, respectively, and their transport properties were computed [104]. The effective diffusion coefficient of point particles diffusing in the void phase as well as static and time-dependent characteristics associated with diffusion-controlled reactions in which the particles are perfectly absorbing traps for diffusing reactants were considered. It was shown that these transport as well as certain geometrical and topological properties of two-phase media derived from decorated stealthy ground states are distinctly different from those of equilibrium hard-sphere systems and spatially uncorrelated overlapping spheres. As the extent of short-range order increases, stealthy disordered two-phase media can attain nearly maximal effective diffusion coefficients over a broad range of volume fractions while also maintaining isotropy, and therefore may have practical applications in situations where ease of transport is desirable.

The Fourier-space based construction procedure described in Section 6.3 has recently been employed to design both phase-inversion-symmetric composites and disordered stealthy hyperuniform dispersions in a matrix with desirable effective conductivities [87]. The stealthy dispersions were shown to possess nearly optimal effective conductivities, while being fully statistically isotropic.

In the context of type-II superconductors, it was shown that vortices with hyperuniform pinning site geometries exhibit enhanced pinning, enabling higher critical currents [355], which is robust over a wide range of parameters. The stronger pinning arises in the hyperuniform arrays due to the suppression of pinning density fluctuations (greater global uniformity), allowing higher pin occupancy and the reduction of “weak links” that lead to easy flow channeling.

Interestingly, it has been shown theoretically that there is a relationship between a dynamical exponent associated with the long-time diffusion coefficient in disordered porous media is related to large-scale volume-fraction fluctuations and, specifically, the exponent α defined by (133) [356]. This link, which enables one to distinguish hyperuniform from nonhyperuniform systems, was recently verified experimentally using diffusion nuclear magnetic resonance methods [357].

14.4. Mechanical properties

By virtue of the similarities between the optimal microstructures for the effective electrical (thermal) conductivity and effective bulk and shear moduli of two-phase composites [115,358], certain decorations of disordered stealthy hyperuniform

point patterns are expected to have nearly optimal effective elastic moduli in the same way that they have nearly optimal effective conductivities [87]. Moreover, the suppression of volume-fraction fluctuations in disordered hyperuniform particulate composites is known to suppress crack propagation within the matrix phase [199]. Thus, appropriately designed disordered hyperuniform composites could have desirable mechanical failure characteristics. Indeed, in a recent study by Xu et al. [85], designed hyperuniform composites were shown to possess a significantly higher brittle fracture strength than nonhyperuniform ones.

14.5. Structurally anisotropic materials

Structural anisotropic many-particle systems and heterogeneous materials generally possess directional-dependent physical properties, including optical, transport, acoustic and elastic behaviors. Such materials with directional hyperuniformity (see Section 13.4) are expected to possess unusual physical properties, but their potential for technological applications has yet to be explored. The collective-coordinate optimization procedure described in Section 13.4 provides a systematic procedure to design hyperuniform anisotropic materials. Such tunability could have technological relevance for manipulating light and sound waves in media in ways heretofore not thought to be possible. Interestingly, although anisotropic stealthy ground-state configurations, such as one shown in Fig. 58, cannot support shear (for similar reasons as in their isotropic counterparts [42]), they are generally elastically anisotropic because the stress tensor is *asymmetric*. Indeed, such configurations generally will possess internal force couples that resist out-of-plane torques [81]. Directional structural hyperuniformity raises the interesting possibility that there may exist disordered many-particle systems in equilibrium that at positive temperature T are incompressible in certain directions and compressible in other directions — a highly unusual situation [81].

15. Effect of imperfections on hyperuniform states

In the same way that there is no infinitely large perfect crystal in practice due to the inevitable existence of imperfections, such as point defects (e.g., vacancies), dislocations and thermal excitations, there is no infinitely large perfect disordered hyperuniform system, whether in thermal equilibrium or not. For instance, in both equilibrium and nonequilibrium systems, point defects can arise and consequently destroy the hyperuniformity, albeit in some cases to a small degree. In addition, we have seen that any compressible ($\kappa_T > 0$) equilibrium system cannot be hyperuniform at positive temperatures due to thermal excitations, which follows from the compressibility relation (78) [40,81]. Moreover, it can be difficult to attain perfect hyperuniformity in disordered nonequilibrium systems due to a *critical slowing down*, as discussed in Sections 11.1.5 and 11.2.1.

Thus, in both experiments and numerical simulations, it is important to understand the extent to which the hyperuniformity can be degraded or destroyed due to such imperfections in an otherwise hyperuniform system. Interestingly, the presence of imperfections can significantly alter the properties of materials. Specifically, point defects and dislocations can substantially enhance the mechanical strength of metals [192,359]. Moreover, impurities can have a dramatic influence on the electronic properties of crystalline solids, e.g., color centers [192,360], doped semiconductors [192,360], and the Kondo effect [361,362].

In what follows, we discuss how the degree of hyperuniformity of a perfect hyperuniform system, either ordered or disordered, is affected by the introduction of imperfections, such as point vacancies, particle displacements, and thermal excitations, following closely the recent work of Kim and Torquato [144]. We start with an initial hyperuniform point process at number density ρ that has a structure factor $S_0(\mathbf{k})$ and a pair-correlation function $g_2^{(0)}(\mathbf{r})$.

Point vacancies in a crystal refers to missing particles at the crystal sites that are fully occupied by particles in the perfect crystal. In many cases, the presence of point defects induces elastic deformations in the crystal, resulting in asymmetric diffuse scattering near Bragg peaks, which is called Huang diffuse scattering [363,364]. If one neglects the effect of deformations, the structure factor of a defective crystal with uncorrelated point vacancies is given by

$$S(\mathbf{k}) = p + (1 - p)S_0(\mathbf{k}), \quad (276)$$

where p is the concentration of vacancies. It is noteworthy that this relation is also applicable to disordered point processes, whether they are hyperuniform or not; see Refs. [364] and [144] for various derivations of this equation. We see that even a small concentration of defects can destroy hyperuniformity, even if to a small degree.

Now consider a perturbed point configuration in which the position of the i th particle \mathbf{r}_i ($i = 1, 2, \dots$) in an initial hyperuniform point configuration is displaced to a new position $\mathbf{r}_i + \mathbf{u}(\mathbf{r}_i)$. When the initial point configuration is a lattice, we call the perturbed system a *perturbed lattice* [365], which is also known as the *shuffled lattice* [27,28,142,143]. Welberry et al. [365] investigated perturbed lattices with Gaussian perturbations in the context of distorted crystals, and Gabrielli [142] and Gabrielli, Joyce and Torquato [138] studied this subject more generally in the context of hyperuniformity.

The structure factor of a perturbed point process, whether it is initially ordered or disordered, can be written as [142,365]

$$S(\mathbf{k}) = 1 + \rho \int d\mathbf{r} e^{-i\mathbf{k} \cdot \mathbf{r}} g_2^{(0)}(\mathbf{r}) \hat{\phi}(\mathbf{k}; \mathbf{r}), \quad (277)$$

where $\hat{\phi}(\mathbf{k}; \mathbf{r}) \equiv \int d\mathbf{u} d\mathbf{v} \exp(i\mathbf{k} \cdot (\mathbf{u} - \mathbf{v})) f_2(\mathbf{u}, \mathbf{v}; \mathbf{r})$ and $f_2(\mathbf{u}, \mathbf{v}; \mathbf{r}) d\mathbf{u} d\mathbf{v}$ is the joint probability that two particles, initially separated by \mathbf{r} , are displaced by \mathbf{u} within a volume element $d\mathbf{u}$ and \mathbf{v} within $d\mathbf{v}$, respectively. Note that relation (277) is valid whether the initial configuration is hyperuniform or not. If the displacements are uncorrelated and identically distributed, the associated joint probability density function is the product of two singlet probability densities, i.e., $f_2(\mathbf{u}, \mathbf{v}; \mathbf{r}) = f_1(\mathbf{u})f_1(\mathbf{v})$, where $f_1(\mathbf{u})$ is the singlet probability density function of a displacement \mathbf{u} . Thus, (277) simplifies as follows [142,143]:

$$S(\mathbf{k}) = 1 - |\tilde{f}_1(\mathbf{k})|^2 + |\tilde{f}_1(\mathbf{k})|^2 S_0(\mathbf{k}), \quad (278)$$

where $\tilde{f}_1(\mathbf{k})$ is the Fourier transform of $f_1(\mathbf{u})$. The fact that $\tilde{f}_1(\mathbf{k}) \rightarrow 1$ as $|\mathbf{k}| \rightarrow 0$ enables one to conclude from (277) that perturbing a hyperuniform point process preserves the hyperuniformity of the original system if the displacements are uncorrelated. However, in all cases, the resulting growth rate of the number variance cannot be slower than that of the original hyperuniform system. For example, depending upon whether the variance of $f_1(\mathbf{u})$ exists, an original class I hyperuniform system can remain class I or may change to class II or III.

Let us now suppose that the displacements \mathbf{u} are isotropic and two of its orthogonal components are uncorrelated when $d \geq 2$. It then follows that $\hat{\phi}(\mathbf{k}; \mathbf{r})$ in (277) for small $|\mathbf{k}|$ must be given asymptotically by

$$\hat{\phi}(\mathbf{k}; \mathbf{r}) = 1 + |\mathbf{k}|^2 [G(\mathbf{r}) - G(\mathbf{0})] + \mathcal{O}(|\mathbf{k}|^4), \quad (279)$$

where $G(\mathbf{r}) \equiv \langle u_1(\mathbf{r} + \mathbf{r}_0)u_1(\mathbf{r}_0) \rangle$ is the displacement-displacement correlation function, $\langle \mathbf{u} \rangle = \mathbf{0}$ due to the isotropy of \mathbf{u} , and thus $G(\mathbf{0}) = \langle |\mathbf{u}|^2 \rangle / d$ if $\langle |\mathbf{u}|^2 \rangle$ exists. Using (279), the structure factor $S(\mathbf{k})$ in (277) for small $|\mathbf{k}|$ is given approximately by [142]

$$S(\mathbf{k}) \approx [|\mathbf{k}|^2 G(\mathbf{0}) + (1 - |\mathbf{k}|^2 G(\mathbf{0})) S_0(\mathbf{k})] + \rho |\mathbf{k}|^2 \tilde{G}(\mathbf{k}) + \rho |\mathbf{k}|^2 \int d\mathbf{r} e^{-i\mathbf{k} \cdot \mathbf{r}} h_0(\mathbf{r}) G(\mathbf{r}), \quad (280)$$

where $h_0(\mathbf{r}) \equiv g_2^{(0)}(\mathbf{r}) - 1$ and $\tilde{G}(\mathbf{k})$ is the Fourier transform of $G(\mathbf{r})$. Note that since $|\tilde{f}_1(\mathbf{k})|^2 \approx 1 - |\mathbf{k}|^2 \langle |\mathbf{u}|^2 \rangle / d = 1 - |\mathbf{k}|^2 G(\mathbf{0})$ for small $|\mathbf{k}|$ if $\langle |\mathbf{u}|^2 \rangle$ exists, the terms in the square brackets in (280) correspond to the right-hand side of relation (278), and the next two terms in (280) describe contributions from correlated displacements. Gabrielli [142] pointed out that when $\tilde{G}(\mathbf{k}) \sim |\mathbf{k}|^\beta$ for small $|\mathbf{k}|$, the perturbed point process is hyperuniform if $\beta > -2$.

Structure factors of crystals in thermal equilibrium have been extensively studied in the past by utilizing approximations for $\hat{\phi}(\mathbf{k}; \mathbf{r})$ in (277). For instance, the Debye–Waller factor $\exp(-\langle (\mathbf{q} \cdot \mathbf{u})^2 \rangle)$ [192], a major contribution to diffuse scattering in harmonic crystals, is obtained from the terms $1 - |\mathbf{k}|^2 G(\mathbf{0})$ in (279). However, previous studies mainly focused on diffuse scattering near Bragg peaks rather than on the small-wavenumber behavior. Thus, it had not been quantitatively understood how thermal excitations effect the behavior of the structure factor for small wavenumbers and hence how they precisely destroy the hyperuniformity of ground-state crystals as the temperature is increased. Recently, Kim and Torquato [144] addressed this question by deriving the structure factor of a classical harmonic hypercubic lattice in thermal equilibrium; in short, they showed that

$$S(\mathbf{k}) \approx \langle |\mathbf{k} \cdot \tilde{\mathbf{u}}(\mathbf{k}, t)|^2 \rangle = |\mathbf{k}|^2 \frac{k_B T}{m \omega_{\parallel}^2(\mathbf{k})} \quad (|\mathbf{k}|a \ll 1), \quad (281)$$

where m is the mass of a single particle, a is lattice constant, $\tilde{\mathbf{u}}(\mathbf{k}, t)$ refers to the normal coordinates of a harmonic crystal [4] at a wave vector \mathbf{k} [essentially the Fourier components of a small displacement $\mathbf{u}(\mathbf{r}, t)$ of a particle initially located at \mathbf{r}] and $\omega_{\parallel}(\mathbf{k})$ is the angular frequency of $\tilde{\mathbf{u}}(\mathbf{k}, t)$ with a longitudinal polarization. In the small-wavenumber limit, (281) recovers the compressibility relation (78) with an isothermal compressibility that is given by

$$\kappa_T = (Ka^{2-d})^{-1}, \quad (282)$$

where K is the spring constant between nearest neighbors. Relation (282) has the same form for other lattices but with different constant parameters [144]. We note in passing that equilibrated 3D hard-spheres systems obtained via molecular dynamics on approach to the fcc jamming point along the stable crystal branch exhibits the same structure factor scaling as in (281) [54].

Interestingly, harmonic crystals in thermal equilibrium can be viewed as correlated perturbed lattices. We learned that uncorrelated perturbed systems, which contribute only to the one-point statistics, cannot arise long-wavelength density fluctuations. However, correlated perturbations can influence the two-point statistics in a point process; if the correlations are sufficiently long-ranged, i.e., $\tilde{G}(\mathbf{k}) \sim |\mathbf{k}|^{-2}$ for small $|\mathbf{k}|$, then the hyperuniformity of an initial point process can be destroyed [142] because the contribution $|\mathbf{k}|^2 \tilde{G}(\mathbf{k})$ from “correlations” in (280) remains a constant for small wavenumbers. Displacement-displacement correlation functions of classical harmonic crystals in thermal equilibrium exactly satisfy this condition, regardless of the space dimension d [144]. For low dimensions ($d \leq 2$), this implies that $\langle |\mathbf{u}|^2 \rangle$ diverges, or equivalently the Debye–Waller factor vanishes, which is consistent with previous theoretical studies [366].

16. Nearly hyperuniform systems

Quantifying large-scale density fluctuations of a many-particle system is of interest, regardless of whether it is hyperuniform. For example, the relative magnitudes of the volume and surface-area coefficients in the asymptotic expansion of

the local number variance $\sigma_N^2(R)$ contain crucial information about the large-scale structure of a many-body system. This was borne out in a recent study concerning amorphous ices and transitions between their different forms [84]. Moreover, understanding structural and physical properties of a system as it approaches a hyperuniform state or whether near hyperuniformity in a system is signaling crucial large-scale structural changes appears to be fundamentally important. In what follows, we briefly review some developments along these lines.

16.1. Growing length scale on approach to a hyperuniform state

In Section 7, we saw that the volume integral of the direct correlation function $c(\mathbf{r})$, i.e., $\tilde{c}(\mathbf{k} = \mathbf{0})$, diverges to $-\infty$ at a hyperuniform state, whether in equilibrium or not, where $\tilde{c}(\mathbf{k})$ is the Fourier transform of $c(\mathbf{r})$. This volume integral is expected to have a large magnitude for any system that is near a hyperuniform state. Thus, it is natural to define the following length scale [50,107]:

$$\xi_c \equiv [-\tilde{c}(\mathbf{k} = \mathbf{0})]^{1/d}, \quad (283)$$

to herald the anomalous suppression of large-scale density fluctuations. In the case of overcompressed nonequilibrium hard-sphere systems, ξ_c grows with increasing density well before the critical hyperuniform state is reached [50,54]. For well-known atomic glass formers, this length scale is able to distinguish subtle structural differences between glassy and liquid states and grows upon supercooling, even as the temperature is lowered past the glass transition temperature and even if these states are only nearly hyperuniform [107]. Moreover, in all of these cases [50,107], as ξ_c grew, so did the nonequilibrium index X , defined by (79). Interestingly, using a revised cell theory, it has been shown that jamming results in a percolation transition described by a static diverging length scale that is proportional to ξ_c [114].

16.2. Amorphous silicon and electronic band gaps

The development of accurate structural models of amorphous silicon (a-Si) and other tetrahedrally coordinated solids has been an active area of research for many decades [367–370], but many challenges and questions remain. The structure of a-Si is approximated well by continuous random network (CRN) models [367,369], which are fully four-coordinated, isotropic disordered networks that contain primarily five, six, and seven atom rings, while maintaining nearly perfect local tetrahedral order. The concept of nearly hyperuniform network (NHN) structures has been proposed [105] as alternatives to the CRN models for amorphous tetrahedrally coordinated solids, such as a-Si, especially after annealing. A NHN has been defined as an amorphous tetrahedral network whose structure factor $S(\mathbf{k})$ at $\mathbf{k} = \mathbf{0}$ is smaller than the liquid value at the melting temperature. As a practical matter, one is interested in cases where $S(\mathbf{k} = \mathbf{0})$ is substantially less, by 50% or more, which implies a substantial reduction in the large-scale density fluctuations and runs counter to the limitations imposed by the “frozen-liquid” paradigm of a glass [371]. Using a novel implementation of the Stillinger-Weber potential for the interatomic interactions [372], Henja et al. [105] showed that the energy landscape for a spectrum of NHNs includes a sequence of local minima with an increasing degree of hyperuniformity that is significantly below the frozen-liquid value and that correlates with other measurable features in the structure factor at intermediate and large wavenumbers. Among other results, it was shown the degree of hyperuniformity correlates with the width of the electronic band gap, i.e., in terms of the “hyperuniformity parameter” H , defined by relation (251), this means that this width increases as H decreases.

On the experimental side, results of highly sensitive transmission X-ray scattering measurements have been reported on nearly fully dense high-purity a-Si samples for the purpose of determining their degree of hyperuniformity [106]. Annealing was observed to increase the degree of hyperuniformity in a-Si where it was found that $S(0) = 0.0075(\pm 0.0005)$, which is significantly below the suggested lower bound based on computational studies of CRN models [371], but consistent with the recently proposed NHN picture of a-Si [105]. Increasing hyperuniformity was shown to be correlated with narrowing of the first diffraction peak and the extension of the range of oscillations in the pair distribution function.

16.3. Polymeric materials: liquid state and glass formation

Here we briefly describe some work that demonstrates that models of polymers in equilibrium and of glassy polymer systems can be made, under certain conditions, to be nearly hyperuniform and, in some cases, nearly stealthy and hyperuniform.

16.3.1. Equilibrium liquids

The Gaussian-core model (GCM), in which particles interact with a purely repulsive Gaussian pair potential, $v_2(r) = \epsilon \exp[-(r/\sigma)^2]$, was introduced by Stillinger [374] as a simple model to mimic effective pair interactions between the centers of mass of two polymer chains. Since then, the GCM has been investigated by many groups [373,375–377]. Zachary, Stillinger and Torquato [373] studied the liquid states of this model in \mathbb{R}^d in various approximations and arbitrary dimensions. Among other results, they employed the d -dimensional generalization of the structure factor in the *mean-field-approximation* (MFA) for the GCM to quantify its large-scale density fluctuations in the high-density limit:

$$S(k) = \frac{1}{1 + \lambda_d \exp\left[-\frac{(k\sigma)^2}{4}\right]}, \quad (284)$$

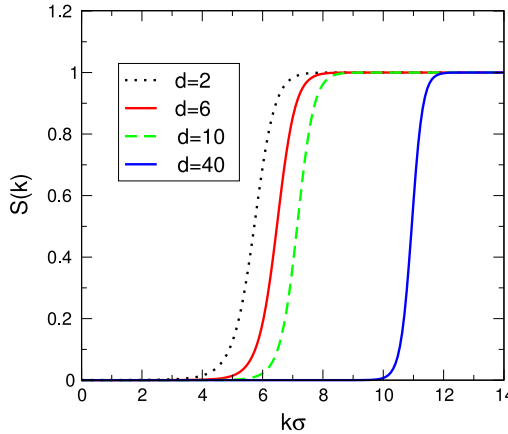


Fig. 62. Structure factor $S(k)$ in the MFA for the GCM at selected d with $\beta\epsilon = 100$ and $\rho\sigma^d = 36/\pi$, as obtained from relation (284) given in Ref. [373].

where $\lambda_d = \beta\epsilon\rho\sigma^d\pi^{d/2}$ is a dimensionless parameter that depends on dimension, $\beta = 1/(k_B T)$ is an inverse temperature, and k_B is Boltzmann's constant. This approximation was first derived by Lang et al. in three dimensions [375] and shown by them to be in excellent agreement with computer simulations. The MFA structure factor (284) is plotted in Fig. 62 for selected dimensions at fixed dimensionless temperature $\beta\epsilon = 100$ and fixed dimensionless density $\rho\sigma^d = 36/\pi$. It is seen that the systems are not only nearly hyperuniform but they are nearly stealthy for a range of wavenumbers that increases as d increases. The degree of hyperuniformity increases as d increases. Thus, the GCM in the high-density regime are examples of disordered systems in equilibrium that at positive temperatures are very nearly hyperuniform and stealthy. To understand this more quantitatively, consider the first two terms in the series expansion of the MFA structure factor (284) about $k = 0$ for any d :

$$S(k) = \frac{1}{1 + \lambda_d} + \frac{\lambda_d}{4(1 + \lambda_d)^2} (k\sigma)^2 + \mathcal{O}(k^4). \quad (285)$$

Thus, for large λ_d , $S(0) \sim \lambda_d^{-1}$. In particular, fixing $\beta\epsilon = 100$ and $\rho\sigma^d = 36/\pi$, as in the cases plotted in Fig. 62, we find that $S(0) \approx 2.8 \times 10^{-4}$, 2.8×10^{-5} , 2.9×10^{-6} , and 1.0×10^{-13} for $d = 2, 6, 10$ and 40 , respectively. Ikeda and Miyazaki studied the high-density equilibrium behavior of the GCM in three dimensions via molecular dynamics [376]. Fig. 5 in this paper shows $S(k)$ at four densities for liquids at the declining freezing temperature, with an insert indicating strong convergence to hyperuniformity [i.e., $S(0) = 0$] upon compression, which is consistent with the aforementioned results.

16.3.2. Glassy systems

Douglas and coworkers explored the utility of information in the static structure factor $S(k)$ to quantify molecular jamming processes that underlie glass-formation in polymeric materials. Their molecular dynamics simulations indicated that polymeric materials (bulk materials composed of flexible polymers [80] and nanoparticle fluids with chains grafted onto their surfaces [83]) are prototypical “soft” materials because the many internal degrees of freedom within the molecules allow for rearrangements at a molecular scale that naturally permit the approach to a hyperuniform solid-like state. In particular, they found that the onset temperature of glass formation T_A may be estimated by a Hansen–Verlet freezing criterion, corresponding to the peak height in the first peak in $S(k)$. In physical terms, when this peak is large the particles have begun to be locally “jammed”. However, this localization is transient in equilibrium liquids because the inertia of the polymer segments ultimately allows them to escape from their “cages”. The temperature T_A is the temperature at which transient particle localization first emerges. They also found that polymer fluids progressively approach a hyperuniform glassy state upon cooling and that the temperature range demarcating the end of glass formation process in measurements may be estimated from the magnitude of the “hyperuniformity parameter H ” [53], defined by relation (251).

Fig. 63 shows structure-factor characteristics as a function of temperature T , normalized energy ϵ , a parameter measuring the strength of the intermolecular cohesive interaction, which was first presented in Ref. [80]. Data is shown for both constant volume V and constant pressure P . From this universal curve, the temperature at which $H = \mathcal{O}(10^{-3})$ can be estimated to be about $T/\epsilon = 0.3$ at constant pressure, a value that is comparable to the characteristic Vogel–Fulcher–Tammann temperature at which the viscosity of the cooled liquid extrapolates to infinity based on measurements performed above the glass-transition temperature. Simulations of nanoparticle fluids in which the nanoparticles have layers of grafted polymer chains also led to fluid materials that are effectively hyperuniform at low temperatures, proving further evidence that “soft molecular fluids in which the molecules have many internal degrees of freedom that can adjust under local jamming conditions are ideal materials for actually achieving effectively hyperuniform materials [83]. One may thus estimate both the “onset” and “end” of the glass-formation process from thermodynamic properties of glass-forming liquids, at least

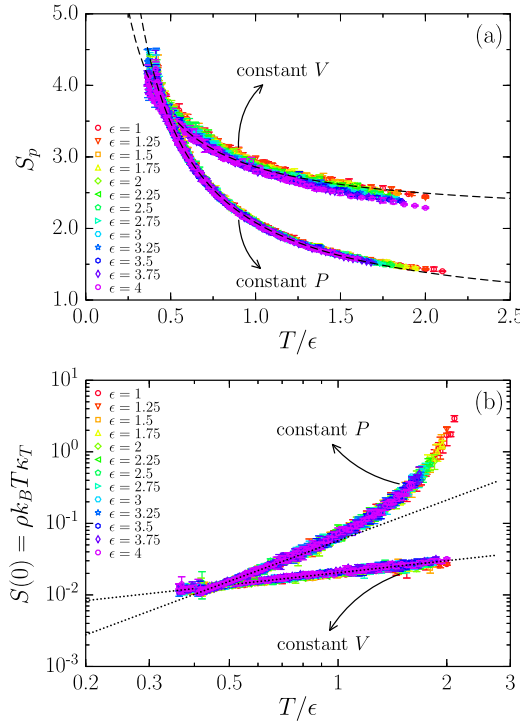


Fig. 63. (a) Height S_p of the first peak of $S(k)$ and (b) $S(0)$ as a function of T/ϵ for various ϵ at constant volume V and constant pressure P . Dashed and dotted lines in (a) and (b), respectively, are fits to the data. This is Fig. 7 of Ref. [80].

under constant pressure conditions. On approaching the glassy state, the liquid evidently shows an opposite tendency in comparison to approaching a liquid critical point, in the sense that the compressibility tends to vanish rather than diverge. Douglas and coworkers emphasize that while the evidence points to a thermodynamic transition underlying glass formation, no phase transition involving the singular changes in the free energy arises as temperature or density is varied.

17. Discussion and outlook

Hyperuniform systems are characterized by an unusually large suppression of density fluctuations at long wavelengths (large length scales) compared to those in ordinary disordered systems, such as typical fluids and amorphous solids. The hyperuniformity concept provides a unified means to classify and structurally characterize crystals, quasicrystals and special disordered systems. While this review article focused attention on disordered hyperuniform systems, we have seen that problems involving the quantification of the hyperuniformity of the ordered kinds, crystals and quasicrystals, have deep connections to problems in pure mathematics (e.g., number theory and discrete geometry) and theoretical physics (e.g., low-temperature states of matter and integrable quantum systems).

Disordered hyperuniform systems and their manifestations were largely unknown in the scientific community about a decade and a half ago, but this survey reveals that such systems arise in a plethora of contexts across the physical, materials, chemical, mathematical, engineering and biological sciences, including disordered ground states, glass formation, jamming, high-pressure states of matter, Coulomb systems, spin systems, quantum states of matter, photonic and electronic band structure, localization of waves and excitations, quantum chaos, self-organization, fluid dynamics, number theory, stochastic point processes, integral and stochastic geometry, the immune system, and photoreceptor cells [13,14,34,36–74,79–107,219,248]. Remarkably, disordered hyperuniform systems can be obtained via equilibrium or nonequilibrium routes, and come in both quantum-mechanical and classical varieties. Such isotropic amorphous states of matter are poised at exotic critical points, and are like perfect crystals in the way they suppress large-scale density fluctuations, a special type of long-range order, and yet are like liquids or glasses in that they are statistically isotropic with no Bragg peaks and hence lack any conventional long-range order. These unusual attributes endow such materials with novel physical properties, including photonic, phononic, electronic, transport and mechanical properties that are only beginning to be discovered, both computationally [86–90,99–102,104,105] and experimentally [59,63,91–95,98,103]. Nonetheless, their full potential in technological applications has yet to be explored or realized. The design and fabrication of novel disordered hyperuniform materials can be accelerated by integrating the output of algorithms that are now available to design disordered hyperuniform systems with targeted spectral functions (both point configurations [36–38,41] and two-phase materials [87,124]) with micro- and nano-scale additive manufacturing techniques [378].

We have also seen that the hyperuniformity concept has illuminated the importance of studying the large-scale structural correlations in amorphous systems, regardless of whether they are hyperuniform, via the quantification of the long-wavelength behavior of their spectral functions or corresponding density fluctuations. Understanding structural and physical properties of a system as it approaches a hyperuniform state or whether near hyperuniformity is signaling crucial large-scale structural changes in a system is fundamentally important and should lead to new insights about condensed phases of matter. The hyperuniformity concept has suggested a “nonequilibrium index” for glasses and novel static correlation functions from which one can extract relevant growing length scales as a function of temperature as a liquid is supercooled below its glass transition temperature.

While the notion of hyperuniformity was introduced in the context of density fluctuations associated with point configurations and subsequently of volume-fraction fluctuations in heterogeneous materials [32], it has very recently been broadened along four different directions [81]. This includes generalizations to treat fluctuations in the interfacial area in heterogeneous media and surface-area driven evolving microstructures, random scalar fields (e.g., spinodal decomposition), random vector fields (e.g., velocity fields in turbulence and transport in random media), and statistically anisotropic many-particle systems (e.g., structures that respond to external fields) and two-phase media. In the instances of random vector fields and statistically anisotropic structures, the standard definition of hyperuniformity must be generalized such that it accounts for the dependence of the relevant spectral functions on the direction in which the origin in Fourier space is approached (nonanalyticities at the origin).

Another obvious and untapped generalization involves hyperuniform stochastic processes in *time*. A temporal hyperuniform process is defined by a spectral function that tends to zero as the *frequency* tends to zero. Ascertaining hyperuniformity in time would involve spectral analysis of time series, which could be applied to real-valued continuous data or discrete data [379]. Such processes arise in host of contexts and applications, including signal processing, control theory, communication theory, statistics, astrophysics, econometrics, quantitative finance, seismology, meteorology, and geophysics.

The connections of hyperuniform states of matter to many different areas of fundamental science appear to be profound and yet our theoretical understanding of them is only in its infancy. Can one identify general organizing principles that drive a system to a hyperuniform state? When a system is at a disordered hyperuniform state, what does it say about the system and the underlying process leading to it? Is it possible to devise a non-perturbative statistical-mechanical theory of stealthy ground states for arbitrary χ that goes beyond the existing small- χ perturbation scheme [40]? Is the hyperuniformity correlation length scale based on the direct correlation function that grows with decreasing temperature upon supercooling a liquid [50,107] related to corresponding growing point-to-set length scales [111–113]? While relatively small hyperuniform materials have been primarily fabricated at millimeter length scales using 3D printing technologies, a fabrication challenge is to design interactions in soft-matter and molecular systems to self-organize to produce large samples of disordered hyperuniform materials with heterogeneity length scales at the micron or smaller level. There similar challenges on the computational side. For example, can new algorithms and/or optimization procedures be devised that efficiently generate very large samples of high-quality disordered hyperuniform systems. When a biological systems is poised at a disordered hyperuniform state, what are the concomitant biological advantages being conferred? This list represents a very small fraction of the open fascinating questions in the field.

Judging from the explosive pace of published articles on disordered hyperuniform systems over the last several years, prospects for exciting future theoretical and experimental developments in this field are very promising. It would not be surprising that by the time this review article is published, such advances will have been made.

Acknowledgments

I am deeply grateful to Frank Stillinger, Obioma Uche, Aleksandar Donev, Robert Batten, Andrea Gabrielli, Michael Joyce, Antonello Scardicchio, Paul Steinhardt, Paul Chaikin, Marian Florescu, Weining Man, Yang Jiao, Chase Zachary, Adam Hopkins, Étienne Marcotte, Gabrielle Long, Sjoerd Roorda, Joseph Corbo, Robert DiStasio, Eli Chertkov, Ge Zhang, Duyu Chen, Jaeuk Kim, Zheng Ma, Steven Atkinson, Remi Dreyfus, Arjun Yodh, Tim Still, Ye Xu, Michael Klatt, Jianxiang Tian, Joshua Socolar, Erdal Oğuz, Chaney Lin, Roberto Car, Fausto Martelli, Nicholas Giovambattista, Enrrique Lomba, Matthew de Courcy-Ireland, and Jean-Jacques Weis with whom I have collaborated on topics described in this review article. I am very thankful to Jaeuk Kim, Duyu Chen, Zheng Ma, Michael Klatt, Jack Douglas, Fausto Martelli, Roberto Car, Matthew de Courcy-Ireland and Yang Jiao for comments that greatly improved this article. The author's work on hyperuniformity since 2003 has been supported by the Office of Basic Energy Sciences under Grant No. DE-FG02-04-ER46108 and the National Science Foundation under Grant Nos. DMS-0312067, DMS-0804431, DMR-0820341 and DMR-1714722.

Appendix. Gauss circle problem and its generalizations

How does the number of points contained within some prescribed domain (window) Ω in which \mathbf{x}_0 (centroidal position) is fixed grow as the size of Ω is uniformly increased? A classic number-theoretic problem involving a specific version of this question asks how many lattice points of a square lattice at unit density lie inside or on a circle of radius R centered at a lattice point, denoted by $N(R)$, which amounts to finding all of the integer solutions of $n_1^2 + n_2^2 \leq R^2$ [135,161]. (This problem is directly related to the determination of the number of energy levels less than some fixed energy in integrable quantum

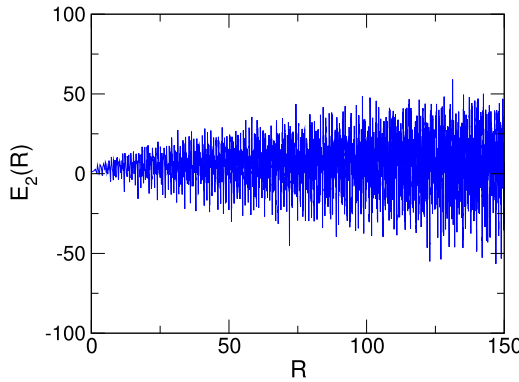


Fig. A.64. The discrepancy $E_2(R) \equiv N(R) - \pi R^2$ versus R for the square lattice at unit number density using a circular window of radius R centered on a lattice point.

systems [15].) Clearly, $N(R)$ asymptotically approaches the window area πR^2 for large R . The *discrepancy* $E_2(R) \equiv N(R) - \pi R^2$ grows with R in apparently “chaotic” manner; see Fig. A.64. Using elementary considerations, Gauss showed that the error $|E_2(R)|$ is bounded from above by some constant times the circumference of the circle, i.e., proportional to R . Since that time, many investigators have sought to improve the bound, a notoriously difficult task. Expressing the error as $|E_2(R)| \leq CR^t$, the best known bounds on the exponent t are $1/2 < t \leq 131/208 = 0.6298\dots$, where C is a constant; see Ref. [380] and references therein.

A d -dimensional generalization of this question asks for the number of points of a d -dimensional lattice at unit density contained within and on a d -dimensional spherical window of radius R , $N(R)$, which asymptotically approaches the volume of a sphere of radius R , $v_1(R)$. An exact expression for the discrepancy $E_d(R) \equiv N(R) - v_1(R)$ in dimension d is immediately obtained from relation (64) for $N(R; \mathbf{x}_0)$, where $N(R) \equiv N(R; \mathbf{x}_0 = 0)$, yielding

$$E_d(R) = (2\pi R)^{d/2} \sum_{\mathbf{q} \neq \mathbf{0}} \frac{J_{d/2}(qR)}{q^{d/2}}. \quad (\text{A.1})$$

Assuming the hypercubic lattice \mathbb{Z}^d and considering the large- R asymptotic limit, we can replace the Bessel function by the first term of its asymptotic expansion and obtain an estimate for the error:

$$|E_d(R)| = \frac{R^{(d-1)/2}}{\pi} \left| \sum_{n \geq 1} \frac{z_m(n) \cos[2\pi \sqrt{nR} - \pi(d+1)/4]}{n^{(d+1)/4}} \right| + \mathcal{O}(R^{(d-2)/2}) \quad (\text{A.2})$$

where $z_m(n)$ is the number of ways of writing n as a sum of m squares. Note that whereas the correction term of order $R^{(d-2)/2}$ involves an absolutely convergent sum, the first sum in (A.2) is conditionally convergent. Improving on the elementary upper bound that $|E_d(R)| \leq CR^{d-1}$ for $d \geq 2$ rests on obtaining sharper R -dependent estimates of the first sum. That such estimates are most difficult to obtain in dimensions two and three is related to the fact that every positive integer cannot always be written as a sum of two and three squares, respectively. (The best known solution in three dimensions is $|E_3(R)| \leq CR^{t+\epsilon}$, where $t = 17/14 = 1.21428\dots$ and $\epsilon > 0$ is arbitrarily small [381].) Lagrange showed that every positive integer can be written as the sum of at most four squares and so one expects that it become easier to estimate the error when $d \geq 4$. Indeed, the problem is settled when $d \geq 5$, where its known that $|E_d(R)| = \mathcal{O}(R^{d-2})$; see Ref. [382] and references therein.

References

- [1] D.J. Venzetti, A new derivation of some fluctuation theorems in statistical mechanics, *J. Math. Phys.* 16 (1975) 31–33.
- [2] R.M. Ziff, On the bulk distribution functions and fluctuation theorems, *J. Math. Phys.* 18 (1977) 1825–1831.
- [3] L.D. Landau, E.M. Lifshitz, *Statistical Physics*, Pergamon Press, New York, 1980.
- [4] P.M. Chaikin, T.C. Lubensky, *Principles of Condensed Matter Physics*, Cambridge University Press, New York, 1995.
- [5] T.M. Truskett, S. Torquato, P.G. Debenedetti, Density fluctuations in many-body systems, *Phys. Rev. E* 58 (1998) 7380–7639.
- [6] J.P. Hansen, I.R. McDonald, *Theory of Simple Liquids*, fourth ed., Academic Press, New York, 2013.
- [7] B. Widom, Equation of state in the neighborhood of the critical point, *J. Chem. Phys.* 43 (1965) 3898–3905.
- [8] L.P. Kadanoff, Scaling laws for ising models near T_c , *Physics* 2 (1966) 263–272.
- [9] M.E. Fisher, The theory of equilibrium critical phenomena, *Rep. Progr. Phys.* 30 (1967) 615.
- [10] H.E. Stanley, *Introduction to Phase Transitions and Critical Phenomena*, Oxford University Press, New York, 1971.
- [11] K.G. Wilson, J. Kogut, The renormalization group and the ϵ expansion, *Phys. Rep.* 12 (1974) 75–199.
- [12] J.J. Binney, N.J. Dowrick, A.J. Fisher, M.E.J. Newman, *The Theory of Critical Phenomena: An Introduction to the Renormalization Group*, Oxford University Press, Oxford, England, 1992.

- [13] M.V. Berry, M. Robnik, Statistics of energy levels without time-reversal symmetry: Aharonov-Bohm chaotic billiards, *J. Phys. A: Math. Gen.* 19 (1986) 649.
- [14] M.L. Metha, *Random Matrices*, Academic Press, New York, 1991.
- [15] P.M. Bleher, F.J. Dyson, J.L. Lebowitz, Non-Gaussian energy level statistics for some integrable systems, *Phys. Rev. Lett.* 71 (1993) 3047–3050.
- [16] A. Wax, C. Yang, V. Backman, K. Badizadegan, C.W. Boone, R.R. Dasari, M.S. Feld, Cellular organization and substructure measured using angle-resolved low-coherence interferometry, *Biophys. J.* 82 (2002) 2256–2264.
- [17] P.J.E. Peebles, *Principles of Physical Cosmology*, Princeton University Press, Princeton, 1993.
- [18] A. Gabrielli, F.S. Labini, M. Joyce, L. Pietronero, *Statistical Physics for Cosmic Structures*, Springer-Verlag, New York, 2005.
- [19] F.C. Grozema, S. Tonzani, Y.A. Berlin, G.C. Schatz, L.D.A. Siebbeles, M.A. Ratner, Effect of structural dynamics on charge transfer in DNA hairpins, *J. Am. Chem. Soc.* 130 (2008) 5157–5166.
- [20] R. Chang, A. Yethiraj, Strongly charged flexible polyelectrolytes in poor solvents: Molecular dynamics simulations with explicit solvent, *J. Chem. Phys.* 118 (2003) 6634–6647.
- [21] Z. Ou, M. Muthukumar, Entropy and enthalpy of polyelectrolyte complexation: Langevin dynamics simulations, *J. Chem. Phys.* 124 (2006) 154902.
- [22] L. Berthier, G. Biroli, J.-P. Bouchaud, W. Kob, K. Miyazaki, D.R. Reichman, Spontaneous and induced dynamic fluctuations in glass formers. I. General results and dependence on ensemble and dynamics, *J. Chem. Phys.* 126 (2007) 184503.
- [23] K. Lum, D. Chandler, J.D. Weeks, Hydrophobicity at small and large length scales, *J. Phys. Chem. B* 103 (1999) 4570–4577.
- [24] A.M. Kulkarni, A.P. Chatterjee, K.S. Schweizer, C.F. Zukoski, Depletion interactions in the protein limit: Effects of polymer density fluctuations, *Phys. Rev. Lett.* 83 (1999) 4554–4557.
- [25] S. Warr, J.-P. Hansen, Relaxation of local density fluctuations in a fluidized granular medium, *Europhys. Lett.* 36 (1996) 589.
- [26] Y. Jiao, H. Berman, T.-R. Kiehl, S. Torquato, Spatial organization and correlations of cell nuclei in brain tumors, *PLoS One* 6 (2011) e27323.
- [27] S. Torquato, F.H. Stillinger, Local density fluctuations, hyperuniform systems, and order metrics, *Phys. Rev. E* 68 (2003) 041113.
- [28] A. Gabrielli, M. Joyce, F.S. Labini, Glass-like universe: Real-space correlation properties of standard cosmological models, *Phys. Rev. D* 65 (2002) 083523.
- [29] D. Shechtman, I. Blech, D. Gratias, J.W. Cahn, Metallic phase with long-range orientational order and no translational symmetry, *Phys. Rev. Lett.* 53 (1984) 1951–1953.
- [30] D. Levine, P.J. Steinhardt, Quasicrystals: A new class of ordered structures, *Phys. Rev. Lett.* 53 (1984) 2477–2480.
- [31] D. Levine, P.J. Steinhardt, Quasicrystals. I. Definition and structure, *Phys. Rev. B* 34 (1986) 596.
- [32] C.E. Zachary, S. Torquato, Hyperuniformity in point patterns and two-phase heterogeneous media, *J. Stat. Mech. Theory Exp.* (2009) P12015.
- [33] E.C. Oğuz, J.E.S. Socolar, P.J. Steinhardt, S. Torquato, Hyperuniformity of quasicrystals, *Phys. Rev. B* 95 (2017) 054119.
- [34] S. Torquato, A. Scardicchio, C.E. Zachary, Point processes in arbitrary dimension from Fermionic gases, random matrix theory, and number theory, *J. Stat. Mech. Theory Exp.* (2008) P11019.
- [35] D. Levesque, J.-J. Weis, J. Lebowitz, Charge fluctuations in the two-dimensional one-component plasma, *J. Stat. Phys.* 100 (2000) 209–222.
- [36] O.U. Uche, F.H. Stillinger, S. Torquato, Constraints on collective density variables: Two dimensions, *Phys. Rev. E* 70 (2004) 046122.
- [37] O.U. Uche, S. Torquato, F.H. Stillinger, Collective coordinates control of density distributions, *Phys. Rev. E* 74 (2006) 031104.
- [38] R.D. Batten, F.H. Stillinger, S. Torquato, Classical disordered ground states: Super-ideal gases, and stealthy and equi-luminous materials, *J. Appl. Phys.* 104 (2008) 033504.
- [39] R.D. Batten, F.H. Stillinger, S. Torquato, Novel low-temperature behavior in classical many-particle systems, *Phys. Rev. Lett.* 103 (2009) 050602.
- [40] S. Torquato, G. Zhang, F.H. Stillinger, Ensemble theory for stealthy hyperuniform disordered ground states, *Phys. Rev. X* 5 (2015) 021020.
- [41] G. Zhang, F. Stillinger, S. Torquato, Ground states of stealthy hyperuniform potentials: I. Entropically favored configurations, *Phys. Rev. E* 92 (2015) 022119.
- [42] G. Zhang, F. Stillinger, S. Torquato, Ground states of stealthy hyperuniform potentials: II. Stacked-slider phases, *Phys. Rev. E* 92 (2015) 022120.
- [43] G. Zhang, F.H. Stillinger, S. Torquato, Can exotic disordered “stealthy” particle configurations tolerate arbitrarily large holes? *Soft Matter* 13 (2017) 6197.
- [44] E. Lomba, J.-J. Weis, S. Torquato, Disordered hyperuniformity in two-component non-additive hard disk plasmas, *Phys. Rev. E* 96 (2017) 062126.
- [45] E. Lomba, J.-J. Weis, S. Torquato, Disordered multihyperuniformity derived from binary plasmas, *Phys. Rev. E* 97 (2018) 010102(R).
- [46] A. Donev, F.H. Stillinger, S. Torquato, Unexpected density fluctuations in disordered jammed hard-sphere packings, *Phys. Rev. Lett.* 95 (2005) 090604.
- [47] M. Skoge, A. Donev, F.H. Stillinger, S. Torquato, Packing hyperspheres in high-dimensional Euclidean spaces, *Phys. Rev. E* 74 (2006) 041127.
- [48] C.E. Zachary, Y. Jiao, S. Torquato, Hyperuniform long-range correlations are a signature of disordered jammed hard-particle packings, *Phys. Rev. Lett.* 106 (2011) 178001.
- [49] Y. Jiao, S. Torquato, Maximally random jammed packings of platonic solids: Hyperuniform long-range correlations and isostaticity, *Phys. Rev. E* 84 (2011) 041309.
- [50] A.B. Hopkins, F.H. Stillinger, S. Torquato, Nonequilibrium static diverging length scales on approaching a prototypical model glassy state, *Phys. Rev. E* 86 (2012) 021505.
- [51] D. Chen, Y. Jiao, S. Torquato, Equilibrium phase behavior and maximally random jammed state of truncated tetrahedra, *J. Phys. Chem. B* 118 (2014) 7981–7992.
- [52] M.A. Klatt, S. Torquato, Characterization of maximally random jammed sphere packings. II. Correlation functions and density fluctuations, *Phys. Rev. E* 94 (2016) 022152.
- [53] S. Atkinson, G. Zhang, A.B. Hopkins, S. Torquato, Critical slowing down and hyperuniformity on approach to jamming, *Phys. Rev. E* 94 (2016) 012902.
- [54] S. Atkinson, F.H. Stillinger, S. Torquato, Static structural signatures of nearly jammed disordered and ordered hard-sphere packings: Direct correlation function, *Phys. Rev. E* 94 (2016) 032902.
- [55] L.E. Silbert, M. Silbert, Long-wavelength structural anomalies in jammed systems, *Phys. Rev. E* 80 (2009) 041304.
- [56] L. Berthier, P. Chaudhuri, C. Coulais, O. Dauchot, P. Sollich, Suppressed compressibility at large scale in jammed packings of size-disperse spheres, *Phys. Rev. Lett.* 106 (2011) 120601.
- [57] R. Kurita, E.R. Weeks, Incompressibility of polydisperse random-close-packed colloidal particles, *Phys. Rev. E* 84 (2011) 030401.
- [58] R. Dreyfus, Y. Xu, T. Still, L.A. Hough, A.G. Yodh, S. Torquato, Diagnosing hyperuniformity in two-dimensional, disordered, jammed packings of soft spheres, *Phys. Rev. E* 91 (2015) 012302.
- [59] J. Ricouvier, R. Pierrat, R. Carminati, P. Tabeling, P. Yazhgur, Optimizing hyperuniformity in self-assembled bidisperse emulsions, *Phys. Rev. Lett.* 119 (2017) 208001.
- [60] I. Lesanovsky, J.P. Garrahan, Out-of-equilibrium structures in strongly interacting Rydberg gases with dissipation, *Phys. Rev. A* 90 (2014) 011603.
- [61] R.L. Jack, I.R. Thompson, P. Sollich, Hyperuniformity and phase separation in biased ensembles of trajectories for diffusive systems, *Phys. Rev. Lett.* 114 (2015) 060601.
- [62] D. Hexner, D. Levine, Hyperuniformity of critical absorbing states, *Phys. Rev. Lett.* 114 (2015) 110602.
- [63] J.H. Weisj, R. Jeanneret, R. Dreyfus, D. Bartolo, Emergent hyperuniformity in periodically driven emulsions, *Phys. Rev. Lett.* 115 (2015) 108301.

[64] E. Tjhung, L. Berthier, Hyperuniform density fluctuations and diverging dynamic correlations in periodically driven colloidal suspensions, *Phys. Rev. Lett.* 114 (2015) 148301.

[65] D. Hexner, D. Levine, Noise, diffusion, and hyperuniformity, *Phys. Rev. Lett.* 118 (2017) 020601.

[66] D. Hexner, P.M. Chaikin, D. Levine, Enhanced hyperuniformity from random reorganization, *Proc. Natl. Acad. Sci.* 114 (2017) 4294–4299.

[67] J.H. Weis, D. Bartolo, Mixing by unstirring: Hyperuniform dispersion of interacting particles upon chaotic advection, *Phys. Rev. Lett.* 119 (2017) 048002.

[68] S. Kwon, J.M. Kim, Hyperuniformity of initial conditions and critical decay of a diffusive epidemic process belonging to the Manna class, *Phys. Rev. E* 96 (2017) 012146.

[69] G. Willis, G. Pruessner, Spatio-temporal correlations in the Manna model in one, three and five dimensions, *Internat. J. Modern Phys. B* 32 (2018) 1830002.

[70] Y. Jiao, T. Lau, H. Hatzikirou, M. Meyer-Hermann, J.C. Corbo, S. Torquato, Avian photoreceptor patterns represent a disordered hyperuniform solution to a multiscale packing problem, *Phys. Rev. E* 89 (2014) 022721.

[71] A. Mayer, V. Balasubramanian, T. Mora, A.M. Walczak, How a well-adapted immune system is organized, *Proc. Natl. Acad. Sci.* 112 (2015) 5950–5955.

[72] G. Zhang, F.H. Stillinger, S. Torquato, The perfect glass paradigm: Disordered hyperuniform glasses down to absolute zero, *Sci. Rep.* 6 (2016) 36963.

[73] G. Zhang, F.H. Stillinger, S. Torquato, Classical many-particle systems with unique disordered ground states, *Phys. Rev. E* 96 (2017) 042146.

[74] R.P. Feynman, M. Cohen, Energy spectrum of the excitations in liquid helium, *Phys. Rev.* 102 (1956) 1189–1204.

[75] H.L. Montgomery, The pair correlation of zeros of the zeta function, *Amer. Math. Soc.* (1973) 181–193.

[76] F.J. Dyson, Correlations between eigenvalues of a random matrix, *Comm. Math. Phys.* 19 (1970) 235–250.

[77] S. Torquato, O.U. Uche, F.H. Stillinger, Random sequential addition of hard spheres in high Euclidean dimensions, *Phys. Rev. E* 74 (2006) 061308.

[78] G. Zhang, S. Torquato, Precise algorithm to generate random sequential addition of hard hyperspheres at saturation, *Phys. Rev. E* 88 (2013) 053312.

[79] S. Torquato, Disordered hyperuniform heterogeneous materials, *J. Phys.: Condens. Matter* 28 (2016) 414012.

[80] W.-S. Xu, J.F. Douglas, K.F. Freed, Influence of cohesive energy on the thermodynamic properties of a model glass-forming polymer melt, *Macromolecules* 49 (2016) 8341–8354.

[81] S. Torquato, Hyperuniformity and its generalizations, *Phys. Rev. E* 94 (2016) 022122.

[82] E. Chertkov, R.A. DiStasio, G. Zhang, R. Car, S. Torquato, Inverse design of disordered stealthy hyperuniform spin chains, *Phys. Rev. B* 93 (2015) 064201.

[83] A. Chremos, J.F. Douglas, Particle localization and hyperuniformity of polymer-grafted nanoparticle materials, *Ann. Phys.* 529 (2017).

[84] F. Martelli, S. Torquato, N. Giovambattista, R. Car, Large-scale structure and hyperuniformity of amorphous ices, *Phys. Rev. Lett.* 119 (2017) 136002.

[85] Y. Xu, S. Chen, P.-E. Chen, W. Xu, Y. Jiao, Microstructure and mechanical properties of hyperuniform heterogeneous materials, *Phys. Rev. E* 96 (2017) 043301.

[86] B.-Y. Wu, X.-Q. Sheng, Y. Hao, Effective media properties of hyperuniform disordered composite materials, *PLoS One* 12 (2017) e0185921.

[87] D. Chen, S. Torquato, Designing disordered hyperuniform two-phase materials with novel physical properties, *Acta Mater.* 142 (2018) 152–161.

[88] M.A. Klatt, S. Torquato, Characterization of maximally random jammed sphere packings. III. Transport and electromagnetic properties via correlation functions, *Phys. Rev. E* 97 (2018) 012118.

[89] M. Florescu, S. Torquato, P.J. Steinhardt, Designer disordered materials with large complete photonic band gaps, *Proc. Natl. Acad. Sci.* 106 (2009) 20658–20663.

[90] M. Florescu, P.J. Steinhardt, S. Torquato, Optical cavities and waveguides in hyperuniform disordered photonic solids, *Phys. Rev. B* 87 (2013) 165116.

[91] W. Man, M. Florescu, E.P. Williamson, Y. He, S.R. Hashemizad, B.Y.C. Leung, D.R. Liner, S. Torquato, P.M. Chaikin, P.J. Steinhardt, Isotropic band gaps and freeform waveguides observed in hyperuniform disordered photonic solids, *Proc. Natl. Acad. Sci.* 110 (2013) 15886–15891.

[92] W. Man, M. Florescu, K. Matsuyama, P. Yadak, G. Nahal, S. Hashemizad, E. Williamson, P. Steinhardt, S. Torquato, P. Chaikin, Photonic band gap in isotropic hyperuniform disordered solids with low dielectric contrast, *Opt. Express* 21 (2013) 19972–19981.

[93] J. Haberko, N. Muller, F. Scheffold, Direct laser writing of three dimensional network structures as templates for disordered photonic materials, *Phys. Rev. A* 88 (2013) 043822.

[94] T. Ma, H. Guerboukha, M. Girard, A.D. Squires, R.A. Lewis, M. Skorobogati, 3D printed hollow-core terahertz optical waveguides with hyperuniform disordered dielectric reflectors, *Adv. Optical Mater.* 4 (2016) 2085–2094.

[95] W. Zhou, Z. Cheng, B. Zhu, X. Sun, H.K. Tsang, Hyperuniform disordered network polarizers, *IEEE J. Sel. Top. Quantum Electron.* 22 (2016) 288–294.

[96] C.D. Rosa, F. Auriemma, C. Diletto, R.D. Girolamo, A. Malafronte, P. Morvillo, G. Zito, G. Rusciano, G. Pesce, A. Sasso, Toward hyperuniform disordered plasmonic nanostructures for reproducible surface-enhanced Raman spectroscopy, *Phys. Chem. Chem. Phys.* 17 (2015) 8061–8069.

[97] R. Degl'Innocenti, Y.D. Shah, L. Masini, A. Ronzani, A. Pitanti, Y. Ren, D.S. Jessop, A. Tredicucci, H.E. Beere, D.A. Ritchie, Hyperuniform disordered terahertz quantum cascade laser, *Sci. Rep.* 6 (2016) 19325.

[98] G. Zito, G. Rusciano, G. Pesce, A. Malafronte, R.D. Girolamo, G. Ausanio, A. Vecchione, A. Sasso, Nanoscale engineering of two-dimensional disordered hyperuniform block-copolymer assemblies, *Phys. Rev. E* 92 (2015) 050601.

[99] O. Leseur, R. Pierrat, R. Carminati, High-density hyperuniform materials can be transparent, *Optica* 3 (2016) 763–767.

[100] S. Yu, X. Piao, J. Hong, N. Park, Bloch-like wave dynamics in disordered potentials based on supersymmetry, *Nature Mater.* 6 (2015) 8269.

[101] L.S. Froufe-Pérez, M. Engel, P.F. Damasceno, N. Muller, J. Haberko, S.C. Glotzer, F. Scheffold, Role of short-range order and hyperuniformity in the formation of band gaps in disordered photonic materials, *Phys. Rev. Lett.* 117 (2016) 053902.

[102] L.S. Froufe-Pérez, M. Engel, J. José Sáenz, F. Scheffold, Transport phase diagram and anderson localization in hyperuniform disordered photonic materials, *Proc. Natl. Acad. Sci.* 114 (2017) 9570–9574.

[103] G. Gkantzounis, T. Amoah, M. Florescu, Hyperuniform disordered phononic structures, *Phys. Rev. B* 95 (2017) 094120.

[104] G. Zhang, F.H. Stillinger, S. Torquato, Transport geometrical and topological properties of stealthy disordered hyperuniform two-phase systems, *J. Chem. Phys.* 145 (2016) 244109.

[105] M. Hejna, P.J. Steinhardt, S. Torquato, Nearly hyperuniform network models of amorphous silicon, *Phys. Rev. B* 87 (2013) 245204.

[106] R. Xie, G.G. Long, S.J. Weigand, S.C. Moss, T. Carvalho, S. Roorda, M. Hejna, S. Torquato, P.J. Steinhardt, Hyperuniformity in amorphous silicon based on the measurement of the infinite-wavelength limit of the structure factor, *Proc. Natl. Acad. Sci.* 110 (2013) 13250–13254.

[107] É. Marcotte, F.H. Stillinger, S. Torquato, Nonequilibrium static growing length scales in supercooled liquids on approaching the glass transition, *J. Chem. Phys.* 138 (2013) 12A508.

[108] V. Lubchenko, P.G. Wolynes, Theory of structural glasses and supercooled liquids, *Annu. Rev. Phys. Chem.* 58 (2007) 235–266.

[109] K.S. Schweizer, Dynamical fluctuation effects in glassy colloidal suspensions, *Current Opinion Coll. Inter. Sc.* 12 (2007) 297–306.

[110] D. Chandler, J.P. Garrahan, Dynamics on the way to forming glass: Bubbles in space-time, *Annu. Rev. Phys. Chem.* 61 (2010) 191–217.

[111] L. Berthier, W. Kob, Static point-to-set correlations in glass-forming liquids, *Phys. Rev. E* 85 (2012) 011102.

[112] G.M. Hocky, T.E. Markland, D.R. Reichman, Growing point-to-set length scale correlates with growing relaxation times in model supercooled liquids, *Phys. Rev. Lett.* 108 (2012) 225506.

[113] B. Charbonneau, P. Charbonneau, G. Tarjus, Geometrical frustration and static correlations in hard-sphere glass formers, *J. Chem. Phys.* 138 (2013) 12A515.

[114] A. Coniglio, M. Pica Ciamarra, T. Aste, Universal behaviour of the glass and the jamming transitions in finite dimensions, *Soft Matter* 13 (2017) 8766–8771.

[115] S. Torquato, *Random Heterogeneous Materials: Microstructure and Macroscopic Properties*, Springer-Verlag, New York, 2002.

[116] M. Sahimi, *Heterogeneous Materials I: Linear Transport and Optical Properties*, Springer-Verlag, New York, 2003.

[117] B.L. Lu, S. Torquato, Photographic granularity—Mathematical formulation and effect of impenetrability of grains, *J. Opt. Soc. Am. A* 7 (1990) 717–724.

[118] B.L. Lu, S. Torquato, Local volume fraction fluctuations in heterogeneous media, *J. Chem. Phys.* 93 (1990) 3452–3459.

[119] J. Quintanilla, S. Torquato, Local volume fraction fluctuations in random media, *J. Chem. Phys.* 106 (1997) 2741–2751.

[120] J. Quintanilla, S. Torquato, Local volume fraction fluctuations in periodic heterogeneous media, *J. Chem. Phys.* 110 (1999) 3215–3219.

[121] C.E. Zachary, Y. Jiao, S. Torquato, Hyperuniformity, quasi-long-range correlations, and void-space constraints in maximally random jammed particle packings. I. Polydisperse spheres, *Phys. Rev. E* 83 (2011) 051308.

[122] C.E. Zachary, Y. Jiao, S. Torquato, Hyperuniformity, quasi-long-range correlations, and void-space constraints in maximally random jammed particle packings. II. Anisotropy in particle shape, *Phys. Rev. E* 83 (2011) 051309.

[123] D. Chen, S. Torquato, Confined disordered strictly jammed binary sphere packings, *Phys. Rev. E* 92 (2015) 062207.

[124] R.A. DiStasio, G. Zhang, F.H. Stillinger, S. Torquato, Rational design of stealthy hyperuniform patterns with tunable order, *Phys. Rev. E* 97 (2018) 023311.

[125] D. Stoyan, W.S. Kendall, J. Mecke, *Stochastic Geometry and Its Applications*, second ed., Wiley, New York, 1995.

[126] A. Scardicchio, F.H. Stillinger, S. Torquato, Estimates of the optimal density of sphere packings in high dimensions, *J. Math. Phys.* 49 (2008) 043301.

[127] A. Lenard, Correlation functions and the uniqueness of the state in classical statistical mechanics, *Comm. Math. Phys.* 30 (1973) 35–44.

[128] S. Torquato, F.H. Stillinger, New conjectural lower bounds on the optimal density of sphere packings, *Exp. Math.* 15 (2006) 307–331.

[129] J.H. Conway, N.J.A. Sloane, *Sphere Packings, Lattices and Groups*, Springer-Verlag, New York, 1998.

[130] S. Torquato, G. Stell, Microstructure of two-phase random media: I. The n -point probability functions, *J. Chem. Phys.* 77 (1982) 2071–2077.

[131] S. Torquato, G. Stell, Microstructure of two-phase random media: II. The Mayer–Montroll and Kirkwood–Salsburg hierarchies, *J. Chem. Phys.* 78 (1983) 3262–3272.

[132] P. Debye, A.M. Bueche, Scattering by an inhomogeneous solid, *J. Appl. Phys.* 20 (1949) 518–525.

[133] P. Debye, H.R. Anderson, H. Brumberger, Scattering by an inhomogeneous solid. II. The correlation function and its applications, *J. Appl. Phys.* 28 (1957) 679–683.

[134] P. Martin, T. Yalcin, The charge fluctuations in classical Coulomb systems, *J. Stat. Phys.* 22 (1980) 435–463.

[135] D.G. Kendall, R.A. Rankin, On the number of points of a given lattice in a random hypersphere, *Q. J. Math.* 4 (1953) 178–189.

[136] L. Heinrich, H. Schmidt, V. Schmidt, Central limit theorems for Poisson hyperplane tessellations, *Ann. Appl. Probab.* 16 (2006) 919–950.

[137] L. Heinrich, M. Spiess, Central limit theorems for volume and surface content of stationary Poisson cylinder processes in expanding domains, *Adv. Appl. Probab.* 45 (2013) 312–331.

[138] A. Gabrielli, M. Joyce, S. Torquato, Tilings of space and superhomogeneous point processes, *Phys. Rev. E* 77 (2008) 031125.

[139] C.E. Zachary, S. Torquato, Anomalous local coordination density fluctuations and void statistics in disordered hyperuniform many-particle ground states, *Phys. Rev. E* 83 (2011) 051133.

[140] J. Beck, Irregularities of distribution I, *Acta Math.* 159 (1987) 1–49.

[141] L.D. Abreu, J.M. Pereira, J.L. Romero, S. Torquato, The Weyl–Heisenberg ensemble: Hyperuniformity and higher landau levels, *J. Stat. Mech. Theory Exp.* 2017 (2017) 043103.

[142] A. Gabrielli, Point processes and stochastic displacement fields, *Phys. Rev. E* 70 (2004) 066131.

[143] A. Gabrielli, S. Torquato, Voronoi and void statistics for superhomogeneous point processes, *Phys. Rev. E* 70 (2004) 041105.

[144] J. Kim, S. Torquato, Effect of imperfections on the hyperuniformity of many-body systems, *Phys. Rev. B* 97 (2018) 054105.

[145] M. Aizenman, S. Goldstein, J. Lebowitz, Bounded fluctuations and translation symmetry breaking in one-dimensional particle systems, *J. Stat. Phys.* 103 (2001) 601–618.

[146] Z. Ma, S. Torquato, Random scalar fields and hyperuniformity, *J. Appl. Phys.* 121 (2017) 244904.

[147] L. Reatto, G.V. Chester, Phonons and the properties of a Bose system, *Phys. Rev.* 155 (1967) 88–100.

[148] A. Gabrielli, B. Jancovici, M. Joyce, J.L. Lebowitz, L. Pietronero, F.S. Labini, Generation of primordial cosmological perturbations from statistical mechanical models, *Phys. Rev. D* 67 (2003) 043506.

[149] B. Jancovici, Exact results for the two-dimensional one-component plasma, *Phys. Rev. Lett.* 46 (1981) 386–388.

[150] J. Kim, S. Torquato, Effect of window shape on the detection of hyperuniformity via the local number variance, *J. Stat. Mech. Theory Exp.* 2017 (2017) 013402.

[151] P. Sarnak, A. Strömbergsson, Minima of Epstein's zeta function and heights of flat tori, *Invent. Math.* 165 (2006) 115–151.

[152] R.A. Rankin, A minimum problem for the Epstein zeta function, *Proc. Glasg. Math. Assoc.* 1 (1953) 149–158.

[153] V. Ennola, On a problem about the Epstein zeta function, *Proc. Camb. Philos. Soc.* 60 (1964) 855–875.

[154] M. Viazovska, The sphere packing problem in dimension 8, *Ann. Math.* 185 (2017) 991–1015.

[155] H. Cohn, A. Kumar, S.D. Miller, D. Radchenko, M. Viazovska, The sphere packing problem in dimension 24, *Ann. Math.* 183 (2017) 1017–1033.

[156] J.E.S. Socolar, P.J. Steinhardt, Quasicrystals. II. Unit-cell configurations, *Phys. Rev. B* 34 (1986) 617.

[157] C. Lin, P.J. Steinhardt, S. Torquato, Hyperuniformity variation with quasicrystal local isomorphism class, *J. Phys.: Condens. Matter* 29 (2017) 204003.

[158] T.C. Hales, A proof of the Kepler conjecture, *Ann. of Math.* 162 (2005) 1065–1185.

[159] S. Torquato, F.H. Stillinger, Toward the jamming threshold of sphere packings: Tunneled crystals, *J. Appl. Phys.* 102 (2007) 093511. 103 (2008) 129902 (erratum).

[160] S. Torquato, Reformulation of the covering and quantizer problems as ground states of interacting particles, *Phys. Rev. E* 82 (2010) 056109.

[161] D.G. Kendall, On the number of lattice points inside a random oval, *Q. J. Math.* 19 (1948) 1–24.

[162] J. Beck, Randomness in lattice point problems, *Discrete Math.* 229 (2001) 29–55.

[163] M.G. Kendall, P.A.P. Moran, *Geometrical Probability*, Griffin, London, 1963.

[164] B. Matérn, Precision of area estimation: a numerical study, *J. Microsc.* 153 (1989) 269–284.

[165] A.T. Chieco, R. Dreyfus, D.J. Durian, Characterizing pixel and point patterns with a hyperuniformity disorder length, *Phys. Rev. E* 96 (2017) 032909.

[166] C.L.Y. Yeong, S. Torquato, Reconstructing random media, *Phys. Rev. E* 57 (1998) 495–506.

[167] Y. Jiao, F.H. Stillinger, S. Torquato, A superior descriptor of random textures and its predictive capacity, *Proc. Natl. Acad. Sci.* 106 (2009) 17634–17639.

[168] S. Torquato, G. Stell, Microstructure of two-phase random media: III. The n -point matrix probability functions for fully penetrable spheres, *J. Chem. Phys.* 79 (1983) 1505–1510.

[169] S. Torquato, G. Stell, Microstructure of two-phase random media: V. The n -point matrix probability functions for impenetrable spheres, *J. Chem. Phys.* 82 (1985) 980–987.

[170] B.L. Lu, S. Torquato, General formalism to characterize the microstructure of polydispersed random media, *Phys. Rev. A* 43 (1991) 2078–2080.

[171] S. Torquato, B. Lu, Rigorous bounds on the fluid permeability: Effect of polydispersity in grain size, *Phys. Fluids A* 2 (1990) 487–490.

[172] L.S. Ornstein, F. Zernike, Accidental deviations of density and opalescence at the critical point of a single substance, *Proc. Akad. Sci.* 17 (1914) 793–806.

[173] M.D. Johnson, P. Hutchinson, N.H. March, Ion-ion oscillatory potentials in liquid metals, *Proc. R. Soc. Lond. Ser. A Math. Phys. Eng. Sci.* 282 (1964) 283–302.

[174] G. Stell, Fluids with long-range forces: Toward a simple analytic theory, in: B.J. Berne (Ed.), *Statistical Mechanics, Part A*, Plenum Press, New York, 1977, pp. 47–82.

[175] K. Huang, *Statistical Mechanics*, John Wiley, New York, 1987.

[176] P.J. Forrester, B. Jancovici, G. Téllez, Universality in some classical Coulomb systems of restricted dimension, *J. Stat. Phys.* 84 (1996) 359–378.

[177] S. Torquato, Statistical description of microstructures, *Ann. Rev. Mater. Res.* 32 (2002) 77–111.

[178] J.R. Crawford, S. Torquato, F.H. Stillinger, Aspects of correlation function realizability, *J. Chem. Phys.* 119 (2003) 7065–7074.

[179] M. Baus, On the compressibility of a one-component plasma, *J. Phys. A: Math. Gen.* 11 (1978) 2451.

[180] E.J.M. Navet, M.R. Feix, Virial pressure of the classical one-component plasma, *J. Physique Lett.* 41 (1980) 69–73.

[181] P. Choquard, P. Favre, C. Gruber, On the equation of state of classical one-component systems with long-range forces, *J. Stat. Phys.* 23 (1980) 405–442.

[182] M. Baus, J.-P. Hansen, Statistical mechanics of simple Coulomb systems, *Phys. Rep.* 59 (1980) 1–94.

[183] S. Serfaty, Ginzburg-Landau Vortices, Coulomb Gases, and Renormalized Energies, *J. Stat. Phys.* 154 (2014) 660–680.

[184] E. Sandier, S. Serfaty, 2D Coulomb gases and the renormalized energy, *Ann. Probab.* 43 (2015) 2026–2083.

[185] S. Serfaty, Coulomb gases and Ginzburg-Landau vortices, in: *Zurich Lecture Notes in Mathematics*, Eur. Math. Soc.

[186] T. Leblé, Logarithmic, Coulomb and Riesz energy of point processes, *J. Stat. Phys.* 162 (2016) 887–923.

[187] M. Petrache, S.R. Nodari, Equirdistribution of jellium energy for Coulomb and Riesz interactions, *Constr. Approx.* 47 (2018) 163–210.

[188] H. Sakai, F.H. Stillinger, S. Torquato, Equi- $g(r)$ sequences of systems derived from the square-well potential, *J. Chem. Phys.* 117 (2002) 297–307.

[189] Y. Fan, J.K. Percus, D.K. Stillinger, F.H. Stillinger, Constraints on collective density variables: One dimension, *Phys. Rev. A* 44 (1991) 2394–2402.

[190] R.D. Batten, F.H. Stillinger, S. Torquato, Interactions leading to disordered ground states and unusual low-temperature behavior, *Phys. Rev. E* 80 (2009) 031105.

[191] S. Martis, É. Marcotte, F.H. Stillinger, S. Torquato, Exotic ground states of directional pair potentials via collective-density variables, *J. Stat. Phys.* 150 (2013) 414.

[192] N.W. Ashcroft, D.N. Mermin, *Solid State Physics*, Thomson Learning, Toronto, 1976.

[193] A. Bácsi, A. Virosztek, Local density of states and Friedel oscillations in graphene, *Phys. Rev. B* 82 (2010) 193405.

[194] C. Hanel, C.N. Likos, R. Blaak, Effective interactions between multilayered ionic microgels, *Materials* 7 (2014) 7689–7705.

[195] A. Sütő, Crystalline ground states for classical particles, *Phys. Rev. Lett.* 95 (2005) 265501.

[196] J.B. Hough, M. Krishnapur, Y. Peres, B. Virág, *Zeros of Gaussian Analytic Functions and Determinantal Point Processes*, Vol. 51, American Mathematical Society, Providence, RI, 2009.

[197] S. Ghosh, J.L. Lebowitz, Generalized stealthy hyperuniform processes: Maximal rigidity and the bounded holes conjecture, ArXiv e-prints [arXiv:1707.04328](https://arxiv.org/abs/1707.04328).

[198] W. Kauzmann, The nature of the glassy state and the behavior of liquids at low temperatures, *Chem. Rev.* 43 (1948) 219–256.

[199] S. Torquato, Modeling of physical properties of composite materials, *Int. J. Solids Struct.* 37 (2000) 411–422.

[200] S. Torquato, F.H. Stillinger, Jammed hard-particle packings: From Kepler to Bernal and beyond, *Rev. Modern Phys.* 82 (2010) 2633.

[201] S. Torquato, F.H. Stillinger, New duality relations for classical ground states, *Phys. Rev. Lett.* 100 (2008) 020602.

[202] S. Torquato, C.E. Zachary, F.H. Stillinger, Duality relations for the classical ground states of soft-matter systems, *Soft Matter* 7 (2011) 3780.

[203] P.G.D. Gennes, J. Prost, *The Physics of Liquid Crystals*, Oxford University Press, Oxford, England, 1995.

[204] E.P. Wigner, On the statistical distribution of the widths and spacings of nuclear resonance levels, *Proc. Cambridge Philos. Soc.* 47 (1951) 790–798.

[205] A.M. Lane, R.G. Thomas, E.P. Wigner, Giant resonance interpretation of the nucleon–nucleus interaction, *Phys. Rev.* 98 (1955) 693–701.

[206] M.L. Mehta, On the statistical properties of the level-spacings in nuclear spectra, *Nuclear Phys.* 18 (1960) 395–419.

[207] R. McWeeny, Some recent advances in density matrix theory, *Rev. Modern Phys.* 32 (1960) 335–369.

[208] F.J. Dyson, Statistical theory of the energy levels of complex systems. I, *J. Math. Phys.* 3 (1962) 140–156.

[209] F.J. Dyson, Statistical theory of the energy levels of complex systems. II, *J. Math. Phys.* 3 (1962) 157–165.

[210] F.J. Dyson, Statistical theory of the energy levels of complex systems. III, *J. Math. Phys.* 3 (1962) 166–175.

[211] M.L. Mehta, F.J. Dyson, Statistical theory of the energy levels of complex systems. IV, *J. Math. Phys.* 4 (1963) 713–719.

[212] T. Mori, K. Tanaka, Average stress in matrix and average elastic energy of materials with misfitting inclusions, *Acta Metall.* 21 (1973) 571–574.

[213] A.M. Odlyzko, On the distribution of spacings between zeros of the zeta function, *Math. Comp.* 48 (1987) 273–308.

[214] Z. Rudnick, P. Sarnak, Zeros of principal L -functions and random matrix theory, *Duke Math. J.* 81 (1996) 269–322.

[215] R.P. Feynman, *Statistical Mechanics*, Westview Press, Boulder, Colorado, 1998.

[216] N. Katz, P. Sarnak, Zeros of zeta functions and symmetry, *Bull. Amer. Math. Soc.* 36 (1999) 1–26.

[217] P.J. Forrester, *Log-Gases and Random Matrices*, Princeton University Press, Princeton, New Jersey, 2010.

[218] T. Tao, V. Vu, Random matrices: Universality of local eigenvalue statistics, *Acta Math.* 206 (2011) 127–204.

[219] M.V. Berry, Semiclassical theory of spectral rigidity, *Proc. R. Soc. Lond. Ser. A Math. Phys. Eng. Sci.* 400 (1985) 229–251.

[220] T. Guhr, A. Müller-Groeling, H.A. Weidenmüller, Random-matrix theories in quantum physics: common concepts, *Phys. Rep.* 299 (1998) 189–425.

[221] V. Balasubramanian, M. Berkooz, S.F. Ross, J. Simón, Black holes, entanglement and random matrices, *Classical Quantum Gravity* 31 (2014) 185009.

[222] J.S. Cotler, G. Gur-Ari, M. Hanada, J. Polchinski, P. Saad, S.H. Shenker, D. Stanford, A. Streicher, M. Tezuka, Black holes and random matrices, *J. High Energy Phys.* 2017 (2017) 118.

[223] L. Laloux, P. Cizeau, J.-P. Bouchaud, M. Potters, Noise dressing of financial correlation matrices, *Phys. Rev. Lett.* 83 (1999) 1467–1470.

[224] V. Plerou, P. Gopikrishnan, B. Rosenow, L.A.N. Amaral, T. Guhr, H.E. Stanley, Random matrix approach to cross correlations in financial data, *Phys. Rev. E* 65 (2002) 066126.

[225] S.N. Majumdar, C. Nadal, A. Scardicchio, P. Vivo, Index distribution of Gaussian random matrices, *Phys. Rev. Lett.* 103 (2009) 220603.

[226] M.A. Rutgers, J.H. Dunsuir, J.Z. Xue, W.B. Russel, P.M. Chaikin, Measurement of the hard-sphere equation of state using screened charged polystyrene colloids, *Phys. Rev. B* 53 (1996) 5043–5046.

[227] P.X. Gallagher, On the distribution of primes in short intervals, *Mathematika* 23 (1976) 4–9.

[228] G. Tenenbaum, *Introduction to Analytic and Probabilistic Number Theory*, Vol. 46, Cambridge University Press, Cambridge, 1995.

[229] G. Zhang, F. Martelli, S. Torquato, Structure factor of the primes, *J. Phys. A Math. Theory* 51 (2018) 115001.

[230] S. Torquato, G. Zhang, M. de Courcy-Ireland, Uncovering multiscale order in the prime numbers via scattering, ArXiv e-prints [arXiv:1802.10498](https://arxiv.org/abs/1802.10498).

[231] S. Torquato, G. Zhang, M. de Courcy-Ireland, Hidden multiscale order in the primes, ArXiv e-prints [arXiv:1804.06279](https://arxiv.org/abs/1804.06279).

[232] G.H. Hardy, J.E. Littlewood, Some problems of ‘partitio numerorum’: III: On the expression of a number as a sum of primes, *Acta Math.* 44 (1923) 1–70.

[233] M. Baake, U. Grimm, Diffraction of limit periodic point sets, *Phil. Mag.* 91 (2011) 2661–2670.

[234] G. Matheron, *Random Sets and Integral Geometry*, Wiley, New York, 1975.

[235] A. Soshnikov, Determinantal random point fields, *Russian Math. Surveys* 55 (2000) 923–975.

[236] R. Burton, R. Pemantle, Local characteristics entropy and limit theorems for spanning trees and domino tilings via transfer-impedances, *Ann. Probab.* 21 (1993) 1329–1371.

[237] K. Johansson, Determinantal processes with number variance saturation, *Comm. Math. Phys.* 252 (2004) 111–148.

[238] Y. Peres, B. Virág, Zeros of the iid Gaussian power series: A conformally invariant determinantal process, *Acta Math.* 194 (2005) 1–35.

[239] O. Costin, J. Lebowitz, On the construction of particle distributions with specified single and pair densities, *J. Phys. Chem. B.* 108 (2004) 19614–19618.

[240] J.D. Coninck, F. Dunlop, T. Huillet, On the correlation structure of some random point processes on the line, *Physica A* 387 (2008) 725–744.

[241] A. Scardicchio, C.E. Zachary, S. Torquato, Statistical properties of determinantal point processes in high-dimensional Euclidean spaces, *Phys. Rev. E* 79 (2009) 041108.

[242] H. Minkowski, Diskontinuitätsbereich für arithmetische Äquivalenz, *J. Reine Angew. Math.* 129 (1905) 220–274.

[243] S. Torquato, F.H. Stillinger, Exactly solvable disordered sphere-packing model in arbitrary-dimensional Euclidean spaces, *Phys. Rev. E* 73 (2006) 031106.

[244] J.B. Hough, M. Krishnapur, Y. Peres, B. Virág, Determinantal processes and independence, *Probab. Surv.* 3 (2006) 206–209.

[245] J. Ginibre, Statistical ensembles of complex, quaternion, and real matrices, *J. Math. Phys.* 6 (1965) 440–449.

[246] R.B. Laughlin, Elementary theory: The incompressible quantum fluid, in: *The Quantum Hall Effect*, Springer, 1987, pp. 233–301.

[247] C. Cavazzoni, G.L. Chiarotti, S. Scandolo, E. Tosatti, M. Bernasconi, M. Parrinello, Superionic and metallic states of water and ammonia at giant planet conditions, *Science* 283 (5398) (1999) 44–46.

[248] J. Sun, B.K. Clark, S. Torquato, R. Car, The phase diagram of high-pressure superionic ice, *Nature Commun.* 6 (2015) 8156.

[249] J.B. Boyce, B.A. Huberman, Superionic conductors: Transitions, structures, dynamics, *Phys. Rep.* 51 (1979) 189–265.

[250] R. Makiura, T. Yonemura, T. Yamada, M. Yamauchi, R. Ikeda, H. Kitagawa, K. Kato, M. Takata, Size-controlled stabilization of the superionic phase to room temperature in polymer-coated agi nanoparticles, *Nature Mater.* 8 (2009) 476–480.

[251] A. Haimi, H. Hedenmalm, The polyanalytic ginibre Ensembles, *J. Stat. Phys.* 153 (2013) 10–47.

[252] A. Donev, F.H. Stillinger, P.M. Chaikin, S. Torquato, Unusually dense crystal ellipsoid packings, *Phys. Rev. Lett.* 92 (2004) 255506.

[253] G. Parisi, F. Zamponi, Mean field theory of hard sphere glasses and jamming, *Rev. Modern Phys.* 82 (2010) 789–845.

[254] R. Connelly, K. Bezdek, A. Bezdek, Finite and uniform stability of sphere packings, *Discrete Comput. Geom.* 20 (1998) 111–130.

[255] S. Torquato, T.M. Truskett, P.G. Debenedetti, Is random close packing of spheres well defined? *Phys. Rev. Lett.* 84 (2000) 2064–2067.

[256] S. Torquato, F.H. Stillinger, Multiplicity of generation, selection, and classification procedures for jammed hard-particle packings, *J. Phys. Chem. B* 105 (2001) 11849–11853.

[257] C.S. O'Hern, S.A. Langer, A.J. Liu, S.R. Nagel, Random packings of frictionless particles, *Phys. Rev. Lett.* 88 (2002) 075507.

[258] C.S. O'Hern, L.E. Silbert, A.J. Liu, S.R. Nagel, Jamming at zero temperature and zero applied stress: The epitome of disorder, *Phys. Rev. E* 68 (2003) 011306.

[259] A. Donev, I. Cisse, D. Sachs, E.A. Variano, F.H. Stillinger, R. Connelly, S. Torquato, P.M. Chaikin, Improving the density of jammed disordered packings using ellipsoids, *Science* 303 (2004) 990–993.

[260] W. Man, A. Donev, F.H. Stillinger, M. Sullivan, W.B. Russel, D. Heeger, S. Inati, S. Torquato, P.M. Chaikin, Experiments on random packing of ellipsoids, *Phys. Rev. Lett.* 94 (2005) 198001.

[261] M. Wyart, L.E. Silbert, S.R. Nagel, T.A. Witten, Effects of compression on the vibrational modes of marginally jammed solids, *Phys. Rev. E* 72 (2005) 051306.

[262] C. Song, P. Wang, H.A. Makse, A phase diagram for jammed matter, *Nature* 453 (2008) 629–632.

[263] M. Mailman, C.F. Schreck, C.S. O'Hern, B. Chakraborty, Jamming in systems composed of frictionless ellipse-shaped particles, *Phys. Rev. Lett.* 102 (2009) 255501.

[264] R. Mari, F. Krzakala, J. Kurchan, Jamming versus glass transitions, *Phys. Rev. Lett.* 103 (2008) 025701.

[265] R. Jadrich, K.S. Schweizer, Equilibrium theory of the hard sphere fluid and glasses in the metastable regime up to jamming. I. Thermodynamics, *J. Chem. Phys.* 139 (2013) 054501.

[266] S. Torquato, A. Donev, F.H. Stillinger, Breakdown of elasticity theory for jammed hard-particle packings: Conical nonlinear constitutive theory, *Int. J. Solids Struct.* 40 (2003) 7143–7153.

[267] A. Donev, S. Torquato, F.H. Stillinger, R. Connelly, Jamming in hard sphere and disk packings, *J. Appl. Phys.* 95 (2004) 989–999.

[268] A. Donev, S. Torquato, F.H. Stillinger, Pair correlation function characteristics of nearly jammed disordered and ordered hard-sphere packings, *Phys. Rev. E* 71 (2005) 011105: 1–14.

[269] S. Torquato, Y. Jiao, Dense packings of the Platonic and Archimedean solids, *Nature* 460 (2009) 876–881.

[270] S. Torquato, Y. Jiao, Dense polyhedral packings: Platonic and Archimedean solids, *Phys. Rev. E* 80 (2009) 041104.

[271] J.D. Bernal, Geometry and the structure of monatomic liquids, *Nature* 185 (1960) 68–70.

[272] J.D. Bernal, The geometry of the structure of liquids, in: T.J. Hugel (Ed.), *Liquids: Structure, Properties, Solid Interactions*, Elsevier, New York, 1965, pp. 25–50.

[273] S. Atkinson, F.H. Stillinger, S. Torquato, Existence of isostatic, maximally random jammed monodisperse hard-disk packings, *Proc. Natl. Acad. Sci.* 111 (2014) 18436–18441.

[274] S.F. Edwards, The role of entropy in the specification of a powder, in: A. Mehta (Ed.), *Granular Matter*, Springer-Verlag, New York, 1994, pp. 121–140.

[275] S. Atkinson, F.H. Stillinger, S. Torquato, Detailed characterization of rattlers in exactly isostatic, strictly jammed sphere packings, *Phys. Rev. E* 88 (2013) 062208.

[276] M.A. Klatt, S. Torquato, Characterization of maximally random jammed sphere packings: Voronoi correlation functions, *Phys. Rev. E* 90 (2014) 052120.

[277] B.D. Lubachevsky, F.H. Stillinger, Geometric properties of random disk packings, *J. Stat. Phys.* 60 (1990) 561–583.

[278] F.H. Stillinger, S. Torquato, H. Sakai, Lattice-based random jammed configurations for hard particles, *Phys. Rev. E* 67 (2003) 031107.

[279] B.D. Lubachevsky, F.H. Stillinger, E.N. Pinson, Disks versus spheres: Contrasting properties of random packings, *J. Stat. Phys.* 64 (1991) 501–524.

[280] S. Torquato, Y. Jiao, Robust algorithm to generate a diverse class of dense disordered and ordered sphere packings via linear programming, *Phys. Rev. E* 82 (2010) 061302.

[281] A. Ikeda, L. Berthier, Thermal fluctuations, mechanical response, and hyperuniformity in jammed solids, *Phys. Rev. E* 92 (2015) 012309.

[282] Y. Wu, P. Olsson, S. Teitel, Search for hyperuniformity in mechanically stable packings of frictionless disks above jamming, *Phys. Rev. E* 92 (2015) 052206.

[283] A. Ikeda, L. Berthier, G. Parisi, Large-scale structure of randomly jammed spheres, *Phys. Rev. E* 95 (2017) 052125.

[284] A. Donev, S. Torquato, F.H. Stillinger, Neighbor list collision-driven molecular dynamics for nonspherical hard particles: I. Algorithmic details, *J. Comput. Phys.* 202 (2005) 737–764.

[285] A. Donev, S. Torquato, F.H. Stillinger, Neighbor list collision-driven molecular dynamics for nonspherical hard particles: II. Applications to ellipses and ellipsoids, *J. Comput. Phys.* 202 (2005) 765–793.

[286] A. Donev, S. Torquato, F.H. Stillinger, R. Connelly, A linear programming algorithm to test for jamming in hard-sphere packings, *J. Comput. Phys.* 197 (2004) 139–166.

[287] P. Chaudhuri, L. Berthier, S. Sastry, Jamming transitions in amorphous packings of frictionless spheres occur over a continuous range of volume fractions, *Phys. Rev. Lett.* 104 (2010) 165701.

[288] Y. Jiao, F.H. Stillinger, S. Torquato, Distinctive features arising in maximally random jammed packings of superballs, *Phys. Rev. E* 81 (2010) 041304.

[289] J. Tian, Y. Xu, Y. Jiao, S. Torquato, A geometric-structure theory for maximally random jammed packings, *Sci. Rep.* 5 (2015) 16722.

[290] G.W. Delaney, P.W. Cleary, The packing properties of superellipsoids, *Europhys. Lett.* 89 (2010) 34002.

[291] S.-X. Li, J. Zhao, X. Zhou, Numerical simulation of random close packing with tetrahedra, *Chin. Phys. Lett.* 25 (2008) 1724.

[292] A. Haji-Akbari, M. Engel, A.S. Keys, X. Zheng, R.G. Petschek, P. Palffy-Muhoray, S.C. Glotzer, Disordered, quasicrystalline and crystalline phases of densely packed tetrahedra, *Nature* 462 (2009) 773–777.

[293] A. Jaoshvili, A. Esakia, M. Porrati, P.M. Chaikin, Experiments on the random packing of tetrahedral dice, *Phys. Rev. Lett.* 104 (2010) 185501.

[294] K.C. Smith, M. Alam, T.S. Fisher, Athermal jamming of soft frictionless Platonic solids, *Phys. Rev. E* 82 (2010) 051304.

[295] J. Baker, A. Kudrolli, Maximum and minimum stable random packings of Platonic solids, *Phys. Rev. E* 82 (2010) 061304.

[296] H. Spohn, Long range correlations for stochastic lattice gases in a non-equilibrium steady state, *J. Phys. A: Math. Gen.* 16 (1983) 4275.

[297] P.L. Garrido, J.L. Lebowitz, C. Maes, H. Spohn, Long-range correlations for conservative dynamics, *Phys. Rev. A* 42 (1990) 1954.

[298] Z. Cheng, P.L. Garrido, J.L. Lebowitz, J.L. Vallés, Long-range correlations in stationary nonequilibrium systems with conservative anisotropic dynamics, *Europhys. Lett.* 14 (1991) 507.

[299] B. Derrida, Non-equilibrium steady states: Fluctuations and large deviations of the density and of the current, *J. Stat. Mech. Theory Exp.* 2007 (2007) P07023.

[300] T. Bodineau, B. Derrida, V. Lecomte, F. van Wijland, Long range correlations and phase transitions in non-equilibrium diffusive systems, *J. Stat. Phys.* 133 (2008) 1013–1031.

[301] H. Hinrichsen, Non-equilibrium critical phenomena and phase transitions into absorbing states, *Adv. Phys.* 49 (2000) 815–958.

[302] S. Lübeck, Universal scaling behavior of non-equilibrium phase transitions, *Internat. J. Modern Phys. B* 18 (2004) 3977–4118.

[303] M. Henkel, H. Hinrichsen, S. Lübeck, *Non-Equilibrium Phase Transitions - Volume 1: Absorbing Phase Transitions*, Springer, New York, 2008.

[304] D.J. Pine, J.P. Gollub, J.F. Brady, A.M. Leshansky, Chaos and threshold for irreversibility in sheared suspensions, *Nature* 438 (2005) 997–1000.

[305] C. Laurent, P.M. Chaikin, J.P. Gollub, D.J. Pine, Random organization in periodically driven systems, *Nat. Phys.* 4 (2008) 420–424.

[306] J.N. Roux, Geometric origin of mechanical properties of granular materials, *Phys. Rev. E* 61 (2000) 6802–6836.

[307] S.-B. Lee, Universality class of the conserved Manna model in one dimension, *Phys. Rev. E* 89 (2014) 060101.

[308] J. Feder, Random sequential adsorption, *J. Theoret. Biol.* 87 (1980) 237–254.

[309] J. Talbot, G. Tarjus, P.R. Van Tassel, P. Viot, From car parking to protein adsorption: An overview of sequential adsorption processes, *Colloids Surf. A* 165 (2000) 287–324.

[310] C. Reichhardt, C.J.O. Reichhardt, Random organization and plastic depinning, *Phys. Rev. Lett.* 103 (2009) 168301.

[311] K.H. Nagamanasa, S. Gokhale, A.K. Sood, R. Ganapathy, Experimental signatures of a nonequilibrium phase transition governing the yielding of a soft glass, *Phys. Rev. E* 89 (2014) 062308.

[312] J.R. Royer, P.M. Chaikin, Precisely cyclic sand: Self-organization of periodically sheared frictional grains, *Proc. Natl. Acad. Sci.* 112 (2015) 49–53.

[313] D. Purves, R.B. Lotto, *Why We See What We Do Redux: A Wholly Empirical Theory of Vision*, Sinauer Associates, Sunderland, Massachusetts, 2011.

[314] C.E. Shannon, Communication in the presence of noise, *Proc. IRE* 37 (1949) 10–21.

[315] D.P. Petersen, D. Middleton, Sampling and reconstruction of wave-number-limited functions in N-dimensional Euclidean spaces, *Info. Control* 5 (1962) 279–323.

[316] A.S. French, A.W. Snyder, D.G. Stavenga, Image degradation by an irregular retinal mosaic, *Bio. Cybernetics* 27 (1977) 229–233.

[317] D.F. Ready, T.E. Hanson, S. Benzer, Development of the drosophila retina. A neurocrystalline lattice, *Develop. Bio.* 53 (1976) 217–240.

[318] D.K. Lubensky, M.W. Pennington, B.I. Shraiman, N.E. Baker, A dynamical model of ommatidial crystal formation, *Proc. Natl. Acad. Sci.* 108 (2011) 11145–11150.

[319] A.H. Lyall, Cone arrangements in teleost retinae, *J. Cell Sci.* 3 (1957) 189–201.

[320] K. Engström, Cone types and cone arrangements in teleost retinae1, *Acta Zool.* 44 (1963) 179–243.

[321] P.A. Raymond, L.K. Barthel, A moving wave patterns the cone photoreceptor mosaic array in the zebrafish retina, *Int. J. Develop. Bio.* 48 (2004) 935–945.

[322] R.F. Dunn, Studies on the retina of the gecko *coleonyx variegatus*: II. The rectilinear visual cell mosaic, *J. Ultrastructure Res.* 16 (1966) 672–684.

[323] N.S. Hart, The visual ecology of avian photoreceptors, *Prog. Retinal Eye Res.* 20 (2001) 675–703.

[324] V.B. Morris, Symmetry in a receptor mosaic demonstrated in the chick from the frequencies, spacing and arrangement of the types of retinal receptor, *J. Comparative Neurology* 140 (1970) 359–397.

[325] Y.A. Kram, S. Mantey, J.C. Corbo, Avian cone photoreceptors tile the retina as five independent, self-organizing mosaics, *PLoS One* 5 (2010) e8992.

[326] D. Chen, W.-Y. Aw, D. Devenport, S. Torquato, Structural characterization and statistical-mechanical model of epidermal patterns, *Biophys. J.* 111 (2016) 2534–2545.

[327] S. Torquato, Relationship between permeability and diffusion-controlled trapping constant of porous media, *Phys. Rev. Lett.* 64 (1990) 2644–2646.

[328] D.J. Wilkinson, D.L. Johnson, L.M. Schwartz, Nuclear magnetic relaxation in porous media: The role of the mean lifetime $\tau(\rho, d)$, *Phys. Rev. B* 44 (1991) 4960–4971.

[329] P.P. Mitra, P.N. Sen, Effects of microgeometry and surface relaxation on nmr pulsed-field-gradient experiments: Simple pore geometries, *Phys. Rev. B* 45 (1992) 143.

[330] J.W. Cahn, J.E. Hilliard, Free energy of a nonuniform system. I. Interfacial free energy, *J. Chem. Phys.* 28 (1958) 258–267.

[331] J. Swift, P.C. Hohenberg, Hydrodynamic fluctuations at the convective instability, *Phys. Rev. A* 15 (1977) 319–328.

[332] G.K. Batchelor, *The Theory of Homogeneous Turbulence*, Cambridge University Press, Cambridge, England, 1959.

[333] A.S. Monin, A.M. Yaglom, *Statistical Fluid Mechanics: Mechanics of Turbulence*, Vol. 2, MIT Press, Cambridge, Massachusetts, 1975.

[334] D.J. Pine, D.A. Weitz, P.M. Chaikin, E. Herbolzheimer, Diffusing wave spectroscopy, *Phys. Rev. Lett.* 60 (1988) 1134–1137.

[335] D.S. Wiersma, The physics and applications of random lasers, *Nat. Phys.* 4 (2008) 359–367.

[336] A. Dogariu, R. Carminati, Electromagnetic field correlations in three-dimensional speckles, *Phys. Rep.* 559 (2015) 1–29.

[337] D. Di Battista, D. Ancora, M. Leonetti, G. Zacharakis, From amorphous speckle pattern to reconfigurable Bessel beam via wavefront shaping, *ArXiv e-prints arXiv:1511.04964*.

[338] E. Komatsu, A. Kogut, M.R. Nolta, C.L. Bennett, M.H. i. G. Hinshaw, N. Jarosik, M. Limon, S.S. Meyer, L. Page, D.N. Spergel, G.S. Tucker, L. Verde, E. Wollack, E.L. Wright, First-year Wilkinson microwave anisotropy probe (WMAP) observations: Tests of Gaussianity, *Astrophys. J. Suppl. Ser.* 148 (2003) 119.

[339] N.F. Berk, Scattering properties of a model bicontinuous structure with a well defined length scale, *Phys. Rev. Lett.* 58 (1987) 2718–2721.

[340] N.F. Berk, Scattering properties of the leveled-wave model of random morphologies, *Phys. Rev. A* 44 (1991) 5069–5079.

[341] M. Teubner, Level surfaces of Gaussian random fields and microemulsions, *Europhys. Lett.* 14 (1991) 403–408.

[342] P.A. Crossley, L.M. Schwartz, J.R. Banavar, Image-based models of porous media—Application to vycor glass and carbonate rocks, *Appl. Phys. Lett.* 59 (1991) 3553–3555.

[343] R. Blumenfeld, S. Torquato, Coarse-graining procedure to generate and analyze heterogeneous materials: Theory, *Phys. Rev. E* 48 (1993) 4492–4500.

[344] A.P. Roberts, M. Teubner, Transport properties of heterogeneous materials derived from Gaussian random fields: Bounds and simulation, *Phys. Rev. E* 51 (1995) 4141–4154.

[345] A.P. Roberts, Morphology and thermal conductivity of model organic aerogels, *Phys. Rev. E* 55 (1997) R1286–R1289.

[346] M. Cross, H. Greenside, *Pattern Formation and Dynamics in Nonequilibrium Systems*, Cambridge University Press, Cambridge, England, 2009, 2009.

[347] J.P. Huang, Z.W. Wang, C. Holm, Computer simulations of the structure of colloidal ferrofluids, *Phys. Rev. E* 71 (2005) 061203.

[348] R.E. Caflisch, J.H. Luke, Variance in the sedimentation speed of a suspension, *Phys. Fluids* 28 (1985) 759–760.

[349] J.M. Ham, G.M. Homsy, Hindered settling and hydrodynamic dispersion in quiescent sedimenting suspensions, *Int. J. Multiphase Flow* 14 (1988) 533–546.

[350] H. Nicolai, E. Guazzelli, Effect of the vessel size on the hydrodynamic diffusion of sedimenting spheres, *Phys. Fluids* 7 (1995) 3–5.

[351] P.N. Segrè, E. Herbolzheimer, P.M. Chaikin, Long-range correlations in sedimentation, *Phys. Rev. Lett.* 79 (1997) 2574–2577.

[352] T. Goldfriend, H. Diamant, T.A. Witten, Screening, hyperuniformity, and instability in the sedimentation of irregular objects, *Phys. Rev. Lett.* 118 (2017) 158005.

[353] M. Mézard, G. Parisi, M. Virasoro, *Spin Glass Theory and beyond: An Introduction to the Replica Method and Its Applications*, Vol. 9, World Scientific Publishing, 1987.

[354] M.C. Rechtsman, S. Torquato, Effective dielectric tensor for electromagnetic wave propagation in random media, *J. Appl. Phys.* 103 (2008) 084901.

[355] Q.L. Thien, D. McDermott, C.J. Reichhardt, C. Reichhardt, Enhanced pinning for vortices in hyperuniform substrates and emergent hyperuniform vortex states, *Phys. Rev. B* 96 (2017) 094516.

[356] L.M. Burcaw, E. Fieremans, D.S. Novikov, Mesoscopic structure of neuronal tracts from time-dependent diffusion, *Neuroimage* 114 (2015) 18–37.

[357] A. Papaioannou, D.S. Novikov, E. Fieremans, G.S. Boutis, Observation of structural universality in disordered systems using bulk diffusion measurement, *Phys. Rev. E* 96 (2017) 061101.

[358] G.W. Milton, *The Theory of Composites*, Cambridge University Press, Cambridge, England, 2002.

[359] G.E. Dieter, *Mechanical Metallurgy*, third ed., McGraw-Hill, New York, 1986.

[360] C. Kittel, *Introduction to Solid State Physics*, eighth ed., Wiley, New York, 2005.

[361] J. Kondo, Resistance minimum in dilute magnetic alloys, *Progr. Theoret. Phys.* 32 (1964) 37–49.

[362] P.W. Anderson, A poor man's derivation of scaling laws for the Kondo problem, *J. Phys. C: Solid State Phys.* 3 (1970) 2436.

[363] K. Huang, X-ray reflexions from dilute solid solutions, *Proc. R. Soc. Lond. Ser. A Math. Phys. Eng. Sci.* 190 (1947) 102–117.

[364] P.H. Dederichs, The theory of diffuse x-ray scattering and its application to the study of point defects and their clusters, *J. Phys. F Met. Phys.* 3 (1973) 471.

[365] T.R. Welberry, G.H. Miller, C.E. Carroll, Paracrystals and growth-disorder models, *Acta Crystallogr. Sect. A* 36 (1980) 921–929.

[366] Y. Imry, Long-range order in two dimensions, *Crit. Rev. Solid State Mater. Sci.* 8 (1979) 157–174.

[367] W.H. Zachariasen, The atomic arrangement in glass, *J. Am. Chem. Soc.* 54 (1932) 3841–3851.

[368] D. Weaire, M.F. Thorpe, Electronic properties of an amorphous solid. I. A simple tight-binding theory, *Phys. Rev. B* 4 (1971) 2508.

[369] R. Zallen, *The Physics of Amorphous Solids*, Wiley, New York, 1983.

[370] N. Mousseau, G.T. Barkema, S.M. Nakhmanson, Recent developments in the study of continuous random networks, *Phil. Mag. B* 82 (2002) 171–183.

[371] A.M.R.D. Graff, M.F. Thorpe, The long-wavelength limit of the structure factor of amorphous silicon and vitreous silica, *Acta Crystallogr. Sect. A* 66 (2010) 22–31.

[372] F.H. Stillinger, T.A. Weber, Computer simulation of local order in condensed phases of silicon, *Phys. Rev. B* 31 (1985) 5262–5271.

[373] C.E. Zachary, F.H. Stillinger, S. Torquato, Gaussian-core model phase diagram and pair correlations in high Euclidean dimensions, *J. Chem. Phys.* 128 (2008) 224505.

[374] F.H. Stillinger, Phase transitions in the Gaussian core system, *J. Chem. Phys.* 65 (1976) 3968.

[375] A. Lang, C.N. Likos, M. Watzlawek, H. Lowén, Fluid and solid phases of the Gaussian core model, *J. Phys.: Condens. Matter* 12 (2000) 5087–5108.

[376] A. Ikeda, K. Miyazaki, Thermodynamic and structural properties of the high density Gaussian core model, *J. Chem. Phys.* 135 (2011) 024901.

[377] H. Cohn, M. de Courcy-Ireland, The Gaussian core model in high dimensions, ArXiv e-prints arXiv:1603.09684.

[378] M. Vaezi, H. Seitz, S. Yang, A review on 3d micro-additive manufacturing technologies, *Int. J. Adv. Manuf. Technol.* 67 (2013) 1721–1754.

[379] M.B. Priestley, *Spectral Analysis and Time Series*, Academic Press, New York, 1981.

[380] M.N. Huxley, Exponential sums and lattice points III, *Proc. Lond. Math. Soc.* 87 (2003) 591–609.

[381] L.G. Arkhipova, Number of lattice points in a sphere, *Moscow Univ. Math. Bull.* 63 (2008) 214–215.

[382] K.-M. Tsang, Counting lattice points in the sphere, *Bull. Lond. Math. Soc.* 32 (2000) 679–688.